

KENYA SOCIETY OF ELECTRICAL AND ELECTRONIC ENGINEERS



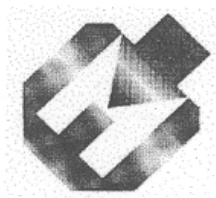
KSEEE 2010

PROCEEDINGS

***ENGINEERING RESEARCH AND INNOVATION AS FUNDAMENTAL REQUIREMENTS
FOR INDUSTRIALIZATION***

Organized by KSEEE

In conjunction with



JAPAN SOCIETY OF APPLIED ELECTROMAGNETICS AND MECHANICS (JSAEM)

5th – 6th August 2010

Multimedia University College of Kenya, Mbagathi, Nairobi, Kenya

CONFERENCE ORGANIZING COMMITTEE

- | | | |
|------------|------------------------|----------------------------------|
| 1. | D B O Konditi | <i>Chairman</i> |
| 2. | A Saito | <i>Patron, KSEEE,</i> |
| 3. | M. Sasaki | <i>Coordinator, JSAEM</i> |
| 4. | D O Owira | <i>Secretary</i> |
| 5. | S Musyoki | <i>Treasurer</i> |
| 6. | J K Makiche | <i>Member</i> |
| 7. | H A Ouma | <i>Member</i> |
| 8. | E K Koech | <i>Member</i> |
| 9. | C A Otieno | <i>Member</i> |
| 10. | V Dharmathikari | <i>Member</i> |

COPYRIGHT

© 2010, by the Kenya Society of Electrical and Electronic Engineers

CONTENTS

PREFACE	v
OPENING PRESENTATION	1
Historical Perspective of KSEEE-JSAEM	1
POLICY PRESENTATION	2
Role of Research in Universities Towards Meeting the 2030 Millennium Goals	2
KEYNOTE ADDRESS	7
Emerging Technologies in Photovoltaic Issues: Measurement Techniques and Characterization	7
INVITED PLANERY PRESENTATION	12
Robot Control Systems Using Bio-potential Signals	12
INVITED PLANERY PRESENTATION	13
Teaching of Communication Skills to Scientists and Engineers	13
IMPROVING ENGINEERING EDUCATION, PROFESSION AND RESEARCH IN KENYA THROUGH CREATION OF INSTITUTES	20
NON LINEAR DYNAMICS: CHAOS AND ITS APPLICATION IN TELECOMMUNICATIONS	25
DETERMINATION OF STRESS INTENSITY FACTORS IN MULTIPLY CRACKED THICK-WALLED CYLINDERS USING MVCCT	28
EVALUATING PERFORMANCE OF WRP AND AODV MANETS ROUTING PROTOCOLS UNDER MOBILITY	37
PERFORMANCE ANALYSIS OF BIODIESEL FOR DOMESTIC USE	43
POWER THEFT IDENTIFIER USING GLOBAL SYSTEM MOBILE COMMUNICATION (GSM) TECHNOLOGY	47
A HYBRID MOM/FDTD FORMULATION FOR EMC/EMI PROBLEMS OF METALLIC ENCLOSURES WITH APERTURES	53
AUTOMATION OF CORPORATE SERVICE AVAILABILITY AND SLA REPORTING	61
FINGER MOTION PATTERN ESTIMATION FROM SURFACE-EMG SIGNALS USING SVM	64
APPLICATION OF MULTI-ANTENNA SYSTEMS IN COMBATING INTERFERENCE AND MULTIPATH FADING IN WIRELESS COMMUNICATION SYSTEMS	71
VOLTAGE STABILITY ANALYSIS USING CP_ANN AND OPTIMISED CAPACITOR BANK PLACEMENT	76
ANALYSIS OF THE EFFECTS OF CONNECTING WIND FARMS TO A DISTRIBUTION NETWORK	84
DEVELOPMENT OF SOLUTION SEARCH ALGORITHM FOR CFD OPTIMIZATION PROBLEM	89
REMOTE MONITORING OF TV/RADIO CHANNELS-USE	94
NEURAL FUZZY BASED DC-DC CONVERTER CONTROLLER OPTIMISED WITH PARTICLE SWARM OPTIMIZATION.	97

OPTIMIZATION OF UNDERDETERMINED BLIND SPEECH DENOISING FOR ENHANCED TELECONFERENCING BY INTERPOLATED FASTICA_25_____ 106

A STUDY OF THE EFFECTS OF URBAN DOMESTIC ELECTRICAL BURDEN ON THE ELECTRICITY GENERATION INDUSTRY OF KENYA _____ 110

ACTIVE POWER FILTER CONTROL USING A COOPERATIVE NEURO-FUZZY SYSTEM FOR HARMONIC MITIGATION _____ 114

DETERMINATION OF REACTIVE POWER COMPENSATION AND TRANSMISSION LINE POWER TRANSFER CAPABILITY IMPROVEMENT OF THE KENYAN POWER SYSTEM _____ 118

MODELLING AND CONTROL OF A FLEXIBLE MANIPULATOR USING FORMULA MANIPULATION_ 124

LIST OF PARTICIPANTS _____ 129



PREFACE

Today, as a country, we are focused on the 2030 development goals dubbed *Vision 2030*. We have the opportunity to make a better future for ourselves and for the generations to come. This is only possible if different institutions play their rightful roles as prescribed in the 2030 development goals. As a learning institution, ours is to teach, research and disseminate knowledge. Since all these require different experiences and expertise, we open our gates to people in similar fields to draw on our collective expertise and experience for mutual benefit. Hence, the spirit and mood in which the KSEEE-JSAEM 2010 International Conference was held.

On behalf of the organizing committee, I thank very sincerely the authors and participants who made this year's conference such a great success. Particular gratitude and appreciation go to Prof. Aimé Lay-Ekuakille (University of Salento, Italy), Prof. Minoru Sasaki (University of Gifu, Japan), Prof. Robert Jallang'o Akello (Masinde Muliro University of Science and Technology, Kenya) for the role they played as the main speakers at the conference. Greatly appreciated too are the contributions made by Prof. H. Kaane (Secretary, Ministry of Higher Education, Kenya Government), Prof. Akihiko Saito, the Patron, KSEEE (Former President, Fukuoka Jo-Gakuin University, Japan) and Prof. James Kulubi (Principal, Multimedia University College of Kenya).

As KSEEE we pay great tribute to Prof. K. Chonnan, formerly, Chairman, Japan Society of Applied Electromagnetics & Mechanics (JSAEM) and his successor, Prof. Minoru Sasaki, together with Prof. A. Saito, who have overwhelmingly supported us by funding the activities of the KSEEE and mobilizing Professors and other researchers to participate and present technical/scientific papers at the Conference. The Conference also enjoyed an overwhelming support from Prof. James Kulubi by way of funding the conference participants from the Multimedia University College of Kenya (MMUCK) and availing transport for participants from abroad. The 2010 KSEEE-JSAEM Conference was held under the serene environment of MMUCK which is geographically somewhat an extension of the Nairobi National Park. The participants thus had the privilege of observing some of the park animals within the campus grounds during the course of the conference.

Turning to the presentations, the plenary talks gave a great challenge and food-for-thought to the audience not only in terms of substance but also as a gauge to how much time and resources go into making a plenary talk worth its salt: The talks were quite well received and valued as truly scientific cutting edge masterpieces! The paper presentation sessions also provided some well-researched works from three continents. Out of the 24 presentations, four were by participants from Japan, one each from Italy, South Africa, Nigeria and Tanzania, and the rest from Kenya. It is worthwhile to note that a good number of the papers involved collaborations of researchers from different institutions and countries thus illustrating further the coming together with an aim to pool our expertise and experience in achieving our common goals.

The very fruitful scientific collaboration between KSEEE and JSAEM in organizing the joint conference over several years now has greatly benefitted many local researchers. The JSAEM commitment is recognized and appreciated especially in view of the financial resources entailed in coming all the way from Japan and back. We hope that the collaboration will continue to grow from strength to strength as we go forward.

Prof. Dominic B. Onyango Konditi, PhD

Chairman, KSEEE and Joint-Chairman, KSEEE-JSAEM 2010 International Conference.

OPENING PRESENTATION

Historical Perspective of KSEEE-JSAEM

Prof. A Saito

Former President,
Fukuoka JoGakuin University Japan,
Patron KSEEE

Summary

The Kenya Society of Electrical and Electronic Engineers was registered on 26th July, 1994, at the Registrar of Societies in Kenya and with the following people as the founding members:

Prof. Alfred Vincent Otieno –	Chairman
Dr. Stephen Marangi Mbogho –	Vice –Chairman
Dr. David K. Murage –	Secretary
Dr. Edward N. Ndung’u –	Assistant Secretary
Prof. Dominic B. Onyango Konditi –	Treasurer
Prof. Akihiko Saito –	Later, Patron
Prof. Stephen M. Kang’ethe –	Member
Mr. Yoshio Iwami –	Member

One of the objectives of the Society was to promote advancement of Electrical & Electronic Engineering and Technology. In order to achieve this, one of the functions was to provide a forum for discussions and a medium for dissemination of knowledge by organizing symposia, seminars, workshops and conferences.

The history of KSEEE dates back to 1991 when the first seminar so called “Electrical and Engineering Department Seminar” was held in JKUCAT. At that seminar only four papers; two from Prof. Saito and one each from Dr. Ndung’u and Prof. Konditi were presented. Thereafter, similar seminars had been held annually up to 1994 with the number of participants increasing each year with more and more countries coming into the fold. The fourth seminar was held on 4th August, 1994. At the end of the Seminar, the seminar organizing committee, held a gala dinner during which the Kenya Association of Electrical & Electronic Engineers (KAEEE) was inaugurated. The Society was officially registered on July 26th, 1994. At the time of registration, the name of the society was changed to KSEEE upon the advice of the Registrar of Societies. It is for this reason that the month of August has become not only special but memorable in the history of KSEEE conferences.

The first KSEEE International Conference was held on 24th August, 1995, at Serena Hotel, Nairobi, and was jointly organized by Japan Society of Applied Electromagnetics and Mechanics (JSAEM) and KSEEE. The Conference realized a modest success as was evident from the number participating countries, namely, Japan, Zimbabwe, Tanzania, and Kenya, with thirty two papers presented in total, not a small number by any stretch of imagination. Then, hence, the conference has been held annually, except in 2008 and 2009, owing to the Post Election Violence in Kenya after 2007 General Election. The response has always been overwhelming.

The Society has enjoyed over the years generous sponsorship from JSAEM, Communication Commission of Kenya, TELKOM Kenya, SAFARICOM Kenya, and Kenya Power & Lighting Co. KSEEE endeavors to stimulate research in our universities and to foster partnerships with our local industries, institutions of higher learning and overseas universities and research centers. The scope of the conference has been limited to Electrical Engineering and Telecommunications as well as limited areas in Mechanical Engineering. However, the scope is being expanded to include areas such as mechatronics, aeronautical engineering, biomedical engineering and applied mathematics. This paradigm shift has been propelled by the fact that electrical, electronic and the allied fields are interleaved in a real practical sense.

Prof. D B O Konditi, KSEEE-JSAEM Conference Chairman

POLICY PRESENTATION

Role of Research in Universities Towards Meeting the 2030 Millennium Goals

Prof. H L Kaane

Secretary to Minister for Higher Education, Kenya
Former Chairman of KSEEE

PRESENTATION SLIDES

Slide 1:

2010 INTERNATIONAL ENGINEERING CONFERENCE


ENGINEERING RESEARCH AND INNOVATION AS FUNDAMENTAL REQUIREMENTS FOR INDUSTRIALIZATION

**PARADIGM SHIFT
FROM RESEARCH TO INNOVATION**


THE DRIVER FOR KENYAN VISION 2030

**BY
HARRY L. KAANE**


**HIGHER EDUCATION, SCIENCE AND TECHNOLOGY SECRETARY
MINISTRY OF HIGHER EDUCATION SCIENCE AND TECHNOLOGY**




Kenya Society of Electrical & Electronic Engineers (KSEEE)



Japan Society of Applied Electromagnetics & Mechanics (JSAEM)



REPUBLIC OF KENYA



MULTIMEDIA UNIVERSITY

Slide 2:

INDUSTRIAL REVOLUTION AND EVOLUTION	
FIRST REVOLUTION:	PLENTY OF CHEAP AND ABUNDANT ENERGY – THE STEAM ENGINE
SECOND REVOLUTION:	THE TRANSISTOR – MECHANIZATION BECAME POSSIBLE
THIRD REVOLUTION:	THE COMPUTER: AUTOMATION – THE INFORMATION ERA
FOURTH REVOLUTION:	INTEGRATION OF SERVICES – KNOWLEDGE ERA

Slide 3:

**KNOWLEDGE DRIVES ECONOMIC AND
HUMAN DEVELOPMENT**

- FROM LABOUR TO CAPITAL TO KNOWLEDGE
- KNOWLEDGE = SCIENCE, TECHNOLOGY AND INNOVATION
- KNOWLEDGE = EDUCATION, SKILLS AND COMPETENCIES
- SHIFT: FROM RESEARCH TO INNOVATION
= NEW PRODUCTS (INCLUDING PROCESSES) ON MARKET

Slide 4:

KENYAN VISION 2030	
FOUNDATION	Infrastructure; Energy; Science, Technology and Innovation Human Resource Development, Land Reforms, Security, Public Service
SOCIAL PILLAR	Education and Training; Health; Water and Sanitation; Environment; Gender, Youth and Vulnerable groups; Housing and Urbanization; Social Equity and Poverty Reduction
ECONOMIC PILLAR	Tourism; Agriculture; Wholesale and Retail; Manufacturing; Business Process Outsourcing; Financial Services
POLITICAL PILLAR	Rule of Law; Electoral and Political Processes; Democracy and Public Participation; Transparency and Accountability; Public Administration and Service Delivery; Security Peace Building and Conflict Management

Slide 5:

STI AND VISION 2030	
TOURISM	Increase numbers and expenditure per tourist
AGRICULTURE	Enhance access to food, add value and enhance food security
WHOLESALE AND RETAIL	Enhance efficiency
MANUFACTURING	Enhance technical capacity and capabilities; efficiency and quality concerns

Slide 6:

STI AND VISION 2030	
FINANCIAL SERVICES	Institutional efficiency and productivity
EDUCATION	Enhance access and quality
HEALTH	Enhance access and quality
ENVIRONMENT	Environmental conservation and management awareness and capabilities

Slide 7:

STI AND VISION 2030	
WATER AND SANITATION	Management capabilities and capacities; water storage
GENDER, YOUTH, VULNERABLE GROUPS	Access to employment opportunities and equity
GOVERNANCE SECURITY AND RULE OF LAW	Enhance integrity, transparency and accountability
ICT	Capacity and capability building BPO

Slide 8:

STI AND VISION 2030	
HOUSING AND INFRASTRUCTURE	Capability and capacity building; housing units; length of roads constructed
LABOUR AND EMPLOYMENT	Aligning skills to labor demands
POPULATION AND URBANIZATION	Management of population growth and urbanization
MACROECONOMIC FRAMEWORK	Enhance domestic component of national investment Increase STI contribution to economic growth
SOCIAL EQUITY AND POVERTY REDUCTION	Equitable access to opportunities for poverty reduction

Slide 9:

INTERVENTIONS	
STI BILL	Restructure the NCST Create the National Innovation Agency
Universities Bill	Restructure the CHE
TIVET Bill	Create the TIVETA
Performance Contracting	Target to achieve selected international performance indicators

KEYNOTE ADDRESS

Professor Aimé Lay-Ekuakille

Dipartimento d'Ingegneria dell'Innovazione
(Dept of Innovating Engineering)
University of Salento, Lecce, Italy
aime.lay.ekuakille@unisalento.it



PROFILE

Aimé Lay-Ekuakille has a permanent position at the University of Salento (Italy) University & post-academic studies: Master Degree in Electronic Engineering, Master Degree in Clinical Engineering, PhD in Electronic Engineering, Post Degree in Environmental Impact Assessment. Professional & scientific aspects: He has been Director of different private companies in the field of: Industrial plants, Environment Measurements, Nuclear and Biomedical Measurements; he was director of Health & Environment municipal department. He has been a technical advisor of Italian government for high risk plants. From 1993 up to 2001, he was adjunct professor of Measurements and control systems in the University of Calabria, University of Basilicata and Polytechnic of Bari. He joined the Department of Innovation Engineering (University of Salento) in September 2000 in the Measurement & Instrumentation Group. Since 2003, he became the leader of the scientific group; hence he is the co-ordinator of Measurement and Instrumentation Lab in Lecce. He has been appointed as UE Commission senior expert for FP-VI (2009-2014). He is still: chair of IEEE -sponsored SCI/SSD Conference and member of Transactions on SSD editorial board, Guest Editor of IEEE Sensors Journal, associate editor of International Journal on Smart Sensing and Intelligent Systems, and of other international journals. He co-chaired the ICST2010. He is the founder and the Editor-in-Chief of the "International Journal of Measurement Technologies and Instrumentation Engineering" (IJMTIE) published by the US IGI Global (Hershey, Pennsylvania, USA). His main researches regard Environmental, industrial and Biomedical instrumentation & measurements.

TITLE OF PRESENTATION:

Emerging Technologies in Photovoltaic Issues: Measurement Techniques and Characterization

Abstract—Recent advances in photovoltaic technologies have increased the use of photovoltaic modules even in locations where it seemed very difficult to use them. The advances are allowing the reduction of production costs, hence the dissemination of renewable energy for small users. Thin film technologies, mainly including amorphous silicon solar cells, microcrystalline silicon solar cells, cadmium telluride thin-film PV modules, Cu(In,Ga) Se₂ thin-film solar cells, and high-efficiency concentrator silicon solar cells are of interest. Testing, monitoring and characterization are key issues for the development and the use of these technologies. Experimental setup for measuring and characterizing must match IEC requirements and specifications not only for indoor tests but also for outdoor ones. Nowadays IEC tests show the previous technologies are ripe and they can be used in a wide range of architectures and situations. Concentrator silicon cells, thanks to their efficiency, are suitable for countries with high level of insolation such as Mediterranean areas of Europe, Africa, south Asia and central-south America. Conversely, interesting but unripe technologies such as organic and plastic cells as well as cells based on nanowires still need developments in terms of efficiency. Testing, monitoring and characterization of PV modules but also of PV systems are a topic of great scientific, technical and economical impacts.

Keywords: *Photovoltaics, solar concentrators, characterization, measurements and test*

INTRODUCTION

Photovoltaic energy is a matter of increasing scientific research and applications in many locations in the world. There is quick evolution in research for photovoltaic cells, modules and systems. Many reasons impact on the evolution, namely, technological, sustainability, and economical. But efficiency is the parameter that represents a connection among the above reasons. Many solar cells have no longer margins of increasing efficiency in a commercial terms; their increasing is quite theoretical.

Table I illustrates the efficiency of different photovoltaic cells according IEC regulations as Green [1]. The ideal solar cell efficiencies referred to, for example, single-junction semiconductor devices suffer from limitations due to the fact the simplest semiconductor cannot absorb below band gap photons. Furthermore, it is also due to the fact that the part of the energy of the absorbed photons in excess of the bandgap is lost as heat. It is sometimes argued that there are other “unavoidable” losses, due to electronic energy transfer to other electrons by Auger effect as Grauvogl [2], Kaiser [3] and Pirozzi [4]. The search for efficiency boosts new progresses for: silicon technologies, CIS (copper indium selenide)-family-based absorbers, III-V and II-VI, organic cells, nanowire-based cells, etc.

EMERGING PV TECHNOLOGIES

In the previous section we mentioned diverse emerging technologies and most of them are ripe for commercial uses. In this section we briefly depict concentration-based photovoltaic and nanowire technologies; however some comparisons with other technologies recalled. High Concentration PhotoVoltaic (HCPV) displays the highest efficiencies in solar PV technologies as CPV [5].

Table I: Efficiency of different technologies

Classification*	Eff. (%)	Area ² (cm ²)	Isc (mA)	Voc (V)	FF (%)	Test centre (ref. data)	Description
Silicon	50.0 ± 0.3	4.00 (40)	0.705	0.735	42.7	82.3 Sandia (1999) ¹	UNSW PERC ¹²
	30.4 ± 0.3	1.00 (10)	0.664	0.664	30.8	80.9 NREL (1990) ¹	IBC-SE ²
	24.7 ± 0.4	4.07 (10)	0.645	0.645	30.8	71.2 Fraunhofer (2011) ³	U. Stuttgart (1.5 sun 1000h) ⁴
II-V cells	40.7 ± 0.3	6.0 (60)	0.697 ⁵	0.697 ⁵	26.7 ⁶	72.1 Fraunhofer (1997) ⁷	U. Stuttgart (1.5 sun 1000h) ⁴
	34.1 ± 0.3	0.08 (10)	0.698	0.698	26.7	84.7 Fraunhofer (1999) ⁷	Radford U. Virginia ⁸
	22.1 ± 0.7	4.02 (10)	0.694	0.694	26.2	79.5 NREL (11/99) ¹	RTI, Ge substrate ⁹
III-V cells	44.4 ± 0.3	4.02 (10)	0.694	0.694	26.2	83.4 NREL (1999) ¹	Space optimal ¹⁰
	39.4 ± 0.3	0.04 (10)	0.716	0.716	31.7	80.3 NREL (10/00) ¹	NREL, GaAs on GaAs ¹¹
	36.7 ± 0.4	16.0 (160)	0.661 ¹³	0.661 ¹³	30.6 ¹⁴	71.1 Fraunhofer (2000) ⁷	U. Upstate, 7 serial cells ¹⁵
	36.7 ± 0.3 ¹⁶	1.02 (10)	0.645	0.645	28.1	71.5 NREL (10/01) ¹	NREL, mesa on GaAs ¹⁶
	34.1 ± 0.3 ¹⁷	1.07 (10)	0.659	0.659	17.5	61.0 NREL (10/01) ¹	U. Stuttgart ¹⁸
	33.5 ± 0.3 ¹⁹	1.07 (10)	0.659	0.659	17.5	61.0 NREL (10/01) ¹	Kanata (2 sun on glass) ²²
	32.2 ± 0.3 ²⁰	1.04 (10)	0.678	0.678	22.8	61.2 AIST (2005) ²¹	Shiga ²³
	32.2 ± 0.3 ²⁰	1.04 (10)	0.678	0.678	22.8	61.1 AIST (12/07) ²¹	Shiga, 9 serial cells ²⁴
	32.2 ± 0.3 ²⁰	1.04 (10)	0.678	0.678	22.8	61.2 AIST (2005) ²¹	Shiga, 9 serial cells ²⁴
	32.2 ± 0.3 ²⁰	1.04 (10)	0.678	0.678	22.8	61.2 AIST (2005) ²¹	Shiga, 9 serial cells ²⁴
	32.2 ± 0.3 ²⁰	1.04 (10)	0.678	0.678	22.8	61.2 AIST (2005) ²¹	Shiga, 9 serial cells ²⁴
	32.2 ± 0.3 ²⁰	1.04 (10)	0.678	0.678	22.8	61.2 AIST (2005) ²¹	Shiga, 9 serial cells ²⁴
Organic polymer	5.15 ± 0.3 ²⁵	1.02 (10)	0.676	0.676	1.09	62.5 NREL (12/16) ¹	Kanaka ²⁶
	1.1 ± 0.3 ²⁷	152.4 (160)	28.3	1.072	5.2	NREL (19/99) ¹	Perovskites (PHIPKBA) ²⁷
	12.0 ± 1.4 ²⁸	3.00 (10)	24.22	11.27	8.65	NREL (18/16)	Perovskites (mesohal)
	10.9 ²⁹	4.0 (10)	24.88	14.22	8.56	JQA (16/16)	Perovskites (mesohal)
	25.8 ± 1.3 ³⁰	4.30 (10)	—	—	—	—	Perovskites (mesohal)
	17.7 ± 0.3 ³¹	14.23 (10)	5.62	3.99	7.13	AIST (09/04)	Perovskites (mesohal)
	17.7 ± 0.3 ³¹	14.23 (10)	5.62	3.99	7.13	AIST (09/04)	Perovskites (mesohal)
	17.7 ± 0.3 ³¹	14.23 (10)	5.62	3.99	7.13	AIST (09/04)	Perovskites (mesohal)
	17.7 ± 0.3 ³¹	14.23 (10)	5.62	3.99	7.13	AIST (09/04)	Perovskites (mesohal)
	17.7 ± 0.3 ³¹	14.23 (10)	5.62	3.99	7.13	AIST (09/04)	Perovskites (mesohal)
	17.7 ± 0.3 ³¹	14.23 (10)	5.62	3.99	7.13	AIST (09/04)	Perovskites (mesohal)
	17.7 ± 0.3 ³¹	14.23 (10)	5.62	3.99	7.13	AIST (09/04)	Perovskites (mesohal)

*CIGS = CuInGaSe₂; a-Si = amorphous silicon/hydrogen alloy.
¹Eff. = efficiency.
²(ap) = aperture area; (t) = total area; (di) = designated illumination area.
³FF = fill factor.
⁴Fraunhofer Institute for Solar Energy Systems; JQA = Japan Quality Assurance; AIST = Japanese National Institute of Advanced Industrial Science and Technology.
⁵Recalibrated from original measurement.
⁶Reported on a 'per cell' basis.
⁷Not measured at an external laboratory.
⁸Stabilized by 800h; 1 sun AM1.5 illumination at a cell temperature of 50°C.
⁹Measured under IEC 60904-3 Ed. 1: 1989 reference spectrum.
¹⁰Stability not investigated.
¹¹Stabilized by 174h; 1 sun illumination after 20 h, 5 sun illumination at a sample temperature of 50°C.
¹²CIGS = CuInGaSe₂; a-Si = amorphous silicon/hydrogen alloy; a-SiGe = amorphous silicon/germanium/hydrogen alloy.
¹³Eff. = efficiency.
¹⁴(ap) = aperture area; (di) = designated illumination area.
¹⁵FF = fill factor.
¹⁶Recalibrated from original measurement.
¹⁷Not measured at an external laboratory.
¹⁸Light soaked at NREL for 1000 hours at 50°C, nominally 1-sun illumination.
¹⁹Measured under IEC 60904-3 Ed. 1: 1989 reference spectrum.

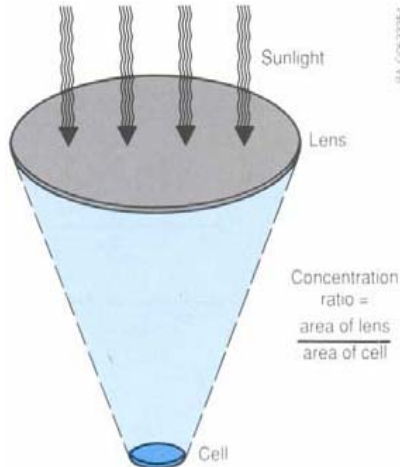


Figure1: HCPV principle

The HCPV principle is described in figure1 the lightweight, cheap and plastic Fresnel lenses are used to concentrate light. The light must be dispersed over cell not focused onto one spot. A cross section of typical complete cell is illustrated in figure 2.

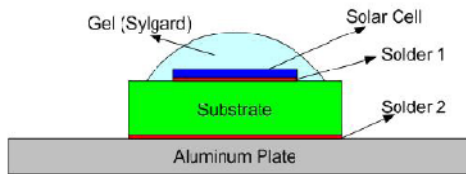


Figure 2: HCPV cell Performances

The solar energy technology is composed of solar cells through which semiconductors transform light into electric power. The difference between the structure of a high concentration photovoltaic (HCPV) system and the traditional solar cell is the former's use of a concentrated-light module to enhance optic-electric transition efficiency. Moreover, an HCPV system uses highly efficient multi-junction solar cells, which are expected to reduce significantly the cost of traditional solar cell system as Garboushian [6], Yamaguchi [7], and Karam [8].

For the HCPV system, when the heat effect dominates the energy-conversion efficiency of solar cell, the other factors of energy loss within the solar cell module can be neglected. The dissipation power of the solar cell can be calculated by the following equation:

$$P_{cell} \approx [P_m \times \beta \times A_{cell}] \times [100\% - \eta] \quad (1)$$

where P_{cell} is the power dissipation of the solar cell, P_{in} is the total power per unit area in the incident sunlight, β is the optical concentration ratio of the lens, A_{cell} is the surface area of the solar cell, and η is the energy conversion efficiency of the HCPV system.

Table II: HCPV types

CPV Type	Optics	Cell Assembly	Cell Type	C. Ratio	Cooling	Tracking
Type I Point focus	Fresnel	One Cell or Beam splitting	•Silicon •III-V	•50<Xg<500 •Xg>500	Passive	Two-axis
Type II Large area point focus	Parabolic dish Central tower	Parquet of cells	•Silicon •III-V	150<Xg<500	Active	Two-axis
Type III Linear systems	Linear lens Parabolic trough	Linear array of cells	•Silicon •III-V	•15<Xg<60 •60<Xg<300	Passive	One axis on parabolic
Type IV Static systems	Non imaging device	Usually linear arrays of cells	Silicon	1.5<Xg<10	Passive	No tracking
Type V Mini point focus	Small lens RXI Device Small parabolic	One single cell	•Silicon •III-V	Xg>800	Passive	Two-axis

HCPV is divided in different types according to IEC 62108 as shown in Table 1. But as a matter of concerns in photovoltaic issues, temperature plays a key role in the operating mode; it is limiting factor for many photovoltaic technologies. If external temperatures, measured in many locations, range between 25°C and 45°C, the efficiency varies between 30% and 32%. We are speaking about the cell efficiency which is different from module and system one; because, when assembling cells to be packed in order to form a module, many problems arise and there is a decreasing of efficiency. However, commercial modules have an efficiency of 25%. That is a lot. Figure 3 shows the behaviour of HCPV cell according to temperature variations. The best way to see the asset of HCPV is to have a comparison with respect to the other PV sources; suffice it to look at figure 4. Semiconductor nanowires, produced by the vapor-liquid-solid (VLS) method, first proposed by Wagner and Ellis [9], are being considered for sensors, field effect transistors, and energy harvesting devices as Gradecak [10]. In particular, photovoltaic devices employing semiconductor nanowires have the potential for lower cost and greater energy conversion efficiency compared to conventional thin film devices due to less material utilization, enhanced photovoltage or photocurrent due to hot carrier or multiexciton phenomena as Luque [11] enhanced light absorption, and freedom from lattice matching requirements due to strain accommodation at the nanowire surfaces, which provides greater freedom in bandgap engineering and substrate selection.

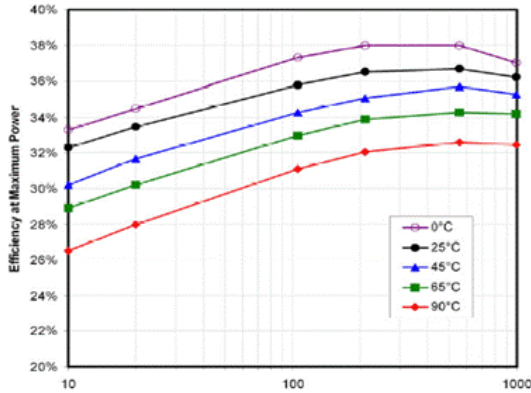


Figure 3: HCPV cell Performances

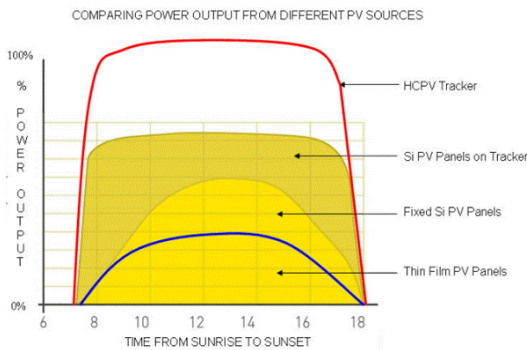


Figure 4: HCPV output power vs other technologies

Of particular interest are coaxial structures in which a doped nanowire core is surrounded by a shell of opposite doping type, forming a core-shell p-n junction as Zhang [12]. The conversion efficiency and fill factor of the devices are calculated using Equations (2) and (3)

$$\eta = \frac{I_m V_m}{P_{sun}} \quad (2)$$

$$FF = \frac{I_m V_m}{I_{sc} V_{oc}} \quad (3)$$

Figure 5 and figure 6 depict the I-V curve of nanowire elements capable of producing current and voltage in particular conditions. For time being, nanowires produce weak quantities with small amount of materials however it is a promising technology.

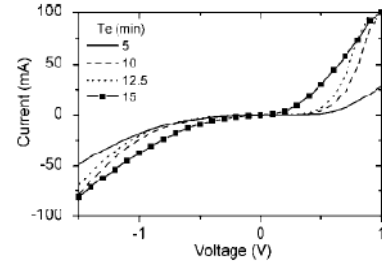


Figure 5: I-V curve of devices with opaque contacts for samples with various Te growth durations.

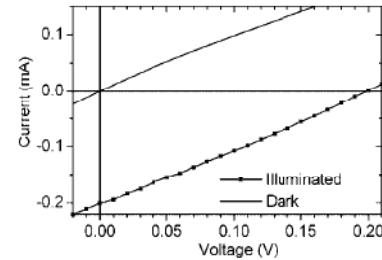


Figure 6: I-V curve of sample in dark and illuminated conditions

CHARACTERIZATION AND RESULTS

Since there are not commercial applications of nanowires for photovoltaic energy, we present here some interesting results limited to HCPV. HCPV plants have been built in different areas and countries. One of the most experience in Europe is related to ISFOC-Institute of Concentration Photovoltaic Systems as Isfoc [13] for which HCPV modules mounted on trackers as shown in figure 7. The ISFOC experience is very instructive because different companies, coming from different countries, notably, Spain, USA, Taiwan, Germany, have decided to build a plant in cooperation with public and private institutions in order to share experience. The 3 MW plant is based on Puertollano and Almuquera area in Spain.



Figure 7: HCPV modules on tracker

However the experience of ISFOC has been anticipated by laboratory and commercial characterizations. Table III and Table IV depict the best results for laboratory and commercial applications respectively. They also report the names of the manufacturers.

Table III: Best HCPV lab results

	Effic (%)	Suns	Manufacturer	Date	Type	Description
1	41.1	454	Fraunhofer ISE	2009	GaInP/GaInAs/Ge	lattice-mismatch
2	40.8	326	NREL	2008	GaInP/GaInAs/GaInAs	lattice-mismatch
3	40.7	240	Spectrolab	2006	GaInP/GaInAs/Ge	lattice-mismatch
4	37.2	500	Sharp	2005	InGaP/InGaAs/Ge	lattice-match
5	35.0	500	Splire	2008	InGaP/GaAs	dual junction

Table IV: Best HCPV commercial results

	Effic (%)	Suns	Company	Type	Location
1	39	500	Emcore / NREL	MJ	USA
2	36	500	Spectrolab	MJ	USA
3	35	500	Splire	MJ	USA
4	35	300	Azur Space	MJ	Germany
5	27	100	Amonix	SI	USA

In section 2, we have reported the influence of temperature on HCPV modules and/or cells. Successive measurements have demonstrated a useful comparison with other technologies as illustrated in figure 8.

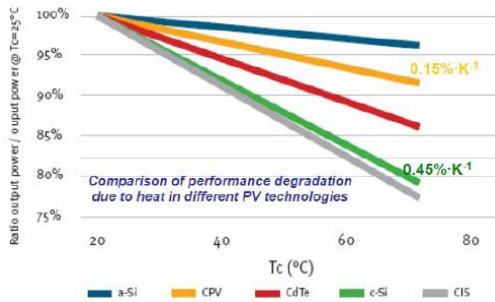


Figure 8: Losses due to temperature

CONCLUSIONS

A survey of PV emerging technologies has been presented in this paper. Two specific technologies have been illustrated. In particular, interesting results have been depicted for HCPV modules and cells. As final comments, it is important to show a comparison between different technologies in terms of LEC (Levelized Energy Cost) that is

necessary for commercial applications; for that, HCPV displays good results as indicated in Table V.

Table V: Comparison based on economic indicators

	Crystalline				Thin-film		CPV		
	c-Si Static optimally tilted	c-Si Single-junction horizontal axis (N/S)	c-Si Single-junction tilted axis (S, 20°)	c-Si Single-junction vertical axis (azimuthal)	c-Si Two-axis	Thin-film: c-Si Static optimally tilted			
Module Efficiency (%)	12.5	12.5	12.5	12.5	12.5	6	7.5	9	23
System efficiency (%)	11.2	11.2	11.2	11.2	11.2	5.3	6.6	8.0	20
Initial annual electricity yield per kWp (kWh/kWp-year)	1380	1225	1835	1863	2000	1380	1380	1380	1870
Initial annual electricity yield per module square meter (kWh/kWp-m²)	172	216	229	233	256	81	105	125	366
LEC (€/kWh)	0.332	0.334	0.315	0.310	0.311	0.332	0.332	0.332	0.354
Initial investment (€/kWp)	5500	6500	6500	6500	7000	5500	5500	5500	7000
Land needed (ha)	16	26	40	56	56	34	25	22	60

Table 5: Average performance and cost-related parameters for different PV technologies under the following conditions: 1000 h of 2000 kWh/m²/year and an 800 Wp installed capacity for each system

Acknowledgements

Author is grateful to Dr. Angelo Sarno and Mr. Franco Invernizzi for their support and suggestions.

References

- Green, M.A., Emery, K., Hishikawa, Y., and Warta, W., Solar Cell Efficiency Tables, Prog. Photovolt: Res. Appl.17, 85–94, 2009.
- Grauvogl, M., Aberle, A., and Hezel, R., 17.1% Efficient Truncated-Pyramid Inversion-Layer Silicon Solar Cells, Proc. 25th IEEE Photovoltaic Specialists Conf., pp.433-436.
- Kaiser, U., Kaiser, M., and Schlinder, R., Texture Etching of Multicrystalline Silicon 1990, Proc. 10th European Photovoltaic Solar Energy Conf., pp 293-294, 1990.
- Pirozzi, L., Garozzo, M., Salza, E., and Margadona, D., The Laser Texturization in a full Screen Printing Fabrication Process of Large Area Poly Silicon Solar Cells, Proc. 12th European Photovoltaic Solar Energy Conf., pp.1025-1028.
- <http://www.concentrationphotovoltaic.com/>
- Garboushian, V., Roubideaux, D., Yoon, S., "Integrated high-concentration PV. Near-term alternative for lowcost large-scale solar electric power," Solar Energy Materials and Solar Cells, vol.47, pp. 315-323, October, 1997.
- Yamaguchi, M., and Luque, A., High efficiency and high concentration in photovoltaics, IEEE Transactions on Electron Devices, Vol. 46, pp.2139-2144, October, 1999.
- Karam, N.H., et al., Recent developments in high-efficiency Ga0.5In0.5P/GaAs/Ge dual- and triplejunction solar cells: steps to next-generation PV cells, Solar Energy Materials and Solar Cells, vol. 66, pp. 453-466, February, 2001.
- Wagner, R. S.; Ellis, W. C. Appl. Phys. Lett., 4, 89, 1964.
- Gradecak, S.; Qian, F.; Li, Y.; Park, H. G.; Lieber, C. M. Appl. Phys. Lett., 87, 173111, 2005
- Luque, A.; Marti, A.; Nozik, A. J. MRS Bull. 2007, 32, 236.
- Zhang, Y.; Wang, L.-W.; Mascarenhas, A. Nano Lett. 2007, 7, 1264.
- www.isfoc.es

INVITED PLANERY PRESENTATION

Professor Minoru Sasaki

Professor of Human and Information Systems Engineering,
Department of Human and Information Systems Engineering,
Gifu University, Japan



PROFILE

Dr. Minoru Sasaki is a professor of human and information systems engineering, Gifu University, Japan. Dr Sasaki has been received his B.Sc. degree in Yamagata University in 1980, his M.Sc. and Ph.D. in Tohoku University, Japan, in 1982, and 1985, respectively. All his degrees were in mechanical engineering. He has an extensive experience in teaching and research: He was a visiting professor at University of California from April 1990 to July 1991 and from October 1997 to December 1997. He was also a visiting professor in George Institute of Technology, The George W. Woodruff School, USA, from January 1998 to March 1998. He is the head of supporting and development centre for technology education in Gifu University. Prof.

Sasaki has published close to 200 papers in refereed journals and conference proceedings. He is a member of ASME, IEEE, JSME (Japan Society of Mechanical Engineers), JSASS (Japan Society of Aeronautical and Space Science), JSAEM(Japan Society of Applied Electromagnetics and Mechanics), SICE (Society of Instrument and Control Engineering). He is an executive board member of JSAEM since 2008, executive director of SICE since 2008, General chair of The 2003 International Conference on Mechatronics and Information Technology.

TITLE OF PRESENTATION:

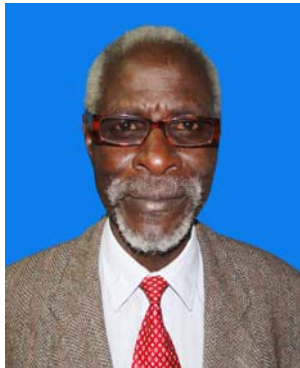
Robot Control Systems Using Bio-potential Signals

Abstract—Robot control systems via human bio-potentials, such as electroencephalographic (EEG), electrooculographic (EOG), and electromagnetic (EMG) signals are developed. Research and development of the technology necessary for estimating and identifying the biological signals themselves through sensing and signal processing, as well as their conversion into control signals is carried out. Experiments to determine the viability of the technology were performed. From sensors attached to an operator's forehead, we attempt to discern his intentions and activity. By mapping signals to commands such as go forward, go backward, stop, turn right and turn left, the operator can control a device through his eye movements, facial muscles and brain waves. These signals can be separated into three frequency bands: a low frequency range of 1-3Hz, a high frequency range of 25-50Hz and the midrange beta wave range from 14-25Hz. CyberlinkTM and ESA-16TM, commercial devices, can acquire and process these signals. A computer analyzes the operator's EEG and EOG in real time. A neural networks further analyzes the EOG to ascertain the operator's intention. After training, the neural network was able to discern whether left or right was desired. Experimental results suggest that with a neural network in the loop, and efficacious assignment of commands, a small device can be controlled using human bio-potentials with few errors.

INVITED PLANERY PRESENTATION

Professor Robert Jalang'o Akello, PhD

Department of Electrical and Communications Engineering,
Faculty of Engineering,
Masinde Muliro University of Science and Technology,
P o Box 190, Kakamega, Kenya



PROFILE

Robert Jallan'go Akello is a full Professor of Electrical and Communications Engineering at Masinde Muliro University of Science and Technology (MMUST), Kakamega, Kenya. He holds an MSc Degree from The Moscow Electrotechnical Institute of Communications (MEIC), where his 1971 thesis was on *The Study of Electromagnetic Compatibility of Pan-African Telecommunications Network (PANAFTEL) with the INTELSAT Systems*. Since then, he briefly worked for The Voice of Kenya (VoK) on Designs of Aerial Microwave Links to replace landlines. On completion of the designs, he was posted to the Kenya Polytechnic to train electrical, telecommunication and technicians. During his tenure at the Kenya Polytechnic, he won a Commonwealth Fellowship Grant to study for a PhD, on *Microwave Integrated Circuit MESFET Amplifiers*, at The School of Electronic Engineering Sciences, University College of North Wales, Bangor, UK. On return to Kenya in 1977, he joined full time teaching at

The University of Nairobi, where he stayed up to 2005, when he joined MMUST. He has taught Electromagnetic Fields and Waves, Microwave Engineering, Circuit Analysis and Synthesis, Antennas and Radiowave Propagation at both undergraduate and postgraduate levels. At the University of Nairobi, Prof. Akello developed an interest in *Lightning*, a phenomenon in which he is currently a consultant to many governments, institutions and companies. At MMUST, the interest in *Scientific and Technical Communication Skills* came on especially because of the increasingly poor sentence construction and handwriting seen on examination scripts and lack of verbal communication skills at project presentations and conferences, notwithstanding the students having undergone *Communication Skills* in the first year of study. Prof. Akello is an author of many papers and articles in *Microwaves*, *Propagation of Radiowaves*, *Electromagnetic Compatibility (EMC)*, *The Lightning Phenomenon* and *Engineering Education*

TITLE OF PRESENTATION:

Teaching of Communication Skills to Scientists and Engineers

Abstract—Scientists and engineers have been known to communicate better with their hands on apparatus and equipment in laboratories, than verbally. For this reason, it is globally agreed that science and engineering students should be trained in Communication Skills not only for presentation of their findings at discussion groups, meetings and conferences but also to market their products. With these objectives, earlier attempts to teach Communication Skills in pioneering universities resulted in students being clustered from disciplines across the divide. Science and engineering students felt slighted when subjected to the bulk of the course content being English, taught by lecturers from the English Departments. A re-think led to specialized presentation of Technical and Scientific Communication Skills, which included reading and verbal interpretation of diagrams and formulae. This paper explores the content and challenges of this course at the pioneering universities and at Masinde Muliro University of Science and Technology.

Key words: *reading, writing, oral presentation, verbal interpretation, relevant english, terminology, drawings, formulae, software, thinking, decision making, examination, interview.*

I. INTRODUCTION:

Engineering is defined as “That profession which uses knowledge in science and mathematics to design and develop gadgets used to make work easier for Man”. Engineers use *symbols* in *formulae* to explain physical processes in the form of mathematical models. The processes are also represented by physical models in the form of *diagrams* and *circuits*.

They have to acquire the theory and underlying principles of Physical Sciences in order to explain the processes. Such theory is proved in laboratories and enhanced by research, from which new findings are presented verbally at colloquia, workshops and conferences, and in written journal articles. Written publications in any medium require editing for verification of content and style, by the peers in the profession. The engineering functions therefore include teaching, and editing.

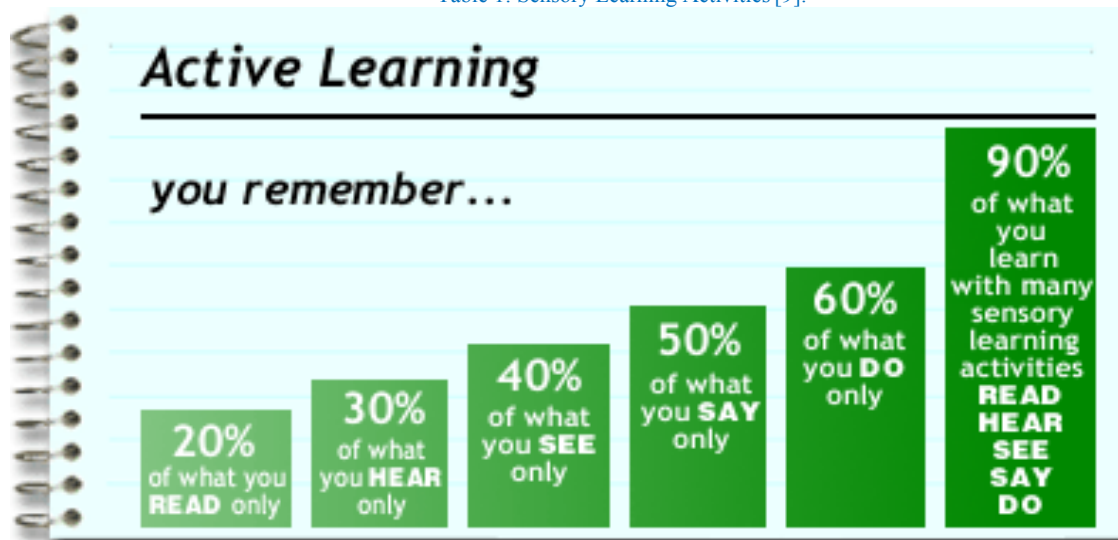
Unlike scientists, engineers go through two more strides: designing and constructing the machines from research, and marketing. Engineers also rise to become managers.

Through all these activities, learning always takes place. Learning in engineering is therefore continuous since the underlying principles in all functions are very dynamic. All these activities require instillation of Communication Skills [1-8].

II. THE SKILLS:

Table 1 below shows some research findings from psychologists on active learning from the five main sensory learning activities. These, and other relevant skills, are what is taught in the course.

Table 1: Sensory Learning Activities [9].



1. READING: [10-13]

Reading takes place throughout a scholar's life. In the course, the content given to students includes *fast*, *efficient*, *active* and *critical* reading strategies of academic texts, typical textbooks and journal articles.

2. LISTENING: [14-15]

At lectures and other verbal presentation fora, listening is very important. Learning by listening is therefore stressed and some *bad listening habits* are spelled out to assist students at lectures.

Some of these bad listening habits are:

- Calling the subject dull
- Criticizing the speaker
- Getting over stimulated
- Listening only for facts
- Trying to outline everything
- Faking attention
- Tolerating distraction
- Choosing only what is easy
- Letting emotion-laden words get in the way

- Wasting the differential between speech and thought speeds

3. WRITING: [16-20]

Characteristics of Professional Writing.

Writing of a scientists and engineers are for proposals, reports, papers for conferences and Journals. Unlike the counterparts in Humanities, scientists and engineers do not write essays. Their writing should be *clear, complete and concise*.

In all disciplines however, long hand writing still prevails over computer writing. In the former case, good handwriting with big scripts is encouraged to increase legibility. In the former case, popular legible scripts should be used.

Relevant English. [21-23]

The English language is most widely used in science and engineering writing. Characteristically, such writing has an *objective tone* with the language of a written text sounding independent from the writer and reader. Therefore, relevant English is taught with a stress on the use of the *objective tone*, which is achieved through the use of impersonal language [24]. Using impersonal language requires the writer to avoid characteristics of *personal language* such as 'I', 'we', 'you', 'our', 'us' to refer to self or the reader. From articles, there are circumstances when "You" may be used in instruction [43] and "We" in reference books, to reflect on a team in a discipline.

Related to the barred personal language are *judgmental words* that indicate feelings about a subject, emotive words such as "worst" and "horrible", and *uncertain descriptions* exemplified by "This", "That", "It". Also unacceptable are run-on expressions, which include phrases such as 'and so forth', 'and so on' or 'etc'.

Furthermore, use *contractions* such as "don't", "can't" and "won't", which should be written in full words, and *conversational language* such as figures of speech, clichés and idioms are not allowed in such writings.

For good writing, attention is also paid to *faulty grammar* and sentence construction. Examples are sentences with clusters of nouns and adjectives modifying a noun and conversely [strings of prepositional phrases](#) after a noun, abstract nouns instead of [action verbs](#), [nonparallel construction](#) of words, phrases, and sentences in enumerations, and [more complicated phrasings than required](#).

Careful *review of any draft* is stressed to the students to make sure they avoid the common writing faults, including types and places of *punctuation marks*.

Note Taking: [25-26]

Note taking at lectures is a writing process. It requires knowledge of the materials presented at previous lectures and attentive listening to note the phrases stressed by the presenter.

Mastering of general spellings and terminology in the discipline is also a requisite. Also necessary is the capability to draw diagrams, graphs and tables freehand. Practicals are given in class to train the students to acquire this ability.

Letters, resumes, e-mails, and memos.

Students are also taught how to write official application letters, e-mails, resumes and memos. Proper language, formatting and etiquette are stressed.

4. THINKING:

For critical thinking [27-28], effective and cognitive strategies are spelled out. Notably, macro-abilities such as predicting and anticipating and remembering, *for example, by picturing, verbal rehearsal and clustering* are stressed.

Since innovation requires creative and imaginative thinking, students are given examples derived from *play and experimentation, discovery and application of new connections and ideas, and through active exploration*.

In experimentation, important ideas are brought from the understanding of cause and effect, and from linking of objects, events and experiences.

Problem solving and editing are two uses of thinking illustrated in the course. The topic *Thinking like a Genius* is addressed citing some behavior traits and characteristics of Yashiro Nakamatsu and Albert Einstein as some examples.

5. ORAL PRESENTATION: [29-32]

Talking during oral presentations follows the rules of writing and uses reading skills. Scientists and engineers have special communication language involving symbols, formulae, diagrams in the form of graphs, mechanical drawings, tables.

Symbols:

Students are taught to pronounce the Greek symbols used in formulae. These are given in Table 2, from alpha to sampi.

Table 2: Greek Symbols

form	full name	aliases	form	full name	aliases
α	\[Alpha]	:a; :alpha;	Α	\[CapitalAlpha]	:A; :Alpha;
β	\[Beta]	:b; :beta;	Β	\[CapitalBeta]	:B; :Beta;
γ	\[Gamma]	:g; :gamma;	Γ	\[CapitalGamma]	:G; :Gamma;
δ	\[Delta]	:d; :delta;	Δ	\[CapitalDelta]	:D; :Delta;
ε	\[Epsilon]	:e; :epsilon;	Ε	\[CapitalEpsilon]	:E; :Epsilon;
ε	\[CurlyEpsilon]	:ce; :cepsilon;			
ζ	\[Zeta]	:z; :zeta;	Ζ	\[CapitalZeta]	:Z; :Zeta;
η	\[Eta]	:h; :eta; :eta;	Η	\[CapitalEta]	:H; :Eta; :Eta;
θ	\[Theta]	:q; :th; :theta;	Θ	\[CapitalTheta]	:Q; :Th; :Theta;
θ	\[CurlyTheta]	:cq; :cth; :ctheta;			
ι	\[Iota]	:i; :iota;	Ι	\[CapitalIota]	:I; :Iota;
κ	\[Kappa]	:k; :kappa;	Κ	\[CapitalKappa]	:K; :Kappa;
κ	\[CurlyKappa]	:ck; :ckappa;			
λ	\[Lambda]	:l; :lambda;	Λ	\[CapitalLambda]	:L; :Lambda;
μ	\[Mu]	:m; :mu;	Μ	\[CapitalMu]	:M; :Mu;
ν	\[Nu]	:n; :nu;	Ν	\[CapitalNu]	:N; :Nu;
ξ	\[Xi]	:x; :xi;	Ξ	\[CapitalXi]	:X; :Xi;
ο	\[Omicron]	:om; :omicron;	Ο	\[CapitalOmicron]	:Om; :Omicron;
π	\[Pi]	:p; :pi;	Π	\[CapitalPi]	:P; :Pi;
π	\[CurlyPi]	:cp; :cpi;			
ρ	\[Rho]	:r; :rho;	Ρ	\[CapitalRho]	:R; :Rho;
ρ	\[CurlyRho]	:cr; :crho;			
σ	\[Sigma]	:s; :sigma;	Σ	\[CapitalSigma]	:S; :Sigma;
ς	\[FinalSigma]	:fs;			
τ	\[Tau]	:t; :tau;	Τ	\[CapitalTau]	:T; :Tau;
υ	\[Upsilon]	:u; :upsilon;	Υ	\[CapitalUpsilon]	:U; :Upsilon;
υ	\[CurlyUpsilon]	:cu; :cupsilon;	Ϛ	\[CurlyCapitalUpsilon]	:cU; :cUpsilon;
φ	\[Phi]	:f; :ph; :phi;	Φ	\[CapitalPhi]	:F; :Ph; :Phi;
φ	\[CurlyPhi]	:j; :cph; :cphi;			
χ	\[Chi]	:c; :ch; :chi;	Χ	\[CapitalChi]	:C; :Ch; :Chi;
ψ	\[Psi]	:y; :ps; :psi;	Ψ	\[CapitalPsi]	:Y; :Ps; :Psi;
ω	\[Omega]	:o; :w; :omega;	Ω	\[CapitalOmega]	:O; :W; :Omega;
ϒ	\[Digamma]	:di; :digamma;	Ϝ	\[CapitalDigamma]	:Di; :Digamma;
ϙ	\[Koppa]	:ko; :koppa;	Ϟ	\[CapitalKoppa]	:Ko; :Koppa;
ς	\[Stigma]	:st; :stigma;	Ϛ	\[CapitalStigma]	:St; :Stigma;
ς	\[Sampi]	:sa; :sampi;	ϛ	\[CapitalSampi]	:Sa; :Sampi;

Formulae:

Formulae are derived and explained from the physical processes. Their interpretations are also illustrated.

A first example starts from the general formula for resistance.

$$R = \rho \frac{l}{A}$$

This simple formula is a mathematical model for a physical process in a wire as the physical model. The following are some of the words used at presentations:

The first presenter states that “*R equals rho multiplied by the ratio of l to A, where R is resistance, rho is the resistivity, l is length and A is the cross sectional area*”.

If a listener closed his eyes and tried to conceptualize the process being described, s/he would not know the type of resistance and the medium.

The second presenter in describing the formula as follows: “*The electrical resistance R of a conducting wire is proportional to the ratio of the wire’s length l to its cross sectional area A , with the coefficient of proportionality being the resistivity of the material, ρ* ”.

This presenter has improved the description by qualifying that the resistance is electrical and the medium is a conducting wire. S/He has used the word ‘proportional’, which makes the listener imagine the variation of the curve with the ‘ratio’. Finally the variables are clearly defined.

The third presenter states: “*The electrical resistance R of a conducting wire is directly proportional to the wire’s length l and inversely proportional to its cross sectional area A , with the coefficient of proportionality being the resistivity of the material, ρ* ”.

Here, the independent variables are separated by qualifying ‘direct’ and ‘inverse’ proportionality, other than ‘ratio; used by the second presenter. This makes the listener imagine how the resistance varies with the wire dimensions and why.

The ‘why’ is answered by the physical process in the wire as a physical model, illustrated by the following words:

Electric current is initiated by movement of charges. On one hand, if many charges are in a line, the ones ahead impede the motion of the ones behind them. The longer the wire, the more the charges are lined up and therefore the bigger the resistance to their movement. On the other hand, the larger the cross sectional area of the wire, the more the charges are available to be moved, the more the current is available to be delivered at the end of the wire, reflecting on low resistance to charge movement.

The second example gives the description of the formula and requires the actual formula to be written. The description is: “*The time dependent forcing function $f(t)$ on a vibrating system of mass m with a displacement x , is defined by the sum of the Newtonian force, a damping force given by the product of beta and the rate of displacement, and the displacement dependent stiffness term $F(x)$. Write the formula.*”

This formula contains one implicit and one explicit differential term as is contained in the Newtonian force $ma = m \frac{d^2x}{dt^2}$, and the damping force dependent on the rate of displacement $\frac{dx}{dt}$, with the coefficient of proportionality being β . Therefore, the formula is

$$f(x) = m \frac{d^2x}{dt^2} + \beta \left(\frac{dx}{dt} \right) + F(x)$$

Diagrams:

Diagrams are generally referred to as figures. They should be explicitly *referred to as labeled*. They should also be accordingly interpreted.

For graphs words, such as *varies linearly, exponentially, parabolically, and hyperbolically*, should be used.

Mechanical drawings are described as either *ellipses, cubes, rectangles, triangles or others*, as in mathematics.

Tables are used in science and engineering to summarize results of dependent and independent variables in form of figures. The row and column widths appropriately selected to fit the figures.

Teaching Aids:

At lectures and conferences, oral presentations are given using teaching aids for power point slides, flip charts and white boards. Apart from writing style and public address skills, the others that are emphasized are slide layout and time management, as is given in [33].

Practicals:

Practicals are on the use of computers to write formulae using both the Equation Editor and MathType.

Students are also trained to use computers for drawing mechanical drawings and electric circuits, and setting of tables. When tables and drawings are big, they are presented in the landscape format to fit all the drawings. For such exercises, they are exposed to the uses of other software such as AUTOCAD and other Knowledge Base Software exemplified by Roads, Sewer, Storm, Water and others as may be found in [34] for Civil Engineers, and MULTISM and Electronic Workbench for Electrical and Electronic Engineers.

6. EXAMINATION: [35]

Examining is the common way of testing understanding of what students have been taught. In the course, presentations are made on what students should do *before the examination, on the examination date, in the examination room, and after the examination.*

On the actual examination paper, the demand by the common words and phrases such as *Define, State, List, Draw, Sketch, Write, Enumerate, Discuss, Explain, Use curves/diagrams to .., Calculate, Determine, Differentiate between.., Compare, Prove that, Show that, Deduce, Derive, Interpret, Relate, Comment on,* and other must be clearly understood before starting to answer the question.

7. INTERVIEW: [36-37]

On graduation, students get interviewed for jobs, initially sometimes by phone and subsequently at a physical appearance. At that stage, they are interviewees. They should generally know the process of the interview and what questions to expect from the interviewing panel and how to answer them. Some of the bad behaviors at interviews are spelled out.

Later on, they join the management cadres at their work places. They should therefore know how to hold themselves as interviewers. Therefore, spelled in the course are what to do and what not to do both as an interviewee and as interviewer.

For this skill, drilling is conducted at mock interviews.

III. END OF THE COURSE

At the end of the course, some materials given to students as future references for long life learning are by Brian Tracey's CD on *Accelerated Learning*, Clayton M. Christensen's *Disrupting Class: How Disruptive Innovation Will Change the Way the World Learns, Career Research Questions and Competency Profile of The English Centre, University of Hong Kong* [5]. Michael Alley, 1996, *The Craft of Scientific Writing (3rd Ed.)* Springer, and [38-43].

IV: CONCLUSIONS AND RECOMMENDATIONS:

Based on the usefulness of this course to all students, teachers and practitioners of scientists and engineering, and on the market demand, it is advisable to keep improving this course by expanding the inter-departmental engagements in practical applications of the skills. To help with continuing learning and in expanding students' exploratory acumen for material, a large source of webpages are given in the references since no modern books on this course are available in most local libraries. Special attention is drawn to materials on *Thinking Skills* which, when supplemented with *Disrupting Class*, lead to the main objectives of scientists and engineers - *problem solution and innovation.*

REFERENCES

1. Natasha Artemeva, *Beyond The Language Barrier. Teaching Communication Skills.pdf*
2. Blay Whitby, *Technical Communication Skills* <http://www.cogs.susx.ac.uk/users/blayw/tcs.html>
3. Rethinking Scholarly Communication: Building the System that Scholars Deserve. D-Lib Magazine, September 2004, Volume 10 Number 9, ISSN 1082-9873
4. <http://unilearning.uow.edu.au/main/html>
5. <http://ec.hku/epc>
6. <http://www.darmouth.edu/acskills/learning/index.html>
7. *Developing oral Communication Skills of Computer Science Undergraduates.* Proceedings of the twenty-fourth SIGCSE technical symposium on Computer science education, Indianapolis, Indiana, United States. pages: 279 - 282 (1993). ISBN:0-89791-565-8

8. *Criteria for Accrediting Programs in the United States*. CSAB Computer Science Accreditation Commission, (November, 1990)
9. *JKU Study Skills Online*. http://www.jcu.edu.au/learningskills/JCUPRD_034938
10. http://startup.curtin.edu.au/study/reading_techniques.cfm
11. <http://web.nps.navy.mil/~menissen/mn3309/readguid.htm>
12. <http://www.mindtools.com/rdstratg.html>
13. http://occawlonline.pearsoned.com/bookbind/pubbooks/lardner_awl/chapter1/custom5/deluxe-content.html
14. Learning by Listening
15. Ten Bad Listening Habits
16. John Ringwood *Hints on Technical Report Writing*. <http://www.eeng.dcu.ie/~ringwoodj/home.html>
17. Gerard M Blair. *How To Write Right*.
18. Writing skills Edinburg.htm
19. www.ee.ed.ac.uk/~gerard/Management/art4.html
20. Writing the Research Proposal.htm
21. <http://www.writing.eng.vt.edu/index.html>,
22. <http://grcltid.grc.nasa.gov>,
23. <http://www.grc.nasa.gov>
24. Academic Writing Words Impersonal Language.htm
25. <http://www.csbsju.edu/academicadvising/default.htm>
26. <http://hsc.uwe.uk/net/student/Default.aspx?pageid=186>
27. <http://www.asa3.org/education/index.html>
28. <http://www.utc.edu/Administration/WalkerTeachingResourceCentre/FacultyDevelopment/CriticalThinking/whatis>
29. Making Effective Oral Presentations. <http://web.cba.neu.edu/skills/oral.htm>
30. Session Guide: Oral Presentation Techniques.
http://dcc2.bumc.bu.edu/prdu/Session_Guides/oral_presentation_techniques.htm
31. A Research Guide for Students: Chapter 3. Presentation Tips for Public Speaking. <http://www.aresearchguide.com>
32. Hand, Harry E., Technical Speech: A Need for Teaching and Research. IEEE Transactions on Engineering Writing and Speech, Volume 10, Issue 2, Dec. 1967 Page(s):48 - 51
33. Pristatymo%20 metodika.pdf, Boston University, School of Public Health.
34. www.civildesigner.com
35. <http://hsc.uwe.uk/net/student/Default.aspx?pageid=191>
36. <http://www.acetheinterview.com/>
37. <http://www.job-interview.net/index.htm>
38. The Elements of Style (online). <http://www.bartleby.com/141/>,
39. <http://www.io.com/~hcexres/textbook/acctoc.html#examples>
40. <http://www.cimms.ou.edu/~schultz/communication.html>
41. <http://io.uwinnipeg.ca/~clark/research/comm/comm.html>
42. <http://www.maths.uwa.edu.au/~alice/scicom/outline.html>
43. *Scientific Style and Format*, The Council of Science Editors. <http://www.councilscienceeditors.org>

IMPROVING ENGINEERING EDUCATION, PROFESSION AND RESEARCH IN KENYA THROUGH CREATION OF INSTITUTES

S. O. Odundo

Department of Electrical & Communication Engineering, Masinde Muliro University of Science & Technology

Abstract—An Institute is defined as a permanent organizational body created for a certain purpose. The main function of institute is research since they are highly specialized in nature. The proposed engineering institutes are to oversee the quality of engineering education, training, practice and research in Kenya.

Keywords: *Institute, Engineer, Engineering, Science, Society, Industry, Technology, Higher Education.*

1. INTRODUCTION

Engineering involves the application of proved scientific knowledge to meet all societal needs, hence the diverse nature of engineering. Since engineering involves the application of proved scientific knowledge, equipped laboratories and specialized training are of great importance.

When engineering education and practice was established in Kenya, high class institutes were developed to improve the quality of engineering profession. These institutes included the following among others;

- Railways Training Institute.
- Kenya College of Communication Technology.
- KPLC training College

The only problem is that these world class institutes were managed by there respective industries which resulted to there quick collapse when the industries faced both financial and management challenges.

This paper presents the establishment of engineering institutes which are independent in order to improve engineering education, training, research and practice.

2. THE ROLE OF ENGINEERING IN SOCIETY: ENGINEERING DESIGN

One of the first sources of confusion, particularly among those who are not engineers or scientists, is the distinction between science and engineering. The primary role of science is to develop knowledge and understanding of the physical universe. As

pointed out by Davis [1] and others, an important distinction is that this pursuit of knowledge (science) may occur largely without regard to societal need (or to societal implications). The direction of scientific research has been described by some as curiosity-based research which is not necessarily driven by the values of society. Societal values (and resulting priorities) do not necessarily define the bounds, direction or scope of scientific curiosity. Given this curiosity-driven process, the base of scientific knowledge about the physical universe may be represented by an amoebae-like structure uneven in its extent in the various directions with current scientific research efforts acting to extend its coverage (Figure 1).

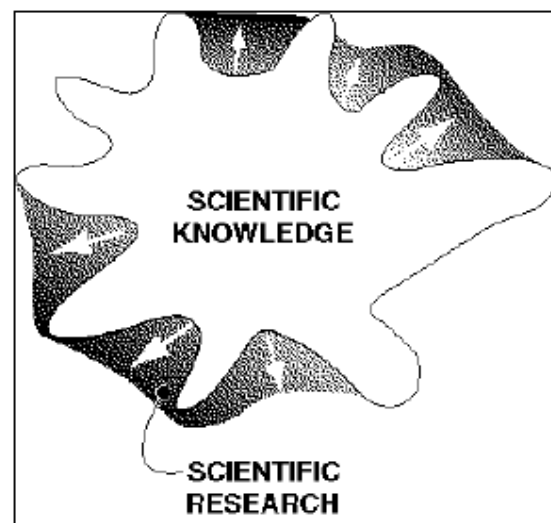


Figure 1:

The utilization of scientific knowledge over time establishes that some of the knowledge is immediately relevant to societal needs while other parts are less immediately relevant (society may never realize the relevance of a particular scientific inquiry). While the congruence of societal need with scientific knowledge is much more complex than indicated in this article, it may be represented for the purpose of this discussion by a Venn diagram as seen in Figure 2. The authors maintain that it is this overlap of scientific knowledge with societal need, more specifically, the application of scientific knowledge to the needs of society, that is the domain of engineering.

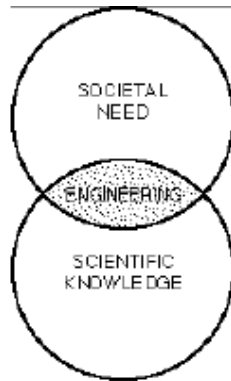


Figure 2:

This analogy can be extended by superimposing the distinction of the creative versus the analytical aspect of the human enterprise. We can represent this aspect of the human intellect by another Venn diagram shown in Figure 3. As indicated in the diagram, one may pursue creative efforts without involving analytical skills, and one may apply analytical skills without entering the domain of creativity. For example, as engineers apply commercial software to the solution of an engineering problem, the application of analytical skills, per se, may involve little or no creativity.

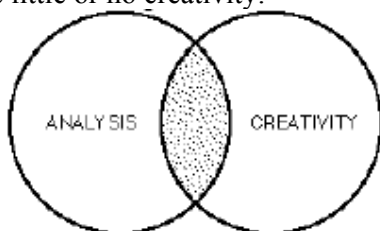


Figure 3:

One may superimpose these two Venn Diagrams and use the resulting diagrams to examine engineering enterprise as shown in Figure 4.

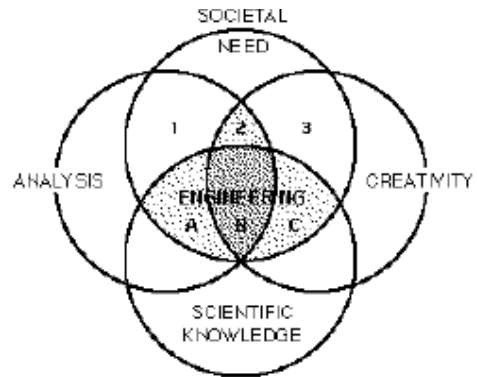


Figure 4:

Considering the intersection of scientific knowledge with societal need (designated as the domain of engineering), the authors will discuss three sectors, shown as A, B, and C.

Sector A represents the intersection of purely analytical talents with the engineering domain. This may be used to represent engineering science, ability to model complex systems and predict their response to various inputs under various conditions. This segment of engineering has, of course, been the subject of intense development over the last half century and has benefited most directly from the availability of fast digital computers.

Sector C, the intersection of our creative capacity with the engineering domain, can be viewed as representing those sudden intuitive leaps often responsible for revolutionary advances in technology called "significant novelty" by Spier [2] as well as those aspects of engineering, not yet fully supported by engineering science, that remain more art than science.

The third sector, B (the intersection of knowledge and need with both creative and analytical capability) can be used to represent engineering design and much "real world" problem solving. This sector includes activities ranging from developing innovative products and processes, to creating an innovative bridge design, to developing a new

control process for petrochemical production and ICT just to mention.

Current approaches to teaching used in engineering schools have been designed more for developing analytical skills (Sector A) than creative skills.

3. THE STRUCTURE FOR ESTABLISHMENT OF ENGINEERING INSTITUTES

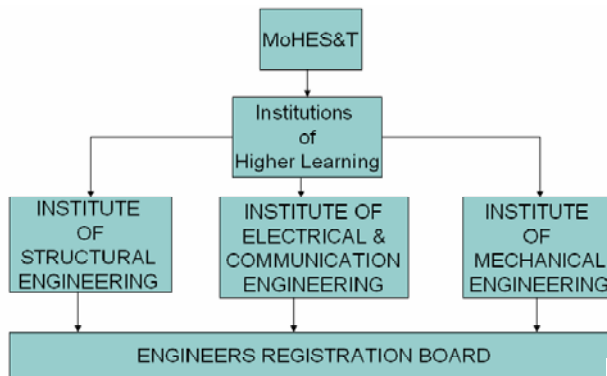


Figure 5: Hierarchy of Organized Engineering Training in Kenya

4. THE MINISTRY OF HIGHER EDUCATION, SCIENCE & TECHNOLOGY (MoHES&T)

The ministry's mandate includes

- Science Technology & Innovation (ST&I) Policy
- Research development.
- Research authorization
- Coordination of Technical Education (TE).

The ministry currently operates with three technical directorates and one SAGA; namely;

- Directorate of Research Development (DRD),
- Directorate of Technical Education (DTE),
- Directorate of Higher Education (DHE)
- National Council for Science and Technology (NCST).

Policy priorities include:

- Strengthening the National ST&I standing and its competitiveness
- Improving the quality, relevance, equity and access to higher education and technical training

- Promoting evidence based policy making and national development
- Encourage private sector participation in ST&I and technical education
- Enhancing capacity of the national ST&I system towards demand driven
- ST&I, quality higher education and technical education services
- Effective use of existing talents and facilities
- Promoting excellence, creativity, innovation and investment in
- ST&I, higher education and technical education.

4.1. Directorate of Research Management and Development.

This directorate;

- Creates regional and international linkages, collaborations and cooperation in ST&I
- Promotes technology transfer and provides of Science, Technology & Innovation (ST&I) information
- Ensures adoption and utilization of ST&I and its conversion into commercial products and services
- Mobilizes resources to support ST&I sector.
- Provides research, Science & Technology accreditation and standards
- Monitors and evaluates research activities in Kenya
- Manages and coordinates ST&I activities at various levels
- Advises scientist in universities and other research organizations on the regulatory requirements relating to ST&I

The Directorate of Research Management and Development has five divisions with distinct areas of specialization in research namely:

- Agricultural and Allied Sciences
- Environmental and Natural Science
- Planning and Social Sciences
- Biomedical and Allied Sciences

4.2. Directorate of Technical Education.

This Directorate in the Ministry of Higher Education Science and Technology performs the following functions:

- Administration of public Technical, Industrial, Vocational and Entrepreneurship Training (TIVET) tertiary institutions which include national Polytechnics, Institutes of Technology and technical Training institutes country-wide
- Provision of bursaries and grants to public TIVET institutions
- Registration of private TIVET institutions
- Planning for the development of technical training institutions.
- Coordinating development and implementation of training programmes.
- Formulation, co-ordination and review of policies and programmes pertaining to Technical, Industrial, Vocational and Entrepreneurship Training (TIVET) in collaboration with other relevant stakeholders, government departments and agencies.
- Administration of budgetary resources for public training institutions.
- Coordination, management and supervision of TIVET institutions.
- Providing professional and policy guidance to managers of existing or newly established TIVET institutions.
- Promotion of access and equity in the provision of TIVET.
- Promotion and facilitation of technical education and training.
- Registration of new TIVET institutions and approval of training programmes.
- Fostering linkages with industry in the provision of quality training.
- Promotion of research and technological innovation within technical training institutions.
- Nurturing entrepreneurial culture through technical education and training.

4.3. Directorate of Higher Education

The Directorate of Higher Education in the Ministry of Higher Education, Science and

Technology has taken this challenge in stride. Constituent University colleges and campuses affiliated to universities have been established to expand access to higher education.

4.4. Role of National Council for Science and Technology (NCST)

The NCST play a major role in science, technology, innovation and research in the country among major achievements they have made for the Kenyan nation is the facilitation of the establishment of the major research institutes, i.e.,

- Kenya Agricultural Research Institute (KARI)
- Kenya Trypanosomiasis Research Institute (KETRI)
- Kenya Forest Research Institute (KEFRI)
- Kenya Plant Health Inspectorate Services (KEPHIS)
- Kenya Medical Research Institute (KEMRI)
- Kenya Industrial Research Development Institute (KIRDI)

Beside the above role NCST does the following

- Advises the Government on science, and technology and innovation
- Advises researchers, Institution of higher learning and research organization on regulatory requirements for science, Technology
- Advises on research programme and scientific capabilities of institutes
- Provides advice on science, technology and innovation requirement for national and sectoral polices Authorizes Research
- Provides fora for dissemination of research results
- Provides information on science, technology and innovation
- Formulates policy and regulations for science, technology, innovation and research

Research Authorization Section

- Provides permits for research
- Receives and acknowledges research applications

- Forwards the applications to the relevant authorities for expert advice
- Receives and dispatches research reports
- Maintains an up to date data bank on all final research reports

5. INSTITUTIONS OF HIGHER LEARNING.

Institutions of higher learning include both local and foreign universities, national Polytechnics, Institutes of Technology and technical Training institutes. Currently we have 7 public Universities, 18 private Universities of which 11 have received university charter and the rest are on letters of interim authority. This number is expected to increase.

6. ENGINEERING INSTITUTES.

This paper introduces engineering institutes into the training program of engineering. Engineering institutes are to perform the following functions.

Examining graduate engineers for registration as members

- Assess engineers for accreditation.
- Link for engineering education and industry.
- Centre of excellence for engineering.
- Skill upgrading centre for engineers
- Developing and updating engineering curriculums for institutions of higher learning.
- Offer specialized training to engineering postgraduate.
- Evaluate engineering industries in Kenya
- Advice the government and society on engineering matters and all engineering projects in Kenya.

In order to perform the required task, these institutes must have well equipped laboratories, space (auditorium/ lecture halls), library and any other facility required in

The academic staffs of engineering institutes must be highly experienced engineering scholar (Academicians) in research and publications, teaching and book writing and also administration.

7. ENGINEERING REGISTRATION BOARD

The Engineering Registration Board is to register qualified graduates from engineering institutes on there areas of specialization as.

- Registered Graduate Technical Engineer.
- Registered Technical Engineer.
- Registered Graduate Engineer.
- Registered Engineer.
- Registered Consulting Engineer.

8. INDUSTRY.

Industry refers to the production of an economic good (either material or a service) within an economy. The engineer in the industry use the knowledge acquired to meet needs of the society.

9. CONCLUSION.

This paper has defined an engineer and also training an engineer towards creativity, innovation and application of new technology. It is important to establish institutes so as to effectively train engineers and hence improving engineering profession. It is also noted that scientist play a very vital role in training engineers and hence a scholar does not need engineering registration.

10. REFERENCES.

1. Davis, Michael. (1995) An Historical Preface to Engineering Ethics. *Science and Engineering Ethics* 1, No. 1, 33-48.
2. Spier, R. (1995) Science, Engineering and Ethics: Running Definitions. *Science and Engineering Ethics* 1: 7.
3. www.erbr.co.ke "Engineers registration Board" website.
4. www.mohest.co.ke "Ministry of Higher Education Science & Technology website"
5. National Academy of Science, Russia. 2001.



Odundo Simon Ochieng' is assistant lecturer in MMUST. His main area of interest is optical and digital communication, electronics and microprocessor technology. At the moment he has successfully worked on 4 publications.

NON LINEAR DYNAMICS: CHAOS AND ITS APPLICATION IN TELECOMMUNICATIONS

Joseph Abok Obadha,
josephabok@yahoo.co.uk

Department of Telecommunication and information Engineering, Jomo Kenyatta University of
Agriculture and Technology

Abstract—This paper examines the salient features of chaos systems, with specific reference to the Lorenz systems that make them appropriate for application in Telecommunications. Lorenz equation is simulated to illustrate these characteristics. Dynamic chaos possesses a combination of properties making it an attractive carrier for communication systems, which includes a high potential rate of data transmission, stability of broadband signals with respect to fading in the case of multipath signal propagation and possibility of providing confidential communications. Furthermore they are suitable for applications that require low cross correlation between the signals being used such as digital spread spectrum and multi-input multi-output radar systems.

INTRODUCTION

Chaos is the word used to describe deterministic behavior for which nevertheless, in view of the computational cost, even if the initial conditions were known to an arbitrary degree of precision, the long term behavior cannot be accurately predicted. This is certainly the case with many natural systems for which in any case we cannot know the initial conditions to an arbitrary degree of precision. A classic example, first considered by E.N Lorenz is the weather [Lorenz 1963]. Edward Lorenz, pioneer in using computers accidentally found in 1960, that in certain kinds of non-linear equations, the result displayed sensitive dependence on initial conditions. This is a distinguishing feature of chaos systems. At the end of the nineteenth century Henry Poincaré was aware of the fact that orbits of three bodies moving under a central force due to gravity are quite complicated and change drastically with a change in initial conditions. He tried to find a theorem to explain more generally the phenomenon the theorem and to establish a theory related to the chaotic paths in a system of differential equations. He showed that three dimensional paths in a system of non linear differential equations can be chaotic but two dimensional paths cannot be chaotic (Poincaré-Bendixon theorem)[1]

The Russian mathematician Lyapunov realized that a single number could be used to represent the change caused by perturbation. He divided the size of the perturbations at one instant in time by its size before. He then performed the computation at various intervals and averaged the results. This

quantity known called Lyapunov multiplier, describes how much on average a perturbation will change. A value less than one means the perturbation will die out and the system is stable. If the value is less than one the perturbation grows and the system is unstable.

NON-LINEAR DYNAMICS-BASIC TERMINOLOGY

Any nonlinear system which can be expressed by a set of mathematical equations includes two types of variables-*dynamic* and *static*. Dynamic variables are the quantities which change with time whereas the static variables, often referred to as the control parameters, remain constant until changed by an outside force. When studying the non linear system, the control parameters are often changed so as to learn how the behavior of the system changes in response. The act of changing a control parameter to change the system behavior is known as perturbation.

State space or *phase space* is the space of the dynamic variables and might in some cases include their derivatives. A point in the state space represents a state of the system at a given time. As the system evolves with time, the state of the system moves from point to point in the state space thus defining a trajectory. A trajectory therefore displays the history of the states of the system.

In nonlinear dynamical theory, the number of degrees of freedom is usually defined as the number of dynamic variables needed to specify the dynamical state of the systems or equivalently as the number of independent initial conditions that can be specified for the system

Chaos is an aperiodic long term behavior in a deterministic system that exhibits sensitive dependence on initial conditions. The three components of the definition are classified as follows:

1. Aperiodic long term behavior means that the system trajectory in phase space does not settle down to any fixed points (steady state), periodic orbits, or quasi-periodic solutions as time tends to infinity. This part of the definition differentiates aperiodicity of for example, a periodically oscillating system that has been momentarily perturbed.
2. “Deterministic” systems can have no stochastic systems (meaning probabilistic) parameters. It is a common misconception that chaotic systems are noisy systems driven by random processes. The irregular behavior of chaotic systems arises from intrinsic non-linearity rather than noise.
3. “Sensitive dependence on initial conditions” requires that trajectories originating from nearly identical conditions will diverge exponentially quickly.[2]

The mathematical model developed, now called, the Lorenz system has been used as a paradigm for chaotic systems satisfy the above definition. The Lorenz system consists of just three coupled first-order differential equations.

$$\begin{aligned} \frac{dx}{dt} &= -\sigma x + \alpha y \\ \frac{dy}{dt} &= -xz + rx - y \\ \frac{dz}{dt} &= xy - bz \end{aligned}$$

Lorenz chose parameter values $\alpha=10$, $b=8/3$ and $r=28$. With these choice for the parameters, Lorenz system is chaotic exhibiting the traits described in the definition given for chaos. For parameter values for which the Lorenz system demonstrates chaotic dynamics, all solutions, regardless of their initial conditions, converge to a set called the strange attractor. The strange attractor can be observed in state space (also called phase space), where each state variable is assigned a respective axis in the x-y-z plane space. Figure 1 illustrates a solution to the Lorenz system tracing out the strange attractor in state space. Since the Lorenz system satisfies the uniqueness theorem [4], no

points of intersection appears on the strange attractor. Nonetheless all solutions eventually converge to the butterfly shaped attractor. Specifically the attractor is composed of two wings, and each wing of the attractor encircles one of the two nontrivial fixed points. The shape of the strange attractor varies for varying parameter values.

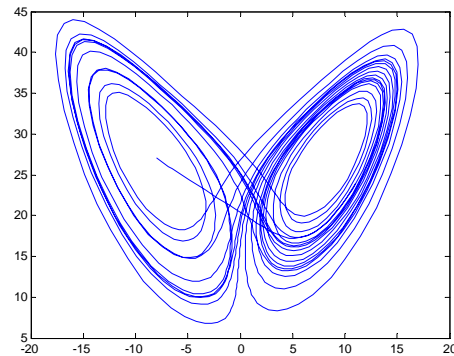


Figure 1: Lorenz strange attractor

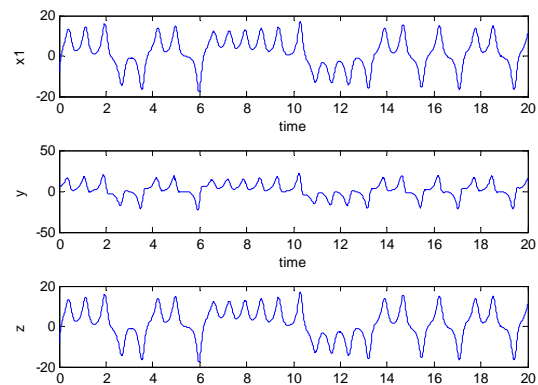


Figure 2: Time series of x, y and z

A time series of x, y and z is shown in Figure 2. The initial conditions can be chosen arbitrarily. From direct observation of the time series, it is reasonable to say that the x, y and z variables are aperiodic.

Chaotic systems exhibit sensitivity to initial conditions. For chaotic systems, two solutions with nearby initial conditions exponentially diverge. To demonstrate that the Lorenz system has this sensitivity, the x state variable from two distinct solutions with nearby initial conditions are shown in Figure 3. As can be seen from this figure, the two signals begin nearby and rapidly diverge from each other. Although only $x(t)$ is shown the same behavior can be observed from both $y(t)$ and $z(t)$.

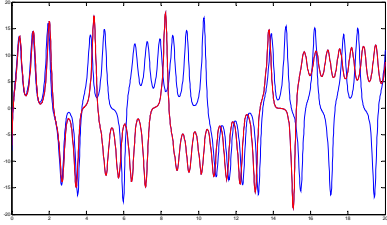


Figure 3: Time series plot for x with a variation in initial conditions

Therefore as can be seen from Figure 2 and Figure 3, the Lorenz system exhibit abounded, aperiodic flow with a sensitive dependence on initial conditions, which is a characteristic of any chaotic system.

APPLICATION OF CHAOS TO TELECOMMUNICATION

Chaotic telecommunication is relatively new field of interest in communications and its major motivation is derived from the facts that on one hand chaotic systems present a complex behavior and on the other hand are governed by some few simple rules. Moreover small changes in input parameters imply large deviations in output.

A direct application of chaos theory to telecommunication systems appear in a conventional digital spread spectrum, where the information is spread over a wider band by using a chaotic signal instead of the usual periodic sequence called the pseudo-noise (PN) sequence, the latter is generated for instance by linear shift registers. The most important characteristic of the periodic sequence are the auto-correlation and the cross correlation. The auto-correlation is important in the synchronization the periodic sequences generate at the transmitter and receiver. The cross correlation between the pseudo sequence must be zero to obtain communication between different users at the same band of frequency and at the same time.

In the same manner multiple input multiple output radar systems demands the generation of multiple signals with the autocorrelation and cross correlation meeting the criteria discussed above. Deterministic chaos can be used to generate a large number of quasi orthogonal waveforms to be used in the radar systems. Chaos synchronization allows applications of chaotic signal $I(t)$ by adding it to a larger chaotic signal and transmitting the superposition of the two signals. Information can

be recovered after the comparison of the received signal $I(t)+n(t)$. In this way chaotic signals in the transmitter and receiver systems must be synchronized. As this way of sending information is difficult to unmask, it is called secure communication [4]



J. A. Obadha received a Bsc.Eng (Electrical and Electronics) from the University of Nairobi (1997) and a Postgraduate Diploma in Education (PGDE) from Kenyatta University (2006). He is writing his dissertation for an MSc in Telecommunication Engineering degree at Jomo Kenyatta University of Agriculture and Technology and also teaches at Kenya Polytechnic University College. My current research interest is in signal processing techniques including non linear models for signal analysis.

REFERENCE

- [1] Thomson J.M.T, “*Non Linear Dynamics and Chaos*, John Wiley and Sons, New York, 2002.
- [2] Arrow, D and Place, C.N *Introduction to Dynamical Systems*, Cambridge University Press, Cambridge, 1990.
- [3] Peterson I.: *Newton’s Clock: Chaos in the solar System*.W.H Freeman, an Francisco
- [4] John Guckenheimer and Philip Holmes. *Nonlinear Oscillations, Dynamical Systems and Bifurcations of Vector fields*, volume 42 of Applied Mathematical Sciences.Springer-Verlag, New York, 1983
- [5] T.Kapitaniak, *CHAOS for Engineers, Theory, Applications, and Control*,

DETERMINATION OF STRESS INTENSITY FACTORS IN MULTIPLY CRACKED THICK-WALLED CYLINDERS USING MVCCT

K. K. Kiragu J. M. Kihiu J. N. Keraita

Department of Mechanical Engineering, Jomo Kenyatta University of Agriculture and Technology, Kenya

Abstract—The stress intensity factors at the crack tip in an internally pressurized pressure vessel with multiple axial cracks were determined using the energy based modified virtual crack closure technique. The Ansys10 Finite Element Analysis software was used to obtain the nodal forces at the crack tip and the nodal displacements in the vicinity of the crack tip. The stress intensity factors obtained using the modified virtual crack closure technique for cylinders with a single crack were found to be very close to those in literature. However this was after assuming that the crack extends by 37.5% of the length of the finite element behind the crack tip. The same assumption was also found to be valid for multiply cracked cylinders.

INTRODUCTION

Multiple radial cracks emanating from the inner surface are often present in thick walled cylinders under internal pressure, for example, pressure vessels employed in the nuclear and chemical industries, barrels of guns, etc. In order to predict the fatigue growth rate of such cracks, and thus the safe life of such cracked pressure cylinders, it is important and essential to know the mode I stress intensity factors (SIF). For many years, a great amount of work has been done on the problems of multiple radial cracks in the thick walled cylinders, and many values of SIF have been obtained by analytical and numerical methods. A radial crack has been studied previously by using the modified mapping-collocation technique [1]. The stress intensity factors due to the internal pressure for one to four radial cracks emanating from the outer surface and for three and four radial cracks emanating from the inner surface of cylinders have also been studied [2]. The stress intensity factors for multiple inner cracks in thick walled cylinders under internal pressure have also been studied using load relief factors [3]. [4] obtained the stress intensity factors for a wide range of thick cylinders with one or two inner and outer radial cracks under polynomial crack face loading by using crack weight functions. An analysis has been performed with a finite element and weight function method for a

uniform array of radial cracks in a partially autofrettaged thick wall cylinder [5]. Stress intensity factors have been calculated for large arrays of up to 1024 radial cracks emanating from the inner surface in the internal pressurized and autofrettaged cylinder by finite element method [6-7]. But most of these studies are limited to a small range of crack configuration parameters. Crack arrays have also been classified as dense or sparse according to inter-crack spacing ratio a/d and several formulae for estimating the stress intensity factors for both dense and sparse crack arrays have been developed [8-9].

The aim of this paper is to use the modified virtual crack closure technique (MVCCT) to determine SIFs in thick-walled multiply cracked internally pressurized cylinders and compare the results with those obtained using other techniques. Ansys10 Finite Element Analysis software was used in this study. This software was used to obtain the nodal forces at the crack tip as well as the displacements in the vicinity of the crack tip. These two parameters were then used in the modified virtual crack closure technique to obtain the stress intensity factors.

Model validation

The radial, hoop and axial stresses obtained from the finite element model were compared

with their corresponding theoretical stresses obtained using the Lamé's equations. Figure 1 shows the comparison of these stresses for a flawless cylinder with a thickness ratio of

$Y=1.5$. From the figure, it was evident that there was very good agreement between the finite element stresses and the theoretical stresses.

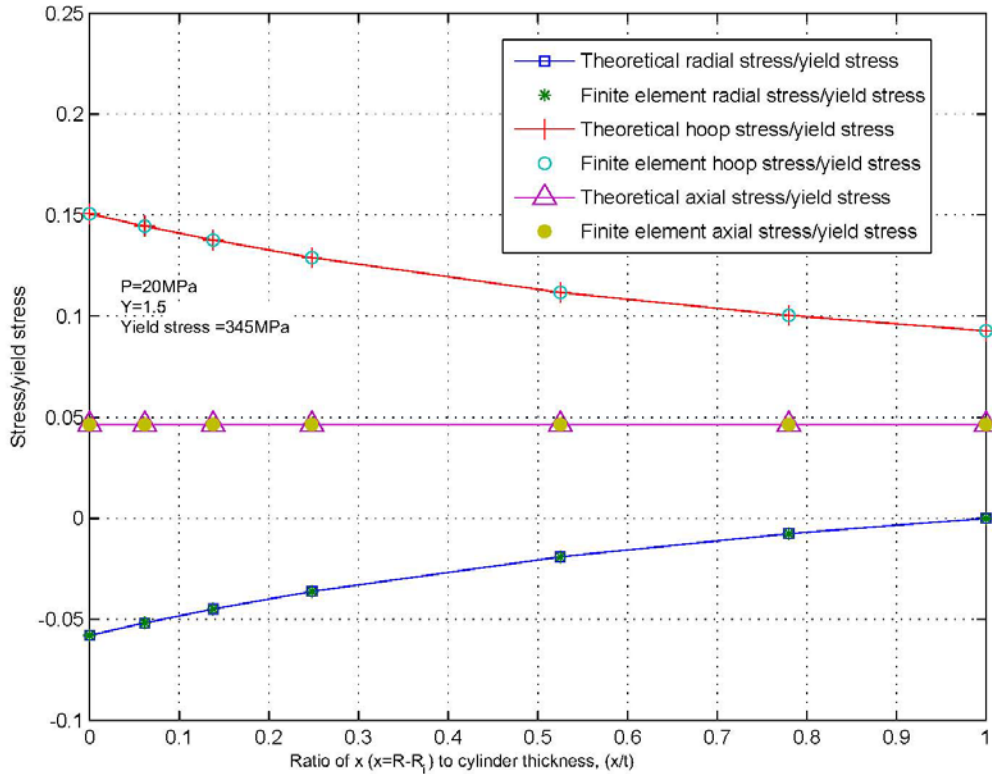


Figure 4: Theoretical versus finite element stresses

Single crack analysis

For cylinders with a single crack, the analysis was done by considering one half of the cylinder so as to take advantage of symmetry. Figure 2 shows the model that was used but the crack size shown has been exaggerated for the sake of clarity. The model structural properties were chosen as E , (Young's modulus of elasticity) $=210\text{GPa}$ and μ , (Poisson's ratio) $=0.3$. It was then meshed using solid-Tet-10node-187 elements. These elements were chosen because they could be arranged in a regular manner around the crack tip and also because they allowed for sufficient mesh

mesh



Figure 5: 3-D Single crack model

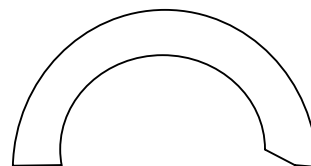


Figure 6: Front view of a single crack model

During the meshing, the model was first freely meshed and then the meshing of the whole model was refined before mesh refinement was done at the crack tip only. The next stage of the analysis involved the application of boundary conditions. The displacement boundary conditions were applied to prevent

the cylinder from rotating about its own axis. The areas in the model were also numbered so as to ensure that the boundary conditions were applied in their appropriate areas. Figure 5 shows the model with displacement boundary conditions.

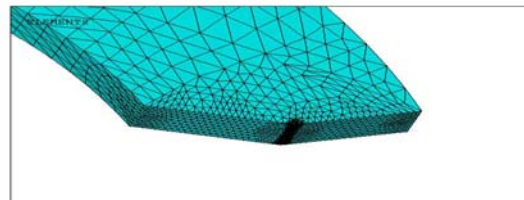


Figure 4: Refined mesh at the crack tip

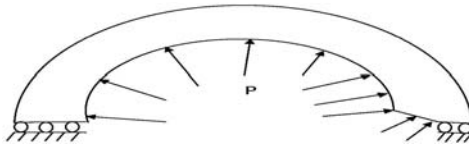


Figure 5: Front view of a model with boundary conditions

Internal pressure was applied on the inner surface of the cylinder as well as on the crack face while making sure that yielding did not occur at any point in the cylinder. The precondition conjugate solver was chosen to carry out the final analysis since it is fast and accurate. After the solution, the deformed and the non-deformed model were observed. The maximum stress was also checked so as to

verify that it was below the model yield stress. Figure 7 shows a plot of the stresses at the crack tip where; f is the distance between point A and C in figure 6. e refers to the distances from A (in the same figure) to the points where the stresses were recorded.

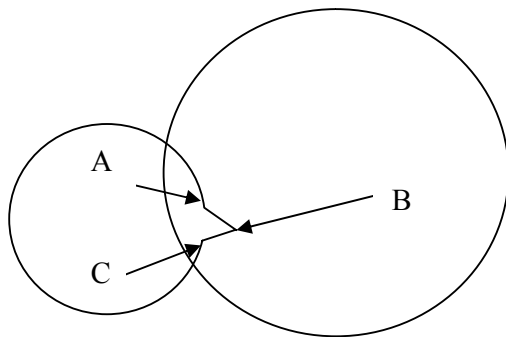


Figure 6: Points A to C where stresses were examined

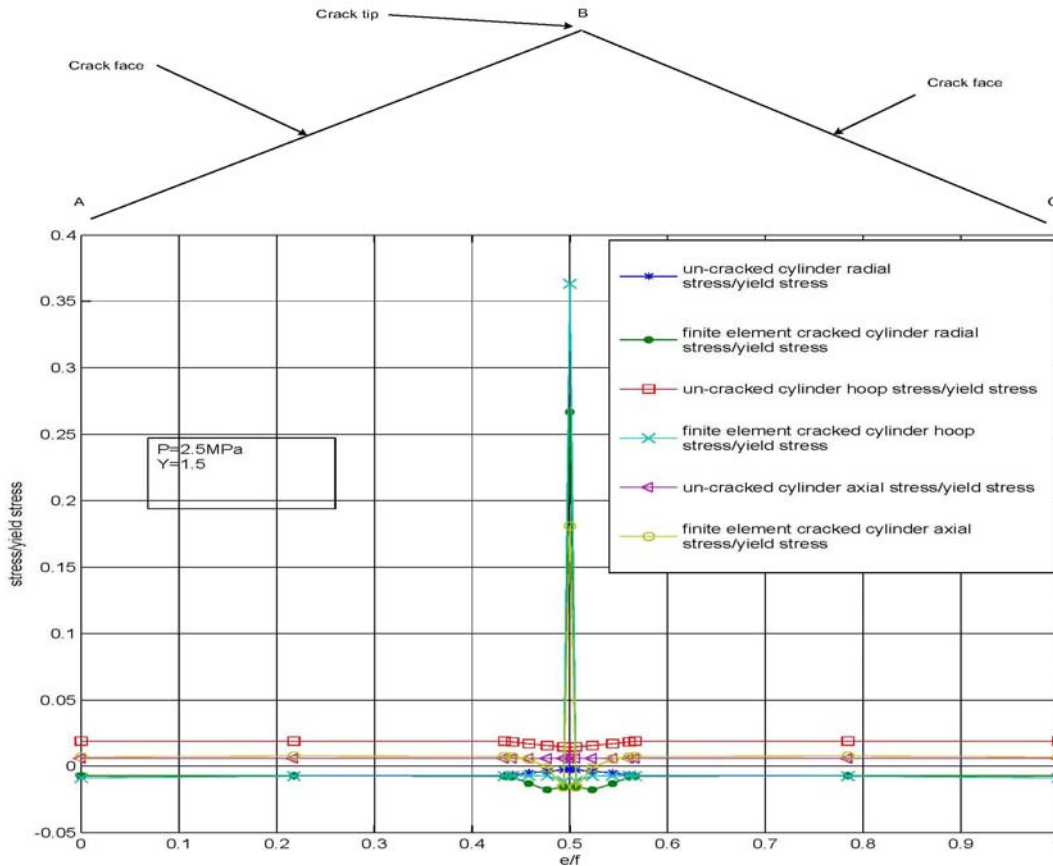


Figure 7: Stress variation along the crack

The node numbering of the whole model was activated and then a section of the crack tip was selected to be used in the analysis. For the selected portion, nodal forces in the hoop/circumferential direction were obtained at five consecutive nodes located along the crack tip. The nodal displacements in the hoop/circumferential direction were also

obtained at other five consecutive nodes near the crack tip. Taking figure 8 as an example, the nodal forces were obtained at nodes 53725, 53307, 53297, 53236 and 53209. The nodal displacements were obtained at nodes 54046, 54032, 54083, 54078 and 54077.

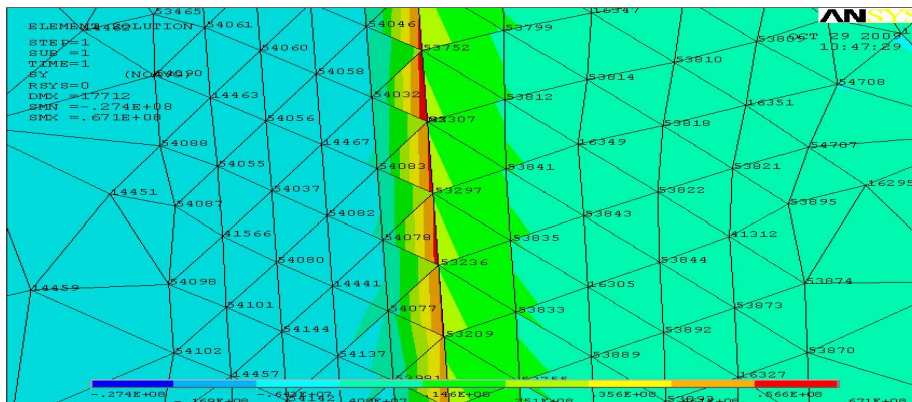


Figure 8: Nodes used for analysis

Application of modified virtual crack closure technique in thick walled cylinders

The modified virtual crack closure technique had earlier been applied in determining stress intensity factors in flat plates subjected to uniform pressure. In thick walled cylinders, the hoop stress that is related to mode I stress intensity factors in radial cracks decreases from the inner surface of the cylinder to the outer surface. Therefore, this method could not be applied in determining stress intensity factors in thick walled cylinders as it had been applied in determining these factors in flat

plates. After thorough investigations, it was found that excellent results were obtained after assuming that the crack extends by an amount equal to 37.5% of the length of the element behind the crack tip. Figures 9 show how varying the length of the element in front of the crack tip causes the SIF obtained using MVCCT (K_m) to vary from the K_k which was obtained from literature [13]. All the stress intensity factors presented are dimensionless i.e they have been divided by $P\pi a$

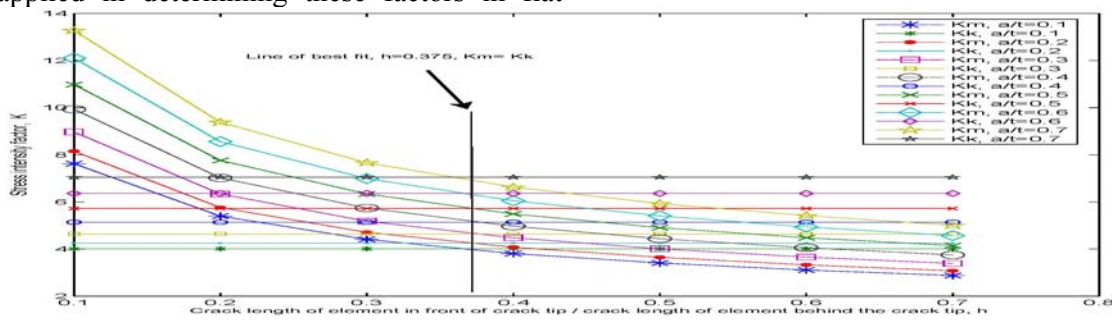


Figure 9: Variation of K_m with h for $Y=1.5$

Multiple crack analysis

For cylinders with an even number of cracks, due to symmetry, the analysis was done by considering a quadrant of the cylinder. For those with an odd number of cracks, again due to symmetry, the analysis was done by considering a half of the cylinder. Figure 10 shows the model that was used in the analysis of a cylinder with three cracks whereas figures 12 show the model that was used for the analysis of a cylinder with six cracks. The

lower half of figure 11 shows the part which was ignored in order to take advantage of the symmetry of the cylinder. For the sake of clarity, the sizes of the cracks have been exaggerated. The procedure for analyzing the cylinders with an even number of cracks is similar to that of analyzing those with an odd number of cracks. In both cases the half crack at the line of symmetry of the model was used for the analysis.

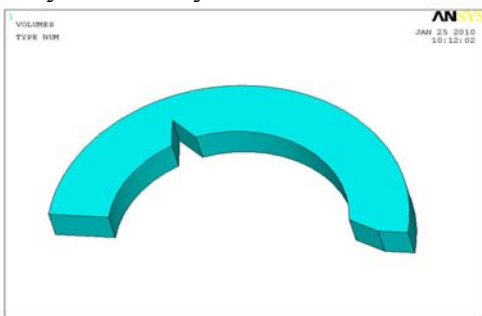


Figure 10: 3-D model for a cylinder with 3 cracks

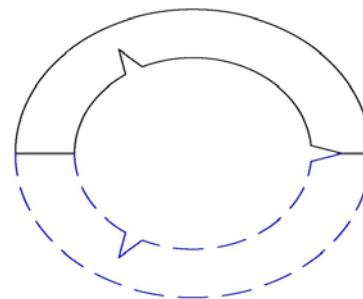


Figure 11: Front view of a model for a cylinder with 3 cracks

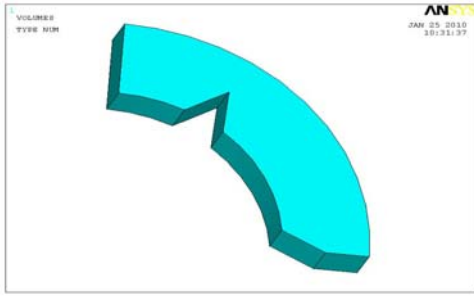


Figure 12: Model for a cylinder with 6 cracks

RESULTS

The stress intensity factors were calculated for $1 \leq n \leq 100$, $1.5 \leq Y \leq 2.5$ and $0.1 \leq a/t \leq 0.7$. The values obtained were compared with those in literature [11]. The maximum value of K was found occur when $n=2$. As the number of cracks increase, the value of K decreases. K also increases with a/t but decreases as Y increases. Figures 13 to 15 show the variation of K with n for various a/t ratios when Y is constant. From figure 13, it was evident that for any a/t ratio, the highest value of K_m occurred when $n=2$. This was in agreement with what had been reported earlier in literature that the two diametrically opposed cracks 'assist' each other in weakening the cylinder [12]. It was also evident from the figure that K_m decreased as n increased from 2. This was attributed to the concept of load

relief whereby the crack opening forces due to the applied pressure were shared by the increasing number of cracks. For $n < 10$, the stress intensity factor was found to increase with a/t and this was mainly due to the fact that, as a/t increased, the remaining cylinder thickness in front of the crack tip was decreasing and the gap between the two pressurized crack faces at the crack tip was reducing. The cracks also being far apart meant there was no interaction with the forces acting on neighboring cracks. For $n > 10$, the value of K_m was found to generally decrease with a decreasing value of a/t except for $a/t=0.1$ where the values of K_m are nearly equal to the values of K_m when $a/t=0.7$. The high values of K_m when $a/t=0.1$ were attributed to the high hoop stress near the inner surface of the cylinder. The values of K_m in figure 13 were in good agreement with those obtained from literature. The results in figure 14 and figure 15 displayed a similar trend with those in figure 13. It was however noted that the values of the stress intensity factors in the three figures decreased as Y increased. This was because strength of the cylinders increases with an increasing value of Y.

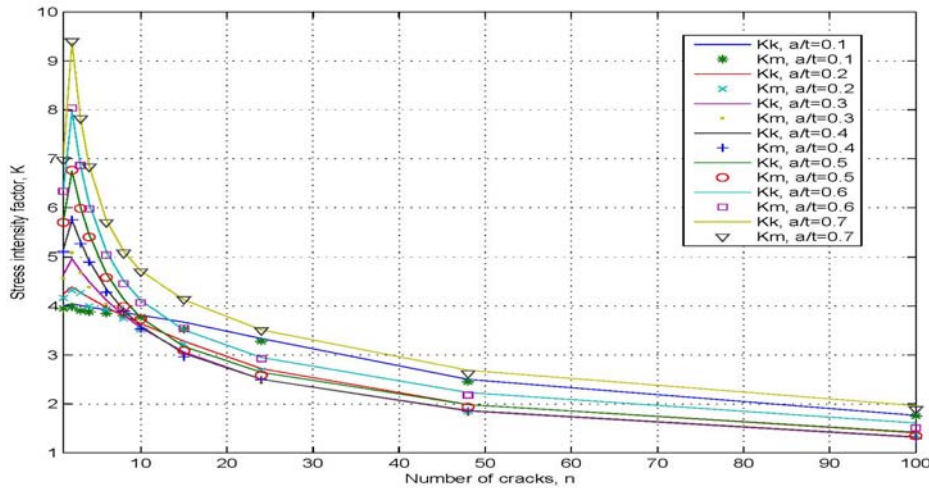


Figure 13: K values for a multiply cracked thick walled cylinder with Y=1.5

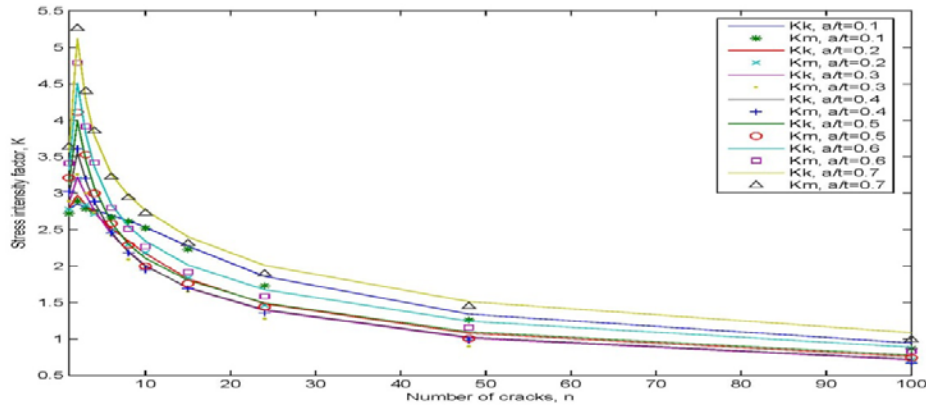


Figure 14: K values for a multiply cracked thick walled cylinder with Y=2.0

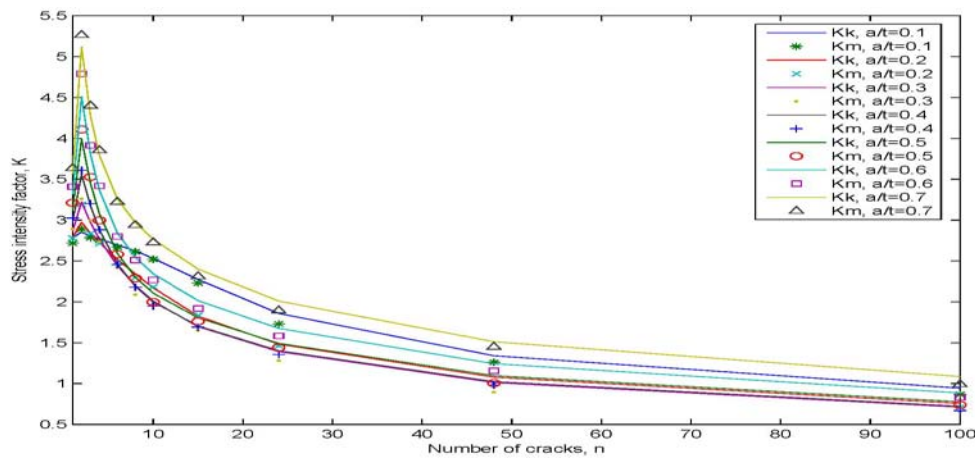


Figure 15: K values for a multiply cracked thick walled cylinder with Y=2.5

Table 1: K values for a multiply cracked thick walled cylinder with Y=1.5

a/t	0.1		0.2		0.3		0.4		0.5		0.6		0.7	
n	K _m	K _k	K _m	K _k	K _m	K _k	K _m	K _k	K _m	K _k	K _m	K _k	K _m	K _k
1	4.01	3.95	4.25	4.17	4.64	4.57	5.14	5.10	5.72	5.70	6.36	6.33	7.05	6.98
2	4.04	3.98	4.39	4.33	4.97	5.08	5.75	5.75	6.75	6.77	7.97	8.04	9.38	9.40
3	4.01	3.90	4.28	4.27	4.72	4.68	5.30	5.26	6.01	5.98	6.85	6.86	7.82	7.82
4	3.98	3.88	4.17	4.00	4.50	4.39	4.93	4.90	5.45	5.40	6.08	5.97	6.86	6.84
6	3.92	3.85	3.98	3.94	4.12	4.04	4.34	4.28	4.67	4.59	5.11	5.04	5.74	5.70
8	3.87	3.80	3.80	3.75	3.81	3.85	3.92	3.90	4.14	3.99	4.52	4.46	5.12	5.08
10	3.81	3.78	3.64	3.52	3.56	3.50	3.59	3.53	3.76	3.73	4.11	4.07	4.72	4.71
15	3.67	3.52	3.28	3.22	3.06	2.99	3.03	2.96	3.17	3.08	3.51	3.55	4.13	4.14
24	3.34	3.28	2.72	2.68	2.50	2.43	2.50	2.50	2.65	2.59	2.95	2.92	3.51	3.50
48	2.50	2.45	1.99	1.85	1.86	1.78	1.87	1.85	1.98	1.93	2.23	2.18	2.69	2.63
100	1.76	1.75	1.41	1.36	1.32	1.30	1.33	1.29	1.42	1.35	1.61	1.51	1.96	1.89

CONCLUSIONS

It was discovered that the modified virtual crack closure technique could not be applied in the analysis of thick walled cylinders in the same way it had been applied in the analysis of flat plates. Thus it was found appropriate to assume that the crack extends by 37.5% of the length of the finite element behind the crack

tip. In this way the SIF values obtained for both single crack and multiply cracked cylinders were found to only have an error of at most 5% in most cases. Despite the assumptions associated with the modified virtual crack closure technique, the SIF values obtained for thick walled cylinders were in good agreement with published results.

Table 2: K values for a multiply cracked thick walled cylinder with Y=2.0

a/t \ n	0.1		0.2		0.3		0.4		0.5		0.6		0.7	
	K _m	K _k	K _m	K _k	K _m	K _k	K _m	K _k	K _m	K _k	K _m	K _k	K _m	K _k
1	2.79	2.72	2.79	2.78	2.86	2.89	2.97	3.02	3.12	3.21	3.31	3.41	3.57	3.63
2	2.85	2.89	2.97	3.19	3.22	3.26	3.56	3.61	3.99	4.11	4.51	4.79	5.12	5.26
3	2.81	2.78	2.84	2.84	2.97	2.99	3.17	3.20	3.45	3.53	3.81	3.91	4.27	4.40
4	2.77	2.75	2.72	2.72	2.76	2.74	2.88	2.88	3.08	3.00	3.36	3.42	3.80	3.85
6	2.70	2.67	2.52	2.49	2.44	2.42	2.47	2.46	2.59	2.58	2.84	2.80	3.26	3.22
8	2.62	2.61	2.34	2.30	2.20	2.09	2.19	2.18	2.30	2.29	2.54	2.51	2.97	2.94
10	2.53	2.52	2.17	2.18	2.01	1.97	2.00	1.95	2.11	2.00	2.34	2.27	2.76	2.72
15	2.27	2.23	1.83	1.84	1.70	1.65	1.70	1.69	1.81	1.76	2.01	1.92	2.40	2.31
24	1.86	1.73	1.48	1.46	1.39	1.28	1.40	1.36	1.49	1.44	1.68	1.58	2.01	1.89
48	1.34	1.26	1.08	1.00	1.01	0.89	1.02	0.98	1.10	1.01	1.24	1.16	1.51	1.45
100	0.94	0.87	0.76	0.71	0.71	0.65	0.72	0.67	0.78	0.74	0.88	0.83	1.09	0.99

Table 3: K values for a multiply cracked thick walled cylinder with Y=2.5

a/t \ n	0.1		0.2		0.3		0.4		0.5		0.6		0.7	
	K _m	K _k	K _m	K _k	K _m	K _k	K _m	K _k	K _m	K _k	K _m	K _k	K _m	K _k
1	2.36	2.35	2.26	2.28	2.23	2.30	2.25	2.33	2.31	2.37	2.41	2.48	2.59	2.64
2	2.43	2.52	2.46	2.54	2.60	2.73	2.81	2.93	3.09	3.22	3.44	3.53	3.88	3.99
3	2.38	2.42	2.33	2.38	2.36	2.38	2.47	2.51	2.64	2.71	2.90	2.99	3.27	3.42
4	2.34	2.29	2.21	2.28	2.17	2.25	2.22	2.23	2.35	2.37	2.58	2.54	2.93	3.13
6	2.25	2.19	2.00	1.98	1.88	1.86	1.88	1.87	1.99	1.92	2.20	2.17	2.56	2.60
8	2.14	2.06	1.81	1.79	1.68	1.65	1.68	1.62	1.78	1.68	1.98	1.95	2.34	2.29
10	2.02	1.95	1.65	1.61	1.53	1.52	1.54	1.49	1.63	1.54	1.82	1.81	2.17	2.08
15	1.72	1.65	1.38	1.30	1.30	1.22	1.31	1.21	1.39	1.32	1.56	1.50	1.87	1.76
24	1.37	1.33	1.12	1.05	1.05	0.99	1.07	0.97	1.15	1.04	1.29	1.21	1.56	1.43
48	1.00	0.95	0.81	0.74	0.76	0.73	0.78	1.69	0.84	0.77	0.95	0.90	1.16	1.09
100	0.70	0.65	0.57	0.51	0.53	0.48	0.55	0.50	0.59	0.53	0.67	0.59	0.83	0.77



Mr. Kenneth Kiragu is a teaching assistant in the department of Mechanical Engineering at the Jomo Kenyatta University of Agriculture and Technology (JKUAT). He received his B.Sc. degree in the same university in 2006 and is also currently pursuing his M. Sc. at the same university. He has worked

as a trainee engineer for heavy engineering limited where he was in charge of penstock installation during the hydro-mechanical works of setting up the Sondumiri hydroelectric project. He is a registered graduate engineer with Engineers Registration Board (ERB).

REFERENCES

- [1] O. L. Bowie and C. E. Freese, Elastic analysis for a radial crack in a circular ring, *Engng Fracture Mech.* **4**, 315-321 (1972)
- [2] P. G. Tracy, Elastic analysis of radial cracks emanating from the outer and inner surfaces of a circular ring. *Engng Fracture Mech.* **11**, 291-300 (1979)
- [3] F. I. Barrata, Stress intensity factors for internal multiple cracks in thick-walled cylinders stressed by internal pressure using load relief factors. *Engng Fracture Mech.* **10**, 691-697 (1978)
- [4] C. P. Andrasic and A. P. Parker, Dimensionless stress intensity factors for cracked thick cylinders under polynomial crack face loading. *Engng Fracture Mech.* **19**, 187-193 (1984)
- [5] S. L. Pu and M. A. Hussain, Stress intensity factor for radial cracks in a partially autofrettaged thick-walled cylinder, *Proc. 14th Symp. on Fracture mechanics*. Volume I: Theory and Analysis ASTM 791, 194-215 (1983)
- [6] M. Perl and R. Arone, Stress intensity factors for large arrays of radial cracks in thick-walled steel cylinders, *Engng Fracture Mech.* **25**, 341-348 (1986)
- [7] M. Perl and R. Arone, Stress intensity factors for a radial multicroaked partially autofrettaged pressurized thick-walled cylinder, *J. Press. Vess. Technol.* **110**, 147-154 (1988)
- [8] L. P. Pook, Stress intensity factor expression for regular crack arrays in pressurized cylinders. *Fatigue Fracture Engng Mater. Struct.* **13**, 135-143, (1990)
- [9] M. Perl, Stress intensity factor approximate formulae for uniform crack arrays in pressurized or autofrettaged cylinders. *Engng Fracture Mech.* **43**, 725-732 (1992)
- [10] R. Hill, *The Mathematical Theory of Plasticity*. Clarendon Press, Oxford (1950).
- [11] H. M. Shu, J. Petit and G. Bezzine, Stress intensity factors for radial symmetrical cracks in thick-walled cylinders, *Engineering Fracture Mechanics*, vol. **49**, pp. 611-623, 1994.
- [12] R. W. E. Shannon, Stress intensity factors for thick-walled cylinders, *International Journal of Pressure Vessels and Piping*, vol. **2**, pp. 19-24, 1974
- [13] R. Bell and J. Kirkhope, Stress intensity factor equations for single and multiple cracked pressurized thick-walled cylinders, *Int. J. Pres. Ves. & Piping*, **40**, 103-111, 1990

EVALUATING PERFORMANCE OF WRP AND AODV MANETS ROUTING PROTOCOLS UNDER MOBILITY

Ephraim W. Mureu S. Musyoki P. Kihato.

ewmureu@yahoo.com, smusyoki@yahoo.com, kamitazv@yahoo.co.uk

Department of Telecommunication and Information Engineering JKUAT,
P O Box 62000 Nairobi, Kenya.

Abstract—The Mobile Ad hoc Networks (MANETs) are wireless networks which have no central bridge, and where each node acts as a destination as well as a router. There are many protocols that have been developed to aid in routing in these types of networks. To achieve effective routing, there are many interdependent parameters that a routing protocol algorithm has to contend with, but which have a great impact on the general performance of the protocol. The Routing protocols designed for MANETs are generally classified as either proactive or reactive. We have simulated WRP (proactive) and AODV (reactive) protocols to study their performance characteristics in face of varying nodes' mobility levels. Performance evaluation is based upon different metrics namely- throughput, packet delivery ratio, end to end delay, messaging overhead and energy consumption. The network simulator used is GloMoSim. Our results demonstrate that the AODV which is a reactive protocol outperforms WRP in many of the measured metrics. The AODV is thus a better for choice MA NETs.

Keywords: *MANET, WRP, AODV, Simulation, GloMoSim.*

1. INTRODUCTION

Mobile ad hoc networks (MANETs)(1) are networks composed of a set of communicating nodes able to spontaneously interconnect without any pre-existing infrastructure. These nodes generally have a limited transmission range and, so, each node seeks the assistance of its neighboring nodes in forwarding packets. In addition to that, these devices are generally mobile.

In order to establish routes between nodes which are further than a single hop, specially designed routing protocols are engaged. The unique feature of these protocols is their ability to trace routes in spite of a dynamic topology. These protocols can be categorized into two main types: reactive and proactive. The nodes in an ad hoc network generally have limited battery power and, so, reactive routing protocols endeavor to save power by discovering routes only when they are essentially required.

In contrast, proactive routing protocols establish and maintain routes at all instants of time so as to avoid the latency that occurs during new route discoveries.

Some of the applications of MANETs are as follows:

- i. Military vehicles on a battlefield with no existing infrastructure.
- ii. A fleet of ships at sea.
- iii. Emergency workers at an earthquake that destroyed the infrastructure
- iv. A gathering of people with notebook computers in an area lacking 802.11.

Selecting a particular protocol for an application or deployment environment involves evaluating many inter-dependent metrics and can be an overwhelming task for an application designer. However, this decision can have a significant impact on the success of a system in terms of performance. Hence, there is need to analyze and compare the performances of various available protocols to determine their suitability in a given network scenario.

Evaluating MANETs is achievable by resorting either to software-based simulators or to experimentation networks (testbeds). Most researchers favor simulators at the expense of testbeds. What prevents (or at least hinders) the use of real-size testbeds is their cost and their inherent lack of flexibility.

This becomes particularly impeding as the size of the experimented network grows. Software-based

simulation then turns out to be a viable alternative and a widely used solution. This paper uses mobile ad hoc network simulator called GloMoSim to evaluate performances of one proactive routing protocol; Wireless Routing Protocol (WRP)(2) and one reactive routing protocol; Ad Hoc On-demand Distance Vector (AODV)(3) protocols under varying nodes' mobility levels.

The rest of the paper is organized as follows: This research paper consists of five sections which are organized as follows: Section one has served as an introduction to the MANETs and need to analyze performance MANETs routing protocols. Section two surveys the literature review of the two mobile ad hoc network routing protocols under study. Section three details the methodology to carry out the MANET simulation. Section four presents the simulation results and Discussion. Section five concludes the paper by describing various observations.

2. DESCRIPTION OF PROTOCOLS

2.1 Wireless Routing Protocol (WRP)

WRP is a proactive routing protocol and was proposed by Murthy (2). WRP eliminates the possibility of routing loops. Nodes in a network using WRP maintain a set of four tables:

1. *Link cost table*. This table contains the cost of the link to each immediate neighbor node and information about the status of the link to each immediate neighbor.
2. *Distance table*. The distance table of a node contains a list of all the possible destination nodes and their distances beyond the immediate neighbors.
3. *Routing table*. The routing table contains a list of paths to a destination via different neighbors. If a valid path exists between a source and a destination node, its distance is recorded in the routing table along with information about the next-hop node to reach the destination node.
4. *Message retransmission list (MRL)*. The MRL of a node contains information about acknowledgement (ACK) messages from its neighbors. If a neighbor does not reply with an ACK to a hello message within a certain time,

then this information is kept in its MRL and an update is sent only to the non-responding neighbors.

WRP works by requiring each node to send an update message periodically. This update message could be new routing information or a simple 'hello' if the routing information has not changed from the previous update. After sending an update message to its all neighbors, a node expects to receive an ACK from all of them. If an ACK message does not come back from a particular neighbor, the node will record the non-responding neighbor in MRL and will send another update to the neighbor node later. The nodes receiving the update messages look at the new information in the update message and then update their own routing table and link cost table by finding the best path to a destination. This best-path information is then relayed to all the other nodes so that they can update their routing tables. WRP avoids routing loops by checking the status of all the direct links of a node with its direct neighbors each time a node updates any of its routing information.

2.2 Ad hoc On-demand Distance Vector Routing (AODV)

Ad Hoc On-Demand Distance Vector Routing (AODV) (3) is an improvement of the Destination-Sequenced Distance-Vector (DSDV) (4) algorithm. It is a reactive protocol and construct route on demand and aims to reduce routing load. It uses a table driven routing framework and destination sequence numbers for routing packets to destination mobile nodes and has location independent algorithm. It sends messages only when demanded and it has bi-directional route from the source and destination. When it has packets to send from source to destinations mobile node then it floods the network with route request (RREQ) packets. When a node receives an AODV control packet from a neighbor, or creates or updates a route for a particular destination or subnet, it checks its route table for an entry for the destination. All mobile nodes that receive the RREQ checks its routing table to find out that if it is the destination node or if it has fresh route to the

destination then it unicast route reply (RREP) which is routed back on a temporary reverse route generated by RREQ from source node, or else it re-broadcast RREQ.

3.0 METHODOLOGY

3.1 Simulation Environment

To evaluate the performances of the two routing protocols, a parallel discrete event-driven simulator, Global Mobile Simulator (GloMoSim) (5), was used. Our simulation experiments were executed on a Compaq Presario CQ60 Notebook PC (Personal Computer) with a Pentium IV processor@ 2.16 MHz with 2GB RAM (Random Access Memory).

3.1.1 GloMoSim

GloMoSim (5) is developed at UCLA (California, USA). It is widely used as wireless network simulator. GloMoSim is written in Parsec and hence benefits from the latter's ability to run on shared-memory symmetric processor (SMP) computers. New protocols and modules for GloMoSim must be written in Parsec too. GloMoSim respects the OSI standard.

3.2 Simulation Experiments

To compare the performance of the two routing protocols described in the previous sections, simulation experiments were performed. Five performance metrics were used to analyze and compare the two protocols.

3.2.1 Performance metrics

We focused on five performance metrics [6] to compare the two routing protocols: packet delivery ratio, mean end-to-end delay, messaging overhead, Energy consumption and Throughput. The five metrics used in our experiments are defined as follows:

i. Packet Delivery Rate

It is the number of received packets divided by the number of sent packets, computed at the application layer. It reflects the routing protocol reliability which is a very important

issue. High values of this metric reflect a good reliability, i.e low packet loss.

ii. Consumed Energy

Because energy resources of devices used in MANETs are limited, energy consumption is an important issue related to routing protocols. A routing protocol is as better as it causes less energy consumption compared with others in the same conditions. GloMoSim's Energy computation is based on NCR Wavelan radio model.

iii. Messaging Overhead

It is the number of packets generated by the routing protocol during the simulation. The generation of an important overhead will decrease the protocol performance. Although control packets are essential to ensure protocol functioning, their number should be less as possible.

iv. Mean End to End Delay

It is the average time separating the data packets sent from the source nodes and their arrival at the destination nodes, at the application layer level. This metric is very important to study the quality of service, especially in real-time applications.

v. Throughput

Throughput refers to how much data can be transferred from one location to another in a given amount of time. It is used to measure the performance of network connections. A high throughput value is desirable as it ensures maximum delivery of data packets.

3.2.2 Experimental Modeling

The control parameter that was used in our simulation experiments is the nodes' mobility. The five performance metrics were then measured for the following three different levels of node mobility: (1) high mobility- pause time 30s; (2) medium mobility- pause time 120s and (3) low mobility- pause time 240s.

Traffic load generated by each source node was modeled by a constant bit rate data

stream, whose transmission rate is defined by packet transmission interval for fixed-size packets. In our case one packet was sent every 1s. Movement of each node was modeled using the random waypoint model. In this model, each node remains stationary for the duration of its ‘pause time’. At the end of a pause time, a node starts moving in a randomly selected direction in the network terrain at a fixed speed. Once a node reaches its new location, it remains stationary during its next pause time. At the end of the new pause time, a node again starts moving in another randomly selected direction in the network. This movement process is continued during a simulation experiment.

The network terrain size was fixed for 2000m x 2000m. The radio signal transmission range was fixed at 175m (radius of 175m). The transmission bandwidth of each link was fixed at 2Mbps and the simulation time was 900s for all the experiments. In every experiment, there were 30 randomly selected pairs of sender and receiver nodes. Data packet size was fixed at 512 bytes. The above parameters were used for both of our simulation experiments.

4. SIMULATION RESULTS AND DISCUSSION

The data obtained from the simulations is as contained in Table 1 and Table 2.

Table 1: WRP Simulation Data

Nodes mobility	Energy (mwHr)	Control Packets	Throughput	Delay (s)	PDR (%)
High	225.16	912.3	1530.125	0.0057	34.61
Medium	225.15	831.73	2519	0.0047	50.14
Low	225.14	797.9	2532.3	0.0054	46.0

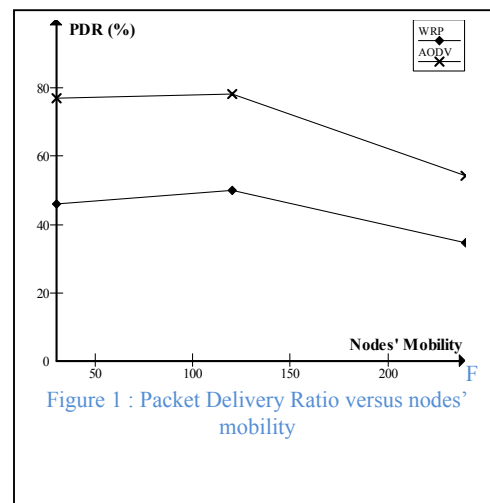
Table 2: AODV Simulation Data

Nodes mobility	Energy (mwHr)	Control Packets	Throughput	Delay (s)	PDR (%)
High	225.023	38.7	1771.125	0.0356	54.20
Medium	225.015	20	2383.8	0.0339	78.21
Low	225.01	14.67	2664.3	0.032	77.05

4.1 Packet Delivery Ratio

In Figure 1, we see that the AODV has a higher PDR compared to WRP in all mobility speeds. The reason for this is that AODV being a reactive protocol reacts more quickly to link failures by each node sending an error packet to all its active neighbors as soon as it detects a link failure thus avoiding excessive packet losses. On the other hand WRP being a proactive protocol sends packets before routing tables converge to a stable state, which leads nodes to take failed routes supposed to be valid and thus suffer from increased packet losses.

For both protocols, PDR decrease when the mobility increases.



4.2 Mean End-to-End Delay

Looking at Figure 2, we remark that WRP has low End-to-End delay compared to the AODV protocol.

This is because WRP being proactive constructs and maintains routing tables permanently, which eliminates the route discovery time as opposed to AODV which constructs routes on demand. In both protocols, the delay is not significantly affected by mobility.

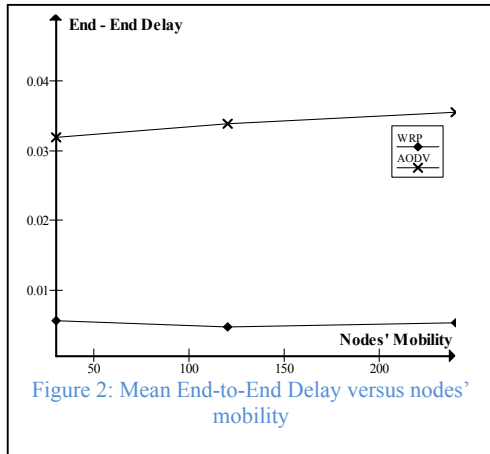


Figure 2: Mean End-to-End Delay versus nodes' mobility

4.3 Messaging overhead

We can see on Figure 3 that WRP generates the most overhead of the two protocols by a factor of 80. This is because WRP being proactive generates periodic messages whereas AODV do not generate overhead unless there is a need for a route or when a route is failed.

The messaging overhead in both protocols increases slightly with increase in mobility. This is because mobility rise implies route failure rise, which causes the generation of more error and route discovery packets.

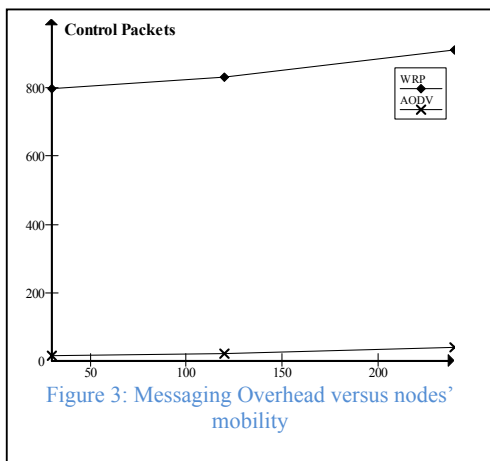


Figure 3: Messaging Overhead versus nodes' mobility

4.4 Energy Consumption

We remark that consumed energy plots (Figure 4), shows that WRP consumes more energy than AODV. The reactive protocols

consume less energy than the proactive ones, because these latter, generally, generate more overhead. Moreover, the sizes of the proactive control packets are longer than those of reactive ones.

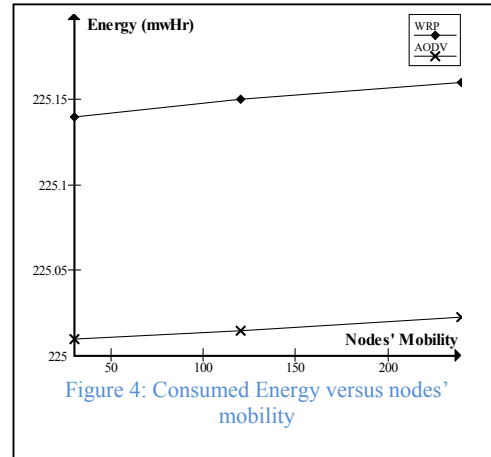


Figure 4: Consumed Energy versus nodes' mobility

4.5 Throughput

It can be seen from Figure 5 that the throughput of both protocols is heavily adversely affected by mobility. This because mobility increases the chances of link failures, which in turn decreases the throughput.

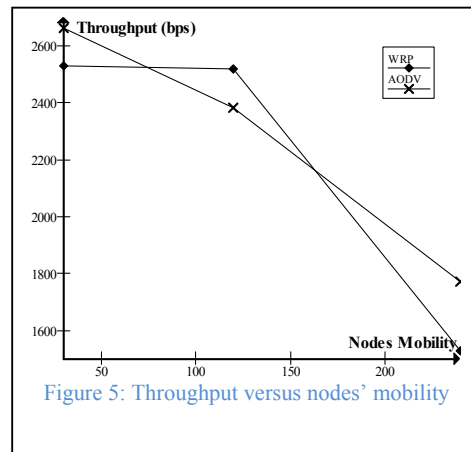


Figure 5: Throughput versus nodes' mobility

5. CONCLUSION

In this paper, we have conducted a GloMoSim based simulation study, to investigate the mobility effects on the performance of two MANETs' routing protocols; A reactive (AODV), and a proactive (WRP). This study is performed by measuring different

quantitative metrics at different mobility levels.

We realize from this study that the mobility, which characterizes MANETs, has negative effects on routing protocols. It causes more energy consumption, more latency, more packet loss, and more congestion (due to the increasing overhead). The results obtained also show that the reactive protocols are more adaptive to MANETs than the proactive protocols. Performances of the proactive protocols go down when the topological change occurs in the network. They generate a great number of routing overhead, resulting in an important power consumption, which is unacceptable for mobile unities supplied by batteries. They also cause an important packets loss. However, the proactive protocols have low latency, since they need no route discovery phase. But this has no significant importance when the mobility appears, because in this case proactive protocols cause an important data packets loss, these packets are not considered when computing delays.

REFERENCES

1. J. Macker and S. Corson, "Mobile Ad Hoc Networks (MANET)," IETF WG Charter., <http://www.ietf.org/html.charters/manet-charter.html>, 1997.
2. Murthy S, Gracia-Luna-Aceves JJ. An efficient routing protocol for wireless networks. *ACM Mobile Networks and Applications Journal*, Special Issue on Routing in Mobile Communications Networks 1996;183–197.
3. C. Perkins, E. Belding-Royer, and S. Das, .Ad hoc on-demand distance vector (aodv) routing,. in *Internet Engineering Task Force (IETF) draft*, July 2003.
4. C. E. Perkins and P. Bhagwat, .Highly dynamic destination-sequenced distance-vector routing (dsv) for mobile computers,. in *Computer*
5. Zeng, X., R. Bagrodia and M. Gerla, Glomosim: A library for parallel simulation of large-scale wireless networks, in: *Workshop on Parallel and Distributed Simulation*, 1998, pp. 154–161.
6. G. Jayakumar and G.Gopinath, "Performance Comparison of MANET protocols based on Manhattan Grid Mobility Model": *Journal of Mobile Communications* 2(1) : 18-26,2008.

PERFORMANCE ANALYSIS OF BIODIESEL FOR DOMESTIC USE

Ademola A. Dare^{1*} Adetokunbo Simon Callender² Adebambo Joseph Badejo²

*ademola_dare@yahoo.com/ademola.dare@mail.ui.edu.ng

¹ Department of Mechanical Engineering, University of Ibadan, Ibadan, Nigeria

² Department of Mechanical Engineering Lagos State University, Lagos, Nigeria

Abstract—There is continued growing demand for alternative energy resources worldwide. One of the emerging energy alternatives being explored is Biodiesel. Biodiesel has been produced from varieties of plant and animal resources. However most of its targets have been for use as fuel for engines with little consideration for domestic purposes. This work has examined the use of biodiesel for domestic use such as cooking. Three grades of biodiesel were produced by mixing ethanol with vegetable oil, diesel or kerosene. The fuel was then tested with a constructed cooking stove. Biodiesel with diesel blend was found not suitable for use in domestic cooking while the blend with either vegetable oil or kerosene was suitable. However, only the kerosene blend gave satisfactory performance for both pressure stove and wool stove. Wool stove also had higher efficiency of 64% as compared with the pressure stove of 60%. The work thus established that a blend of kerosene with ethanol can be used for domestic cooking without incurring any hazards. Equally it is established that biodiesel will perform creditably better with a wool stove.

Keywords: *Energy resources, Renewable, Biodiesel, domestic use*

INTRODUCTION

The continual search for alternative energy resource has been on the increase. One of the now considered viable alternatives is Biodiesel. At present Biodiesel is an alternative fuel for diesel engines that is gaining attention in the United States after reaching a considerable level of success in Europe (see Figures 1 and 2). Its primary advantages are that it is one of the most renewable fuels currently available and it is also non-toxic and biodegradable (Gerpen *et al*, 2004)

Research on biodiesel has focused on three main areas namely: production source, production techniques and productions costs. These three are being pursued in making biodiesel a viable alternative to existing/ upcoming energy sources. It is envisaged that by 2030 the production cost would have been reasonably low (see Figure 3).

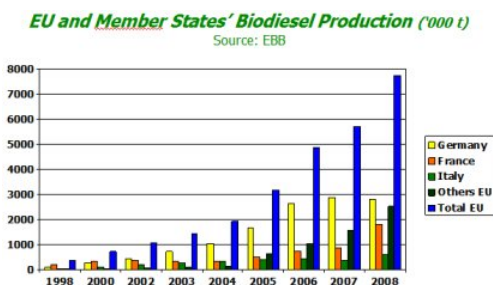


Figure1: EU and Member State Biodiesel Production (in metric tonnes)

Source: European Biodiesel Board, 2009

* Total EU27 biodiesel production for 2008 was over 7.7 million metric tonnes, an increase of 35.7% from the 2007 figures.

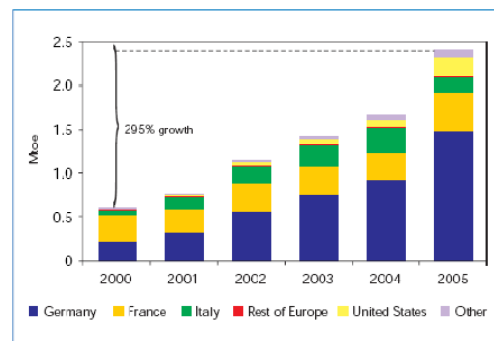


Figure 2: Biodiesel Production: Europe and other Nations.

Source: IEA Energy Technology Essential- Biofuel Production, ETR 02 2007

Biodiesel is typically made from plant oils combined with alcohol to form esters. The esters can be burned as a fuel. In addition to vegetable oils from soybeans, rapeseed, or palm oil, biodiesel can also be made from used cooking oil, animal fats, or oils

produced by certain types of microalgae.(Encarta Premium 2009). Considerable efforts have been made to produce biodiesel from many plant sources (Figure 3). The use of jatropa curcas was considered by Tomomatsu and Swallow (2007). The study largely rules out jatropa as a plantation type of crop under current economic conditions, the opportunity for smallholder farmers in value chain development were discussed. The use of High Iodine Number Candelnut Oil in Biodiesel production was reported by Sulistyo *et al* (2008). The biodiesel obtained had properties similar to those of diesel oil, except for the viscosity that was higher.

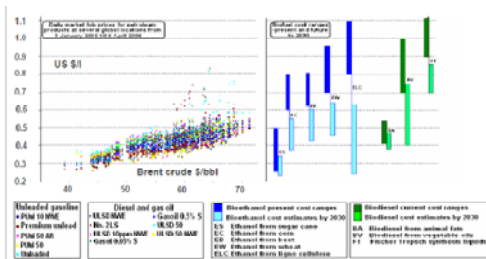


Figure 3: Current and Projected Cost of Biofuel compared with Conventional Wholesale Gasoline

Source: IEA Energy Technology Essential- Biofuel Production ETR 02, 2007

With increased attention being paid to its production, improved production processes were being investigated. Gerpen (2010) emphasis on the need for proper production process as this affects the quality and suitability for use as fuel for engine. Dhar and Khitania(2009) suggested techniques for recovering excess methanol in biodiesel production. The production of biodiesel from low cost raw materials received lot of attention. Abiney et. al. (2008) investigated the use of tin (II) chloride dehydrate as a catalyst on the ethanolysis of oleic acid, which is the major component of several fat and vegetable oils feedstock. Tin chloride efficiently promoted the conversion of oleic acid into ethyl oleate in ethanol solution and in soybean oil samples, under mild reaction conditions. The SnCl₂ catalyst was shown to be as active as the mineral acid H₂SO₄. Its use has relevant advantages in comparison to mineral acids catalysts, such as less corrosion of the reactors and as well as avoiding the unnecessary neutralization of products. Kapilakarn and Peugtong (2007) in their study found that the optimal condition that minimizes the operating cost for biodiesel is the ratio of methanol to oil at 6:1 (or

0.238:1 by wt.), the reaction temperature at 70°C, and the reaction time of 20 minutes. In addition, for the same production rate, the process with double size of the reactor improves the product purity (from 96.62 % to 98.21 %). For the number of reactors, it is found that two half-size reactors give better product purity and operating cost than the single reactor with the equivalent size

It should however be noted that efforts so far has largely been geared towards production of biodiesel for engine use. This has therefore necessitated this present work which is aimed at assessing the performance of different grades of biodiesel for domestic use. The performance of biodiesel when in use for stoves was carried out as this may further assist in reducing energy burdens in the rural communities.

Materials and Methods

A cooking stove was first constructed. Thereafter different grades of biodiesel were prepared. Various tests such as Flammability Test, Combustibility Test, Wool Stove Test, Pressure Stove Test, Environmental Test Miscibility Test, Mechanical Test, and Lubricity Test were then carried out The cooking stove was tested with biodiesel when operating normally and when pressurized.

APPARATUS USED IN PRODUCTION

- 1) A cooking stove or a gas burner.
- 2) 1 funnel.
- 3) 3 plastic bottles.
- 4) A thermometer.
- 5) NaOH (caustic soda).
- 6) Ethanol.
- 7) Pure vegetable oil.
- 8) Mixing bowl.
- 9) Stirrer.
- 10) Chemical balance scale.
- 11) Kerosene.
- 12) Diesel.
- 13) Spatula.
- 14) 4x (250ml) beakers.
- 15) 2 conical flasks.

Description of Experiment

Three different grades of biodiesel mixtures were made. Biodiesel grade A consists of a mixture of

ethanol and vegetable oil. Biodiesel grade B consists of a mixture of ethanol and diesel while Biodiesel grade C consists of a mixture of ethanol and kerosene. The methods of preparation of each grade are presented below

METHOD OF PREPARATION OF BIODIESEL GRADE A

- All apparatus was clean, washed and dried
- 200ml of pure vegetable oil was measured into a beaker and placed in a pot containing water. The oil in the beaker was heated to a temperature of about 55°C, using a burner or a gas stove.
- 1000ml of pure ethanol was measured and poured into a stirring bowl.
- 3.5g of NaOH (Caustic soda) was added to ethanol and stir continuously until the CAUSTIC SODA crystals dissolve completely inside the ethanol.
- After reaching the desired temperature the hot vegetable oil was poured into a stirring bowl and stir continuously. The stirring was continued for about 30 min, until the mixture becomes lighter than the original oil.
- The mixture was subsequently left to settle for 24hrs in a tall vessel. By then the biodiesel floated to the top and a whitish precipitate of glycerin is formed at the bottom was filtered out as by product which can be used for production of quality soap

METHOD OF PREPARING BIODIESEL GRADE B and GRADE C

The same procedure for production of grade A was adopted. However the ratio of ethanol to diesel was 2:1(grade B) and ethanol to kerosene was also 2:1(grade C).

RESULTS AND DISCUSSION

(a) Effect and Observation of Biodiesel Grades on Pressurized Cooking Stove.

Biodiesel grade A

When Biodiesel grade A was poured inside the tank of the pressurized stove and pumped at a pressure of 2.5kg/cm²(35pounds /sq in), the air inside the tank diffuses partially inside the biodiesel and due to the effect of pressure it flows through its stem and up to the hole in the burner nipple. When the biodiesel is

ignited on the spirit cup, the flame rises and heats up the remaining biodiesel coming from the burner nipple. The heating effect then produces a flame. After some minutes of burning; the flame extinguishes itself due to the formation of saturated oil which is produced at the hole of the burner nipple.

Biodiesel grade B

For this grade, the combustion was very excessive and could not be used for the cooking stove. However this grade made can be used on diesel engines and generators.

Biodiesel grade C

When biodiesel grade C is poured inside the tank of the pressurized stove and pumped at a pressure of 2.5kg/cm²(35 pounds /Sq in),the air inside the tank diffuses partially inside the biodiesel and due to the effect of pressure it flows through the stem and up to the hole in the burner nipple. When the biodiesel is ignited in the spirit cup, the flame rises and heats up the remaining biodiesel coming from the burner nipple. The heating effect then produces a flame. After some minutes the flame rises from the hole of the burner nipple and it is sustained due to the exerted pressure already in the tank. A summary of the observation is presented in Table 1

Table 1: Comparison of the Grades of Biodiesel on Stoves

Grades	Effect on Pressure Stove	Effect On Wool Stove
A	Poor Not Suitable.	Fair Performance.
B	Not Usable.	Not Usable.
C	Can Be Used.	Can Be Used.

(b) Results of Test on Biodiesel

The results of tests carried out on the three grades of biodiesel produced are summarized in Table 2

Comparison Burn Time of Pressure Stove and Wool on Stove

Since the kerosene blend biodiesel was found most suitable for use, the performance of the biodiesel for both pressure stove and wool on stove was compared. This was carried out by comparing the time taken for each stove to evaporate completely 25cl of water using the biodiesel as against the time taken using kerosene. The efficiencies are thus calculated as below.

EFFICIENCY OF PRESSURE STOVE

$$= \frac{\text{Burn time of 25cl biodiesel used}}{\text{Burn time of 25cl kerosene used}}$$

$$= (45\text{mins}/75\text{mins}) = 0.60 = 60\%$$

(7)

EFFICIENCY OF WOOL STOVE

$$= \frac{\text{Burn time of biodiesel used}/25\text{cl vol}}{\text{Burn time of kerosene used}/25\text{cl vol}}$$

$$= (48 \text{ mins}/75\text{mins}) = 0.64 = 64\%$$

(8)

The wool stove thus gave better performance than the pressure stove using kerosene blend biodiesel.

Table 2: Tests On Various Grades Of Biodiesel

Property Grades	Flammability	Volatility	Colour of Liquid	Viscosity	Colour of ppt after Burning.
A	Partially flammable	Not volatile	Light Yellow	Highly viscous	Light brown
B	Extremely Flammable	Volatile	Dark brown	Partially viscous	Black
C	Highly Flammable	Volatile	Off White	Partially Viscous	Dark White

CONCLUSION AND RECOMMENDATION

This study has established the viability of biodiesel for domestic use. The analysis showed that a biodiesel formed from a blend of ethanol and kerosene performed excellently well for both pressure stove and wool stove and is thus recommended for use. Equally since wool stove gave better performance, it is thus recommended that the biodiesel be used with wool stove.

REFERENCES

Abiney L. Cardoso, Soraia Cristina Gonzaga Neves and Marcio J. da Silva(2008). Esterification of Oleic Acid for Biodiesel Production Catalyzed by SnCl₂: A Kinetic Investigation. *Energies* , 1, 79-92; DOI: 10.3390/en1020079

Bipro Ranjan Dhar, Kawnish Kirtania (2009).Excess Methanol Recovery In Biodiesel Production Process

Using A Distillation Column: A Simulation Study. *Chemical Engineering Research Bulletin* 13 , 55-60

Hary Sulisty, Suprihastuti S. Rahayu, Gatot Winoto, I M. Suardjaja(2008). Biodiesel Production from High Iodine Number Candlenut Oil. *World Academy of Science, Engineering and Technology* 48, 485-488.

IEA Energy Technology Essentials-Biofuel Production, ETR 02 , 2007

J. Van Gerpen, B. Shanks, R. Pruszko, D. Clements and G. Knothe(2004). Biodiesel Production Technology. NREL/SR-510-36244.

Jon Van Gerpen. Biodiesel Production and Fuel Quality. Retrieved from www.uiweb.uidaho.edu/bioenergy/biodieselIED/publication/01.pdf on 15th June, 2010

Kulchanat Kapilakarn and Ampol Peugtong(2007). A Comparison of Costs of Biodiesel Production from Transesterification *International Energy Journal* 8, 1-6

Microsoft ® Encarta ® 2009. © 1993-2008 Microsoft Corporation

Statistics: the European Biodiesel Industry European Biodiesel Board 2003-2009

Yuka Tomomatsu and Brent Swallow(2007). Jatropha curcas Biodiesel Production in Kenya Economics and Potential Value Chain Development for Smallholder Farmers, *World Agroforestry Centre Working Paper* # 54

POWER THEFT IDENTIFIER USING GLOBAL SYSTEM MOBILE COMMUNICATION (GSM) TECHNOLOGY

K.Senthil¹
ksenthil_856@yahoo.com

K.Manikandan²
Starmk2015@yahoo.com

D.B.O. Konditi³
onyango_d@yahoo.co.uk

¹ Department of EEE, St. Joseph College of Engineering & Technology, Dar Es Salaam, Tanzania. ² Department of EEE, S.R.M University, Chennai, India. ³ Department of ECE, Multimedia University College of Kenya, Nairobi

Abstract—The most challenging problems that distribution utilities are facing are energy losses. At present we are able to find that energy theft is happening somewhere, but the particular location at which it happens is unknown. This paper finds out the particular area and transformer where the energy theft happens and immediately traces the place and transformer number will be transferred to the nearby EB station through SMS by using C programmed language for monitoring the authorized and total load current and to check whether the total load current is greater than the authorized load current. If it is greater then immediately message would be sent to the specified number indicating the area where the energy theft happens. It gives a remedy for detecting the particular area in which energy theft happens so that we could find out the person engaged in it. Therefore we could reduce the commercial losses. It is to identify energy theft, Electrification network and tampered meters. It is based on a central observer meter that is responsible for metering the overall energy of a group of consumers. When a power theft happens at any distribution transformer immediately the location will be transferred to nearby Electricity Board station. The Electricity Board station will immediately send the person to that location and find the people. The data transfer is through GSM Technology.

Keywords: *Power theft, GSM, Millennium development goal, Energy losses, Sustainable development.*

I. INTRODUCTION

Loss of distribution utilities are defined as the net result of the difference between the generated or purchased energy and the energy effectively billed. Basically there are two types of losses namely Technical loss and Commercial loss. Technical losses are related to non idealities of electric equipment such as transformers, transmission lines and other equipments associated with distribution. These losses can be reduced by replacing old equipment by new efficient one and designing efficient distribution networks. Commercial losses are due to theft of energy. These losses can be reduced by reducing the energy theft. This paper gives a remedy for detecting the particular area in which energy theft happens so that we could find out the person engaged in it. Therefore we could reduce the commercial losses.

In Brazil, one of the most challenging problems that distribution utilities are facing is energy losses [1] [2]. Losses of distribution utilities are defined as the net result of the difference

between the generated and or purchased energy and the energy effectively billed. They can be arranged in two types: technical and commercial losses. Technical losses are related to non idealities of electric equipment: transformers, transmission lines and other equipment have, for instance, ohm losses and even the meters are not lossless. In order to reduce technical losses, several actions can be carried out by the utility: replacing old equipment by more efficient equipment, designing and building more efficient distribution networks, etc.

Commercial losses are the net difference between the energy effectively supplied by the distribution utility and the effectively billed energy of the consumers. Theft of energy and meters that don't work properly are one of the major causes of commercial losses. *Also*, problems in the billing system may cause commercial losses to the distribution utility. Checking the billing procedures of the utility can be the first step to reduce commercial losses. To

do that, the consumer database must be always updated, reflecting any change verified in the field with the smallest time delay. This database is important not only for auditing the billing. It is crucial for discovering energy frauds, as it maintains key information such as the class of the consumers (residential, commercial, industrial, etc.), the address, technical aspects of the metering installation (for example, number of phases), the distribution transformer to which the consumer is connected, etc.

Another way to reduce the utility’s commercial losses is to enhance the observability of the consumers. A possible action can be regularly visiting the consumers’ metering installations to check them in order to find out any problem. This should be done by specialized and well-trained teams. However, these visits are expensive if carried out for the whole set of consumers of the utility. Because of that, utilities

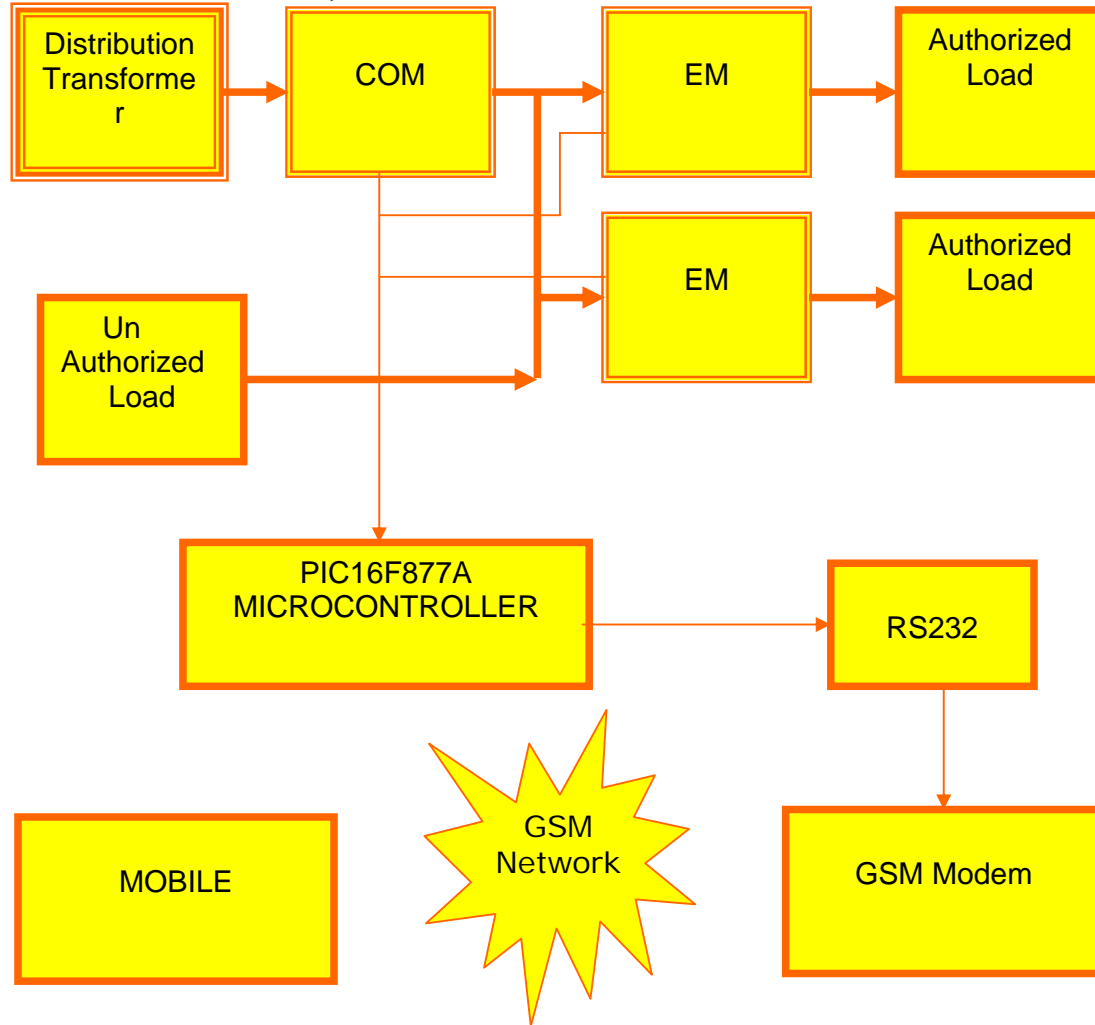


Figure 1.: Block Diagram of Power Theft Identifier using GSM Technology

usually adopt a statistical approach to select the consumers [3] to be inspected and, consequently, they don’t find out the existing problems of all installations. One possible alternative, reported in the literature [4], is substituting the conventional electromechanical meters for

electronic ones, with anti-tampering characteristics. Singhal, discusses revenue protection features brought by electronic measurement.

The drawback of these arrangements is that it is necessary to change from the conventional metering to the electronic metering in all the installations. Improving the observability can be done by installing observer meters outside the metering installations, normally out of the residence of the consumers. At first, an observer meter is necessary for each consumer. A possible approach to overcome commercial losses in this sense should be the centralized system depicted in [1].

In this scheme, there isn't any metering inside the consumer's premises and, besides, all the meters of a particular neighborhood should be accommodated in the same case. The observability of metering would be improved, as the metering could be viewed by everyone. Besides, energy bypasses would be easily discovered. This arrangement also includes a central observer meter, installed next to the distribution transformer. By comparing the register of this observer meter with the sum of the registers of all meters connected to the transformer, any problem can be found out straightforwardly.

Nevertheless, the difference between the observer meter and all the consumers' meters is not enough to point out which consumer has problems in his installation at a first glance. The investigation of metering faults by analysis of the metering readings have already been reported in the literature [6]. Chambers, R.G. [6] shows a systematic procedure with the purpose of discovering discrepancies between main meters

and another meter readings focused on large generators.

II. GSM DATA CALLS

Data calls can be made using this modem. Data calls can be made to a normal PSTN modem/phone line also (even received). Data calls are basically made to send/receive data streams between two units either PC's or embedded devices. The advantage of Data calls over SMS is that both parties are capable of sending/receiving data through their terminals.

III. MEASURING CONCEPTS

The main concept behind measurement is shown in block diagram below. The parameter will be measured and then it will be converted to a proportional DC voltage. This DC voltage will be converted from analog to digital using microcontroller PIC 16F877. The digital data will be compared and if the total load current is greater than the authorized load current an interrupt is produced in the GSM modem through RS 232 communications. From the GSM modem message is transferred to the EB station indicating the area of power theft.

A. Central Observer Meter

This is the basic block diagram of central observer meter where we perform the energy calculation and transmit data, when power theft happens. From transformer the current and voltage values are measured and the energy calculations are performed. The comparison of both distributed amount of power and total power used is done here. In case if there is a power theft an interrupt is

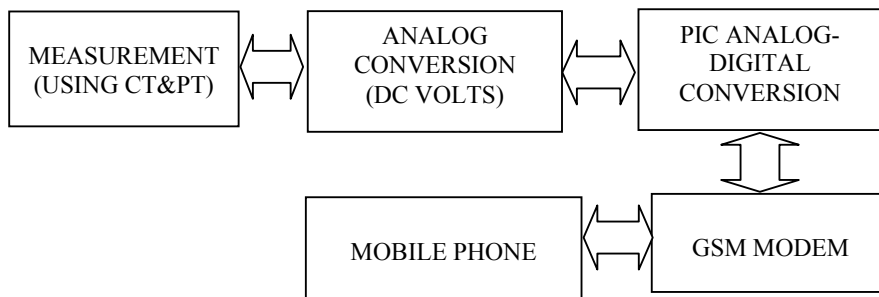


Figure 2. Block Diagram of Measuring Unit

B. Parameter Being Measured and calculated

Parameters being measured are Current, Voltage, Total load current, Authorized load current.

These are the parameters which are not measured but calculated from the parameters being measured.

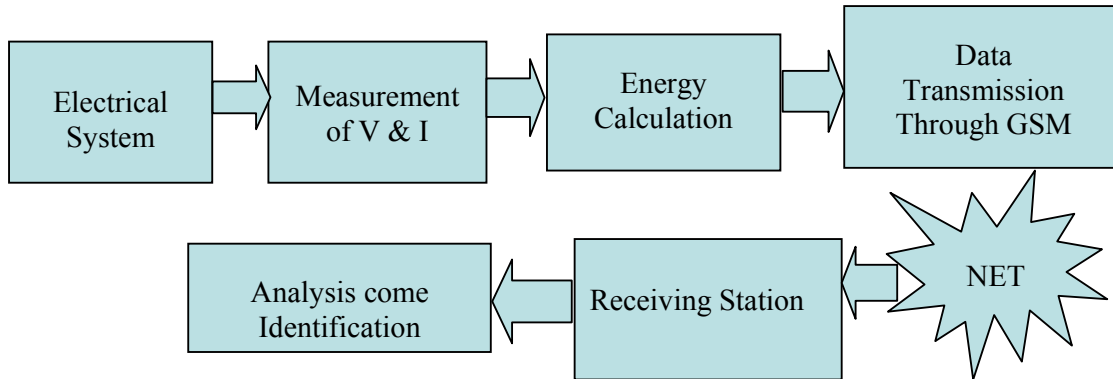


Figure 3. Block Diagram of Central Observer Meter

B. Voltage Measurement Block

This block is used for voltage measurement. There is rectifier been placed for converting the available AC to DC. Here we have current limiting resistors & a filtering capacitor. The supply is given from the potential transformer. The output is given to the ADC circuit in the PIC controller. The ADC circuit converts the output into samples.

C. Current Measurement Block

The current measurement block has bridge rectifier for converting the available AC to DC. The current limiting resistors are added for limiting excess current passing on to the components. The filter capacitors are used for filtering the harmonics in the circuit. The output of the current measurement block is given to the ADC circuit for conversion of samples.

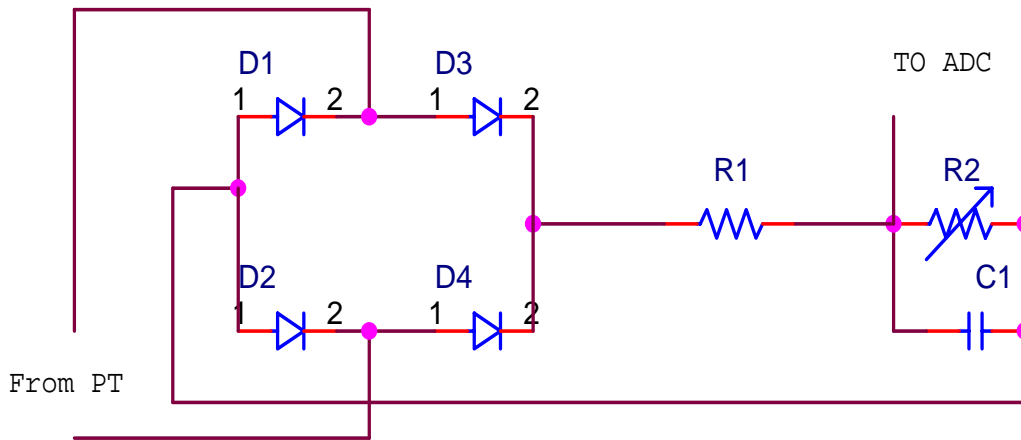


Figure 4. Block Diagram of Voltage Measurement

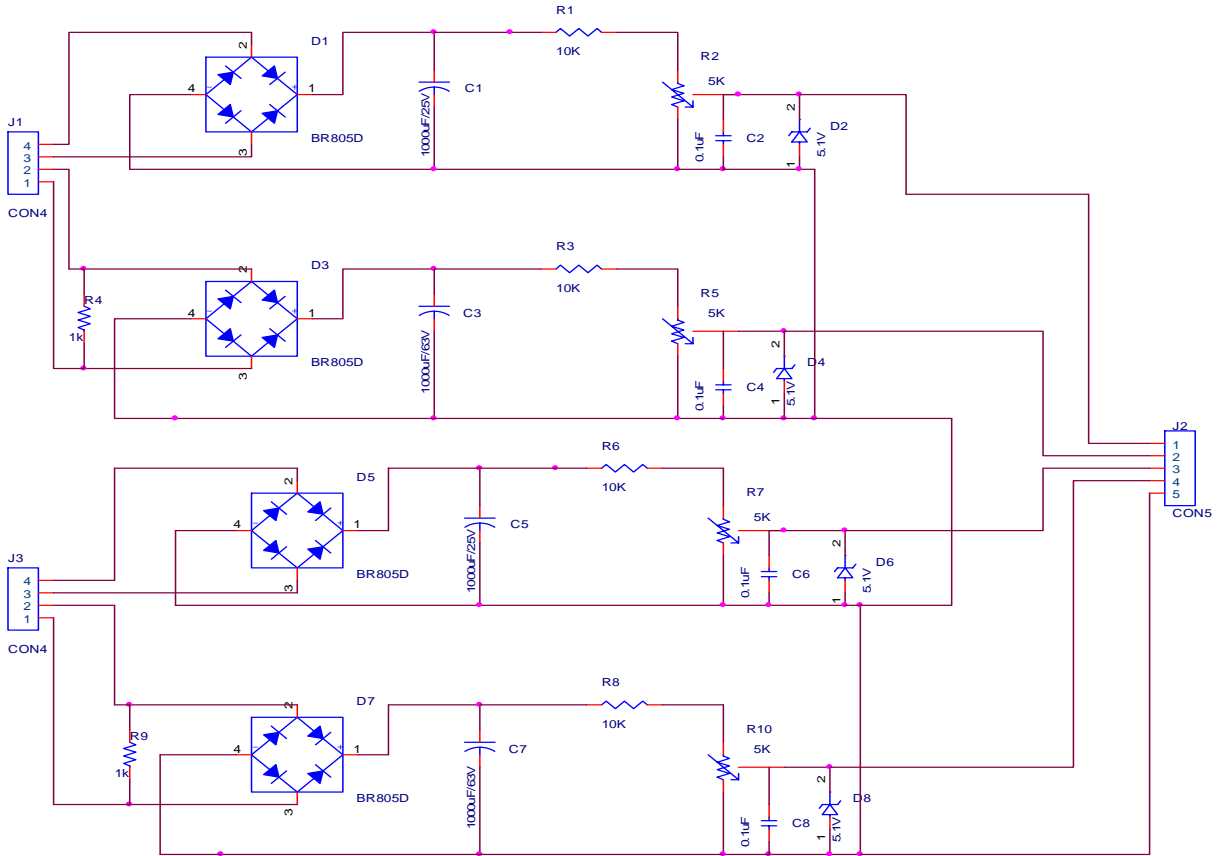


Figure 5. Block Diagram of Voltage & Current Measurements

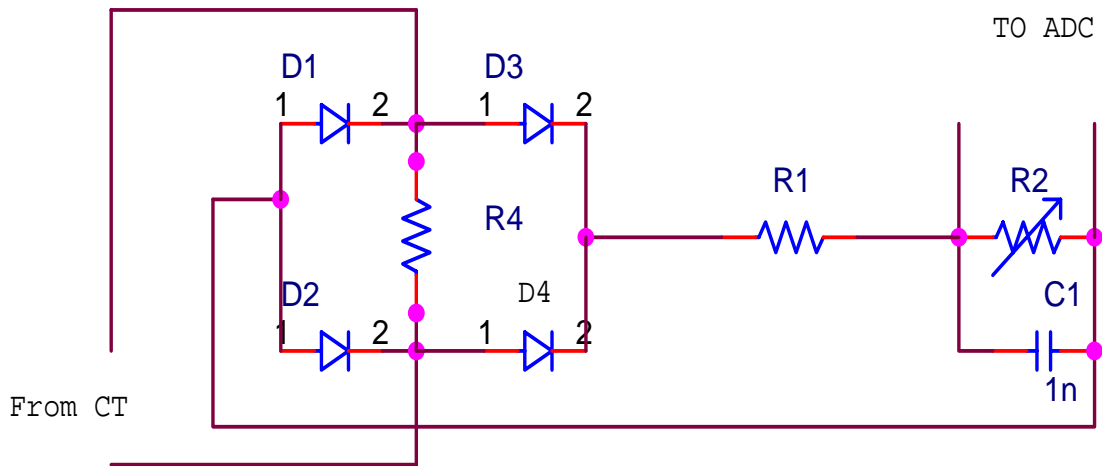


Figure 6. Block Diagram of Current Measurement

IV. RESULT & DISCUSSION

This paper finds out the particular area and transformer where the energy theft happens and immediately the place and transformer number will be transferred to the nearby EB station through SMS by using C programmed language for monitoring the authorized and total load current and to check whether the total load current is greater than the authorized load current. If it is greater then immediately message would be sent to the specified number indicating the area where the energy theft happens. It gives a remedy for detecting the particular area in which energy theft happens so that we could find out the person engaged in it. Therefore we could reduce the commercial losses. This project helps us in reducing the energy theft and also finding out the tampered meters. Here the data transfer is made possible through GSM technology. The algorithms developed here associate the measurements of a group of consumers under investigation with a central observer meter, registering the total energy of that set of consumers. This method is particularly inexpensive, as it uses a single observer meter for a large number of consumers.

ACKNOWLEDGEMENT

The authors gratefully acknowledge the authorities of St. Joseph college of Engineering and Technology, Dar Es Salaam, Tanzania for the facilities offered to carry out this work.

REFERENCES

- [1] Gama, S.Z., et alli - "Uma Nova Abordagem Tecnológica de Combate h Perdas Comerciais" - XV Seminário Nacional de Distribuição de Energia Elétrica - SENDI 2002, Brazil, 2002.
- [2] Bandim, C.J., Pinto Junior, A.V., Alvarenga, L.M., Loureiro, M.R.B., Santos, J.C.R., Galvez-Durand, F., - "Loss Evaluation in Distribution Systems" - Congreso Internacional De Distribución Eléctrica, Cidrel Argentina 2002
- [3] Nilsson, H. , "Random sampling of and a scheme for reporting of malfunctions in electricity meters in Sweden" , Metering and Tariffs for Energy Supply, 1999.Ninth International Conference on (Conf. Publ.No. 462)), Aug 1999 ,Birmingham, UK

- [4] Misra, R.B. Patra, S, "Tamper detection using neuro-fuzzy logic [static energy meters] " , Metering and Tariffs for Energy Supply, 1999. Ninth International Conference on (Conf. Publ. No. 462), Aug 1999, Birmingham, UK.
- [5] Singhal, S., "The role of metering in revenue protection" , Metering and Tariffs for Energy Supply, 1999.9th International Conference on (Conf. Publ. No. 462), Aug 1999 Birmingham, UK
- [6] Chambers, R.G., "Early diagnosis of tariff metering faults by a systematic analysis of maidcheck metering discrepancies " , Metering and Tariffs for Energy Supply, 1999. Ninth International Conference on (Conf. Publ. No. 462)), Aug 1999, Birmingham, UK.
- [7] Bandim, C.J., Souza, F.C., Alvarenga, L.M., Pinto Junior, A.V., Luiz, F.C., Alves Junior, J.E.R., Galvez-Durand, F., Loureiro, M.R.B., Dantas, A.R.,- "Centralized Metering System In Buildings" - Congreso Internacional De Distribución Eléctrica, Cidrel Argentina 2002
- [8] Costa, R.S. , Caldas, R.P., Alvarenga, L.M., Pinto Jr., A.V., Souza, F.C., Pimentel, J.C.G., Bandim, C.J. - "A New Concept Of Electrical Energy Metering In Buildings" - ERE, 1994.
- [9] C. J. Bandim, J. E. R. Alves Jr., A. V. Pinto Jr, F. C. Souza, M. R. B. Loureiro, C. A. Magalhães and F. Galvez-Durand . "Identification of Energy Theft and Tampered Meters Using a Central Observer Meter: A Mathematical Approach" – IEEE, 2003



PROFILE

K. Senthil received the Master of Engineering in Power Systems from the Faculty of Engineering & Technology, Annamalai University, Chidambaram, India in 2008. Currently, he is a Lecturer of Electrical & Electronics Engineering Department,

St. Joseph College of Engineering & Technology, Dar Es Salaam, Tanzania. He was a Lecturer in the Department of Electrical & Electronics Engineering, at Lord Venkateshwaraa Engineering College, Puliambakkam, Kanchipuram, India and E.S.College of Engineering & Technology, Villupuram, India from 2007 to 2008. He is an author of three international journals & four Conference papers. His areas of research include Economic Dispatch, Emission Dispatch and Power system optimization. He is a member of Institution of Engineers India (IEI), Member of Indian society for technical education (MISTE), Member of Engineers Registration Board (ERB), Dar Es Salaam, Tanzania and Member of Ecological Society of Eastern Africa (ESEA), Kenya.

A HYBRID MOM/FDTD FORMULATION FOR EMC/EMI PROBLEMS OF METALLIC ENCLOSURES WITH APERTURES

Josiah K. Makiche¹
jkmakiche@yahoo.co.uk

Dominic B. O. Konditi²,
konditi_dom@yahoo.co.uk

Heywood A. Ouma³
houma@ieee.org

¹Department of Telecommunication and Information Engineering, Jomo Kenyatta University of Agriculture and Technology. ²Faculty of Engineering, Multimedia University College of Kenya. ³Department of Electrical and Information Engineering, University of Nairobi

Abstract—In this work a hybrid Method-of-Moments/Finite-Difference-Time-Domain (MoM/FDTD) formulation for the analysis of a metallic enclosure with an aperture is developed. The equivalence principle is used to divide the problem into two regions, region 1 and region 2, each of which is treated separately. The induced aperture magnetic currents are obtained via a moments method solution of the mixed potential integral equation using the generalized network formulation and triangular patch modeling. The computed magnetic current is directly incorporated into FDTD formulations as a source to determine the fields in the interior of the enclosure (region 2). The formulations are implemented in a computer code and used to analyze a typical problem of a rectangular enclosure with an aperture. The results are validated using data available in literature.

Keywords: *Shielding effectiveness, metallic enclosures, method of moments, finite difference time domain, EMI/EMC.*

I. INTRODUCTION

The modern society has witnessed a proliferation of high speed electronic devices. The fast current transients characterizing the operation of these devices cause undesirable electromagnetic emissions to be generated. The emissions can interfere with the operation of other neighboring electronic devices constituting electromagnetic interference (EMI). Electromagnetic compatibility (EMC) is an emerging technology which seeks to ensure that all electronic devices adhere to set standards and regulations regarding the levels of EMI.

Many approaches to limit the level of EMI by a device have been developed. One technique commonly used is to enclose the device in a metallic enclosure. Consequently, electronic devices are usually covered in metal coated enclosures for EMI/EMC reasons. These enclosures normally have various apertures for ventilation, cabling, displays among other reasons. The apertures adversely affect the ability of the enclosure to provide the required electromagnetic shielding. It is for this reason that EMI/EMC analysis has taken a prominent role in electronic system design.

An important parameter in enclosure studies is shielding effectiveness (SE). SE of an enclosure may be defined as the ratio of the electromagnetic energy level due to a source at a point without the enclosure to the electromagnetic energy at the same point with

the enclosure. In terms of the electric field, SE may be expressed as

$$SE = -20 \log \left(\frac{|\mathbf{E}|}{|\mathbf{E}_0|} \right) = -20 \log \left(\frac{E}{E_0} \right) \quad (1)$$

where $|\mathbf{E}| = E$ is the magnitude of the electric field at point P with the enclosure and $|\mathbf{E}_0| = E_0$ is the magnitude of the electric field at the same point without the enclosure.

SE of an enclosure can be estimated analytically, numerically or experimentally. Analytical methods include transmission line analogy [2] and circuit theory [3]. Analytical techniques demand that considerable simplification of the problem be made so that existing closed mathematical formulae can be applied. This simplicity is achieved at the expense of accuracy of final solution. These techniques are therefore only applicable to problems with simple geometries. Experimental methods, while potentially the most reliable, can be expensive and time consuming even for simple problems. Numerical methods provide a convenient way of determining the SE of an enclosure where experimental work can be time consuming and/or analytical expressions become too complicated. This is because most of the computational work involved can be carried out by a computer. The full wave analysis of Maxwell's equations characterizing numerical techniques also ensure that the solution can be carried to any desired

order of accuracy depending on the available computational resources.

An excellent survey of numerical methods commonly used is given in [4]. These techniques include Finite Difference Time Domain (FDTD), Method of Moments (MoM), Finite Element Method (FEM) and Transmission Line Matrix (TLM). The merits and demerits of each technique are discussed in literature.

The choice of numerical technique to use generally depends on the geometry of the problem and the accuracy of desired solution. Some problems may have complex geometries with inhomogeneities so that application of one numerical method is not computationally feasible. In such cases, the equivalence principle [5] is used to sub-divide the problem into various smaller problem segments. Each problem segment is solved independently using the most suitable technique. The final solution to the entire problem is a cascaded combination of the solutions to the various problem segments. Such solution techniques are termed hybrid or mixed. Some hybrid solutions to EMI/EMC problems are reported in [6-8].

II. GEOMETRY OF THE PROBLEM

Figure 1 shows a typical rectangular metallic enclosure with dimensions $l \times w \times h$ and one rectangular aperture on its left end face. The enclosure is illuminated by a z polarized incident plane wave. The enclosure walls are assumed to be made of PEC material. This means that the penetration of the fields inside and outside the enclosure is only through the aperture. The main goal is to determine the shielding effectiveness of the enclosure using equation (1).

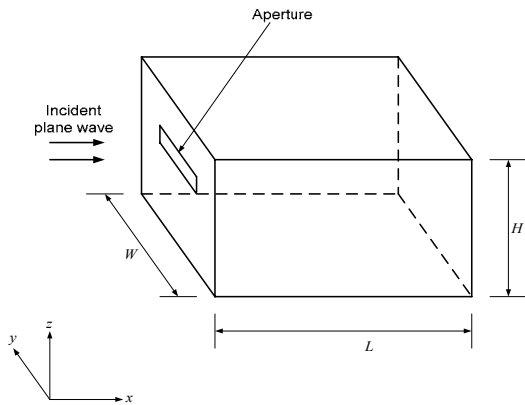


Figure 1: Geometry of the problem

III. FORMULATION OF THE PROBLEM

Determination of Equivalent Aperture Magnetic Currents

The original problem in figure 1 can be separated into two regions, region 1 and region 2 as shown in figure 2. The fields in region 1 are a superposition of the incident fields \mathbf{H}^i and the fields due to equivalent surface magnetic currents $2\mathbf{M}_1$ over the aperture region radiating into free space. The field in region 2 is only due to the equivalent surface magnetic current $-\mathbf{M}_1$ over the aperture region. The total magnetic field in region 1 is

$$\mathbf{H}_1^{tot} = 2\mathbf{H}_1^t(\mathbf{M}_1) + \mathbf{H}_i^t \quad (2)$$

where \mathbf{H}_1^{tot} the total magnetic field in region 1 while $\mathbf{H}_1^t(\mathbf{M}_1)$ and \mathbf{H}_i^t , is the tangential magnetic field due to magnetic current and tangential incident magnetic field respectively. In region 2,

$$\mathbf{H}_2^{tot} = -2\mathbf{H}_2^t(\mathbf{M}_1) \quad (3)$$

where \mathbf{H}_2^{tot} and $\mathbf{H}_2^t(\mathbf{M}_1)$ are the total tangential magnetic field and tangential magnetic field due to magnetic current in region 2 respectively. To

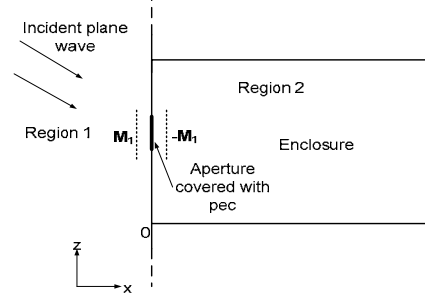


Figure 2: Equivalent problem for the interior and exterior regions

ensure that the electric field is continuous through the aperture, equation (3) and (4) must be equal i.e.

$$2\mathbf{H}_1^t(\mathbf{M}_1) + \mathbf{H}_i^t = -2\mathbf{H}_2^t(\mathbf{M}_1) \quad (4)$$

Equation (4) is an operator equation which can be solved using the method of moments. The solution is based on the generalized network formulation for aperture problems as discussed in [5, 9]. The unknown magnetic currents are first expanded to obtain

$$\mathbf{M}_1 = \sum_n V_n \mathbf{M}_n \quad (5)$$

where V_n are unknown coefficients to be determined and M_n is a suitable expansion (basis) function. By choosing an inner product of the form

$$\langle \mathbf{A}, \mathbf{B} \rangle = \iint_{\text{aperture}} \mathbf{A} \cdot \mathbf{B} dS' \quad (6)$$

where S' is the area of the aperture, and testing function W_m , equation (5) can be reduced into a matrix equation of the form

$$[Y_1 + Y_2] \mathbf{V} = \mathbf{I}_i \quad (7)$$

where

$$[Y_1] = 2[\langle W_m, H_1^t(M_n) \rangle]_{N \times N} \quad (8)$$

is the admittance matrix for region 1.

$$[Y_2] = 2[\langle W_m, H_2^t(M_n) \rangle]_{N \times N} \quad (9)$$

is the admittance matrix for region 2.

$$\mathbf{I}^i = [-\langle W_m, H_i^t \rangle]_{N \times 1} \quad (10)$$

is the matrix containing the incident field and

$$\mathbf{V} = [V_n]_{N \times 1} \quad (11)$$

is the vector of unknown coefficients (voltage vector). Therefore the resultant voltage vector is

$$\mathbf{V} = [Y_1 + Y_2]^{-1} \mathbf{I}_i \quad (12)$$

This gives the vector of coefficients which can be used to determine \mathbf{M}_1 according to equation (6).

Evaluation of Matrix Elements

Since there are no sources at the boundary between the two regions, and assuming time harmonic fields, the magnetic potential integral equation for the aperture may be written as

$$\mathbf{H}_i^t = -j\omega \mathbf{F}(\mathbf{r}) - \nabla \phi(\mathbf{r}) \quad (13)$$

where $\mathbf{F}(\mathbf{r})$ and $\phi(\mathbf{r})$ are the electric vector potential and magnetic scalar potentials respectively. These potentials may be expressed as

$$\mathbf{F}(\mathbf{r}) = \varepsilon_0 \iint_S \mathbf{M}_1(\mathbf{r}) G(\mathbf{r}, \mathbf{r}') dS' \quad (14)$$

$$\phi(\mathbf{r}) = -\frac{\nabla \cdot \mathbf{F}}{j\omega \varepsilon_0 \mu_0} = \frac{j}{\omega \mu_0} \iint_S \nabla \cdot \mathbf{M}_1(\mathbf{r}) G(\mathbf{r}, \mathbf{r}') dS' \quad (15)$$

Equation (16) is the Lorenz gauge transformation. If we denote the magnetic charge density as ρ^m the magnetic current will be related to its corresponding

charges density by the equation of continuity which may be written as

$$-j\omega \rho^m(\mathbf{r}') = \nabla \cdot \mathbf{M}_1(\mathbf{r}') \quad (16)$$

The scalar potential may then be expressed in terms of the magnetic charge density as

$$\phi(\mathbf{r}) = \frac{1}{\mu_0} \iint_S \rho^m(\mathbf{r}') G(\mathbf{r}, \mathbf{r}') dS' \quad (17)$$

$G(\mathbf{r}, \mathbf{r}')$ is the three dimensional Green's function given by

$$G(\mathbf{r}, \mathbf{r}') = \frac{e^{-jk|\mathbf{r}-\mathbf{r}'|}}{4\pi|\mathbf{r}-\mathbf{r}'|} \quad (18)$$

\mathbf{r} and \mathbf{r}' denote the field and source point coordinates respectively.

We use triangular patch modeling proposed in [10]. The aperture region is subdivided into small triangular cells each of which is treated separately. A pair of triangular faces denoted T_n^+ and T_n^- and having an n^{th} edge AB as their common edge are shown in the figure 3. The local and global position vectors at any point within the triangle are denoted $\bar{\rho}_n^\pm$ and \mathbf{r} respectively. Any point within a particular triangle may be located with respect to the local co-ordinate system or the global co-ordinate system as shown. A vector basis function associated with the n^{th} edge is defined as [14]

$$\mathbf{M}_n = \begin{cases} \frac{l_n}{2A_n^+} \mathbf{r} \text{ in } T_n^+ \\ \frac{l_n}{2A_n^-} \mathbf{r} \text{ in } T_n^- \\ 0 \quad \text{otherwise} \end{cases} \quad (19)$$

where l_n is the length of the n^{th} edge and A_n^\pm is the area of the triangle T_n^\pm . The designation T_n^+ and T_n^- is determined by choosing a positive current reference direction for the n^{th} edge, which is assumed to be from T_n^+ to T_n^- . The associated equivalent magnetic charge density for the n^{th} edge is given using (17) as,

$$\rho_n^m = \frac{1}{j\omega} \nabla \cdot \mathbf{M}_n = \begin{cases} \frac{-I_n}{j\omega A_n^+} & \text{rin } T_n^+ \\ \frac{+I_n}{j\omega A_n^-} & \text{rin } T_n^- \\ 0 & \text{otherwise} \end{cases} \quad (20)$$

It is found that ρ_n^m is constant in each triangle and the total charge associated with T_n^+ and T_n^- is zero.

For simplicity, we follow Galerkin's procedure so that $\mathbf{W}_m = \mathbf{M}_m$. Implementing equations (14-18) over the region in Figure 3 and following the procedure described by Konditi and Sinha [11], the integrals over T_m^\pm are approximated by their values at the centroids of the triangles to obtain

$$Y_{mn}^r = -2l_m \left\{ j\omega \left[\mathbf{F}_n(\mathbf{r}_m^{c+}) \cdot \frac{\bar{\rho}_m^{c+}}{2} + \mathbf{F}_n(\mathbf{r}_m^{c-}) \cdot \frac{\bar{\rho}_m^{c-}}{2} \right] + \phi_n(\mathbf{r}_m^{c-}) - \phi_n(\mathbf{r}_m^{c+}) \right\} \quad (21)$$

where Y_{mn}^r is an element of the admittance matrix in the r^{th} region and

$$\mathbf{F}_n(\mathbf{r}_m^{c\pm}) = \varepsilon^r \iint_{T_n^\pm} \bar{G}(\mathbf{r}^{c\pm}, \mathbf{r}') \cdot \mathbf{M}_n(\mathbf{r}') ds \quad (22)$$

$$\phi_n(\mathbf{r}_m^{c\pm}) = \frac{-1}{j\omega\mu^r} \iint_{T_n^\pm} \nabla \bar{G}(\mathbf{r}^{c\pm}, \mathbf{r}') \cdot \mathbf{M}_n(\mathbf{r}') ds \quad (23)$$

In the above equations, $\bar{\rho}_m^{c\pm}$ are the local position vectors of the centroids of T_m^\pm and $\mathbf{r}_m^\pm = (\mathbf{r}_m^{1\pm} + \mathbf{r}_m^{2\pm} + \mathbf{r}_m^{3\pm})/3$ are the position vectors of the centroids of T_m^\pm with respect to the global co-ordinate system. An element of the excitation vector in equation (11) may be written as

$$I_m^i = -l_m \left(\mathbf{H}_t^i(\mathbf{r}_m^{c+}) \cdot \frac{\bar{\rho}_m^{c+}}{2} + \mathbf{H}_t^i(\mathbf{r}_m^{c-}) \cdot \frac{\bar{\rho}_m^{c-}}{2} \right) \quad (24)$$

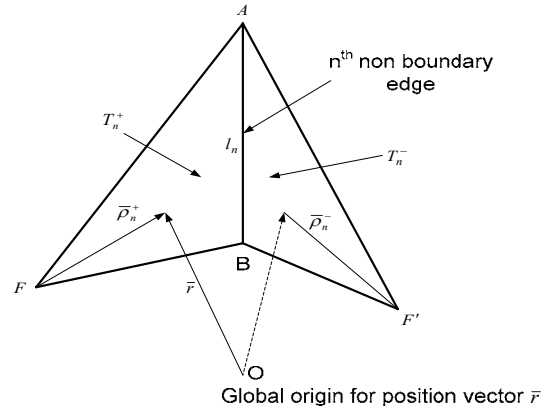


Figure 3: Triangle pair associated with the n^{th} edge

The evaluation of the integrals in equation (22) depends on whether the Kernel of a particular integral is bounded or unbounded over the integration domain. If the kernel is bounded, numerical quadrature is used. For unbounded Kernels, we use a procedure proposed in [10]. The evaluation of the elements of the excitation vector also follows the procedure detailed in [11].

FDTD Formulations

Thus far, the induced magnetic currents at the aperture by the known incident fields in region 1 have been determined using the method of moments. The next step is to use these currents to obtain the fields in region 2. One approach would be to compute these fields using the potentials with these induced aperture currents as the source. This approach however has three main limitations: Firstly, the Kernels of the resultant integral equations are usually difficult to integrate. Secondly, such an approach would only be applicable to an empty or homogeneously filled enclosure and finally, the results obtained only apply to a single mode. To overcome these limitations, FDTD is proposed for the analysis of the fields in region 2. FDTD is based on the direct solution to Maxwell's curl equations given as

$$\nabla \times \mathbf{E} = -\mu \frac{\partial \mathbf{H}}{\partial t} + \mathbf{M} \quad (25)$$

$$\nabla \times \mathbf{H} = \varepsilon \frac{\partial \mathbf{D}}{\partial t} + \mathbf{J} \quad (26)$$

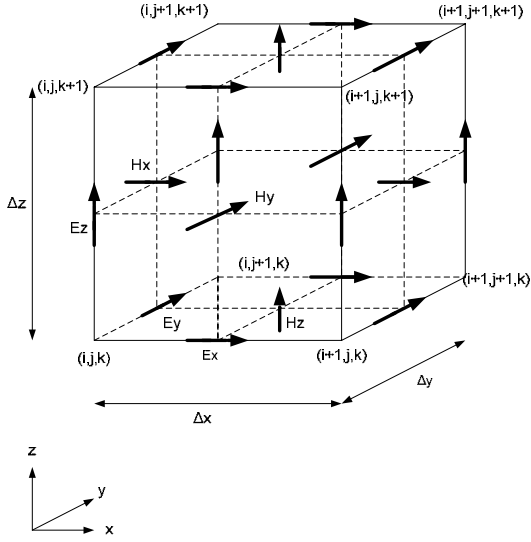


Figure 4: Three dimensional Yee cell

The FDTD procedure entails discretization of the region through which the field propagates using the Yee cell shown in figure 4. The fields can then be iteratively determined at specific points in the Yee cell using equations (26) and (27) with the spatial and temporal derivatives replaced with central finite differences. Using the indices i, j, k, n where $x = i\Delta x$, $y = j\Delta y$, $z = k\Delta z$ and $t = n\Delta t$, the following system of update equations are obtained from (25) and (26),

$$H_x^{n+\frac{1}{2}}(i, j + \frac{1}{2}, k + \frac{1}{2}) = H_x^{n-\frac{1}{2}}(i, j + \frac{1}{2}, k + \frac{1}{2}) + \frac{\Delta t}{\mu(i, j + \frac{1}{2}, k + \frac{1}{2})} \cdot \left(\frac{E_y^n(i, j, +\frac{1}{2}k + 1) - E_y^n(i, j + \frac{1}{2}, k)}{\Delta x} - \frac{E_z^n(i, j + 1, k + \frac{1}{2}) + E_z^n(i, j, k + \frac{1}{2})}{\Delta y} \right) + M_x \quad (29)$$

$$H_y^{n+\frac{1}{2}}(i + \frac{1}{2}, j, k + \frac{1}{2}) = H_y^{n-\frac{1}{2}}(i + \frac{1}{2}, j, k + \frac{1}{2}) + \frac{\Delta t}{\mu(i + \frac{1}{2}, j, k + \frac{1}{2})} \cdot \left(\frac{E_z^n(i + 1, j, k + \frac{1}{2}) - E_z^n(i, j, k + \frac{1}{2})}{\Delta x} - \frac{E_x^n(i + \frac{1}{2}, j, k + 1) + E_x^n(i + \frac{1}{2}, j, k)}{\Delta y} \right) + M_y \quad (30)$$

$$H_z^{n+\frac{1}{2}}(i + \frac{1}{2}, j + \frac{1}{2}, k) = H_z^{n-\frac{1}{2}}(i + \frac{1}{2}, j + \frac{1}{2}, k) + \frac{\Delta t}{\mu(i + \frac{1}{2}, j + \frac{1}{2}, k)} \cdot \left(\frac{E_x^n(i + \frac{1}{2}, j + 1, k) - E_x^n(i + \frac{1}{2}, j, k)}{\Delta y} - \frac{E_y^n(i + 1, j + \frac{1}{2}, k) + E_y^n(i, j + \frac{1}{2}, k)}{\Delta z} \right) + M_z \quad (31)$$

$$E_x^{n+1}(i + \frac{1}{2}, j, k) = E_x^n(i + \frac{1}{2}, j, k) + \frac{\Delta t}{\varepsilon(i + \frac{1}{2}, j, k)} \left(\frac{H_z^{n+\frac{1}{2}}(i + \frac{1}{2}, j + \frac{1}{2}, k) - H_z^{n+\frac{1}{2}}(i + \frac{1}{2}, j - \frac{1}{2}, k)}{\Delta y} - \frac{H_y^{n+\frac{1}{2}}(i + \frac{1}{2}, j, k + \frac{1}{2}) + H_y^{n+\frac{1}{2}}(i + \frac{1}{2}, j, k - \frac{1}{2})}{\Delta z} \right) \quad (32)$$

$$E_y^{n+1}(i, j + \frac{1}{2}, k) = E_y^n(i, j + \frac{1}{2}, k) + \frac{\Delta t}{\varepsilon(i, j + \frac{1}{2}, k)} \left(\frac{H_x^{n+\frac{1}{2}}(i, j + \frac{1}{2}, k + \frac{1}{2}) - H_x^{n+\frac{1}{2}}(i, j + \frac{1}{2}, k - \frac{1}{2})}{\Delta z} - \frac{H_z^{n+\frac{1}{2}}(i + \frac{1}{2}, j + \frac{1}{2}, k) + H_z^{n+\frac{1}{2}}(i - \frac{1}{2}, j + \frac{1}{2}, k)}{\Delta x} \right) \quad (33)$$

$$E_z^{n+1}(i, j, k + \frac{1}{2}) = E_z^n(i, j, k + \frac{1}{2}) + \frac{\Delta t}{\varepsilon(i, j, k + \frac{1}{2})} \left(\frac{H_y^{n+\frac{1}{2}}(i + \frac{1}{2}, j, k + \frac{1}{2}) - H_y^{n+\frac{1}{2}}(i - \frac{1}{2}, j, k + \frac{1}{2})}{\Delta x} - \frac{H_x^{n+\frac{1}{2}}(i, j + \frac{1}{2}, k + \frac{1}{2}) + H_x^{n+\frac{1}{2}}(i, j - \frac{1}{2}, k + \frac{1}{2})}{\Delta y} \right) \quad (34)$$

Before implementing (29-34), suitable cell dimensions $\Delta x, \Delta y, \Delta z$ need to be established. The selected cell size should be able to give a sufficiently accurate solution with minimum computation resources. Experience has shown that for sufficiently accurate results, the cell dimension should at least be a tenth of the shortest wavelength (wavelength at highest frequency). Also to avoid dispersion errors, the smallest cell dimension should at least be a third of the highest cell dimension. For example, if Δx is the smallest cell dimension and Δz is the largest, $\Delta x \geq \Delta z/3$. The choice of Δt is dictated by the Courant stability condition which requires that

$$\Delta t \leq \frac{1}{c(1/\Delta x^2 + 1/\Delta y^2 + 1/\Delta z^2)^{1/2}} \quad (35)$$

The induced aperture magnetic currents are directly incorporated into FDTD update equations as sources thereby eliminating the need for integral equations altogether. Also FDTD is most suited for problems involving complex geometries with inhomogeneities and is therefore an ideal choice since the enclosure must enclose some object in the general EMI/EMC problems of practical interest.

Since MoM is a frequency domain technique while FDTD is in time domain, some form of matching is needed for the hybrid model to be realizable. To achieve this, the magnitude of the current is directly incorporated into the FDTD update equations but its phase is interpreted as a time delay [13]

IV. NUMERICAL RESULTS

The preceding formulations were implemented in a computer code. In this section, some results obtained using the hybrid MoM/FDTD formulations developed are presented.

Validation of Formulation

To validate the formulations, a rectangular enclosure measuring 30cm × 30cm × 12cm with a rectangular aperture located at the centre of the front wall measuring 20cm × 3cm as shown in figure 5 below is chosen. This choice is dictated by the fact that the results for this problem are available in literature.

Variation of Aperture Width, Length constant

Shielding effectiveness is computed at the centre of the enclosure using the formulation developed. The results are compared with those available in reference [10] and found to be in agreement as shown in the figure 6 below.

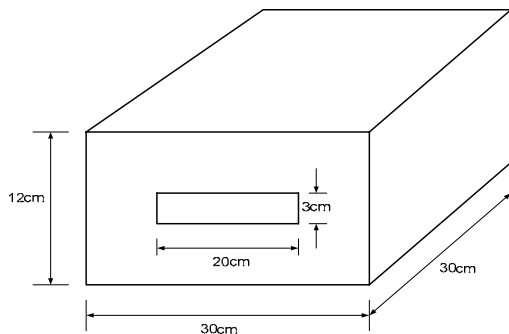


Figure 5: Enclosure used for validation with a centrally located 20 × 3cm aperture

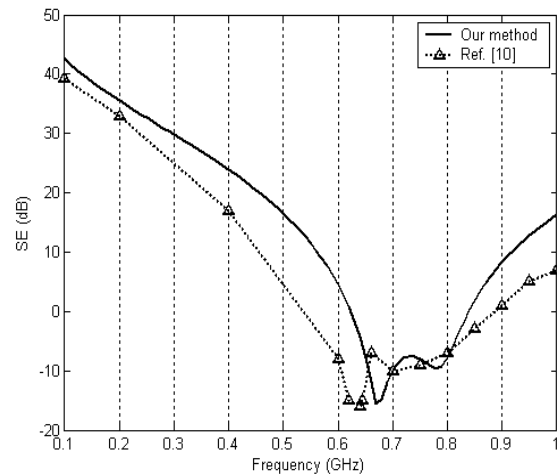


Figure 6: Electric shielding effectiveness at the centre of a 30cm × 30cm × 12cm rectangular enclosure with a centrally located 20cm × 3cm aperture

From the figure it is deduced that the first resonance frequency is approximately 0.68GHz. Due to the presence of the aperture, the first resonance drops to about 0.68GHz from 0.707GHz for a completely closed enclosure.

To study the effect of varying the width of the aperture with the length kept constant, an enclosure with dimensions 55cm × 50cm × 40cm is considered. An aperture measuring 20cm × 2cm is centrally located on the front face just like the previous case shown in figure 5.

From the plots, it is seen that no major variation of shielding effectiveness occurs for varying aperture width. This is in line with the well known fact that SE depends on the longest dimension of the aperture and not aperture area.

Variation of Aperture Length/Width Ratio, Area Constant

The enclosure used in the previous study is considered. In this case however, the aperture length to width ratio is varied but the area of the aperture is kept constant at 40cm². Like in the previous case, the electric shielding effectiveness at the centre of the enclosure is computed and the data obtained plotted in figure 8.

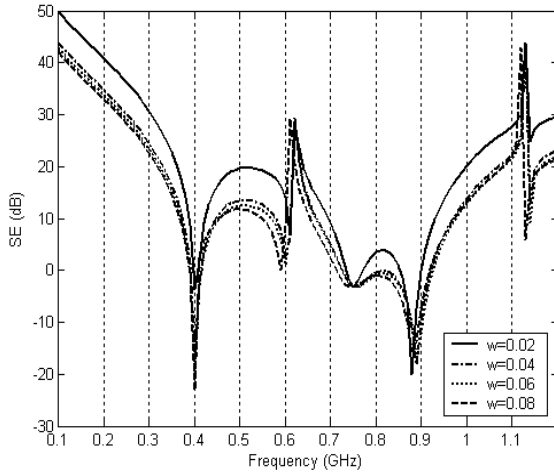


Figure 7: Shielding effectiveness of a rectangular $55\text{cm} \times 50\text{cm} \times 40\text{cm}$ enclosure with a centrally located aperture with its length to width ratio varied while area kept constant at 40cm^2

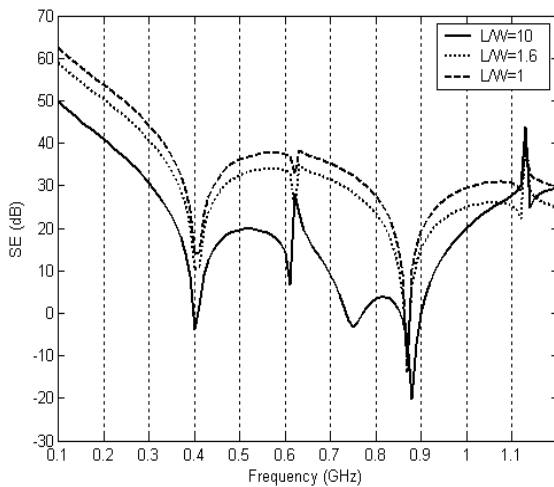


Figure 8: Electric shielding effectiveness at the centre of a $55\text{cm} \times 50\text{cm} \times 40\text{cm}$ rectangular enclosure with a centrally located aperture with its length to width ratio varied while area kept constant at 40cm^2

From the figure, it is observed that the higher the length/width ratio the lower the shielding effectiveness. This observation only applies for cases where $l > w$. Hence, square apertures are better than rectangular apertures provided that the horizontal dimension of the aperture is greater than the vertical dimension. In all these cases however, the resonant frequencies don't change.

Shielding Effectiveness Computed at Different Positions in the Enclosure

Shielding effectiveness is computed at different locations within the same enclosure considered in the previous studies. The locations considered are points P located on a central axis perpendicular to the $20\text{cm} \times 2\text{cm}$ aperture as shown in Figure 9

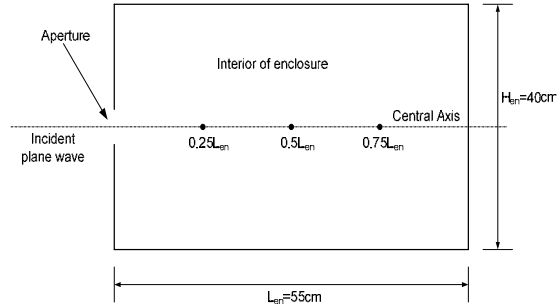


Figure 9: Cross-sectional view of enclosure showing various positions at which SE is computed.

We denote the length of the enclosure by L_{en} . Shielding effectiveness is computed at points $P = 0.25L_{en}$, $P = 0.5L_{en}$, and $P = 0.75L_{en}$ and results plotted in figure 10.

From the figure is observed that SE improves as point P is moved deeper into the enclosure. This is expected since the further P is from the aperture, the less the likelihood of external electromagnetic interferences. Hence, noisy devices should be situated as far as possible from the aperture.

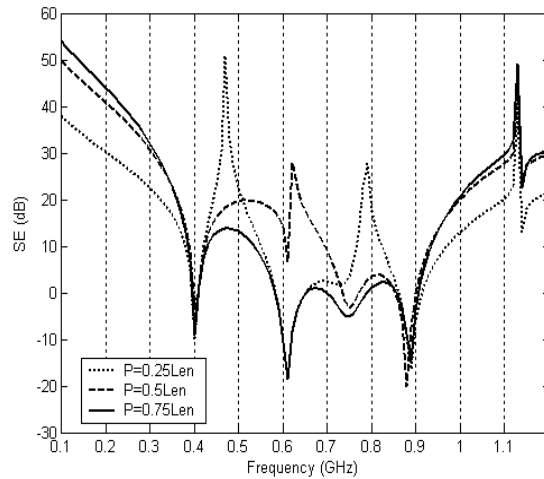


Figure 10: Electric shielding effectiveness at the centre of a $55\text{cm} \times 50\text{cm} \times 40\text{cm}$ rectangular enclosure with a centrally located $20\text{cm} \times 3\text{cm}$ aperture at various positions within the enclosure.

V. CONCLUSION

The electric shielding effectiveness of a rectangular 55cm × 50cm × 40cm enclosure with one rectangular aperture on the end face is investigated using a hybrid MoM/FDTD formulation. The results obtained agree fairly well with the data in open literature. Although the study here is limited to one aperture, the formulation can be applied to an aperture of any shape [11] and to any number of apertures. The use of FDTD for the enclosure region makes it possible to introduce inhomogeneities in the interior of the enclosure without generating additional numerical difficulties. Also the need for an absorbing boundary condition is eliminated since the computational domain is terminated in a perfect electric conductor (PEC) material.

REFERENCES

- [1] Archambeault, B., Brench, C. and Ramahi, O. M., *EMI/EMC computational modeling handbook (2nd Ed.)*, Kluwer Academic Publishers.
- [2] R. Azaro, S. Caorsi, M. Donelli, G. L. Gagnani, "Evaluation of the effects of an external incident electromagnetic wave on metallic enclosure with rectangular apertures", *Microwave and Optical Technology Letters*, Vol. 28, No. 5, March 2005.
- [3] J. E. Bridges, "An Update on the circuit approach to calculate shielding effectiveness", *IEEE Transactions on Electromagnetic Compatibility*, Vol. 30, No. 3, 1998, pp. 211-221.
- [4] Hubing T. H., "Survey of Numerical Modeling Techniques", University of Missouri-Rolla, Electromagnetic Compatibility Laboratory, Report No. TR91-1-001.3, September 1991.
- [5] Harrington R.F, *Field Computation by Moment Methods*, The Macmillan Co., New York, 1968.
- [6] C. Feng and Z. Shen, "A hybrid FD-MoM technique for predicting shielding effectiveness of metallic enclosures with apertures", *IEEE Transactions on Electromagnetic Compatibility*, Vol. 47, 2002, pp. 456-462.
- [7] G. Cerri et al., "Development of a hybrid MOMTD/FDTD technique for EMC problems: analysis of the coupling between ESD transient fields and slotted enclosures", *Int. J. Numer. Model.: Electronic Networks, Devices and Fields*, 12, 245-256, 1999.
- [8] S. Yenikaya, A. Akman, "Hybrid MoM/FEM modeling of loaded enclosure with aperture in EMC problems", *International Journal of RF Microwave Computer Aided Engineering*, Wiley Periodical, 2008.
- [9] A. W. Glisson, D. W. Wilton, "Simple and efficient numerical methods for problems of electromagnetic radiation and scattering from surfaces", *IEEE Transactions on Antennas and Propagation*, Vol. AP-28, No. 5, September 1980.
- [10] S. M. Rao, D. R. Wilton and A. W. Glisson, "Electromagnetic scattering by surfaces of arbitrary shape", *IEEE Trans. Ant. Prop.*, Vol. AP-30, pp. 409-418, 1982.
- [11] D. B. O. Konditi and S. N. Sinha, "Electromagnetic transmission through apertures of arbitrary shape in a conducting screen", *IETE Technical Review*, Vol. 18, Nos. 2&3, March-June 2001, pp. 177-190.
- [12] Peterson A. F., Ray S. L., Mittra R., *Computational Methods for Electromagnetics*, IEEE Press Series on Electromagnetic Waves, 1998.
- [13] Karl S. Kunz, Raymond J. Luebbers, *Finite Difference Time Domain method for Electromagnetics*, CRC Press, Boca Raton, 1993.

AUTOMATION OF CORPORATE SERVICE AVAILABILITY AND SLA REPORTING

G.K. Waguchu J.N. Nderu D.B.O Konditi
gwaguchu@yahoo.com, jnnderu@yahoo.com, dkonditi@mmu.ac.ke

Department of telecommunications Engineering, Jomo Kenyatta University of Agriculture and Technologies

Abstract—The rapid growth of the telecommunication industry has brought with increasing competition of providers with customers increasingly focusing on service quality. The result is an emerging demand for service level guarantees from most corporate customers. Network operations teams are facing challenges in achieving end to end service assurance since the bulky of Service Level Agreements(SLA) are manually managed collecting end data from a number of sources which is a labor intensive, time consuming process and highly prone to human error. Therefore need for researchers to move from reactive management and historical SLA reporting to truly proactive service assurance, in which they monitor, detect, and resolve problems in applications before customer service is impacted. This paper presents the results for real-time automated SLA reports for corporate customers to meet End to End service assurance. This will help to avoid discrepancy between customers and service providers with respect to the service levels defined; in the contract i.e. service level availability (SLA).

Keywords: *SLA- Service level availability, MTBF-Mean Time between Failures, TMM -Total Monthly Minutes, MTTR - Mean Time to Restore.*

I INTRODUCTION

The mobile telephone service provider (MTSP) in Kenya is estimated over 20 million subscribers shared among four network services. With increasing competition in the industry, the four have in various occasion restored to price cuts and promotions to keep or acquire new customers into their network. However customers are no longer interested in price wars by service providers but on quality services [2]. Service Level Agreements (SLA) is signed between two parties for satisfying clients, managing expectations, regulating resources and controlling costs. In order to be competitive in the markets of today, a common way of improving the quality of service is automation of corporate SLA reports [1] that have been manually managed. SLA are fundamental to contract between providers and customers. The measurement of the actual performance against these targets forms the basis for controlling and improving the quality of the service throughout the life of the Agreement. In the event that provider fails to meet the Service Levels and subject to the conditions specified in this SLA, provider will be subjected to the Penalties. The SLA records a common understanding about services, priorities, responsibilities,

guarantees, and warranties. Service providers lack automated systems and methods for determining whether the actual level service provided to a consumer of the service corresponds to the contractual SLA commitment. If a consumer of a service alleges that the actual level of service has failed to meet the contractual SLA commitment, the service provider may need to complete an audit of various records to determine the validity of the complaint. Such an audit may be an onerous process conducted manually by service provider personnel.

Additionally, the records available to a service provider may lack the service level measurements necessary to conduct an audit. Even if records containing service level measurements exist it maybe difficult to correlate the measurements to the commitment. Consumers of the service are unlikely to notify the service provider regarding an actual level of service that exceeds a contractual SLA commitment. Accordingly, service providers may not realize when the actual level of service exceeds such a contractual commitment [3]. Customer service departments of service providers may collect data regarding service

issues. Such data is commonly referred to as a trouble ticket, or simply a ticket, and may be stored in a database system utilized by the customer service department. Tickets generally serve the narrow purpose of facilitating repairs related to the service issue identified therein. However, an aspect of this facilitation may include the recording of certain service level measurements in a ticket.

II NETWORK CHALLENGES

Network operations teams face challenges in achieving end to end service assurance [4]. Therefore the bulky of SLA are manually managed collecting data from a number of sources is a labor intensive, time consuming process and highly prone to human error. Because of the importance of the critical business services to their customers, operations teams must move from reactive management and historical SLA reporting to truly proactive service assurance.

III METHODOLOGY

We make reporting on SLA compliance automatic to simplify “end-of” time periods that can otherwise be extremely rushed, error-prone. Research in the SLA can be performed within the following procedures. This is the first step to identify the problem on the ground and has been cited in the introduction ; For automated SLA reporting, first things is to minimize customers and technicians involvement on reporting time when the fault occurred and fixing problem respectively. This minimize Mean Time to Repair (MTTR) by finding and fixing problems quickly Increase MTBF by preventing problems from occurring in the first .Complicating the topic of SLAs is the issue of the locations from which these measurements are taken.

In order to ensure that guaranteed SLAs can be evaluated and their compliance measured, it is necessary that raw measurement data be collected about the managed system. The instance data collected has to be modeled in the high performance database and a data warehouse so that service level agreements can be monitored on top of the modeled data. The high performance database is updated for every transaction instance data that is received. This

system SLA was only consider normal working hour from 8.am to 5.am excluding lunch hour.

On proposed system database for SLA client was created defining current link status. Script for SLA formulation was developed. Service availability will be maintained at the minimum levels of 99.9% averaged over a period of one (1) month’s service outage occurrence: The service availability objective was calculated using the following formula:

$$\text{Availability (A)} = \frac{(\text{TMM} - \text{MTTR})}{\text{TMM}} \times 100\% \quad (\text{EQ 1})$$

where TMM is Total monthly minutes and MTTR is mean time to restore.

IV RESULTS AND DISCUSSION

Automated corporate weekly SLA report was generated by proposed system as shown in table 1 and table 2 below. Table 1 results show availability connectivity per SLA client while table 2 shows availability for SLA clients. All the outages were stored on database Each Sla client was assigned with unique user ID as shown in the tables. To generate SLA report client is signed up and database is successfully created.

Report link for any outages occurring on client was built, signal was triggered by clicking the mouse and it was automatically stored in the database as start time when the outages happened on client link.

Repairing outages on client link was conducted and to ensure controllability on the system Stall and resume signals were triggered .This was recorded on the database .Final signal coding end time signal was triggered by clicking of mouse and automatically stored on database showing link was restored. Query was made by selecting client availability report option (daily weekly and monthly) and report was generated automatically. Daily, weekly& monthly MTTR was the cumulative total for all outages occurred on the link and was stored on database to generate report.

V CONCLUSION

The purpose of this research was automating corporate service availability and SLA reporting. We developed a system for automating SLA report. It can be concluded that the built system successfully generated weekly availability report and our objective for this search was meet.

[5]. Long T P, Jong W B, Woon HJ. Management of service level agreements for multimedia Internet service using a utility model. IEEE communications Managezine Vol 39, no.5, May 2001 proceedings of NOMS 96.

Table 1: Weekly SLA report

Repair Logs			
userid	ticket	time reported	report
e19	33600	2010-06-30 23:35:58	Start
e19	33600	2010-06-30 23:36:07	Stall
e19	33600	2010-06-30 23:36:16	Resume
e19	33600	2010-06-30 23:36:25	End
e30	13931	2010-07-05 20:52:09	Start
e30	13931	2010-07-05 20:52:31	Stall
e30	13931	2010-07-05 20:52:41	Resume
e30	13931	2010-07-05 20:53:10	End
e32	40509	2010-07-06 10:52:33	Start
e32	40509	2010-07-06 10:55:38	Stall
e32	40509	2010-07-06 10:56:14	Resume
e32	40509	2010-07-06 10:56:29	End

Client records selected for display is: e30

13931:
Seconds: 29 + 22 = 51
minutes 0.85

Total minutes 0.85

Available connection: 99.991145833333%

Table 2: Availability for Sla clients.

Service Availability Report				
userid	Current link status		Service Availability	
	main	redundancy	Core network	Access network expected
e30	Healthy	none	99.99%	99.991145833333%
e32	Healthy	none	99.99%	99.965277777778%

VI REFERENCES

[1] Sahai A, Durante A, Machiraju V. Towards Automated SLA Management. HPL-2001-310

[2] Ajay R.Mishra.Advanced cellular network planning and optimization John Wiley &Son LTD pg 412-414.2007

[3] Bhoj P, Singhal S, Chutani S. SLA Management in a federated Environment. HPL-98-203.

[4]. Lewis D, Bjerring L. An inter-domain Virtual Private Network Management System. In the

FINGER MOTION PATTERN ESTIMATION FROM SURFACE-EMG SIGNALS USING SVM

Kazuki Kojima
o3128010@edu.gifu-u.ac.jp

Satoshi Ito
satoshi@gifu-u.ac.jp

Minoru Sasaki
sasaki@gifu-u.ac.jp

Human and Information Systems Dept. Faculty of Engineering, Gifu University
1-1 Yanagido Gifu, Gifu JAPAN 501-1193

Abstract—This paper introduces the Support Vector Machine (SVM) and its application to the classification of finger motion patterns from EMG (Electromyography). The voltage levels of EMG signals are low and susceptible to noise. This makes it difficult to accurately classify EMG signals to ascertain motion patterns. The Support Vector Machine has characteristics which are advantageous in reducing the effect of noise. This paper examines the effectiveness of the Support Vector Machine in classifying EMG signals for motion estimation. The estimates, which proved to be correct over 70% of the time, were applied to the control of a prosthetic arm.

1 INTRODUCTION

The EMG signal is considered to be applicable to the control of prosthetic arms and legs. Many studies have been done in this area [1], [9], [12]. Otto Bock Corporation in Germany manufactures a prosthetic hand typical of the ones available today [13]. The product is able to perform “Grasp” and “Open” but is still expensive and inconvenient. Other motions such as the flexing and extension of the fingers and wrist would be required before the product can see wide usage.

A surface-EMG consists of a set of complex signals from many muscle fibers around the measuring electrode. This signal is affected by many different muscle fibers [2], thus the action of an individual muscle is hard to discern. Furthermore, the voltage level of an EMG signal is very low and susceptible to noise. Nevertheless, EMG signals have many advantages. Surface-EMGs are easily measured by electrodes attached to a person’s skin. Moreover, it is possible to estimate force from EMG signals. This makes the EMG signal an excellent candidate for the control of prosthetics. As a first step, this paper aims to estimate finger motion pattern from surface-EMG signals.

Many aspects of EMG signals and their application have been studied [10], [11], [14], [15]. Of special interest were finger angle estimation by fuzzy methods [6] [7]. These studies indicate that pattern recognition or a learning algorithm is necessary for motion estimation, especially since the EMG signals varies from person to person.

In this paper, we introduce the use of a Support Vector Machine for pattern recognition in order to

classify and distinguish finger movements. The characteristics of a Support Vector Machine are summarized by its generalization and its kernel, the proper selection of which allows it to classify unseen data. Good performance is expected from the Support Vector Machine in this application and we intend to investigate the achievable recognition rate. If complex motions can be recognized from their EMGs, bio-signals may be used in human interfaces for such applications as video games and rehabilitation equipment in the near future.

2 SUPPORT VECTOR MACHINE

Support Vector Machines (SVMs) are learning systems that use a hypothesis space of linear functions in a higher dimensional feature space [3]. SVMs are designed for pattern classification. Accurate classification depends on suitable values for the SVM’s generalization and kernel.

Consider an input vector: $\mathbf{x} = (x_1, \dots, x_n)^T$, The vector: \mathbf{w} defines a direction perpendicular to the hyperplane, while varying the value of b moves the hyperplane parallel to itself. And the hyperplane defined by the equation $\langle \mathbf{w} \cdot \mathbf{x} \rangle + b = 0$. We consider the case where $f(x)$ is a linear function of $x \in X$, so that it can be written.

$$\begin{aligned} f(x) &= \langle \mathbf{w} \cdot \mathbf{x} \rangle + b \\ &= \sum_{i=1}^n w_i x_i + b \end{aligned}$$

The kernel is a function K defines by the equation.

$$K(\mathbf{x}, \mathbf{z}) = \langle \phi(\mathbf{x}) \cdot \phi(\mathbf{z}) \rangle$$

For all $x, z \in X$ is a mapping from X to an inner product feature space F . It is a fixed non-linear mapping which transforms the data to a feature space for classification. The high dimensional property of the feature space enhances the classification process by the linear learning machine.

We use a RBF (radial basis function) kernel which has the form

$$K(\mathbf{x}, \mathbf{z}) = \exp(-\lambda \|\mathbf{x} - \mathbf{z}\|^2)$$

The generalization of a Support Vector Machine refers to its ability to classify data not in its training set. It is this generalization ability which allows the recognition of un-seen data. Theoretical investigations of generalization were done by Vapnik and Chervonenkis. Reference [3] provides more detail.

3 EXPERIMENT EQUIPMENT

A WEB-9500 Multi Telemeter System by Nihon Kohden Industry Corporation is used for EMG measurement. The system consists of a wireless receiver and transmitter pair. The actual EMG signals were measured with Ag/AgCl electrodes applied using bio-signal pastes to decrease impedance. Figure 1 shows a diagram of the measurement system.

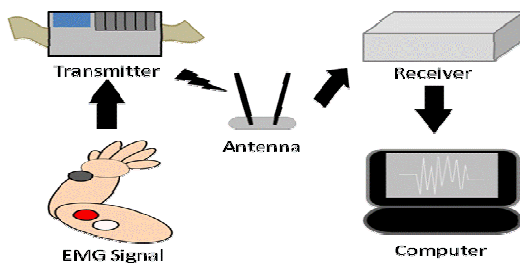


Figure 1 Measurement system

The Support Vector Machine algorithm was implemented using Lib-SVM by Prof. Lin of National Taiwan University. It is available at http://www.support-vector-machines.org/SVM_soft.html.

4 EXPERIMENT METHOD

One goal of this paper is to examine whether a Support Vector Machine can successfully classify finger motion patterns based on EMG signals. Four electrodes were attached to obtain data from the following muscles: a) the Flexor digitorum

superficialis muscle, b) the Flexor digitorum profundus muscle, c) the Flexor pollicis longus muscle, and d) the Extensor digitorum muscle.

Three male subjects are asked to perform two different kinds of motions: individual motion and pair motion. In the individual motion, each finger was quickly flexed and then extended individually twice. And in the pair motion, the thumb and one of fingers were simultaneously flexed and then extended twice. Thus, one series of the data contains ten flexion-and-extensions in the individual motion, with eight from pair motion. Three series were executed continuously in both measurements with short intervals intervening.

During the measurements, four channels of surface-EMG signal were recorded with a 2kHz sampling rate. A 60Hz ham filter was used to avoid AC interference. Finally, averaged rectified values (ARV) were calculated from these signals.

The ARV data is processed to generate teaching and test data. In order to detect the data area that contains actual motion, the peak point in the sum of four ARV signals was found. Then, the surrounding 200 points of time-series data was extracted as the data area so that this peak point became the center. From this area, a quaternity of ARV data was constructed simultaneously from four series of EMG signals. Consequently, 200 4-dimensional discrete data (we call them one data set) was obtained from one series of measurement data.

Two sets of discrete data can be prepared for the same flexion-and-extension because the subject executed such motion twice. Thus, the data set from the first motion was used as the teaching data while the data set from the second motion as the test data. Nine combinations of the teaching and test data were possible: (1,1), (1,2), (1,3), (2,1), (2,2), (2,3), (3,1), (3,2), (3,3), where (3,2), for example, means that the data set in the third measurements was used as the teaching data, and the data set in the second measurements was used as the test data.

4-dimensional teaching data were inputted to Lib-SVM. After the learning, each test data was inputted. The Support Vector Machine then outputted classification results. The rate of the correct classification was investigated.

5 EXPERIMENT RESULT

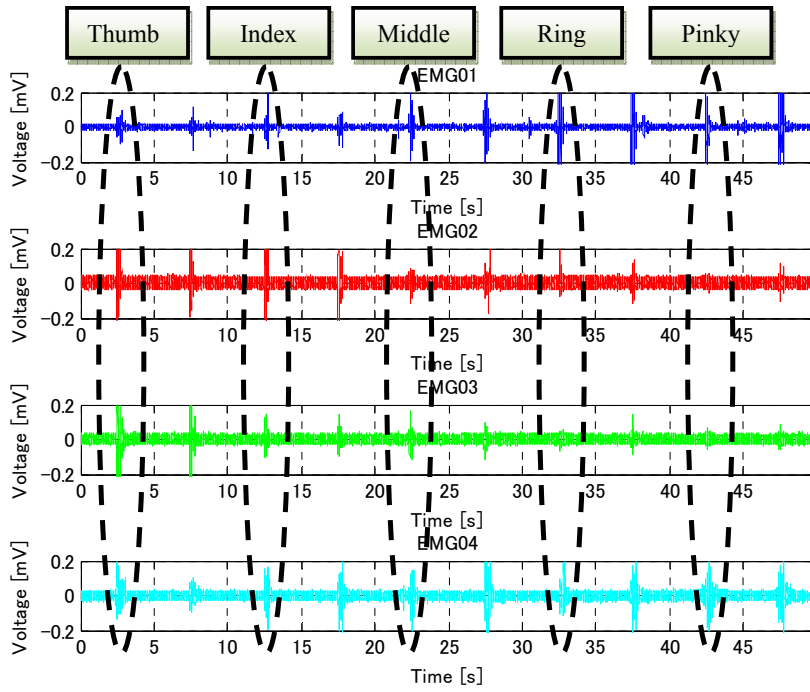


Figure 2 (a) Teaching-data of subject 1 from first measurement.

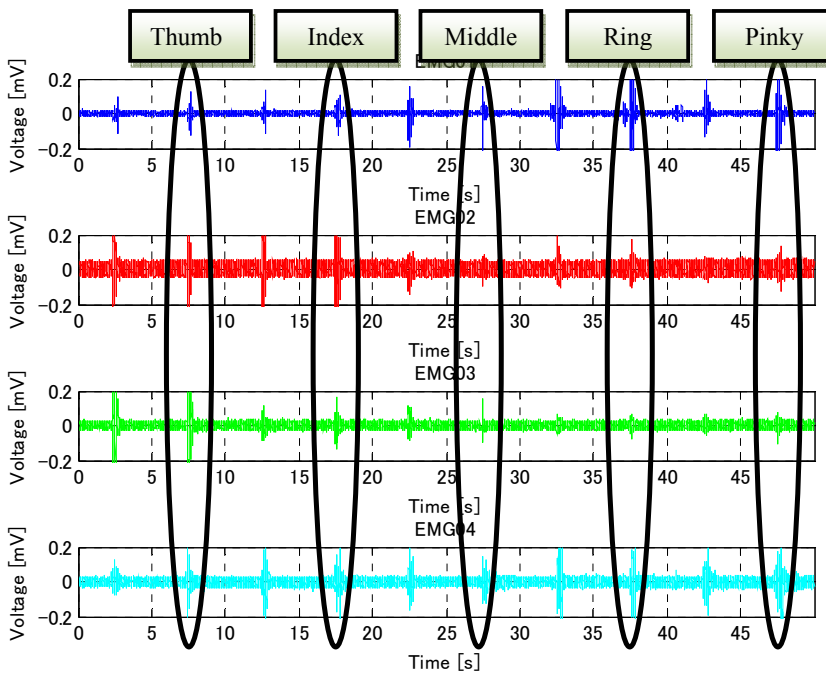


Figure 2 (b) Test-data of subject 1 from second measurement.

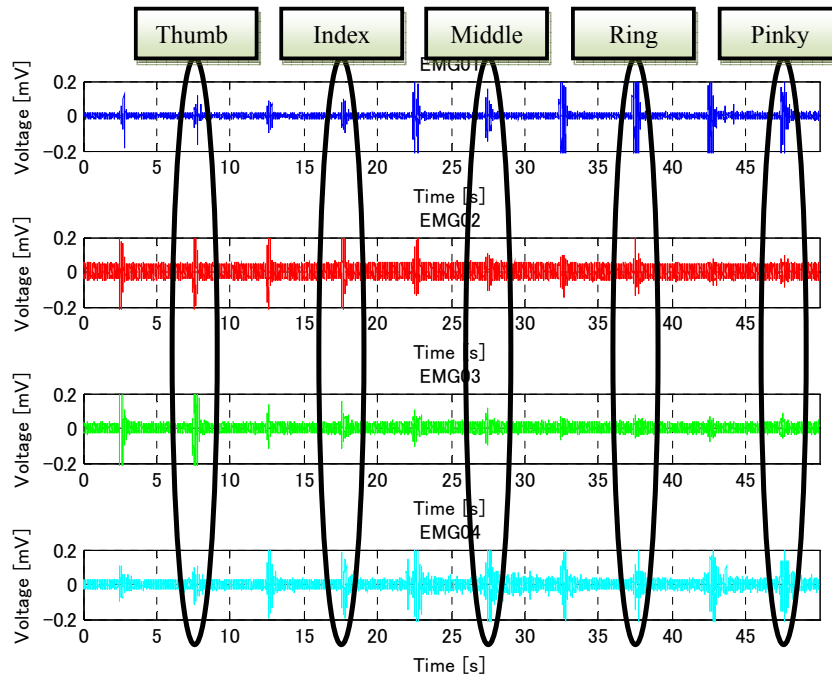


Figure 2 (c) Test-data of subject 1 from third measurement.

5.1 Individual motion measurements.

Time based plot of the EMG signals from a) Flexor digitorum superficialis muscle, b) Flexor digitorum profundus muscle, c) Flexor pollicis longus muscle, d) Extensor digitorum muscle are shown in Figure 2 in this order. In these graphs, one flexion-and-extension was included in each 5-second duration, i.e., all ten motions were expressed in these four graphs.

The rate of the correct classification is summarized in Table 1. The average goes to 77.5%.

Table 1 Classification result of individual motion

Subject 1	Test data 1	Test data 2	Test data 3
Teach-data 1	-	66.3%	66.0%
Teach-data 2	88.1%	-	83.0%
Teach-data 3	92.2%	65.2%	-

Subject 2	Test data 1	Test data 2	Test data 3
Teach-data 1	-	95.3%	62.5%
Teach-data 2	79.9%	-	78.2%
Teach-data 3	53.5%	49.6%	-

Subject 3	Test data 1	Test data 2	Test data 3
Teach-data 1	-	86.4%	89.1%
Teach-data 2	83.3%	-	96.1%
Teach-data 3	92.3%	68.1%	-

5.2 Pair motion measurements. Figure 3 shows time-based plot of the EMG signals. The order is the same as Figure 2. All eight pair motions were included in these four graphs.

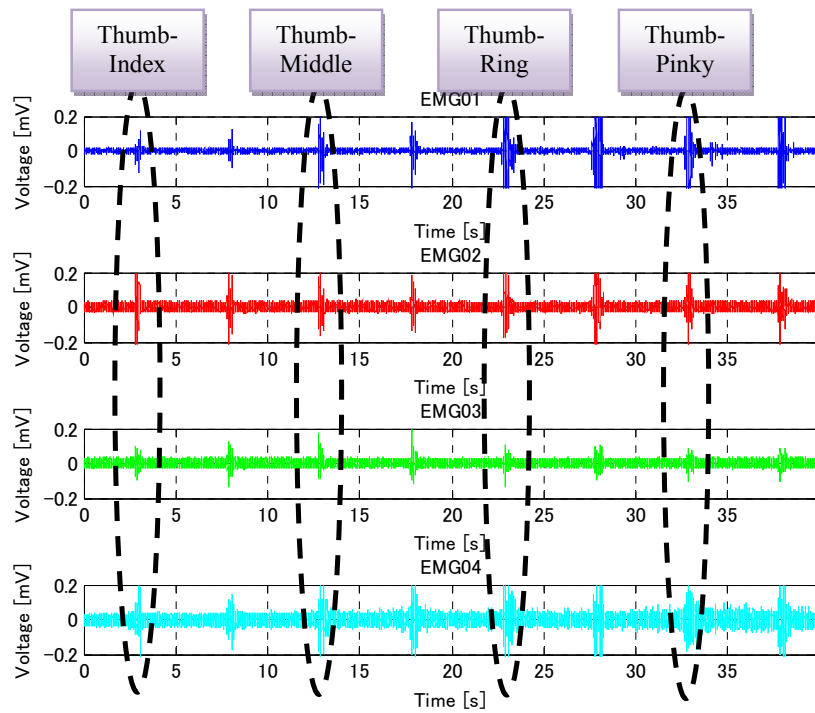


Figure 3 (a) Teaching-data of the subject 1 from first measurement.

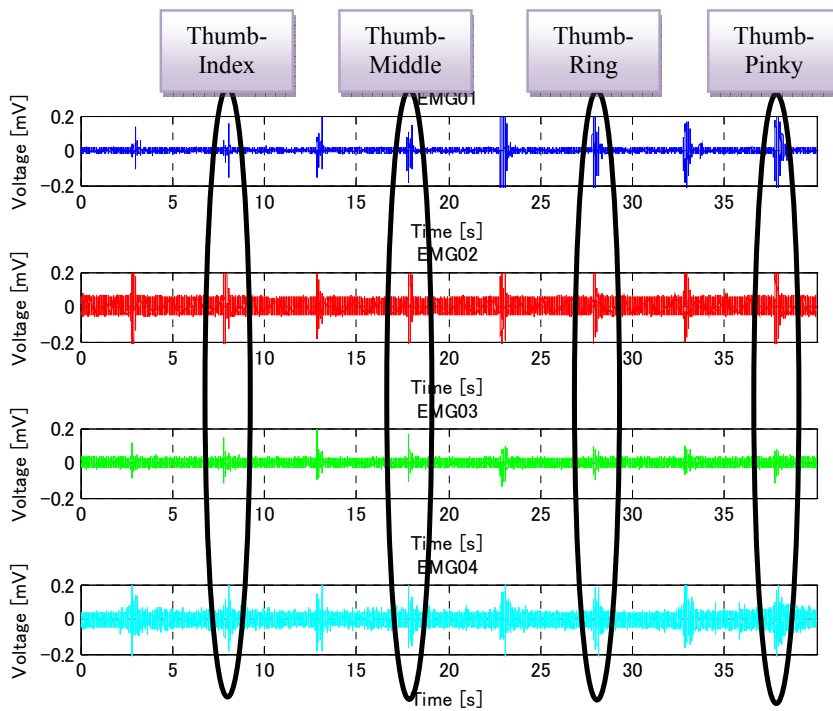


Figure 3 (b) Test-data of the subject 1 from second measurement.

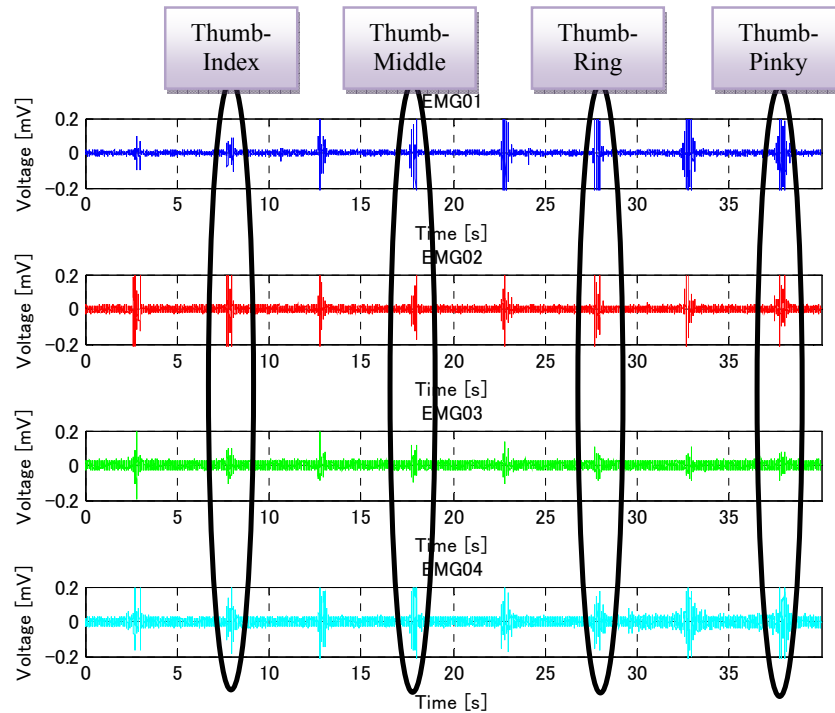


Figure 3 (c) Test-data of the subject 1 from third measurement.

Table 2 shows the classification result. The rate of the correct classification was 87.5% in average.

Table 2 Classification result of pair motion

.Subject 1	Test data 1	Test data 2	Test data 3
Teach-data 1	-	92.4%	81.4%
Teach-data 2	97.2%	-	80.7%
Teach-data 3	85.9%	96.8%	-

Subject 2	Test data 1	Test data 2	Test data 3
Teach-data 1	-	94.0%	77.5%
Teach-data 2	69.0%	-	82.8%
Teach-data 3	99.4%	91.8%	-

Subject 3	Test data 1	Test data 2	Test data 3
Teach-data 1	-	98.1%	68.8%
Teach-data 2	92.1%	-	93.2%
Teach-data 3	76.7%	98.7%	-

6 CONCLUSION

This paper presents finger motion pattern classification from a four-channel EMG measurement using a Support Vector Machine. Two kind of finger motion are examined:

individual flexion-and-extension of the finger or the thumb, and pair flexion-and-extension of the thumb and each finger. In both, the rate of correct classification was comparatively high: 77.5% in the individual motion and 87.5% in the pair classification. However, this is too low for commercial use. Some improvements can be considered. The effects of electrode position should be examined more precisely. Different kernels for the Support Vector Machine should be tried. Prescreening of the teaching data and increasing its quantity may improve performance.

Additionally, variation in EMG data between individuals presents a difficult problem. An on-site Support Vector Machine may be used to customize the system just prior to actual use. With these points in mind, we will continue to strive for a more reliable system through the use of engineering, statistical and medical knowledge.

7 REFERENCES

1. Claudio Castellini, Patrick van der Smagt, Surface EMG in advanced hand prosthetics, biological Cybernetics 100: pp. 35-47, 2009.
2. Kizuka Tomohiro, Masuda Tadashi, Kiryu Tohru, Sadoyama Tsugutake, Biomechanism Library Practical Usage of Surface Electromyogram, Tokyo Denki University Press, Japan, 2006.

3. Nello Cristianini, John Shawe-Taylor, An introduction to Support Vector Machines, Cambridge University Press, 2000.
4. Atsushi KATAYAMA, Duk SHIN, Yasuharu KOIKE, Estimation of Finger Posture with EMG signals for human interface, IEICE Technical Report MVE2006-79, pp.7-12, 2007.
5. Satoshi MORITA, Katsunari SHIBATA, Xin-Zin ZHENG, Koji ITO, Human-EMG Prosthetic Hand Interface using Neural Network, IEICE Technical Report MBE99-167, pp. 37-42, 2000.
6. Osamu FUKUDA, Toshio TSUJI, A Human-Assisting Manipulator Teleoperated by EMG Signals and Arm Motions, IEEE Transactions on Robotics and Automation Vol.19 No.2, pp. 210-222, 2003.
7. Atsushi KISO, Hirokazu SEKI, Hideaki MINAKATA, Susumu TADAKUMA, Human Forearm Motion Discrimination Based on Myoelectric Signal by Fuzzy Inference, Rehabilitation Robotics ICORR 2009 IEEE International Conference, pp. 295-299, 2008.
8. Sebastian Bizter, Patrick van der Smagt, Learning EMG control of a robotic hand: Towards Active Prostheses, IEEE International Conference on Robotics and Automation, pp. 2819-2823, 2006
9. Yosuke HIRATE, Goro OBINATA, Kazunori KASE, Atushi NAKAYAMA, YoungWoo KIM, Estimation of Hand Motions from Surface Electromyogram by Independent Component Analysis, Society of Biomechanisms Japan Vol. 33, pp. 134-141, 2009.
10. Peter Ju, Leslie Pack Kaelbling, Yoram Singer, State-based Classification of Finger Gestures from Electromyographic Signals, Proceedings of the 17th International Conference on Machine Learning, USA, pp. 439-446, 2000.
11. Narender P. Reddy, Vineet Gupta, Toward direct biocontrol using surface EMG signals: Control of finger and wrist joint models, Medical Engineering & Physics 29 pp. 398-403, 2007.
12. M.B.I. Reaz, M.S. Hussain, F. Mohd-Yasin, Techniques of EMG signals analysis: detection, processing, classification and applications, Biological Procedures Online 8(1): pp. 11-35, 2006.
13. Otto Bock Co. Ltd., <http://www.ottobock.com/>
14. Ryan J. Smith, Francesco Tenore, David Huberdeau, Ralph Etienne-Cummings, and Nitish V. Thakor, Continuous Decoding of Finger Position from surface EMG signals for the Control of Powered Prostheses, 30th Annual International IEEE EMBS Conference, pp. 197-200, 2008.
15. Yi-Hung Liu, Han-Pang Huang, Towards a High-Stability EMG Recognition System for Prosthesis Control: a One-Class Classification Based Non-Target EMG Pattern Filtering Scheme, Proceedings of the 2009 IEEE International Conference on Systems, Man, and Cybernetics, pp. 4897-4902, 2009.

APPLICATION OF MULTI-ANTENNA SYSTEMS IN COMBATING INTERFERENCE AND MULTIPATH FADING IN WIRELESS COMMUNICATION SYSTEMS

N. R. Muiga¹

S. Musyoki¹

D. B. O. Konditi²

¹Jomo Kenyatta University of Agriculture and Technology. ²Multimedia University College of Kenya

Abstract—Wireless communication channels are generally band-limited and behave like narrow pipes that can not accommodate rapid flow of data. At the same time unlike Gaussian channel, the wireless channel suffers from attenuation due to destructive addition of multipaths in the propagation media and interference from other users. Severe attenuation makes it impossible for the receiver to determine the transmitted signal unless some less-attenuated replica of the transmitted signal is provided to the receiver. Deploying multiple transmit and receive antennas improves the spectral efficiency and the performance of a wireless systems by increasing the amount of diversity. This paper proposes the use of multiple transmit and receive antennas (multiple-input multiple-output (MIMO) channel) which improve the signal quality at the receiver by use of multiple antennas at the transmitter and/or the receiver. The final analysis proposes a diversity matrix which can be used to optimize wireless communication systems design that achieve high spectral efficiency, low bit error rate, and higher throughput. This must also go with transmit/receive units that have acceptable physical size, reasonable cost and low current drain. These configurations will enable designers to compare the opportunity cost between redesigning the existing systems and adding antenna elements to the most convenient of the transmit and/or receive systems in any network. In other words, the new scheme may be a cost effective way to address the market demands for quality and efficiency without complete redesign of the existing systems and therefore a candidate for the next generation wireless communication systems.

Keywords: *Diversity, Multi-antenna systems, multiple-input multiple-output (MIMO), maximum likelihood estimator. Co-channel interference.*

INTRODUCTION

Multiple antennas are an important means to improve the performance of wireless systems. The spectral efficiency of a system with multiple transmit and receive antennas is much higher than that of the conventional single-antenna systems. [4]. Multiple antennas are used to increase the amount of diversity or the number of degrees of freedom in wireless communication systems.

SIGNAL IMPROVEMENT

Equalization, diversity, and channel coding are the three techniques which can be used independently or in tandem to improve received signal quality and link performance over small scale times and distances. Equalization compensates for inter-symbol interference (ISI) created by multipath within time dispersive channels. Channel coding improves the small-scale link performance by adding redundant data bits in the transmitted message so that if an instantaneous fade occurs in the channel, the data may still be recovered at the receiver. Diversity technique

is used to compensate for fading channel impairments, and is usually implemented by using two or more transmitting and/or receiving antennas.

DIVERSITY

Diversity is a widely known technique in combating channel impairments arising due to multipath fading. In diversity several replicas of the same information carrying signal are received over multiple channels with comparable strengths and exhibit independent fading. As with an equalizer, diversity improves the quality of a wireless communications link without altering the common air interface, and without increasing the transmitted power or bandwidth. [2].

Diversity is usually employed to reduce the depth and duration of the fades experienced by a receiver. Diversity techniques are often employed at both the transmitter (Transmit Diversity) and/or the receiver (Receive Diversity). For a broad class of interference-dominated wireless systems including mobile, personal communications, and wireless LAN networks, a significant increase in systems

capacity can be achieved by use of multiple antennas. Use of diversity is made more compelling by decrease in the cost of digital signal processing hardware and the advances in adaptive signal processing.

There are different kinds of diversity commonly employed in wireless communication systems; frequency diversity, time or temporal diversity, and space or antenna diversity. [1][5]. In temporal diversity, channel coding in conjunction with time interleaving is used. Thus replicas of the transmitted signal are provided at the receiver in the form of redundancy in temporal domain. Frequency diversity utilizes the fact that signals transmitted on different frequencies induce different multipath structure in the propagation media. Thus replicas of the transmitted signals are provided to the receiver in the form of redundancy in the frequency domain.

In Antenna diversity, spatially separated or differently polarized antennas are used. The replicas of the transmitted signal are provided to the receiver in the form of redundancy in spatial domain. This is provided with no penalty in bandwidth efficiency. Space Diversity is the most common diversity technique and it provides an attractive means for improving the performance of wireless communication systems. Unlike frequency diversity where additional bandwidth may be required and time diversity where additional time may be required, in space diversity no additional bandwidth or transmission time is required.

MULTI-ANTENNA SYSTEMS

However, situations arise where the designers have to contend with diverse limiting factors when designing wireless communication systems. In some cases the transmit unit may be the one remotely located in which case current drain may be the main limiting factor like in satellite communications and in meteorological systems. Therefore, the arguments advanced by most papers that only receive unit are limited by physical size and current drain may not always apply. To enhance flexibility in design a matrix

depicting the performance in terms of spectral efficiency, bit error rate and data rates of different design setup based on the number of transmit and/or receive antennas is investigated.

Multiple antenna systems have been known to increase diversity to combat channel fading. Each pair of transmit and receive antennas provides a signal paths from the transmitter to the receiver. By sending signals that carry the same information through different paths, multiple independently faded replicas of the data symbol can be obtained at the receiver end; hence more reliable reception is achieved. [4]. In a slow Rayleigh fading environment with one transmit and n receive antennas, the transmitted signal is passed through n different paths. If the fading is independent across antenna pairs, a maximal diversity gain of n can be achieved. [2][3]. The average error probability is known to decay by $1/SNR^n$ at high SNR in contrast to SNR^{-1} for the single input single output (SISO) system. With multiple transmit antennas, m and one receive antenna, the underlying idea is still averaging over multiple path gains to increase the reliability. It has been shown that with m transmit antennas and one receive antenna, a diversity gain within 0.1dB of that of n receive antennas with one transmit antenna can be achieved. [8].

CAPACITY OF MULTI-ANTENNA SYSTEMS

In a system with m transmit and n receive antennas, assuming the path gains between individual antenna pairs are independent and identically distributed (i.i.d.) Rayleigh faded, the maximal diversity gain is mn which is the total number of fading gains that one can average over. Foschini [9] has shown that the capacity of a channel with m transmits and n receive antennas and i.i.d. Rayleigh faded gains between antennas pair is given by;

$$C(SNR) = \min(m, n) \log SNR + 0(1)$$

The number of degree of freedom is thus the minimum of m and n . Thus if the number of receiving antennas equals the number of

transmitting antennas, the capacity of the channel grows approximately linearly with this number. Multiple-input multiple-output systems can therefore achieve increased spectral efficiency over limited bandwidth. [10].

A 2×2 MIMO CHANNEL WITH MAXIMUM LIKELIHOOD EQUALIZATION

For a 2 transmit 2 receive (2x2) MIMO channel the Maximum Likelihood (ML) decoding receiver structures gives the best performance than; **Zero Forcing (ZF) equalization, Minimum Mean Square Error (MMSE) equalization, Zero Forcing equalization with Successive Interference Cancellation (ZF-SIC), ZF-SIC with optimal ordering and MIMO with MMSE SIC and optimal ordering**

Maximum Likelihood (ML) decoding gives a better performance than minimum mean square error (MMSE) equalization with optimally ordered Successive Interference Cancellation. We will assume that the channel is a flat fading Rayleigh multipath channel and the modulation is BPSK. [6].

In a 2×2 MIMO channel, probable usage of the available 2 transmit antennas can be as follows: we consider that we have a transmission sequence $x_1, x_2, x_3, \dots, x_n$. In normal transmission, we will be sending x_1 in the first time slot, x_2 in the second time slot, x_3 and so on. However, as we now have 2 transmit antennas, we may group the symbols into groups of two. In the first time slot, send x_1 and x_2 from the first and second antenna. In second time slot, send, x_3 and, x_4 from the first and second antenna; send, x_5 and, x_6 in the third time slot and so on. We note that as we are grouping two symbols and sending them in one time slot, we need only $n/2$ time slots to complete the transmission and therefore the data rate is doubled.

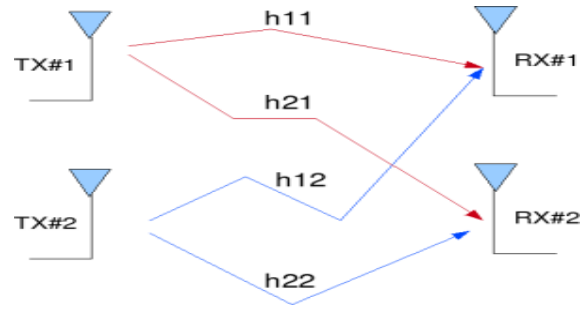


Figure 1: 2 Transmit 2 Receive MIMO channel

In the first time slot, the received signal on the first receive antenna is,

$$y_1 = h_{11}x_1 + h_{21}x_2 + n_1$$

$$= [h_{11} \ h_{21}] \begin{bmatrix} x_1 \\ x_2 \end{bmatrix} + [n_1]$$

The received signal on the second receive antenna is,

$$y_2 = h_{12}x_1 + h_{22}x_2 + n_2$$

$$= [h_{12} \ h_{22}] \begin{bmatrix} x_1 \\ x_2 \end{bmatrix} + [n_2]$$

where y_1 and y_2 are the received symbol on the first and second antenna respectively, h_{11} is the channel from 1^{st} transmit antenna to 1^{st} receive antenna, h_{21} is the channel from 2^{nd} transmit antenna to 1^{st} receive antenna, h_{12} is the channel from 1^{st} transmit antenna to 2^{nd} receive antenna, h_{22} is the channel from 2^{nd} transmit antenna to 2^{nd} receive antenna, x_1 and x_2 are the transmitted symbols and n_1 is the noise on 1^{st} receive antennas and n_2 is the noise on 2^{nd} receive antennas.

We assume that the receiver knows h_{11}, h_{12}, h_{21} and h_{22} . The receiver also knows y_1 and y_2 . The unknowns are x_1 and x_2 . For convenience, the above equation can be represented in matrix notation as follows:

$$\begin{bmatrix} y_1 \\ y_2 \end{bmatrix} = \begin{bmatrix} h_{11} & h_{12} \\ h_{21} & h_{22} \end{bmatrix} \begin{bmatrix} x_1 \\ x_2 \end{bmatrix} + \begin{bmatrix} n_1 \\ n_2 \end{bmatrix}$$

Equivalently, $y = Hx + n$

The assumptions were that that the channel is flat fading, in simple terms; it means that the multipath channel has only one tap. So, the convolution operation reduces to a simple multiplication. The channel experienced by

each transmit antenna is independent from the channel experienced by other transmit antennas. For the i^{th} transmit antenna to j^{th} receive antenna, each transmitted symbol gets multiplied by a randomly varying complex number h_{ij} . As the channel under consideration is a Rayleigh channel, the real and imaginary parts of h_{ij} are Gaussian distributed having mean $\mu_{h_{ij}}=0$ and variance $\sigma^2_{h_{ij}}=1/2$. The channel experienced between each transmit to the receive antenna is independent and randomly varying in time. On the receive antenna, the noise n has the Gaussian probability density function with $\mu=0$ and $\sigma^2=N_0/2$ and the channel h_{ij} is known at the receiver. [7].

MAXIMUM LIKELIHOOD RECEIVER

The Maximum Likelihood receiver tries to find \bar{x} which minimizes, $J = \|y - H\bar{x}\|^2$.

$$J = \begin{bmatrix} y_1 \\ y_2 \end{bmatrix} - \begin{bmatrix} h_{11} & h_{12} \\ h_{21} & h_{22} \end{bmatrix} \begin{bmatrix} \bar{x} \\ \bar{x} \end{bmatrix}^2$$

Since the modulation is BPSK, the possible value of x_1 is +1 or -1; similarly x_2 also take values +1 or -1. So, to find the Maximum Likelihood solution, we need to find the minimum from the all four combinations of x_1 and x_2 .

$$J_{+1+1} = \begin{bmatrix} y_1 \\ y_2 \end{bmatrix} - \begin{bmatrix} h_{11} & h_{12} \\ h_{21} & h_{22} \end{bmatrix} \begin{bmatrix} +1 \\ +1 \end{bmatrix}^2$$

$$J_{+1-1} = \begin{bmatrix} y_1 \\ y_2 \end{bmatrix} - \begin{bmatrix} h_{11} & h_{12} \\ h_{21} & h_{22} \end{bmatrix} \begin{bmatrix} +1 \\ -1 \end{bmatrix}^2$$

$$J_{-1+1} = \begin{bmatrix} y_1 \\ y_2 \end{bmatrix} - \begin{bmatrix} h_{11} & h_{12} \\ h_{21} & h_{22} \end{bmatrix} \begin{bmatrix} -1 \\ +1 \end{bmatrix}^2$$

$$J_{-1-1} = \begin{bmatrix} y_1 \\ y_2 \end{bmatrix} - \begin{bmatrix} h_{11} & h_{12} \\ h_{21} & h_{22} \end{bmatrix} \begin{bmatrix} -1 \\ -1 \end{bmatrix}^2$$

The estimate of the transmit symbol is chosen based on the minimum value from the above four values i.e. if the minimum is $J_{+1+1} \gg [1 \ 1]$, if the minimum is $J_{+1-1} \gg [1 \ 0]$, if the minimum is $J_{-1+1} \gg [0 \ 1]$ and if the minimum is $J_{-1-1} \gg [0 \ 1]$.

SIMULATION MODEL

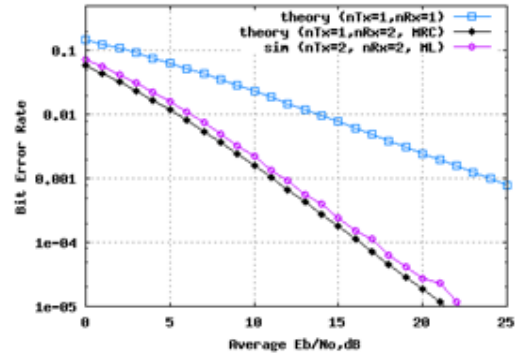


Figure 2: BER plot 2x2 MIMO Rayleigh channel with Maximum Likelihood equalization

CONCLUSIONS

The 2x2 MIMO with Maximum Likelihood (ML) equalization achieve a performance closely matching the 1 transmit 2 receive antenna Maximal Ratio Combining (MRC) case.

ACKNOWLEDGEMENT

The author wishes to acknowledge the invaluable contribution and guidance from Prof. D. B. O. Konditi of Multimedia University College and Dr. Stephen Musyoki the chairman department of Telecommunication and Information Engineering, Jomo Kenyatta University of Agriculture and Technology. I also acknowledge the valuable discussions with my colleagues Mr. Kanai, Mr. Mureu, Mr. Kidegho and Mr. Ombati.

REFERENCES

- [1] Hafeth Hourani, "An overview of diversity techniques in wireless communication systems", Communications Lab, Helsinki University of Technology.
- [2] Theodore Rappaport. *Wireless Communications: Principles and Practice*. Prentice Hall, New Jersey, 1996.
- [3] Alamouti S.M., "A Simple Transmit Diversity Technique for Wireless Communications", IEEE Journal on Selected Areas in Communications, Vol. 16, Issue 8, Oct 1998, pp. 1451-1458
- [4] Lizhong Zheng, "Diversity and Multiplexing: A fundamental Tradeoff in Multi-Antenna Channels", IEEE Journal on Information Theory, Vol. 49, No 5, May 2003, pp 1073 – 1096.
- [5] Tarokh, V., Seshadri, N., Calderbank, A.R. "Space-Time Codes for High Data Rate Wireless Communications: Performance Criterion and Code Construction", IEEE Trans. Of Inf. Th., Vol 44, No 2, 1998, pp. 744-765

- [6] John G. Proakis, "*Digital Communications*", McRAW- Hill International Editions 1995.
- [7] Bernard Sklar, "*Digital Communication Fundamentals and Application*", 2nd Edition Prentice Hall PTR 2001
- [8] J. H. Winters, "*The diversity gain of transmit diversity in wireless systems with Rayleigh fading*", IEEE, Vol 47, No 1, Feb 1998.
- [9] G. J. Foschini, "*Layered space-time architecture for wireless in a fading environment when using multi-element antennas*"
- [10] Wei Zhang, "*Multi-antenna Gaussian Channel (MIMO)*", University of Notre Dame. Spring 2003

VOLTAGE STABILITY ANALYSIS USING CP_ANN AND OPTIMISED CAPACITOR BANK PLACEMENT

Muriithi C. M Ngoo L. M Nyakoe G. N Njoroge S. N
cmmuriithi@eng.jkuat.ac.ke mwalughangoo@yahoo.com nyakoe@eng.jkuat.ac.ke lechnjugunatss@hotmail.com

School of Electrical, Electronic and Information Engineering, Department of Electrical & Electronics Engineering, Jomo Kenyatta University of Agriculture & Technology, P.O. Box 62000-00200, Nairobi, Kenya

Abstract–Voltage Stability refers to the ability of power system to maintain steady voltage at all buses in the system after being subjected to a disturbance from a given initial operating condition. In this paper, the IEEE 30-bus system is subjected to different loading and contingency conditions that simulate probable line faults and a load flow study is conducted with each configuration of load and contingency. The results are used to train a Counter Propagating Artificial Neural Network (CPANN) to classify the buses according to weakness. From the solution for the idealized system, the reduced Jacobian is used to determine the impact of the reactive power injection in the form of system voltage improvement at optimized capacitor bank locations.

Keywords: *Load flow, CP_ANN, Neural Networks, Reduced Jacobian.*

I. INTRODUCTION

The main objectives of LF studies is to determine the voltage magnitude and phase angle at all the buses, reactive powers and at generator buses, real and reactive power flows (line flows) in the transmission line and power losses in the system.

In general, the voltages of the buses within a power system are required to remain within a particular margin from the specified voltage [1]. Most systems have this margin as 4% or 5% of the nominal bus voltage. During conditions of disturbances e.g. faults, switching or lightning surges or load changes, there are fluctuations of voltage magnitudes on the buses. If a system is able to maintain the bus voltages within these margins even during these disturbances, then it can be said to be **voltage stable**.

With the advent of artificial intelligence, in recent years, expert systems, pattern recognition, decision tree, neural networks and fuzzy logic methodologies have been applied to many power system problems [2, 3]. CP_ANN systems provide a practical approach for implementing a pattern mapping task, since learning is fast in this network [4]. The effectiveness of the proposed method based approach is demonstrated by computation of bus voltage magnitudes and angles following different single line-outage contingency at different loading conditions on IEEE 30-bus system. Optimum capacitor bank placement is one way of improving the voltage profile of PQ buses in the system.

In this paper, the Newton Raphson method of load flow solution is adopted due to the quadratic convergence and high accuracy. It consumes memory space but with new computation systems, memory is of little hindrance. In addition, the Jacobian matrix utilized in the solution is essential in optimizing the capacitor bank placement by deriving the reduced Jacobian matrix.

II. METHODOLOGY

A. POWER FLOW PROBLEM

The objective of power flow study is to determine the voltage and its angle at each bus, real and reactive power flow in each line and line losses in the power system for specified bus or terminal conditions.

From the nodal current equations, the total current entering the i^{th} bus of n bus system is given by

$$I_i = V_i \sum_{j=0}^n Y_{ij} - \sum_{j=1}^n Y_{ij} V_j \tag{1}$$

The power injected into a bus is given by

$$\frac{P_i - jQ_i}{V_i^*} = I_i \tag{2}$$

Substituting yields the following equation

$$\frac{P_i - jQ_i}{V_i^*} = V_i \sum_{j=0}^n Y_{i0} - \sum_{j=0}^n Y_{i0} V_j \tag{3}$$

From the above relation, the mathematical formulation of the power flow problem results in a system of algebraic non linear equations which must be solved by iterative techniques. For large power systems the Newton-Raphson method is found to be more efficient and practical. The power flow equations are solved to give

$$\begin{bmatrix} \Delta\delta \\ \Delta|V| \end{bmatrix} = \begin{bmatrix} J_1 & J_2 \\ J_3 & J_4 \end{bmatrix}^{-1} \begin{bmatrix} \Delta P \\ \Delta Q \end{bmatrix} \quad (4)$$

where J_1, J_2, J_3 and J_4 are the elements of the Jacobian matrix while $\Delta\delta$'s and ΔV 's gives the correction vector i.e. $\Delta\delta$'s for all the PV and PQ type buses and ΔV 's for all the PQ type buses, which are used to update the earlier estimates of δ 's and V 's. Newton-Raphson method requires more time per iteration. It provides accurate results and is the most reliable AC power flow method.

To get accuracy in power flow solution, the NR power flow program has been developed in this paper and run to generate several training / testing patterns. A total of 100 different training sets each from a different loading and contingency combination were used with the results being the training data for the CP_ANN system.

B. WEAK BUS ID USING CP_ANN

CP_ANN are very similar to the Kohonen Maps and are essentially based on the Kohonen approach, but combines characteristics from both supervised and unsupervised learning [5]. The CP_ANN net is based on a single layer of neurons arranged in a two-dimensional plane having a well defined topology which means that each neuron has a defined number of neurons as nearest neighbors, second-nearest neighbor, etc. There is an additional output layer with same layout as input layer.

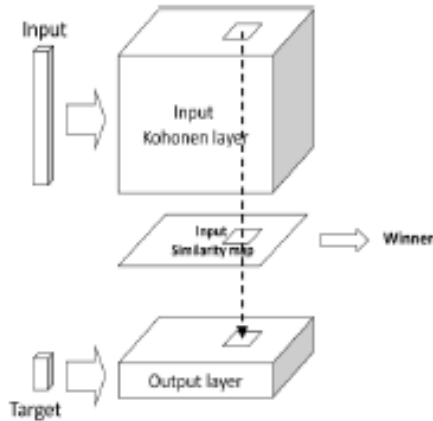


Figure 1: CP_ANN Net Layout

Principle Component Analysis (PCA) is done on the result to analyze the various weights the net appropriates to different variables. It involves a mathematical procedure that transforms a number of possibly correlated variables into a smaller number of uncorrelated variables called principal components. The first principal component accounts for as much of the variability in the data as possible, and each succeeding component accounts for as much of the remaining variability as possible.

Weak buses are buses within the system that have the lowest voltage magnitude and have the least capacity of reactive power during normal operation. In case of a large disturbance, the voltage at these buses is likely to sag to unfeasible levels triggering a voltage collapse. Weak buses have previously been identified based on Fuzzy Logic [6], Load Flow Equations [7], and using power capacity [8].

The variables from the load flow set of solutions are fed into the CP_ANN net to classify the buses according to weakness. The variables chosen are $|V|, \delta$, sub matrix elements J_{1ii}, J_{4ii} and the element Y_{ii} from the Y-bus for each bus in each solution. Based on these data, the CPANN was trained for 100 epochs to produce the top map.

D. COMPUTING THE REDUCED JACOBIAN

The technique implements a simple computation on the elements of the reduced Jacobian to find the suitable bus for capacitor placement as seen in the later section. The reduced Jacobian [9] is formulated from the Jacobian of the load flow. A brief description of the formulation of the reduced Jacobian is given before proceeding further.

The load flow equations are given by

$$f(\theta, V) = 0, \quad (5)$$

$$g(\theta, V) = 0, \quad (6)$$

f represents the active power mismatch equation, g represents the reactive power mismatch equation.

Equation 7 gives the known matrix model of the load flow.

$$\begin{bmatrix} \Delta P \\ \Delta Q \end{bmatrix} = \begin{bmatrix} J_1 & J_2 \\ J_3 & J_4 \end{bmatrix} \begin{bmatrix} \Delta\theta \\ \Delta V \end{bmatrix} \quad (7)$$

P and Q are the active and reactive power injections,

V and θ are the state variable vectors, namely voltage magnitude and bus angle, respectively,

ΔP is the difference in active power injection,
 ΔQ is the difference in reactive power injection,

$\Delta\theta$ is the change in bus angle,
 ΔV is the change in bus voltage magnitude,

J1 represents $\partial f / \partial \theta$,
 J2 represents $\partial f / \partial V$,
 J3 represents $\partial g / \partial \theta$,
 J4 represents $\partial g / \partial V$.

The reduced Jacobian used in this technique assumes that change in active load i.e. $\Delta P = 0$. Substituting this in (7), we get

$$J_1 \Delta\theta + J_2 \Delta V = 0, \quad (8)$$

$$J_3 \Delta\theta + J_4 \Delta V = \Delta Q, \quad (9)$$

Putting $\Delta\theta$ from (8) in (9), we get

$$\Delta Q = (J_4 - J_3 J_1^{-1} J_2) \Delta V, \quad (10)$$

$$\Delta Q = J_R \Delta V, \quad (11)$$

$$\Delta V = J_R^{-1} \Delta Q, \quad (12)$$

where J_R is the reduced Jacobian. The reduced Jacobian serves as the tool on which the proposed methodology yields the results regarding the capacitor location.

E. REDUCED JACOBIAN TECHNIQUE

The reduced Jacobian J_R gives a relationship describing ΔQ in terms of ΔV [9]. The inverse describes ΔV in terms of ΔQ . The elements in each column of the inverse matrix J_R^{-1} can be made to represent the change in voltage of every load bus for a given injection of reactive power into the bus corresponding to that column. The concept can be explained using a sample matrix like the one in (13) which shows J_R^{-1} as a (3 X 3) matrix.

$$[\Delta V] = \begin{bmatrix} A_{11} & A_{12} & A_{13} \\ A_{21} & A_{22} & A_{23} \\ A_{31} & A_{32} & A_{33} \end{bmatrix} [\Delta Q] \quad (13)$$

A_{11} , A_{21} , and A_{31} represent partial derivatives of voltages of load buses 1, 2 and 3 of the system with respect to reactive power at load bus i ,

ΔQ represents the vector of change in reactive power modeled by a fixed amount of reactive power injection,

ΔV represents the vector of change in voltage.

This implies that for studying the change in voltage ΔV as a result of the reactive power injection into load buses separately or individually, the corresponding element of ΔQ , say ΔQ_i alone must be made 1 p.u. and the others 0. Upon implementing this, the corresponding column i in J_R^{-1} directly gives ΔV [9]. Thus one needs to only study the elements of the particular column i of the reduced Jacobian to get the change in voltage as an effect of 1 p.u. reactive power injection at that bus i .

$$A_{1i} = \Delta V_1, \quad (14)$$

$$A_{2i} = \Delta V_2, \quad (15)$$

$$A_{3i} = \Delta V_3, \quad (16)$$

The sum of the elements of that column i of J_R^{-1} further gives the total improvement of system voltage $\Delta V_{total\ i}$ as an effect of the injection at the bus i . This is shown in (17).

$$A_{1i} + A_{2i} + A_{3i} = \Delta V_{total\ i} \quad (17)$$

On comparison of the sums of all individual columns of J_R^{-1} , the bus corresponding to the column i which yields maximum $\Delta V_{total\ i}$ is determined as the bus required.

$$bus_i : \Delta V_{total\ i} = \max\{\Delta V_{total\ 1}, \Delta V_{total\ 2}, \Delta V_{total\ 3}\} \quad (18)$$

corresponding to the matrix given in (13).

bus_i is not the i th bus in the system but the it load bus in the system as the buses involved in the analysis are only load buses.

It should be noted that the term $\Delta V_{overall}$ depicts the total improvement in system voltage where as the individual change in the bus voltage information come with the individual elements of J_R^{-1} .

III. TEST RESULTS.

A. CP_ANN WEAK BUS CLASSIFICATION

The IEEE-30 bus system, which is composed of 30 buses has been used to test the proposed methodology. The data for IEEE-30-bus is given in the appendix. The Newton Raphson method was used to obtain the steady state solution and the results provided the variables $|V|$, δ , sub matrix

elements J_{1ii} , J_{4ii} and the element Y_{ii} from the Y-bus for training the CP_ANN net. The resulting top map was analyzed using Principle Component Analysis (PCA).

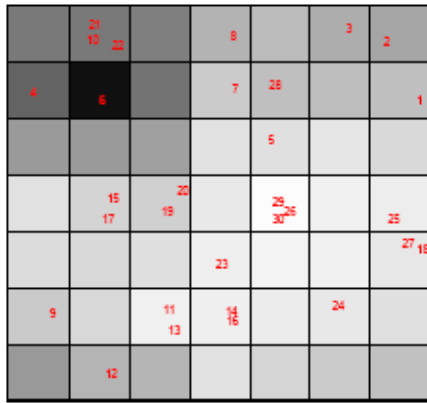


Figure 2: IEEE 30-bus CP_ANN top map

The dark neurons represent strong buses while lighter shading is an indication of weakness.

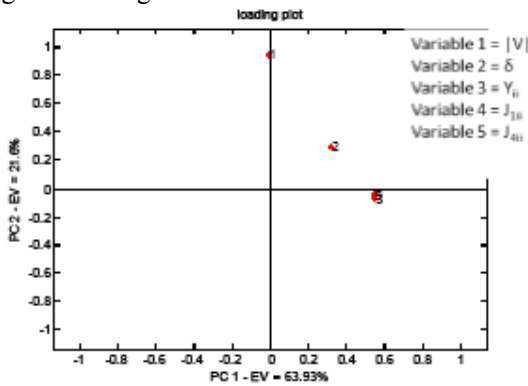


Figure 3: PCA Analysis on IEEE top map

The PCA shows that the first axis extracted almost 3/5th of the variation in the entire data set. In addition, Y_{ii} , J_{1ii} and J_{4ii} are clustered together implying that they play a greater role than the voltage magnitude and angle in determining the strength of a bus, from the variables fed into the CP_ANN net for the load flow study.

Further analysis of the top map shows bus 6 to be the strongest. An evaluation of that neuron's weight (Figure 4) shows strong values of, Y_{ii} , J_{1ii} and J_{4ii}

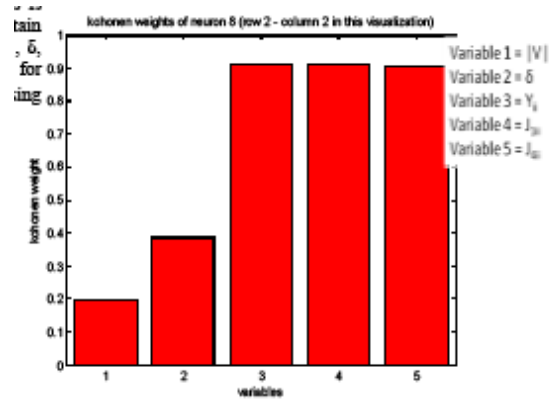


Figure 4: Neuron Weights for bus 6

This is seen as bus 6 is heavily interconnected and thus can be considered voltage stable even though its voltage magnitude and angle weights are low. It's also interesting that bus 6 is not loaded and has a direct connection with bus 2 which has a generator. Next to the neuron with bus 6 is bus 4 which is also well interconnected, has direct connections to generators at bus 2 and bus 1 and is thus considered a strong bus.

In contrast, buses 26, 29 and 30 are clustered together in one neuron as the weakest buses in the system. An evaluation of the neuron weights (Figure 5) shows weak weights for, Y_{ii} , J_{1ii} and J_{4ii} .

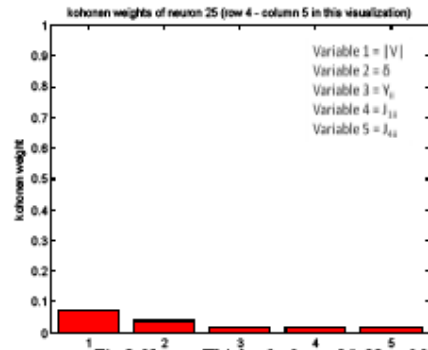


Figure 5: Neuron Weights for Buses 26, 29 and 30

These buses are not only far from the generator but also very weakly interconnected. This makes them particularly susceptible to voltage sags and hence their classification as weak buses.

Bus 5 is placed next to these buses and ranks low in weakness yet it has synchronous condensers connected to it. This is explained by its heavy loading that greatly reduces its voltage stability margin.

This idea can be extended for 100 different loading and contingency arrangements. These were run

using the Newton Raphson load flow solution method by creating a random line contingency and randomizing the loading to within $\pm 50\%$ of the nominal loading. The CP_ANN net was trained with the 100 epochs and had 49 neurons. The top map generated was as in (Figure 6).

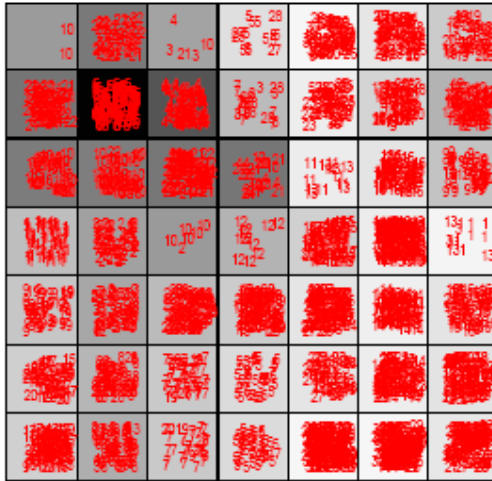


Figure 6: IEEE 30-bus CP_ANN top map for 100 LF solutions

The PCA was similar as that for 1 solution as shown in Figure 7

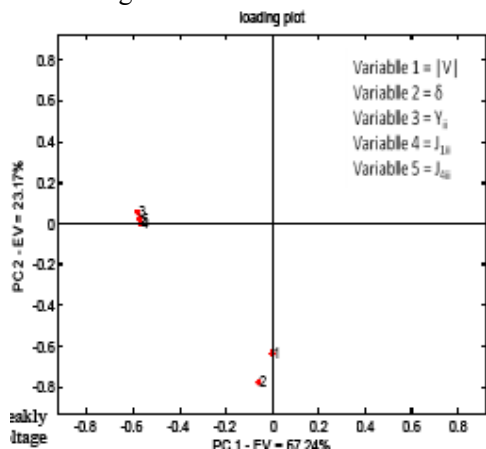


Figure 7: PCA Analysis on IEEE top map for 100 LF solutions

Again, the variables Y_{ii} , J_{1ii} and J_{4ii} are clustered together and account for about 4/5th of all the variation. They thus carry more weight in determining if a bus is weak or strong. From the top map, bus 6 is still ranked as the strongest bus within the system. The neuron weight for bus 6 is (Figure 8)

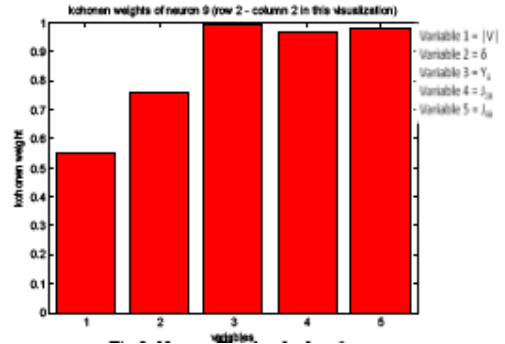


Figure 8: Neuron Weights for bus 6

The voltage magnitude and angle weights improve and the other variable weights are still high. Bus 4 is still clustered near bus 6 as a strong bus. The factors for this clustering remain the same even with line contingencies within the system namely the close proximity to generator buses, light loading and many interconnections.

The top map still classifies buses 26, 29 and 30 as weak buses. Their neuron weight is shown in (Figure 10).

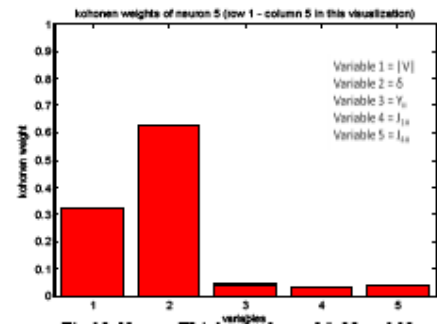


Figure 10: Neuron Weights for buses 26, 29 and 30

Their variables for buses 26, 29 and 30 have very low weights but the weightings for voltage magnitude and voltage angle improve. Bus 5 is still clustered next to them.

B. OPTIMUM CAPACITOR BANK PLACEMENT

From the ideal IEEE 30-bus system, the reduced Jacobian was constructed and the optimum capacitor location identified as bus 26 while the least effect was at bus 7. An idealized static capacitor VAR value of 5MVAR was introduced and the load flow solution obtained for both locations. The voltage profile for the PQ buses showed marked improvement with capacitors at bus 26 and little improvement with capacitors at bus 7. The voltage profile increased with increase in injected VARs (Figure 11).

C. CONCLUSION

The CP_ANN net was trained with data from load flow studies and was able to give a classification of buses according to weakness. This shows that neural networks can be used to predict bus weakness in an online situation and prevent voltage collapse. The variables for prediction can be increased to give a stringer indication of bus strength. For the reduced Jacobian, the improved

voltage profile for optimized capacitor placement shows that optimization may be taken as a tool in improving PQ bus voltages in large systems, saving costs of widespread VAR injection. Optimization spreads the effect of capacitors to other buses within the system. This could be important for developing countries.

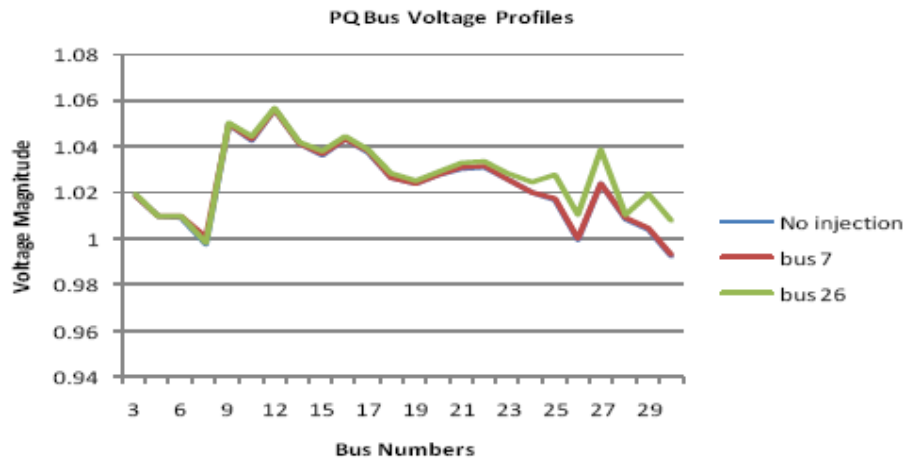


Figure 11: Voltage Profiles for PQ Buses

REFERENCES

- [1] Asnal Effendi, Sasongko Pramono Hadi, Soedjatmiko : Voltage Stability Analysis Of Power System Electrical Supply To Sumbagteng System (Sumbar-Riau-Jambi) : Proceedings of the International Conference on Electrical Engineering and Informatics Institut Teknologi Bandung, Indonesia : June 2007 : pp1.
- [2] Krishna J, Srivastava L, Counterpropagation Neural Network for Solving Power Flow Problem, International Journal of Intelligent Systems and Technologies, Winter 2006, Page 57-62
- [3] Vlachogiannis J. G, Mamdani fuzzy flow method, Engineering Intelligent Systems, 2004, CRL Publishing Ltd, Page 45-52
- [4] J.-S. Roger Jang, C.-T. Sun and E. Mizutani, Neuro-Fuzzy and Soft Computing: a computational approach to learning and machine intelligence, 1996, Prentice-Hall.
- [5] Muriithi C. M., Ngoo L. M., Nyakoe G. N., "Load Flow Analysis with a Neuro-Fuzzy Model of an Induction Motor Load", IEEE AFRICON 2009
- [6] R.A. Alammari : Fuzzy System Applications For Identification of Weak Buses in Power Systems: Electrical Engineering Department, University of Qatar, Doha, Qatar : October 2002
- [7] C. Subramani, Subhransu Sekhar Dash, M. Jagadeeshkumal : Voltage Stability Based Collapse Prediction and Weak Cluster Identification : ISSN 1990-7958 : 2009
- [8] Mehrdad Ahmadi Kamarposhti, Hamid Lesani, Mostafa Alinezhad : A New Method for Contingencies Ranking Using MLP Index : 9th IEEE AFRICON Conference Proceedings : September 2009
- [9] Sivaramakrishnan Raman, Amit Jain, M. Ramamoorthy and Ashok Vaghamshi, A Methodology for Selective Localization of Capacitor Banks for Power Systems, 2009 Third International Conference on Power Systems, Kharagpur, INDIA, December, 318
- [10] William D. Stevenson, Jnr, Elements of power system analysis, 4th edition, McGraw-Hill, New York, 1982
- [11] J. Nagrath, D.P. Kothari, Power System Engineering, , McGraw-Hill ,1994
- [12] Saadat Hadi, Power System Analysis, McGraw-Hill, ISBN 0-070912235-0, -P 691, 2002.

APPENDIX

Table A1: IEEE 30 Bus system Load Bus Data

Bus No	Load	
	MW	MVA _r
2	21.7	12.7
3	2.4	1.2
4	7.6	1.6
5	94.2	19
7	22.8	10.9
8	30	30
10	5.8	2
12	11.2	7.5
14	6.2	1.6
15	8.2	2.5
16	3.5	1.8
17	9	5.8
18	3.2	0.9
19	9.5	3.4
20	2.2	0.7
21	17.5	11.2
23	3.2	1.6
24	8.7	6.7
26	3.5	2.3
29	2.4	0.9
30	10.6	1.9

Table A2: IEEE 30 Bus system Line Data

Bus No	Bus No	R pu	X pu	B/2 pu	Transformer tap setting
1	3	0.0452	0.1852	0.0204	1
2	4	0.057	0.1737	0.0184	1
3	4	0.0132	0.0379	0.0042	1
2	5	0.0472	0.1983	0.0209	1
2	6	0.0581	0.1763	0.0187	1
4	6	0.0119	0.0414	0.0045	1
5	7	0.046	0.116	0.0102	1
6	7	0.0267	0.082	0.0085	1
6	8	0.012	0.042	0.0045	1
6	9	0	0.208	0	0.978
6	10	0	0.556	0	0.969
9	11	0	0.208	0	1
9	10	0	0.11	0	1
4	12	0	0.256	0	0.932
12	13	0	0.14	0	1
12	14	0.1231	0.2559	0	1
12	15	0.0662	0.1304	0	1
12	16	0.0945	0.1987	0	1
15	18	0.1073	0.2185	0	1
18	19	0.0639	0.1292	0	1
19	20	0.034	0.068	0	1
10	20	0.0936	0.209	0	1
10	17	0.0324	0.0845	0	1
10	21	0.0348	0.0749	0	1
10	22	0.0727	0.1499	0	1
21	22	0.0116	0.0236	0	1
15	23	0.1	0.202	0	1
22	24	0.115	0.179	0	1
23	24	0.132	0.27	0	1
23	24	0.132	0.27	0	1
24	25	0.1885	0.3292	0	1
25	26	0.2544	0.38	0	1

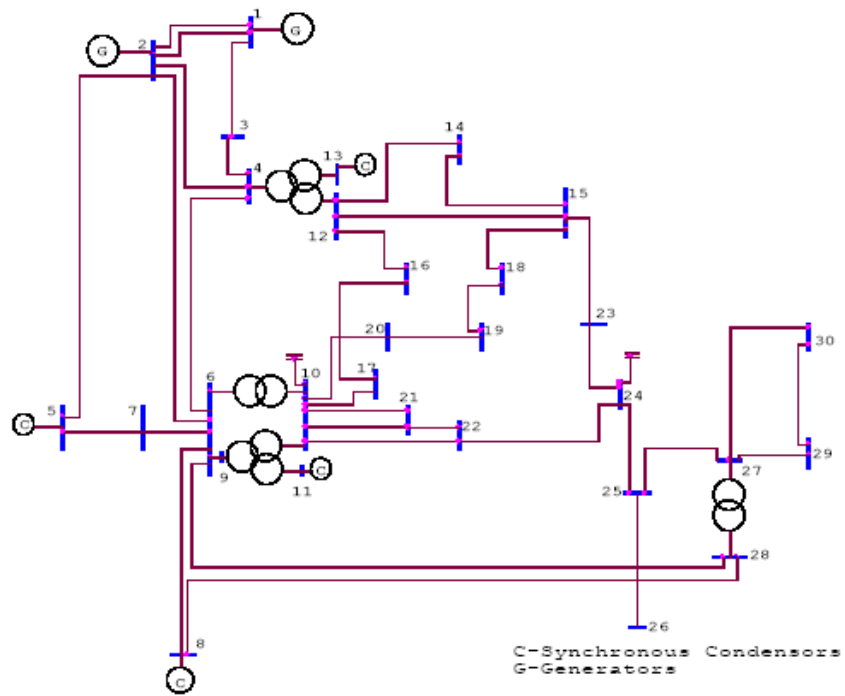


Figure A1: IEEE 30-bus system

ANALYSIS OF THE EFFECTS OF CONNECTING WIND FARMS TO A DISTRIBUTION NETWORK

WD Juma
jumadw@tut.ac.za

BB Monchusi
monchusibb@tut.ac.za

JL Munda
mundajl@tut.ac.za

AA Jimoh
jimohaa@tut.ac.za

Department of Electrical Engineering, Tshwane University of Technology, Pretoria, South Africa

Abstract—South Africa has an energy intensive economy which is highly reliant on fossil fuels, and sees economic growth based on energy intensive industries as a key means to development. This paper investigates the impacts of a wind farm connected at Harterbeespoort substation in South Africa in terms of voltage stability of the distributed power system. Double-Fed Induction Generator and the traditional Induction Generator wind turbines were employed in this study. The resulting P-V and Q-V curves from load flow studies are presented and analyzed. All the models for this study were implemented in DigiSILENT PowerFactory.

Keywords: *Wind power, distributed power system, voltage control, voltage stability*

I. INTRODUCTION

The South Africa's energy sector is a large-scale industry that bears the full imprint of a strong reliance on cheap coal that exists in large quantities. For that, South Africa has become one of the biggest CO₂ emitters in the world. The giant energy monopolist ESKOM is one of the lowest-cost energy suppliers globally. Today it generates more than half of all generated power on the African continent and has a total installed generating capacity of some 42,000MW (Net 36,200 MW, Peak 34,200 MW) with already new peak capacity in demand in the recent past. Of this total power production capacity, 93% is coal based (10 large plants), 5% nuclear and 2% hydroelectric. Small power stations and back-up gas-turbines represent less than 1% of the national output, another 3% is used for own consumption by independent power producers. It is anticipated that this capacities will be outstripped by energy demand by 2011[1].

With the continued reliance on fossil fuels, energy crisis and environmental concerns, it has become critical to call alternative sources of energy into the energy mix. Indeed, South Africa has set some target to generate 10,000GWh from renewable energy sources by 2013 – an equivalent to 4% of the forecasted power demand by then [2]. Of this, close to 70% of the country renewable energy needs are anticipated to come from wind.

Renewable energy can in many ways provide the least cost alternative sustainable energy supply, particularly when the social and environmental costs are considered, with wind power having the greatest potential as compared to other renewable.

Unlike the conventional power plants, wind power introduction into the grid comes with a number of technical challenges, quite notably the voltage stability. This will always affect the operation and security of wind farms and the larger power grid. Intermittency nature of wind power is still a challenge. Many studies have been performed on grid-connected wind farms and their associated power quality issues. A model to investigate the power quality impact during normal operation on power system is given in Ref. [3]. The performance of a large wind farm connected to an external grid is discussed in Ref. [4]. The effects of short circuit power capacity at the point of common coupling and the reactive power compensation on the system stability were determined in Ref. [5].

In this paper, the steady state model of grid-connected wind farm connected at Harterbeespoort substation is studied. The steady-state voltage stability analysis is conducted. Wind turbines model used in load flow calculation is implemented in the power system simulation tool DigiSILENT

PowerFactory. The P-V and V-Q curves obtained from power flow are used in the determination of the voltage stability of the power system with increased wind power penetration levels. For comparison different wind turbine technologies are considered.

II. SIMULATION TOOL

A versatile power systems analysis software DIgSILENT PowerFactory is used to develop the models and for the entire system simulations. It is an integrated tool for power system analysis with the functionality to perform load flow, RMS and transient simulations all in one package.

III. WIND ENERGY BACKGROUND

The amount of power captured from a wind turbine is specific to each turbine and is governed by equation 1 [6].

$$P_T = \frac{1}{2} \rho A C_p (\lambda \beta) v_w \tag{1}$$

where P_T is the turbine power, ρ is the air density (Kg/m^3), A is the swept turbine area (m^2), C_p is the coefficient of performance and is the wind speed (m/s). The coefficient of performance of a wind turbine is influenced by the tip-speed to wind ratio or TSR given as in equation 2.

$$TSR = \frac{\omega r}{v_w} \tag{2}$$

where ω is the turbine rotational speed (rad/s) and r is the turbine radius (m). A typical relationship indicates that there is one specific TSR at which the turbine is most efficient [6]. In order to achieve maximum power the TSR should be kept at the optimal operating point for all wind speeds.

IV. MODEL OF THE WIND FARM

A. The system configuration

The two types of wind turbine models based on different generator technologies - traditional induction generator (IG) and doubly fed induction generator (DFIG) with identical rated power 5.6MW are used in the study. Figure 1, shows a simple configuration of the two types of wind turbines.

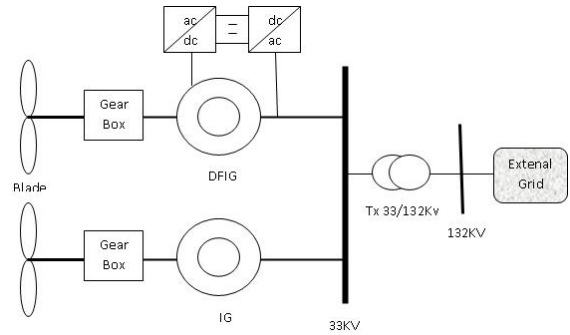


Figure 1: Configuration of DFIG and IG based wind turbines and interconnection to the grid

B. Wind Farm Model Description

The wind farm with up to 80MW maximum rated power is connected to the distribution grid through an existing 33 kV feeder as shown in Figure 1. The very feeder supplies the local distribution grid with a load of 200MVA. A single-line schematic diagram of the modelled system is shown in Figure 4. For the purpose of the analysis presented by this study, the wind farm is modelled as one aggregated wind turbine generator. A real wind farm of this rating would normally have much more number of wind turbines. The normalized (per unit) parameters of the aggregated model are the same as those of an individual generator, save for the rated power which is the sum of the whole group of generators.

C. Induction generator model

The mathematical expression for an IG is as shown in equation 3 [7]. The steady-state equivalent circuit of the induction generator is as given in Figure 2.

$$T_g = u_{ds} i_{ds} + u_{qs} i_{qs} \tag{3}$$

where T_g is the electromechanical torque, and u_{ds} and u_{qs} are the voltages associated with the direct and quadrature axes while i_{ds} and i_{qs} are the currents associated with the direct and quadrature axes.

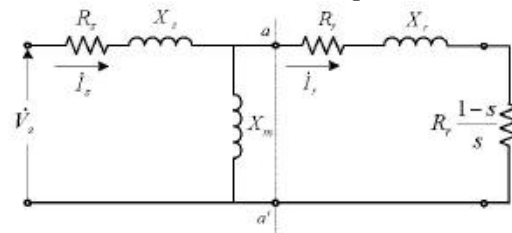


Figure 2: Steady-state equivalent circuit of induction generator

The steady-state equivalent circuit of an induction generator could be simplified as in figure 3. From this figure, we can deduce the power expressions as in equation 4.

$$P_e = \frac{V^2 R_{eq}}{\sqrt{R_{eq}^2 + X_{eq}^2}} \text{ and } Q_e = \frac{V^2 X_{eq}}{\sqrt{R_{eq}^2 + X_{eq}^2}} \quad (4)$$

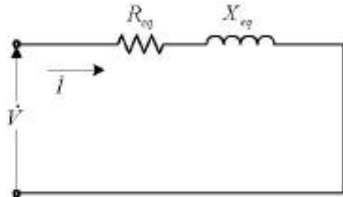


Figure 3: Simplified steady-state equivalent circuit of induction generator

From equation 4, it is clear that the induction generator active and reactive power are directly related to the terminal voltage, and the slip, of the IG. V_s

V. DESCRIPTION OF THE STUDIED SYSTEM

Using the power system simulation software DIgSILENT PowerFactory 13.1 the network under study was implemented as shown is Figure 4. The studied system is a simulation of an actual regional power grid integrating a wind farm into its 33kV distribution network via a Point of Common Connection (PCC). The models for the power system network are from the DIgSILENT PowerFactory library while their parameters are provided by the utility.

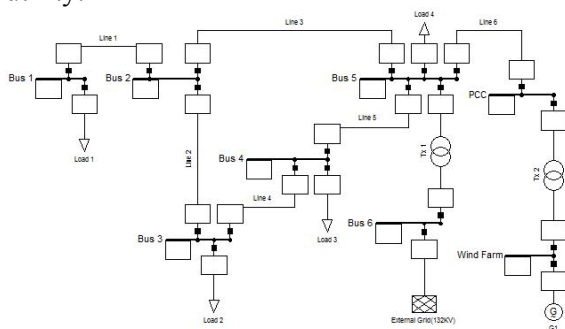


Figure 4: Single line diagram of the studied system

VI. STEADY-STATE VOLTAGE STABILITY ANALYSIS

Wind farms based on different turbine-generator technologies would have distinctive impacts on the power system voltage stability

[8]. In this section, the steady-state voltage stability limit of wind farms based on different wind turbine technologies is assessed. Two cases were investigated; wind turbines equipped with no-load compensated induction generator and wind turbines equipped with DFIG controlling the PCC as a PQ bus. The simulation results from these two cases are compared to determine how the wind power integration affects the grid in terms of voltage stability.

A. P-V curve analysis of wind farm

Wind farms based on different types of wind turbines are interconnected into the distribution grid. When the active power output of wind farm is low, the PCC voltage is not affected significantly but when wind power injection into the PCC increases by a large value then the voltage decreases fast. The P-V curves of the wind farms as wind farm active power output increases are plotted in figure 5.

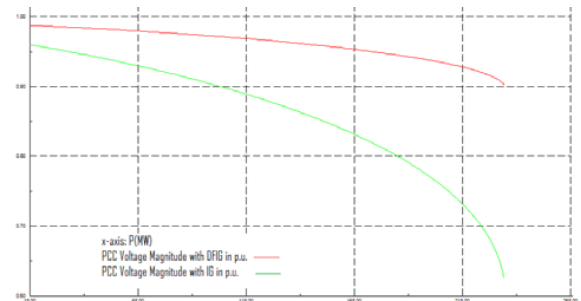


Figure 5: P-V curve of wind farm based on IG and DFIG wind turbines

From Figure 5, it can be seen that the steady-state voltage stability limits of induction generator based wind farm with no-load compensation is less than 50MW. When more real wind power is injected into the PCC than this, the voltage will collapse. When the DFIG based wind farm with constant power factor control that controls the PCC as a PQ bus with $Q = 0$ MW is applied, the steady-state voltage stability limits are tremendously increased to over 100MW. Even with increased real wind power injection into the grid beyond 100MW, the voltage stability can still remain within acceptable margin.

The voltage stability limits with an induction generator based wind farm can be improved

significantly by full-load compensation using a shunt capacitor [10].

B. Q-V curve analysis of wind farm

The operational wind farms may have adverse effects on the system voltage stability since the main factor causing voltage instability is the deficiency of reactive power in the system [12]. Hence the study of Q-V curves of wind farm integrated to the grid is very important.

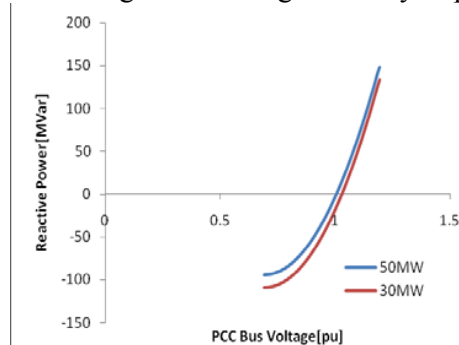


Figure 6: Q-V curve of wind farm based on IG wind turbines

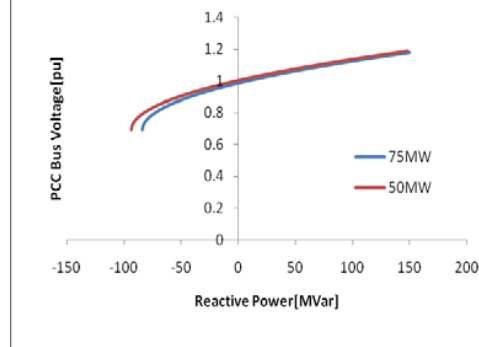


Figure 7: Q-V curve of wind farm based on DFIG wind turbines

The Q-V curves of different active power output of wind farms based on IG and DFIG wind turbines are shown in Figures 6 and 7. The induction generator based wind farm has a reactive power margin of 2MVar when the wind farm’s active power output is 50MW. With a DFIG turbine based wind farm, there is a 3MVar reactive power margin when the wind farm active power output is 50MW. As seen, the acceptable injected real wind power increases significantly when a DFIG-based wind turbine is used. This is because a DFIG-based wind turbine can provide the reactive power to keep a constant power factor of the entire wind farm. Hence a DFIG-based wind farms would improve the voltage stability of the local network integrating wind power.

VII. CONCLUSIONS

The main limitation with respect to maximum rating and integration of the wind power into the grid may be associated with voltage stability of the local network. Because of this voltage control assessments and reactive power compensation are very important to consider when planning for development of large-scale wind power integration.

In this paper the impacts of wind power integration using the two different types of wind turbines were investigated and a comparison was made. Wind turbines equipped with simple induction generator are not provided with reactive power regulation capability. Voltage stability deterioration is mainly due to the large amount of reactive power absorbed by the wind turbine generators during the continuous operation and system contingencies. On the other hand, wind turbines equipped with doubly fed induction generators (DFIG) are capable of reactive power regulation. The adverse affect of the wind power on the local network voltage stability can be suppressed more with DFIG-based wind generators.

ACKNOWLEDGMENT

The authors would like to acknowledge the support of Tshwane Electricity, South Africa.

REFERENCES

- [1] There is wind in Africa, African wind energy association, 2008, [Online]. Available: http://www.afriwea.org/en/south_africa.htm, accessed on May 20, 2010.
- [2] Energy Security Master Plan - Electricity. Department of minerals and Energy, Pretoria; 2007
- [3] Hansen AD, Sorensen P, Janosi L, Bech J. Wind farm modelling for power quality. In: 27th Annual Conference of the IEEE Industrial Electronics Society 29 Nov–2 Dec 2001, vol. 3. Denver, CO, USA: IECON '01; 2001. 1959–1964.
- [4] Huan-ping Li; Jin-ming Yang; , "The performance research of large scale wind farm connected to external power grid," *Power Electronics Systems and Applications, 2009. PESA 2009. 3rd International Conference on* , vol., no., pp.1-5, 20-22 May 2009
- [5] Muyeen, S.M.; Ali, M.H.; Takahashi, R.; Murata, T.; Tamura, J.; Tomaki, Y.; Sakahara, A.; Sasano,

- E.; , "Comparative study on transient stability analysis of wind turbine generator system using different drive train models," *Renewable Power Generation, IET* , vol.1, no.2, pp.131-141, June 2007.
- [6] Baroudi, J.A.; Dinavahi, V.; Knight, A.M.; , "A review of power converter topologies for wind generators," *Electric Machines and Drives, 2005 IEEE International Conference on* , vol., no., pp.458-465, 15-15 May 2005
- [7] Yongning Chi; Yanhua Liu; Weisheng Wang; Huizhu Dai; , "Voltage Stability Analysis of Wind Farm Integration into Transmission Network," *Power System Technology, 2006. PowerCon 2006. International Conference on* , vol., no., pp.1-7, 22-26 Oct. 2006
- [8] Fengquan Zhou; Joos, G.; Abbey, C.; , "Voltage stability in weak connection wind farms," *Power Engineering Society General Meeting, 2005. IEEE* , vol., no., pp. 1483- 1488 Vol. 2, 12-16 June 2005
- [9] Chen Z. Issues of connecting wind farms into power systems. IEEE/PES Transmission and Distribution Conference and Exhibition: Asia and Pacific Dalin, China, 2005.
- [10] Palsson, M.P.; Toftveag, T.; Uhlen, K.; Tande, J.O.G.; , "Large-scale wind power integration and voltage stability limits in regional networks," *Power Engineering Society Summer Meeting, 2002 IEEE* , vol.2, no., pp.762-769 vol.2, 25-25 July 2002
- [11] Guido Schwartz; Analysis of the Energy Political Framework in South Africa for the Introduction of Wind Energy, 2004.
- [12] Ha, L.T.; Saha, T.K.; , "Investigation of power loss and voltage stability limits for large wind farm connections to a subtransmission network," *Power Engineering Society General Meeting, 2004. IEEE* , vol., no., pp.2251-2256 Vol.2, 10-10 June 2004



PROFILE

Professor Josiah Munda received MSc degree in electrical distribution from Moscow Power Institute and Tver State Technical University in 1991, and DEng degree in electrical engineering

from the University of the Ryukyus in 2002. Josiah was a lecturer at KCCT from 1994-1995, before moving to JKUAT where he stayed until 2004. He is currently an associate professor of electrical engineering and the Director, Centre for Energy and Electric Power at Tshwane University of Technology, South Africa. His research areas are power system stability, renewable energy supplies, distributed generation and intelligent control. He is a member of IEEE and a senior member of SAIEE.

DEVELOPMENT OF SOLUTION SEARCH ALGORITHM FOR CFD OPTIMIZATION PROBLEM

Ken'ichi Yano¹
yanolab-paper@gifu-u.ac.jp

Yoshifumi Kuriyama¹
n3812202@edu.gifu-u.ac.jp

Yoshifumi Suzuki²
yoshifumi-suzuki@janis-kogyo.co.jp

¹Faculty of Engineering, Gifu University, 1-1 Yanagido, Gifu, Japan₁

²JANIS, Co., Ltd. 2-88 Karasaki Tokoname Aichi Japan₂

Abstract—Optimization with a computational fluid dynamics (CFD) simulator has gained attention in various fields recently. Optimization is hampered by the increased computing time used by many localized solutions that complicate the calculation by needing a vast amount of space for solution generation and distribution. Therefore, researchers hope to speed the process and make the analytical time highly effective. In this paper, we propose an algorithm that reaches the best solution neighborhood from a complex solution space at high speed, and obtains the best solution. We have applied the algorithm to a real problem, and it worked.

1 INTRODUCTION

The numerical simulator for fluid analysis based on computational fluid dynamics (CFD) is focused on analyzing the behavior of a fluid around an object, or its thermal hydraulics. With the development of computing power and the price plummet of personal computers, the CFD simulator has become a useful and realistic tool (1). Furthermore, CFD is now used not only for analyzing of the behavior of a fluid but also for optimization of a fluid's shape or flow for improved quality or performance.

That said, the optimization with a CFD simulator for improved quality or performance still has many problems. For example, the solution space formed by the solution of optimization using a CFD simulator has become a multimodal space with a lot of local minimums. As a method of searching efficiently for a complex solution space, the meta-heuristic algorithm is a heuristic technique (2). As an algorithm with the greatest general versatility, the genetic algorithm (GA) is generally used. However, in cases such as analyzing a problem that has a lot of local solution, the solution that incorporates the general GA is highly likely to derive local solution. Of course, this problem can be solved by enlarging the number of population members, the number of generations and the mutation evolution; on the other hand, the computational time for one condition was a few minutes and the optimization requires hundreds of repeated computations. Thus the optimization using the CFD simulator needs a lot of time to finish the task.

The purpose of this study was to design a solution search algorithm using fewer populations and generations to derive the optimized solution more efficiently for an optimization problem by using a CFD simulator. Specifically, focusing on an external solution in a multimodal space, we propose the External Distribution Sorting Algorithm (EDSA), which searches intensively at the improving point in the nearly external solution. The effectiveness of the proposed method is shown through experiments in actual die-casting plants for deriving the optimum plunger input.

2 THE EXTREMAL DISTRIBUTION SORTING ALGORITHM (EDSA)

In this study, to derive the optimum solution in a multimodal space in a CFD optimization problem with low calculation frequency, we propose the External Distribution Sorting Algorithm (EDSA). The EDSA distinguishes a progressive area and analyzes the solution space of a CFD optimization problem and the tendency toward the improvement of the solution by using the approximation curve of the evaluation value and the extreme value.

2.1 Deriving the extreme value. Though all individuals inside the generation are handled as the next generation candidates in the GA, an excellent individual is analyzed by priority in the EDSA. Thus the n -dimensional CFD optimization problem is replaced with two-dimensional space by the evaluation value and one variable, and the algorithm searches for the tendency to the solution to each variable by repeating the operation n times. First, each extreme value and the neighborhood of the evaluation value and the approximation curve are obtained. When the evaluation value of the CFD

simulator is assumed to be $f(x)$, the extreme value cannot be derived by the differentiation because it is discontinuous.

Therefore, whether k th variables and the i th individual is an extreme value is judged by using the following Equations (1),(2).

$$\begin{aligned} & (f(x_{i+1,k}) - f(x_{i,k})) \times (f(x_{i,k}) - f(x_{i-1,k})) \\ & < 0 \\ & 0 < (f(x_{-(i+1,k)}) - f(x_{-(i,k)})) \end{aligned} \tag{1}$$

When (1) is filled at the same time, $x_{i,k}$ is the maximum value

$$\begin{aligned} & (f(x_{i+1,k}) - f(x_{i,k})) \times (f(x_{i,k}) - f(x_{i-1,k})) \\ & < 0 \\ & (f(x_{-(i+1,k)}) - f(x_{-(i,k)})) < 0 \end{aligned} \tag{2}$$

When (2) is filled at the same time, $x_{i,k}$ is the minimum value.

When $x_{i,k}$ is judged as an extreme value, x_i is preserved as an extreme value. When thinking about the extreme value neighborhood of $x_{i,k}$ the minimum unit e_k of the variable is used. Afterwards, the two points $x_{i,k} + e_k$ and $x_{i,k} - e_k$ that adjoin $x_{i,k}$ are substituted for the extreme value.

2.2 Deriving the approximate curve.

The approximation curve of the evaluation value to comprehend the tendency to the solution is derived. It depends on a complex solution space like Figure1 by using the approximation curve, and it searches for the area where the improvement of the solution is expected. The approximation curve used to search for the solution is derived by the least-squares method, as follows Equation (3), where N : the number of samples, n :the degree of the CFD optimization problem, m : the degree of the approximation curve, $x_{i,k}$:the k th, i th individual, J_i : the evaluation value of i th individual. The degree of the approximation curve m is changed in proportion to the number of samples N . Condition m

is that 5th dimensions are assumed to be the maximum degree in this study.

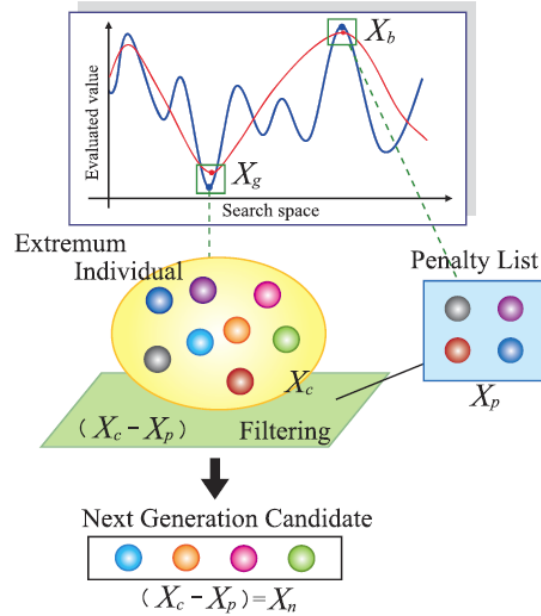


Figure1: The individual selection

2.3 Election of the next generation individual.

After deriving the extreme value of the CFD simulator from the evaluation value and the approximation curve, the next generation's candidates are elected based on those tendencies.

The parents are elected based on the extreme value of the evaluation value. First, a set of the individual with a bad extreme value and its neighborhood is assumed to be X_b . A set of the penalty X_p is also listed it based on X_b to exclude the next generation's candidates. Moreover, an individual that doesn't fill the restriction is added to X_p .

Next, a set of the individual with a good extreme value and its neighborhood is assumed to be X_g . Note that if the extreme value whose evaluation value is larger than the mean value of the maximum value $\bar{f}(x_g)$,

$$\begin{pmatrix} N & \sum_{i=0}^N x_{i,k} & \sum_{i=0}^N x_{i,k}^2 & \dots & \sum_{i=0}^N x_{i,k}^m \\ \sum_{i=0}^N x_{i,k} & \sum_{i=0}^N x_{i,k}^2 & \sum_{i=0}^N x_{i,k}^3 & \dots & \sum_{i=0}^N x_{i,k}^{m+1} \\ \vdots & \vdots & \vdots & \vdots & \vdots \\ \sum_{i=0}^N x_{i,k}^m & \sum_{i=0}^N x_{i,k}^{m+1} & \sum_{i=0}^N x_{i,k}^{m+2} & \dots & \sum_{i=0}^N x_{i,k}^{2m} \end{pmatrix} \begin{pmatrix} a_0 \\ a_1 \\ \vdots \\ a_m \end{pmatrix} = \begin{pmatrix} \sum_{i=0}^N y_i \\ \sum_{i=0}^N x_{i,k} \cdot J_i \\ \vdots \\ \sum_{i=0}^N x_{i,k}^m \cdot J_i \end{pmatrix}$$

(3)

$$f(x_g) > \bar{f}(x_g) \quad (4)$$

only the extreme value that fills Equation (4) is preserved as a set of candidate X_c , which makes an inquiry into X_p . If there is a corresponding individual to X_p in X_c , it is excluded from X_c . The conceptual diagram of the above operation is shown in Figure1.

In addition, the candidate's exclusion is done based on the following conditions. When you compare the extreme value of the approximation curve with that of the evaluation value, the latter is preserved by priority because it is dependable. A good extreme value of the evaluation value is assumed to be x_g . In addition, only the individual that fills Equation (4) is made a candidate x_c from among x_g . A bad extreme value of the evaluation value is assumed to be x_b , and its neighborhood is assumed to be x_{g+e} , x_{b+e} . A good extreme value of the approximation curve is assumed to be x_{Ag} , and a bad extreme value of the approximation curve is assumed to be x_{Ab} , and the neighborhood is assumed to be x_{Ag+e} , x_{Ab+e} . Candidates are chosen based on the following condition:

$$x_c > x_b > x_{g+e} > x_{Ag} > x_{b+e} > x_{Ab} > x_{Ag+e} > x_{Ab+e} \quad (5)$$

Candidates are preserved as x_n based on Equation (5). The best solution in a generation is added to the candidate as the elite to continue the improvement of the solution. Finally, these candidates are preserved as the parents of the next generation individual x_n .

2.4 Simplex crossover.

The parent's individual that generates the next generation individual is elected from X_n . The roulette selection is applied to the election method. The roulette selection is the method of selecting the individual according to the selection rate corresponding to the evaluation value. The probability P_i that a certain individual is selected is expressed in Equation (6).

$$P_i = \frac{f(x_i)}{\sum_{j=1}^{Ng} f(x_j)} \quad (6)$$

In the use of Equation (6) and simplex crossover (SPX), next generation individuals are generated.

SPX is a crossover method for a real-coded genetic algorithm (RCGA) (6). The RCGA uses the crossover method for treating not the variable as bit

strings but the real vectors. Especially, it is an effective crossover method for solving a continuous optimization problem, and it is an effective way to consider the dependence among variables. Moreover, information on the parent's individual can be easily passed on to the child individual. The RCGA has several kinds of crossover methods.

In the proposal algorithm, in spite of the dependence among variables or the scale problem, SPX is employed to deal with any optimization problems. Moreover, the n -dimensional CFD optimization problem is replaced with two-dimension space by the evaluation value and one variable. The individual with the extreme value of each variable is distinguished. Therefore, other values of the variables can be operated as crossover while maintaining the value of a variable that became an extreme value.

The procedure of SPX is as follows. When the intended CFD optimization problem is R_n , $n+1$ th parents $\overrightarrow{Px_0}, \dots, \overrightarrow{Px_n}$ are elected from X_n according to Equation (6). Next, the bar centric position \vec{G} is derived based on the parents.

$$\vec{G} = \frac{1}{n+1} \sum_{i=1}^k \overrightarrow{Px_i} \quad (7)$$

The range of formation of the next generation is decided based on G , and the next generation individual is generated by using the uniform random number.

$$\overrightarrow{p_0} = \vec{G} + \varepsilon (\overrightarrow{Px_0} - \vec{G}) \quad (8)$$

$$\overrightarrow{c_0} = \vec{0} \quad (9)$$

$$\overrightarrow{p_j} = \vec{G} + \varepsilon (\overrightarrow{Px_j} - \vec{G}) \quad (10)$$

$$\overrightarrow{c_j} = r_{j-1} (\overrightarrow{p_{j-1}} - \overrightarrow{p_j} + \overrightarrow{c_{j-1}}), (j = 1, \dots, n) \quad (11)$$

Note that r_{j-1} is calculated from the uniform random number $u(0,1)$ in section $[0,1]$.

$$r_{j-1} = (u(0,1))^{\frac{1}{j+1}} \quad (12)$$

And, the next generation C_x is the following equation.

$$\vec{C} = \overrightarrow{x_n} + \overrightarrow{C_n} \quad (13)$$

When the relation between the number of individuals in generation N and the degree of the CFD optimization problem k is $N > k$, the selection of the parents and the generation of the next generation

individuals are repeated until the number of individuals reaches N . And, if the restriction is not filled or does not conform to penalty lists X_p , the next generation individual is not preserved.

3 APPLICATIONS TO DIE-CASTING

Determining the optimum velocity to reduce the quantity of air entrainment enables the production of high-quality products. The target actual casting plants can be control the multistep velocity, and the velocity pattern, which has five phases, is derived from past studies. Figure2 shows an overview of the mesh setting, and Table 1 shows the parameters of the mesh setting. The plunger velocity is expressed as shown in Figure3, and Table 1 shows the parameters of the mesh setting, where x_{fill} is filling position which is a constant value.

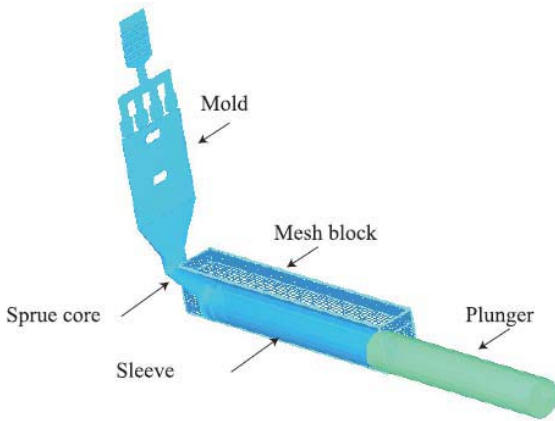


Figure2: Mesh setting for CFD simulation

Table 1: Mesh parameter

	Cell size	Number of cell
X-direction	0.004	20
Y-direction	0.002 ~ 0.006	132
Z-direction	0.0022 ~ 0.0035	29
Total number of cell		76500

As seen in Figure2, the sleeve is symmetrical to the X axis. Thus, the analyzing area is set as only a one-sided model to reduce the analyzing time to, only about ten minutes. Table 1 shows the minimum settings to do calculations quickly and accurately.

The optimization problem was defined with a cost function equivalent to the sum of the weighted quantity of air entrainment and the weighted filling time, as shown in Equation (14),

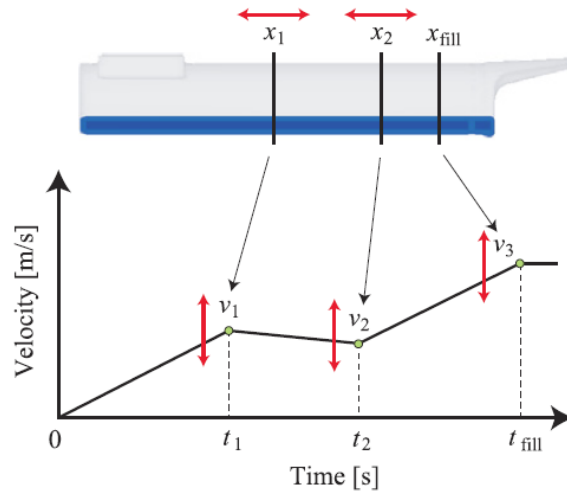


Figure3: Die-casting simulation model

minimize

$$J = w_a A(v_i(t), x) + w_t t_f(v_i(t), x) + K_p + A_{shut} \quad (14)$$

subject to:

$$\begin{aligned} 0.02 &\leq v \leq 0.60 \\ 0.02 &\leq x \leq 0.35 \\ 0 &\leq t \leq 2.0 \quad A_{shut} \leq 2.0 \end{aligned} \quad (15)$$

where A is the quantity of air entrainment, t_f is the filling time, x is the acceleration distance, and $w_a = 1.0$ and $w_t = 0.1$ are the weighting factors. A_{shut} is the volume of trapped air when the plunger injection is switched from low speed to high speed, where K_p is the penalty. Each time, the penalty conditions shown in Equation (15) hold, the penalty $K_p=10^8$, which is big enough to avoid the penalty conditions, will be added to satisfy the specifications.

3.1 Optimization of Die-casting.

The parameters for the EDSA are, the number of generation is 60, the number of population is 30, the number of elite preservation is 2, the order of fitting curve is 5, and the parameters for the GA to be compared with the EDSA are , the number of generation and the number are same, the number of elite preservation is 1, the crossover fraction is 0.80, the mutation fraction is 0.01, where the initial population is the same for each algorithm, allowing us to calculate under the same conditions.

Table 2 shows the cost determined by the EDSA and the GA. Based on these results we conclude that the proposed method can derive the optimized solution with few repeated computations.

Table 2. Performance comparison sample

Parameter	EDSA	GA
Evaluated value	0.3441	0.4622
Air entrainment	0.1682	0.2737
Finish time	1.76	1.89
Optimum termination	41	19

3.2 Verification by Experiment.

Experiments for an actual die-casting plant were performed with the obtained optimum velocity input derived using the EDSA and the GA. The plunger velocity parameters are shown in Table 3. The result of the blister examination, the obtained optimum velocity input derived using the EDSA can about 30 percent reduction of air entrapment less than using the GA

Table 3. Experimental plunger velocity parameters

EDSA	Time	Velocity	Position
1	1.23[s]	0.26[m/s]	0.160[m]
2	1.34[s]	0.50[m/s]	0.200[m]
3	1.76[s]	0.29[m/s]	0.367[m]
GA	Time	Velocity	Position
1	1.32[s]	0.220[m/s]	0.145[m]
2	0.440[s]	0.440[m/s]	0.245[m]
3	0.560[s]	0.560[m/s]	0.367[m]

4 CONCLUSION.

The purpose of this study was to design a search algorithm that used smaller number of populations and a generation that can derive the optimized solution more efficiently for an optimization problem using a CFD simulator. The effectiveness of the proposed method is shown through experiments in actual die-casting plants for deriving the optimum plunger input. The effectiveness of the proposed method was clarified by experimental results, which showed that the amount of air entrainment by using the EDSA was better than that resulting from using the GA.

REFERENCES

1. P. Stefano P. Carlo M. Martin, "Integrating Multibody Simulation and CFD : toward Complex Multidisciplinary Design Optimization," JSME international journal. Ser. B, Fluids and thermal engineering, vol.48, no.2, 2005, pp. 224-228
2. P. Moscato, "gentle introduction to memetic algorithm," Handbook of Metaheuristics, 2003, pp. 105-144
3. S. Tsutsui, M. Yamamura, "Simplex Crossover in Real Coded Genetic Algorithms," Proceedings of the

REMOTE MONITORING OF TV/RADIO CHANNELS-USE

Ojenge Winston

tojenge@yahoo.com

Department of Electrical and Electronic Engineering, School of Engineering, Science and Technology
Kenya Polytechnic University College, P.O. Box 52428 – 00200, Nairobi, Kenya

Abstract–TV/Radio broadcasters do the business of informing and entertaining its listeners/viewers. Their returns is in the amount of listenership / viewership that they pull, as advertisers of goods use them as a medium to reach potential buyers. The broadcasters themselves, advertisers, among other stakeholders, frequently need to determine the amount of listenership/viewership for each channel/program. Currently, they carry interview/questionnaire survey of sample populations. This is plagued by inherent survey inaccuracies. The proposed system attempts to remotely ‘listen’ to the frequencies that individual receivers are tuned into. The frequencies are constantly cumulated over a given region to determine the listenership/viewership of a channel / program.

1. INTRODUCTION.

Broadcasting is cut-throat business as various broadcasters fight to achieve the most viewer/listener-base. Access to viewer/listener-base makes a broadcaster a convenient advertisement medium for the hundreds of thousands of products that occupy retail stores.

To charge appropriately for the exposure they give to these products, broadcasters may need to qualify their viewer/listener-base.

Currently, broadcasters and other interested entities do a survey, asking viewers and listeners what channels and programs they favor (Thompson (1)). This technique is not very reliable in the sense that listeners and viewers may not provide accurate information. The survey is also likely to have significant sampling error margins.

A technique, that discreetly ‘listens’ to the frequency tuned into by a remote viewer/listener, is most reliable.

The focus of this study is to;

1. Re-design a super-heterodyne receiver system that sends a signal containing both, the frequency it is tuned into and a code that identifies the individual receiver.
2. Utilize the mobile telephone infrastructure to harvest the signals from the remote individual receiver.
3. Design a system that receives the signals nation-widely, analyses them and determines the receiver- and viewer-base of individual channels and programs.

2. CURRENT SITUATION

Figure 1 below illustrates the operation of the generic super-heterodyne radio/TV receiver;

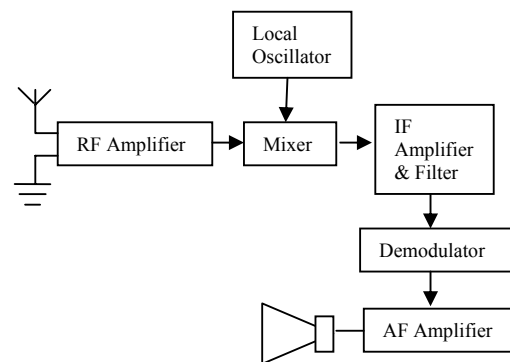


Figure 1:

Only one intermediate frequency (IF), usually 455 KHz in AM broadcasts, is allowed to the demodulator (Whitaker (2)). The demodulator converts it to audio frequency (AF), which is the message frequency. To achieve the single IF, the mixer is designed to get the algebraic sum of the local oscillator and the radio frequency (RF). During tuning, the user chooses a local oscillator frequency which, when mixed with the frequency of the desired channel, results into an algebraic sum of 455 KHz (Nahin (3)). If the oscillator frequency could be known, it would be easy to determine the frequency tuned into, and subsequently, the channel being listened to.

There is always some radiation from such receivers, and in the initial stages of RAFTER, a World War II operation undertaken by the British MI5, they simply attempted to locate clandestine

Nazi receivers based on picking up the super-heterodyne signal with a quiet sensitive receiver that was custom built (Wright (4)). This was not always easy because of the increasing number of domestic radios and televisions in people's homes.

By accident, one such receiver for MI5 mobile radio transmissions was being monitored when a passing transmitter produced a powerful signal. This overloaded the receiver, producing an audible change in the received signal. Quickly the agency realized that they could identify the actual frequency being monitored if they produced their own transmissions and listened for the change in the super-heterodyne tone.

Such remote sensing of the local oscillator frequency can be used to remotely detect the channels an individual receiver is tuned into.

3. METHODOLOGY

The following proposed techniques focus on a slight redesign of the super-heterodyne receiver, the use of mobile telephony infrastructure and finally, the constant region-wide analysis of the tuned-into channels, in order to determine the favorite channels and programs.

3.1. Use of the mobile telephony infrastructure

Currently, the infrastructure that is laid down elaborately enough to access nearly every receiver in the country is the networks of the mobile telephony service providers. Their base stations are found in almost every nook of the provinces. If the reach of the oscillator echo is adequate, the base stations may be used to capture the signals. Each base station is identified. It therefore is possible to maintain a running record of listener/viewer tuning profile around each base station, which is cumulated over the relevant region.

However, two or more receivers may be close together and both tuned to the same station. How are the two differentiated? This is possible by slightly redesigning the super-heterodyne receiver as follows;

3.2. Redesign of the super-heterodyne receiver

The key to differentiating between any two neighboring receivers tuned to the same channel lies in the most likely feature about which two receivers would be different. Any two or more

receivers close together may differ in such factors as;

- size
- make / model
- height at which they are placed
- volume level

Of all the above features, a survey has established that the factor most likely to differentiate the receivers is volume level.

Greatwall apartments, in Mlolongo township, occupies an area of about 100 m by 100m, with 500 households. 270 radio and TV receivers were tested for volume level using a VU meter. Only two recorded the same levels at certain selected reference points. That implies 0.74%. The study assumes that although two slightly different speaker volumes may be tuned at same level in terms of output voltage for volume control, the likelihood of two users tuning the same output voltage level is as rare as the findings of the survey.

The study proposes to use output voltage level for volume control, to code the local oscillator signal before it is transmitted out of the receiver. The output voltage level of each receiver is first converted to voltage-dependent frequency, which is used to modulate the local oscillator frequency. The modulated signal is now channeled to an antenna. At the base station, the two signals are separated. An analytical module then uses the modulating signal to identify every local oscillator frequency signal.

3.3. Analysis of the tuned-into channels region-wide

The identities of the individual receivers can be established with permanency as volume control and channel selection shall be as dynamic as the alternating whims of the many users within a household. However, it would still be possible to monitor the usage, in terms of number of listeners and viewers, to all channels at any single moment. The analysis of the dynamic usage, in order to identify which programs are more popular would need artificial intelligence analytical techniques, as the changing of the channels and programs reflect whimsical human habits that are only possible to monitor and establish patterns for, using Artificial Intelligence.

The entire proposed system is illustrated in the block diagram in Figure 2 below;

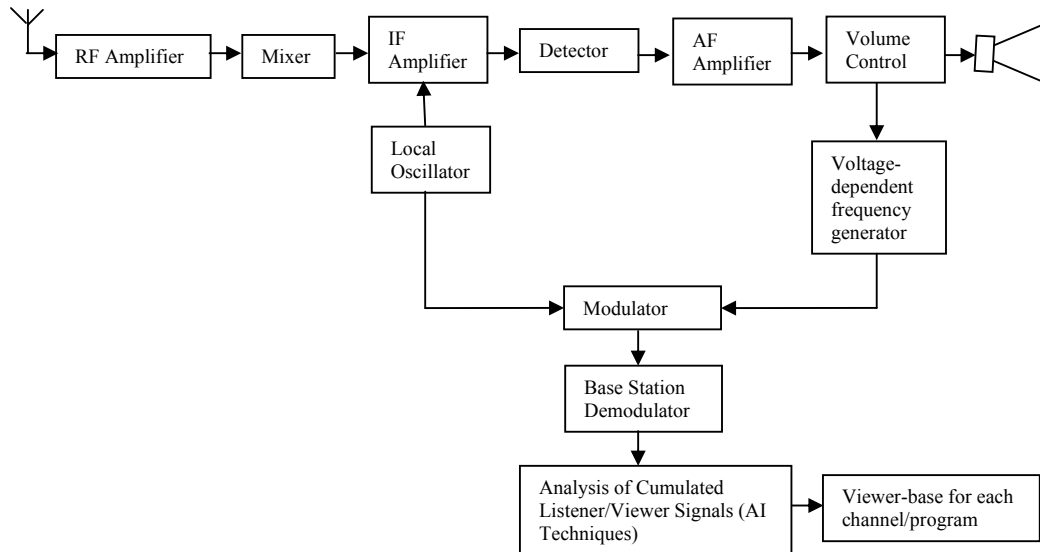


Figure 2:

4. REFERENCE.

1. Thompson, S., TV: The Medium of Choice in a Recession?, 2009 SThompson@wfofr.com
2. Wright, P., Spycatcher: The Autobiography of a Senior Intelligence Officer, 1987.
3. Whitaker, J., The Electronics Handbook. CRC Press. pp. 1172. ISBN 08-493834-55, 1996.
4. Nahin, P., The Science of Radio. Page 91. Figure 7.10. Chapter 7. ISBN 0-387-95150-4.

NEURAL FUZZY BASED DC-DC CONVERTER CONTROLLER OPTIMISED WITH PARTICLE SWARM OPTIMIZATION.

M.M Kanai J.N Nderu P.K Hinga

Department of Electrical and Electronics Engineering, Jomo Kenyatta University of Agriculture and Technology. cheptora@yahoo.com, jnnnderu@yahoo.com

Abstract—This paper presents an application of Adaptive Neuro-Fuzzy Inference System (ANFIS) controller for DC – DC converter optimized with swarm collective intelligence. First, an adaptive Neuro-Fuzzy controller of the DC-DC converter is designed and simulated using MATLAB/SIMULINK package; the ANFIS has the advantage of expert knowledge of the Fuzzy inference system and the learning capability of neural networks. Secondly, the ANFIS is optimized by Particle Swarm optimization methodology. Digital simulation results demonstrates that the designed ANFIS-Swarm controller realize a good dynamic behavior of the DC-DC converter, a perfect voltage tracking with smaller overshoot, steady state error and short settling time as well as high robustness than those obtained by ANFIS controller. The results are compared with conventional PID controller.

Keywords: *DC-DC converter; Neural Fuzzy controller; Particle Swarm Optimization (PSO); Adaptive Fuzzy Neural Network.*

I INTRODUCTION

Every electronic circuit is assumed to operate off some supply voltage which is usually assumed to be constant. DC-DC converter is a voltage regulator (a power electronic circuit that maintains a constant output voltage irrespective of changes in load current or line voltage). Many different types of voltage regulators with a variety of control schemes are used. With the increase in circuit complexity and improved technology a more severe requirement for accurate and fast regulation is desired. This has led to need for newer and more reliable design of dc-dc converters. With the advent of digital signal processors, advanced control methodologies through Artificial Intelligence has been applied in most of the industrial applications. Power supplies have emerged as an independent industry which is inevitable in all electrical and electronic components. The practical challenge in most of the SMPS is to design the advanced control strategies to tackle the nonlinearity, stability and uncertainty of parameters. DC-DC converter controllers can be implemented in numerous conventions these includes: Voltage mode control, Current mode control, V^2 mode control in analog controllers [1], Fuzzy Logic

Controller [2] Neural Network controllers [3]; or a combination of these: Fuzzy-Neural Networks [4], [5].

For many years, control design for converters has been carried out through analog circuits with Negative feedback being employed for voltage regulation regardless of disturbances in input voltage, load current, or variations in component values. The duty cycle is varied in the feedback loop to compensate for these variations. The conventional voltage mode and current mode control depends on speed of error amplifier on load variations which slows down compensation. To improve further on speed of response, V^2 control mode control [1] is introduced. The unique feature of V^2 control is its fast transient speed and simple compensation design. The transient speed is maximized by using the output voltage as a ramp signal.

To counter the effects of input voltage variations, Barry and Dragan [6] designed a feed-forward controller to improve line regulation in applications with a wide range of input voltages and load currents. Inherent advantages over various inner-feedback techniques, such as current-mode

programming include simplicity, absence of stability problems, and the fact that the converter low open loop output impedance is not affected. However, direct sensing of the input voltage through a feed-forward loop may induce large signal disturbances that could upset the normal duty cycle of the converter.

Analog controllers also suffer from lower sensitivity to changes in environment such as temperature, supply voltage fluctuation and aging of components. In general they are neither robust nor adaptive [7].

In recent years, there has been a growing interest in the implementation of digital control concepts in high frequency low-medium power DC-DC converters. Digital control is well recognized for its flexibility and programmability, reduced design time, less susceptibility to aging and better noise immunity, ability to handle complex control schemes and to implement communication functions for fault and status information and easy reconfigurability for different applications [8].

However, as compared to analog control, digital control suffers from a reduced control loop bandwidth due to the presence of time delays inherent to the digital control structure. Therefore, the improvement of digital control performance is a key issue that needs to be assessed and solved in order to make digital control a viable technological option [9].

II INTELLIGENT CONTROLERS

Intelligent control achieves automation via the emulation of biological intelligence. It either seeks to replace a human who performs a control task or it borrows ideas from how biological systems solve problems and applies them to the solution of control problems.

The control laws for power converter and inverter topologies are based mainly on linear control theory even though most topologies are characterized by non-linearity and discontinuities. Using human linguistic terms and common sense, several fuzzy logic

controllers have been developed and implemented for dc-dc converters. These controllers have shown promise in dealing with nonlinear systems and achieving voltage regulation. Fuzzy logic control uses human-like linguistic terms in the form of IF-THEN rules to capture the nonlinear system dynamics [10].

There are several design concerns that one encounters when constructing a fuzzy controller. First, it is generally important to have a very good understanding of the control problem, including the plant dynamics and closed-loop specifications. Second, it is important to construct the rule base very carefully. If you do not tell the controller how to properly control the plant, it cannot work well. Third, for practical applications you can run into problems with controller complexity since the number of rules used grows exponentially with the number of inputs to the controller, if you use all possible combinations of rules. In general, although it has achieved many practical successes, fuzzy control has not been viewed as a rigorous science due to lack of formal analysis and synthesis techniques.

An NN is an interconnection of a number of artificial neurons that simulates a biological brain system. It has the ability to approximate an arbitrary function mapping and can achieve a higher degree of fault tolerance. NNs have been successfully introduced into power electronics circuits to generate the switching signals for converters. An Artificial Neural Network (ANN) is an information-processing paradigm that is inspired by the way biological nervous system, such as brain, process information. The key element of this paradigm is the novel structure of the information processing system. It is composed of large number of highly interconnected processing elements (neurons) working in unison to solve problems [11].

There are several design concerns with neural network controllers that you encounter in solving the function approximation problem

using gradient methods (or others) to tune the approximator structure. First, it is difficult to pick a training set that you know will ensure good approximation. Second, the choice of the approximator structure is difficult. While most neural networks (and fuzzy systems) satisfy the “universal approximation property,” so that they can be tuned to approximate any continuous function on a closed and bounded set to an arbitrary degree of accuracy, this generally requires that you be willing to add an arbitrary amount of structure to the approximator. Due to finite computing resources we must then accept an “approximation error.” How do we pick the structure to keep this error as low as possible? This is an open research problem. Third, it is generally impossible to guarantee convergence of the training methods to a global minimum due to the presence of many local minima. Hence, it is often difficult to know when to terminate the algorithm. Finally, there is the important issue of “generalization,” where the neural network is hopefully trained to nicely interpolate between similar inputs. It is very difficult to guarantee that good interpolation is achieved. Normally, all we can do is use a rich data set (large, with some type of uniform and dense spacing of data points) to test that we have achieved good interpolation. If we have not, then you may not have used enough complexity in your model structure, or you may have too much complexity that resulted in over fitting (over-training) where you match very well at the training data but there are large excursions elsewhere.

III. NEURALFUZZY-ANF CONTROLLERS

The integration of neural network architectures with fuzzy inference system has resulted in a very powerful strategy known as adaptive network-based fuzzy inference system (ANFIS). It essentially consists of combining fuzzy inference system and neural networks and implementing within the framework of adaptive networks [12].

Two control topologies of adaptive network-based fuzzy inference system (ANFIS) for

control of the DC-DC converter are developed and presented in [5]. The developed ANFIS has the ability to learn about the non-linear dynamics and external disturbances of the converter with a stable output, small steady error and fast disturbance rejection. It can adapt and generalize its learning to other tasks. It can also provide abstraction particularly when Sensory measurements are contaminated with noise. The input to the controller is output voltage and inductor current. In [4] ANFIS is used to control dc-dc converter with output error voltage and derivative of error as the inputs to the controller. Both fuzzy logic principles and learning functions of neural networks are employed together to construct the adaptive fuzzy network inference system for the control topology. Initially, a basic fuzzy logic controller is set up utilizing linguistic rules. Then, numerical data are used for training the controller. The number of membership functions is chosen so as to cover the entire input space. The controllers are shown to be robust, adaptive, and capable of learning.

The subsequent to the development of ANFIS approach, a number of methods have been proposed for learning rules and for obtaining an optimal set of rules. Jang and Mizutani [13] have presented application of Lavenberg-Marquardt method, which is essentially a nonlinear least squares technique, for learning in ANFIS network, this method is always stable and efficient. Jang also in [12] introduced four methods to update the parameters of ANFIS structure, as listed below according to their computation complexities:

1. Gradient descent only: all parameters are updated by the gradient descent.
2. Gradient descent only and one pass of LSE: the LSE is applied only once at the very beginning to get the initial values of the consequent parameters and then the gradient descent takes over to update all parameters.
3. Gradient descent only and LSE: this is the hybrid learning.
4. Sequential LSE: using extended Kalman filter to update all parameters. These

methods update antecedent parameters by using GD or Kalman filtering.

The training of network is through Gradient Descent (GD) and Least Square Estimation (LSE) methods leads to slow convergence of parameters and finding the best learning rate is very difficult. The methods also depends on initial value of parameters which if not well chosen may lead to local minimum.

A. ADAPTIVE NEURO-FUZZY PRINCIPLE

A typical architecture of an ANFIS is shown in Figure 1, in which a circle indicates a fixed node, whereas a square indicates an adaptive node. For simplicity, we consider two inputs x, y and one output z . Among many FIS models, the Sugeno fuzzy model is the most widely applied one for its high interpretability and computational efficiency, and built-in optimal and adaptive techniques. For a first order Sugeno fuzzy model, a common rule set with two fuzzy if-then rules can be expressed as:

Rule 1: if x is A_1 and y is B_1 , then $z_1 = p_1 x + q_1 y + r_1$ (1)

Rule 2: if x is A_2 and y is B_2 , then $z_2 = p_2 x + q_2 y + r_2$ (2)

Where A_i and B_i are the fuzzy sets in the antecedent, and p_i, q_i and r_i are the design parameters that are determined during the training process. As in Figure 1, the ANFIS consists of five layers [12]:

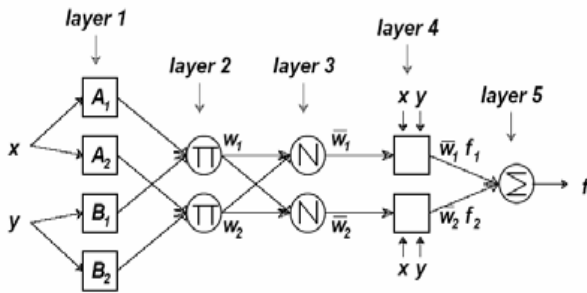


Figure 1: The equivalent ANFIS (type-3 ANFIS)

Layer 1: Every node i in the first layer employ a node function given by:

$$\begin{aligned} O_i^1 &= \mu_{A_i}(x), i = 1, 2 \\ O_i^1 &= \mu_{B_{i-2}}(y), i = 3, 4 \end{aligned} \tag{3}$$

Where μ_{A_i} and μ_{B_i} can adopt any fuzzy membership function (MF).

Layer 2: Every node in this layer calculates the firing strength of a rule via multiplication:

$$O_i^2 = w_i = \mu_{A_i}(x) \mu_{B_i}(y), i = 1, 2 \tag{4}$$

Layer 3: The i -th node in this layer calculates the ratio of the i -th rule's firing strength to the sum of all rules firing strengths:

$$O_i^3 = \bar{w}_i = \frac{w_i}{w_1 + w_2}, i = 1, 2 \tag{5}$$

Where w_i is referred to as the normalized firing strengths.

Layer 4: In this layer, every node i has the following function:

$$O_i^4 = \bar{w}_i z_i = \bar{w}_i (p_i x + q_i y + r_i), i = 1, 2 \tag{6}$$

Where W_i is the output of layer 3, and $\{p_i, q_i, r_i\}$ is the parameter set. The parameters in this layer are referred to as the consequent parameters.

Layer 5: The single node in this layer computes the overall output as the summation of all incoming signals, which is expressed as:

$$O_i^5 = \sum_{i=1}^2 \bar{w}_i z_i = \frac{w_1 z_1 + w_2 z_2}{w_1 + w_2} \tag{7}$$

The output z in Figure 1 can be rewritten as:

$$z = (\bar{w}_1 x) p_1 + (\bar{w}_1 y) q_1 + (\bar{w}_1) r_1 + (\bar{w}_2 x) p_2 + (\bar{w}_2 y) q_2 + (\bar{w}_2) r_2 \tag{8}$$

B. Adaptive Neuro-Fuzzy controller Design

The ANFIS controller generates change in the reference voltage V_{ref} , based on speed error e and derivate in the speed error de defined as:

$$e = V_{ref} - V \tag{9}$$

$$de = [d(V_{ref} - V)]/dt \tag{10}$$

where V_{ref} and V are the reference and the actual speeds, respectively.

In this study first order Sugeno type fuzzy inference was used for ANFIS and the typical fuzzy rule is:

If e is A_i and de is B_i then $z = f(e, de)$ (11)

Where A_i and B_i are fuzzy sets in the antecedent and $z = f(e, de)$ is a crisp function in the consequent.

The significances of ANFIS structure are:

Layer 1: Each adaptive node in this layer generates the membership grades for the input Vectors $A_i, i=1, \dots, 5$. In this paper, the node function is a triangular membership function:

$$\mu_{A_i}(e) = \begin{cases} 0 & e_i \leq a_i \\ \frac{e - a_i}{b_i - a_i} & a_i \leq e \leq b_i \\ \frac{c_i - e}{c_i - b_i} & b_i \leq e \leq c_i \\ 0 & c_i \leq e \end{cases} \tag{12}$$

Layer 2: Each node output represents the activation level of a rule:

$$O = w_i = \min(\mu_{A_i}(e), \mu_{B_i}(e)), i=1, \dots, 5 \tag{13}$$

Layer 3: Fixed node i in this layer calculate the ratio of the i -th rule's activation level to the total of all activation level:

$$O_i^1 = \frac{w_i}{\sum w_j} \tag{14}$$

Layer 4: Adaptive node i in this layer calculate the contribution of i -th rule towards the overall output, with the following node function:

$$O_i^1 = \frac{w_i}{\sum w_j} Z_i = \frac{w_i}{\sum w_j} (p_i e + q_i de + r_i) \tag{15}$$

Layer 5: The single fixed node in this layer computes the overall output as the summation of contribution from each rule:

$$O_i^5 = \sum_{i=1}^2 \frac{w_i Z_i}{w_i + w_j} \tag{16}$$

The parameters to be trained are a_i, b_i and c_i of the premise parameters and p_i, q_i , and r_i of the consequent parameters. Training algorithm requires a training set defined between inputs and output.

IV. PARTICLE SWARM OPTIMIZATION (PSO)

The PSO, which is a member of the evolutionary routines family, mimics the social behavior of a swarm of birds (particles) seeking the richest food source in a large field [14–16]. The algorithm exploits a population of randomly generated potential solutions in order to detect the global minimum of a highly nonlinear multimodal objective function. The PSO is a derivative-free algorithm, which utilizes cooperation, competition, and experience of the population individuals along with probabilistic transition rules of search.

The algorithm starts with a randomly generated population of individual particles representing potential solutions to the optimization problem. Each particle signifies a position in the search space, at which the objective function is evaluated. The particles move in the search space affected by three factors, namely, the previous movement of the same particle, the position of the best particle of the current population (local best), and the position of the best particle over the previous iterations (global best). The new velocities of the particles are probabilistically determined

as given in Equation 17, while the new positions are computed as shown in Equation 18. One distinct attribute of PSO, compared to other evolutionary techniques, is that it does not employ the “survival of the fittest” concept as it does not implement a direct selection function. In other words, particles of low fitness can survive and probably visit any point in the search space.

$$v_i^{k+1} = \omega v_i^k + \alpha(P_{i-} - x_k) + \beta(P_{g-} - x_i^k) \quad (17)$$

$$x_i^{k+1} = x_i^k + v_i^{k+1} \quad (18)$$

- v_i^{k+1} = the velocity vector of the i^{th} particle at the $(k + 1)^{th}$ iteration,
- ω = inertia weighting factor
- v_i^k = the velocity vector of the i^{th} particle at the k^{th} iteration,
- α = bounded positive uniformly distributed random vector,
- P_{i-} = the position vector of the local best particle at the k^{th} iteration,
- x_i^k = the position vector of the i^{th} particle at the k^{th} iteration,
- β = bounded positive uniformly distributed random vector,
- P_{g-} = the position vector of the global best particle up to the k^{th} iteration,
- x_i^{k+1} = the position vector of the i^{th} particle at the $(k + 1)^{th}$ iteration.

One evident advantage of PSO is the ease of implementation. Once the particle positions and velocities are randomly initialized, Equations 17 and 18 above are used to iterate on the fitness till convergence.

Optimal ANFIS Controller Design with PSO

To design the optimal ANFIS controller, the PSO algorithms are applied to find the globally optimal parameters of the ANFIS. The structure of the DC-DC converter with ANFI- PSO controller is shown in Figure 7.

In this paper, the chromosomes of the PSO algorithms contains two parts: the range of the

membership functions (Ke and Kde) and the shape of the membership functions ($e1\sim e5$ and $de1\sim de5$). It gives the optimal output voltage, such that the steady-state error of the response is zero. The genes in the chromosomes are defined as: $[Ke, Kde, e1, e2, e3, e4, e5, de1, de2, de3, de4, \text{ and } de5]$.

V. RESULTS

Three different controllers are designed for the DC-DC Buck Converter (steps 12 volts to 5 volts output). First, the PID controller is designed based on the expert experience; best results were obtained with;

$Kp=3, Ki= 1.5e4, Kd=0.$

- where:
- Kp =proportional gain
- Ki =integral time
- Kd =derivative time

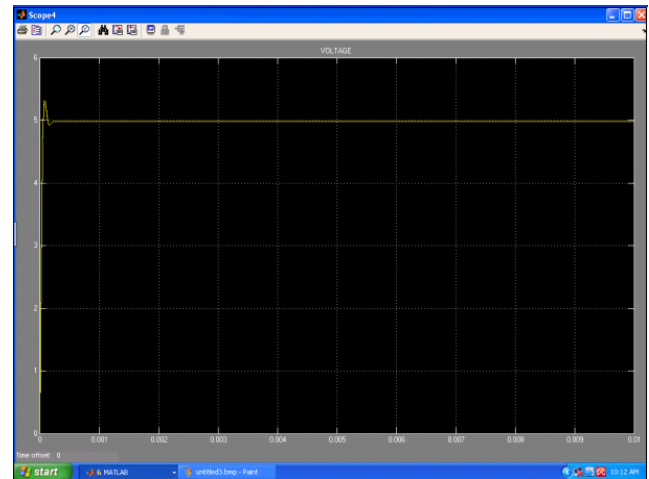


Figure 2: Output voltage with PID controller

Second, the fuzzy logic controller is designed based on the neural networks (ANFIS) to find the optimal range of the membership functions.

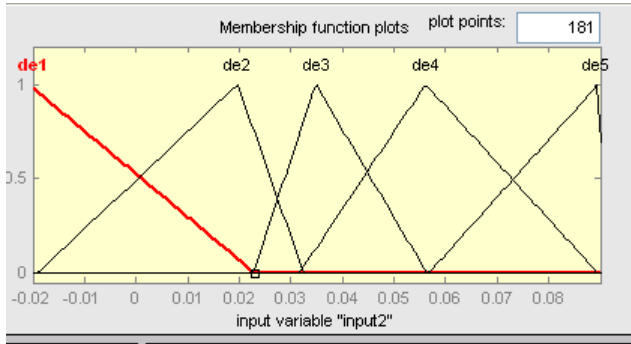


Figure 3: Change in error membership functions

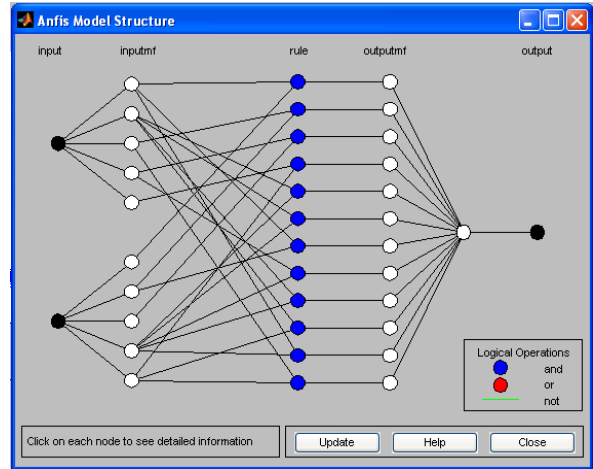


Figure 6: Anfis model structure

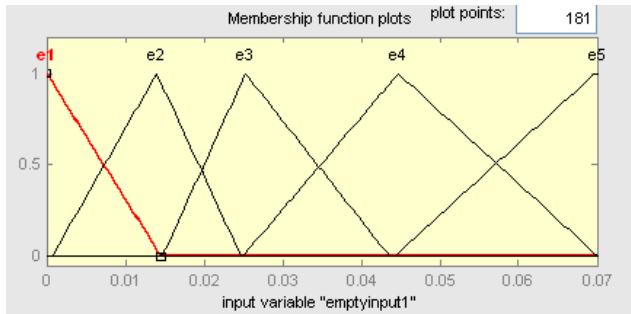


Figure 4: Error membership functions

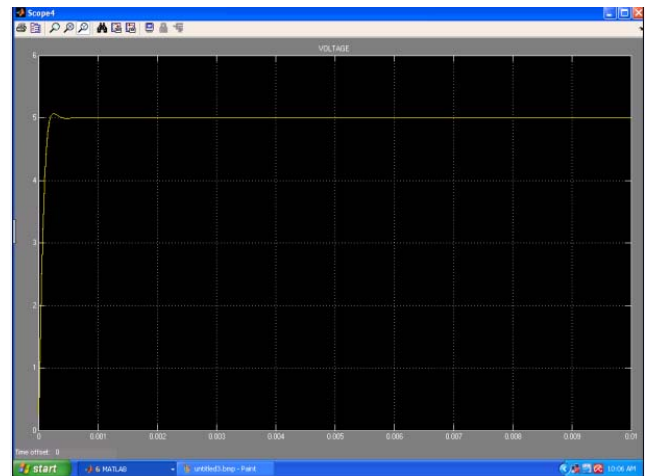


Figure 7: output voltage with ANFIS controller

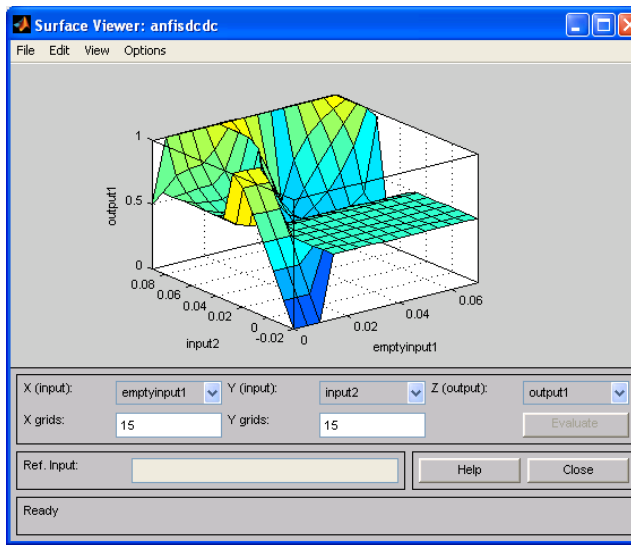


Figure 5: Matlab surface view

After that, the optimal fuzzy controller (ANFIS) is designed based on the PSO to search the optimal range of the membership functions, the optimal shape of the membership functions (ANFIS with PSO).

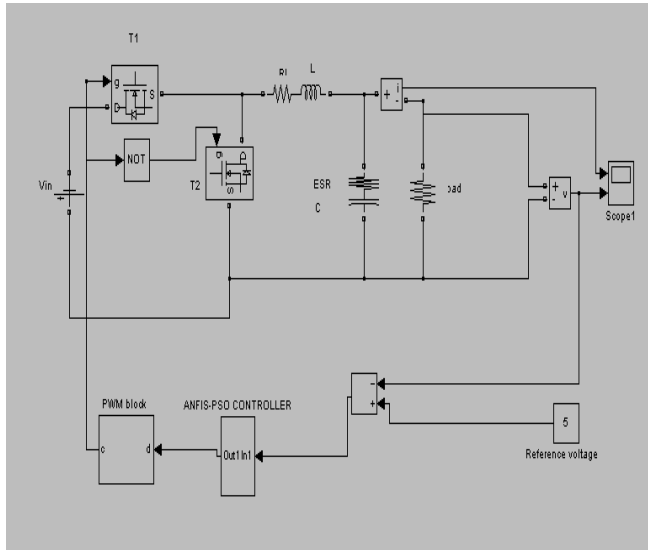


Figure 8: Buck (12V-5V) DC-DC converter

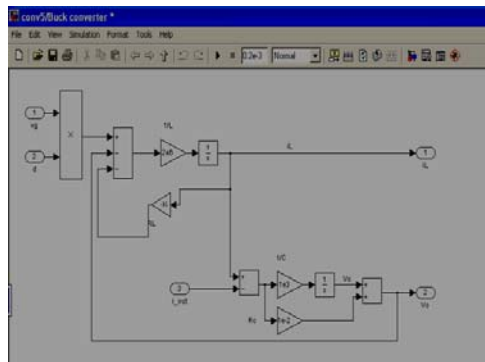


Figure 9: Simulink diagram of buck converter

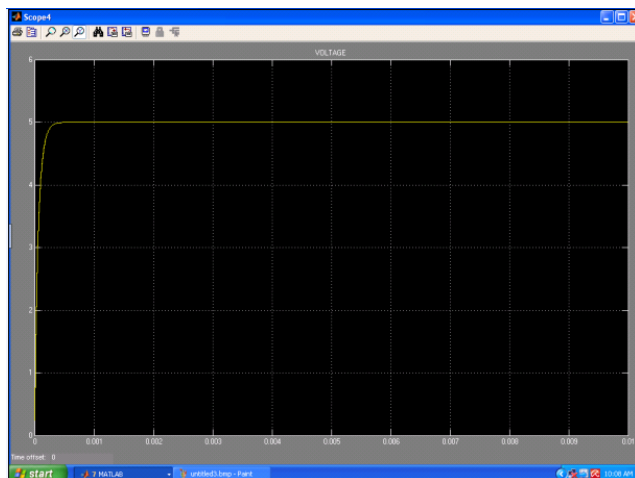


Figure 10: Output voltage with ANFIS-PSO controller

VI.CONCLUSION

In this paper, the optimal ANFIS controller is designed using Particle Swarm Optimization algorithms. The ANFIS-Swarm presents satisfactory performances and possesses good robustness; no overshoot, minimal rise time and zero Steady state error (deadbeat response) as presented in simulation in figure9 and table1. The system operating conditions, which influence the controller parameters, are determined. PSO is utilized to obtain the parameters of the controller, which maintain deadbeat response, at selected load points within the reasonably wide range of operation. Data resulting from PSO are used to train ANFIS agents to predict the controller parameters at different loads within the operating regions. The comparison shows the superiority of the proposed technique over ANFIS and PID controllers.

Table 1: Comparative Analysis

Results	PID controller	(ANFIS) controller	ANFIS-PSO controller
Rise time(sec.)	2e-4	2e-4	1.8e-4
Steady-state error	5%	2%	0%
Overshoot	2%	1%	0%

REFERENCES

- [1] Saurabh Kasat, Analysis, Design and Modeling of dc-dc converter using Simulink, Masters Thesis, December, 2004.
- [2] Guang Feng , Wanfeng Zhang and Yan-Fei Liu, An Adaptive Current Mode Fuzzy Logic Controller for DC-to-DC Converters, Department of Electrical and Computer Engineering, Queen’s University Kingston, Canada, 2003
- [3] S.G. Kadwane, Amit kumar, B.M. Karan, T Ghose, Online Trained Simulation and DSP Implementation of Dynamic Back Propagation Neural Network for Buck Converter, ACSE Journal, Volume (6), Issue (1), January, 2006.
- [4] Ahmed Rubaai, Abdul R. Ofoli, Legend Burge and Moses Garuba, Hardware Implementation of an Adaptive Network-Based Fuzzy Controller for DC–DC Converters, IEEE Transaction Industry Applications, VOL.41,NO.6, November/December2005 pp 1557-1565.
- [5] Ahmed Rubaai and Abdul Ofoli, Hardware Implementation of an Adaptive Network-based

- Fuzzy Controller for DC-DC Converters, Howard University Electrical and Computer Engineering Department, 2004.
- [6] B.Arbetter and D. Maksimovic, “Feed-Forward Pulse Width Modulators for Switching Power Converters,”IEEE Trans. Power Electron. vol. 12, no. 2, pp. 361–368, Mar. 1997.
- [7]Mohan,Underland,Robbins.Power Electronics Converters, Applications and Design. John Wiley & sons, inc. 2003, pp 322-341.
- [8] Praveen Jain, CHiL Semiconductor, Digital Control in the Voltage Regulators for Computers, 2007.
- [9] Yoichi Ishizuka, Yosuke Asako, Masao Ueno and Hirofumi Matsuo,A Design of a Low-Delay DPWM Control Circuit for DC-DC Converter, Nagasaki University, Sanken Electric Co., Ltd., 2007.
- [10] Johnson Asumadu and Eugene Ho, A Multivariable Fuzzy Logic Controller (MFLC) For A Buck DC-DC Converter, Annual IEEE Power Electronics Specialists Conference ,Aachen Germany, 2004.
- [11] N. Rajarajeswari and K. Thanushkodi, Design of an Intelligent Bi-Directional DC-DC Converter with Half Bridge Topology, European Journal of Scientific Research ISSN 1450-216X Vol.22 No.1 (2008), pp.90-97© Euro-Journals Publishing, Inc. 2008.
- [12]Jang, J.-S.R., “ANFIS: Adaptive-Network-based Fuzzy Inference System”, IEEE Transactions on Systems, Man and Cybernetics, Vol. 23, No. 3 , 1993, pp. 665 –685.
- [13] Jang, J.-S. R., and Mizutani, E., “Levenberg-Marquardt Method for ANFIS Learning”, Biennial Conference of the North American Fuzzy Information Processing Society, June 1996, pp. 87 –91.
- [14] A.Soundarrajan, Member, IAENG, Dr.S.Sumathi, C.Sundar, Particle Swarm Optimization Based LFC and AVR of Autonomous Power Generating System, IAENG International Journal of Computer Science, 37:1, IJCS_37_1_2010.
- [15] Mohamed A. Awadallah, Ehab H. E. Bayoumi, Hisham M. Soliman, Adaptive Deadbeat Controllers for Brushless Dc Drives Using PSO and ANFIS Techniques, Journal of Electrical Engineering, vol. 60, no. 1, 2009, 3–11
- [16] Kurniawan E. P. and Siti Z. M. , Fuzzy Membership Function Generation using Particle Swarm Optimization, Int. J. Open Problems Compt. Math., Vol. 3, No. 1, March 2010.

OPTIMIZATION OF UNDERDETERMINED BLIND SPEECH DENOISING FOR ENHANCED TELECONFERENCING BY INTERPOLATED FASTICA_25

Denis Ombati Dr. E N Ndun'gu
denist2009@yahoo.com

Department of Telecommunication and Information Engineering, JKUAT

Abstract—This paper proposes a new method for optimization of blind source separation for enhanced teleconferencing. Independent component analysis ICA and sparse representation SR are the main tools employed to obtain source signals from observed data containing both original signals and white Gaussian noise. This is called “cocktail-party problem”. The aim of this research is to separate source signals and de-noising them thereof, using optimal FastICA. The method will take the advantages of statistical independence and non-Gaussianity of signal components. The signals considered here are instantaneous in nature. Several sparse algorithms have been proposed so far in literature though with different complexities to realize its objectives. The proposed methodology for this research will follow the following procedure. A model room environment in a microphone array and exploit underdetermined blind sources separation. An algorithm that will exploit spatial diversity in time domain to optimize decomposition to obtain independent speech subset. The research looks maximizing SNR and eventually low signal distortion. Our results simulated in MATLAB software based algorithm will be developed to realize optimal modelled blind source separation for separation and de-noising, to mimic real world. Any further direction on this research will be outlined to facilitate future realization of effective separation of many kinds of signals, such as speech or biomedical data, teleconferencing.

Keywords: *Blind Source Separation, Independent Component Analysis, Sparse Representation, Sparse Decomposition*

1. INTRODUCTION

In blind source separation BSS we obtain an estimate of each source signal from the sensor observations with little information as possible about the number of sources, the speech sources, or the mixing process, and additive noise. Therefore blind techniques do not have knowledge of on-times of various sources, and such information will only be gotten by estimating the separated signals. Considering [1] [2] an array of M microphones (sensors) where the output of the m^{th} microphone is denoted by $x_m(k)$, where k is the discrete-time sample index. Assuming n sources whose signals are given by $s_n(k)$, the output of the m^{th} microphone is the convolved mixture whose mathematical equation can be viewed as:-

$$x(k) = B * s(k) + v(k). \tag{1}$$

where $x_m(k)$ the sensor observations, $s_n(k)$ is the source signal, B is the mixing system (impulses), $v_m(k)$ is the added noise. The output signal $\hat{s}_m(k)$ of each will be the point of interest; an estimate of sound source $s_n(k)$. It is generally assumed that the source signals are mutually statistically independent.

In this research proposal an optimal underdetermined blind speech de-noising algorithm, practically free from prior weakness, is

to be developed for analysis of telecommunication systems with more emphasis on teleconferencing room. The separation of the signals is achieved by sparse decomposition and filtering. This paper proposes an improved way of sparse representation SR focusing Pursuit algorithm as one of its aspects. Pursuit algorithms help to solve optimization problems of the signal dictionary. Sparse representation (factorization) of a data matrix based on the following model and alongside Figure (1) below.

$$X = BS; \tag{2}$$

where the $X = [x(1); \dots ; x(N)] \in \mathbf{R}^{m \times N}$ ($N \gg 1$) is a known data matrix, $B = [b(1) \dots b(m)] \in \mathbf{R}^{m \times n}$ is a $m \times n$ basis matrix, $S = [s(1); \dots ; s(N)] = [s_{ij}]_{n \times N}$ is a coefficient matrix, also called a solution corresponding to the basis matrix B . Generally, $m < n$, which implies that the basis is overcomplete dictionary.

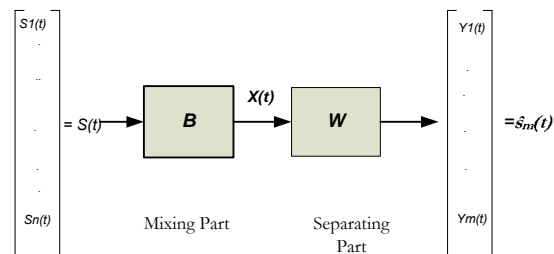


Figure 1. Mixing and Separating Parts.

The Mixed Model, ICA and Sparsity.

In this section, we formulate the instantaneous mixing model for underdetermined Blind Source Separation [1]. Given M mixtures of N sound sources such that $M \leq N$, our goal is to recover the underlying sources up to a scale factor. For a data frame of T samples, we can represent the mixture X , as an $M \times T$ matrix which is the result of the product of an unknown mixing matrix B and the $N \times T$ source matrix S . Matrix B is an $M \times N$ matrix with each column corresponding to the direction of arrival of one source. Without loss of generality, we assume that 2 mixtures and 3 sources are available. The m th mixture can be represented as follows

$$x_m = \sum_{n=1}^N b_{m,n} s_n \tag{3}$$

However, several authors have found that sound signals exhibits very high sparsity in alternative representations such as time-frequency [1], and have successfully exploited this in algorithms such as pursuit. We now extend the above model for overcomplete dictionaries.

Given an overcomplete dictionary $D = \{d_k\}_{k=1}^K$, such that each atom d_k is a $T \times 1$ vector and $K \gg T$, we can represent the n th source vector as,

$$s_n = \sum_{k=1}^K c_{n,k} d_k \tag{4}$$

where $c_{n,k}$ is the coefficient associated to the k th dictionary atom. Subsequently, we can represent the mixture signals in terms of the source signals, dictionary atoms, mixing matrix columns and associated coefficients. The resulting representation is,

$$x_m = \sum_{n=1}^N \sum_{k=1}^K b_{m,n} c_{n,k} d_k \tag{5}$$

Sparse decomposition SD algorithm can be used to find a representation with few non-zero coefficients.

2. MULTICHANNEL DECOMPOSITION

2.1 Independent component analysis ICA

ICA is a technique for performing blind source separation. The equation (2) above is known as ICA model. The conditions that must be satisfied for ICA and the fore guarantee separation are

given by Darmois Theorem, which state that the sources S must be:-

- a. non-Gaussian and
- b. statistically independent.

These two assumptions are used to estimate the un-mixing matrix and the unmixed signals. The original mixed signals which we try to find in BSS are known as independent components.

To solve the cocktail party problem we must be able to separate the signals $x_1(t)$ and $x_2(t)$ to produce two signals $\hat{s}_1(t)$ and $\hat{s}_2(t)$ which are as close as possible to the original signals $s_1(t)$ and $s_2(t)$. This un-mixing process can be represented by the mathematical equation where W is the un-mixing matrix:

$$\hat{S} = WX \tag{6}$$

2.2 FastICA_25

FastICA_25 [2] is one of the practical implementation for ICA problems used in BSS. It uses non-Gaussianity as an estimate for independence to find a separating matrix

$W \in \mathbf{R}^{n \times n}$ to make the separated source signals non Gaussian.

Pre-processing by centering and whitening are necessary and important for the ICA performance. Centering is the process of subtracting the mean of the mixture of the independent components from the independent components so that the mixture of the independent components has a zero mean. This has no effect on the mixing matrix and is described by [3] as the “most usual and necessary pre-processing” for ICA. It is assumed in all of the ICA methods mentioned in this chapter.

To satisfy the assumption (b), the mixed signal is first whitened restricting the search space for the mixing matrix to the space of orthogonal matrices. During whitening the mixture is transformed so that its components are uncorrelated and its variances are unity. The mixture is said to be white [1]. Whitening is performed by Principal Components Analysis (PCA) by the most popular techniques of whitening: Eigenvalue Decomposition, demonstrated as follows:-

$$\hat{x} = ED^{-1/2}E^T x \tag{7}$$

Equation 7 shows the mathematical formula for performing eigenvalue decomposition. \hat{x} is the whitened transformation of the vector x . E is the matrix of eigenvectors of the covariance matrix of

x. D is the diagonal matrix of the eigenvalues of the covariance matrix of x.

To measure the non-gaussianity, kurtosis or differential entropy called negentropy can be used. Since kurtosis is not a robust measure of nongaussianity, especially with outliers. We consider negentropy in this paper.

2.3 ICA Using Negentropy in FastICA_25

The function J_G in equation (8), a maximizing entropy equation can be used as a gradient approximation of negentropy

$$J_G(w) = [E\{G(w^T x)\} - E\{G(v)\}]^2 \quad (8)$$

where G is a non quadratic function, v is a standardized Gaussian variable of zero mean and unit variance and w can be found under the constraint $E\{(w^T x)^2\} = 1$

i. $G_1(s) = \frac{1}{\pi} \log \cosh \pi s$

where $1 \leq s \leq a$

ii. $G_2(s) = -\exp\left(-\frac{s^2}{2}\right)$

Then FastICA_25 algorithm demonstrated in this paper uses this approximation of negentropy objective functions. Estimation of W is a measure of minimization of mutual information and maximization of negentropy which can be interpreted as estimation of single Independent component. The unmixing matrix W is estimated by maximizing the contrast function with respect to W given by:

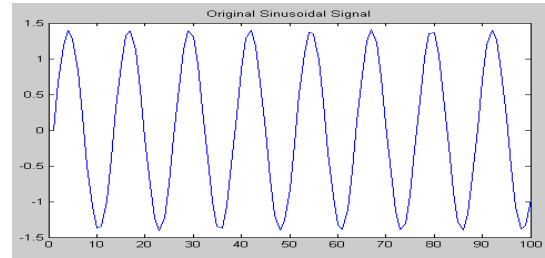
$$W = \sum_{i=1}^n \sum_{j=1}^m G(w_i^T x_j) \quad (9)$$

For optimal fast independent component analysis (Optimal FastICA) the objective function G is estimated by:

$$G_2(s) = -\exp\left(-\frac{s^2}{2\sigma}\right) \quad (10)$$

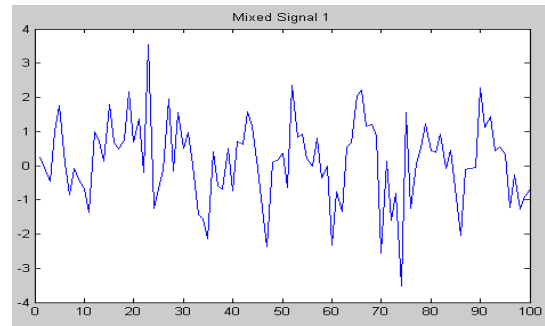
where $\sigma = k^x$ a parameter that gives a measure of distribution, Optimal value of K can be found from experimentation.

3 EXPERIMENTAL RESULTS



B_Mixing_Matrix =

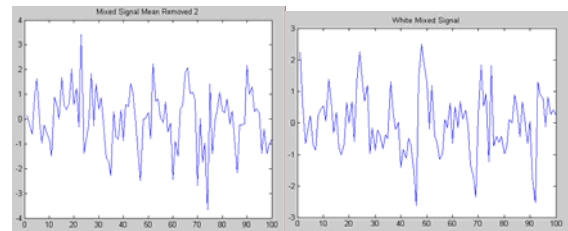
0.6028	0.2967	0.0855	0.9289
0.7112	0.3188	0.2625	0.7303
0.2217	0.4242	0.8010	0.4886
0.1174	0.5079	0.0292	0.5785



3.1 Preprocessing for ICA

3.1.1 Centering

This function is needed by FASTICA it removes the mean of row vectors and returns the new vectors and the mean.

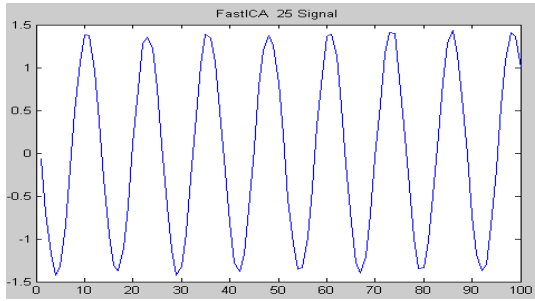


3.1.2 Whitening

This function is Eigen value decomposition by PCA.

$$\hat{x} = E D^{1/2} F^T x$$

3.1.3 FastICA_25



B =

0.4690	-0.1175	-0.1440	0.8634
-0.6193	0.5449	-0.4558	0.3344
-0.3732	0.0724	0.8541	0.3550
-0.5072	-0.8271	-0.2051	0.1288

W =

0.4690	-0.6193	-0.3732	-0.5072
-0.1175	0.5449	0.0724	-0.8271
-0.1440	-0.4558	0.8541	-0.2051
0.8634	0.3344	0.3550	0.1288

We estimate the independent components in the mixed signal and its corresponding demixing matrix W from which the sources are separated. Using OFastICA and BSS_Eval Matlab Toolbox the SIR components were to be compared by;

$$SNR = 10 \log_{10} \frac{\|mixed\ signal\|^2}{\|noise\|^2}$$

4.0 CONCLUSION

The demonstrated Gaussian ICA is used to solve the problem of Source Separation. Experimental result shows that there is a better quality of separation of the mixed signals using FastICA algorithms. The signal quality as demonstrated is well attained by the reconstructed signal. Nevertheless the effectiveness of the algorithm is the selection of the negentropy based function that can give optimal solution. The simplicity of using a modified gaussian function is the main criteria in this algorithm.

REFERENCES

[1] Vikrham B. Gowreesunker and Ahmed H. Tewfik, Blind source separation using monochannel

overcomplete Dictionaries, University of Minnesota, Dept. of Electrical and Computer Engineering, 2008.

[2] Zhong Zhang and Xudong Zhang “A New Mixing Matrix Identification Algorithm for Underdetermined Blind Source Separation” *ICSP2008 Proceedings*, Beijing, China 2008

[3] Hyvarien A. & Oja E. 1999 Independent component Analysis: A Tutorial Available at: http://www.cis.hut.fi/aapo/papers/IJCNN99_tutorialweb/.

[4] Ahmed Rubaai, Abdul R. Ofoli, Legand Burge and Moses Garuba, Hardware Implementation of an Adaptive Network-Based Fuzzy Controller for DC-DC Converters, *IEEE Transaction Industry Applications*, VOL. 41, NO. 6, November/December 2005 pp 1557-1565.

[5] Fevotte C, Gribonval R, Vincent R, BSS_EVAL Tool box http://www.irisa.fr/metiss/bss_eval/.

[6] Aapo Hyvärinen and Erkki Oja Independent Component Analysis: Algorithms and Applications. FIN-02015 HUT, Finland *Neural Networks*, 13(4-5):411-430, 2000

[7] Zhong Zhang and Xudong Zhang “A New Mixing Matrix Identification Algorithm for Underdetermined Blind Source Separation” *ICSP2008 Proceedings*, Beijing, China 2008

A STUDY OF THE EFFECTS OF URBAN DOMESTIC ELECTRICAL BURDEN ON THE ELECTRICITY GENERATION INDUSTRY OF KENYA

Gideon G. Kidegho
kideghoee@eng.jkuat.ac.ke

Marangi S. Mbogho
mbogho_ms@yahoo.co.uk

Oriedi A. Akumu,
oriedi@eng.jkuat.ac.ke

Department of Electrical and Electronic Engineering, Jomo Kenyatta University of Agriculture and Technology, P.O. Box 62000, Nairobi Kenya.

Abstract—Electrical energy in Kenya is the largest prime mover of the economy. Despite this fact, this energy source is in short supply. To satisfy the demand for electrical energy countrywide, available resources have been exploited. Currently electrical power generation is by; hydro, geothermal, petroleum fuels, wind and some solar PV in the rural areas. This paper investigates the effects of the urban domestic electrical burden on the power generation industry. The study uses Microsoft Excel to analyze the electrical burden. Further, the study would extrapolate the domestic burden to observe its effects nationally. Preliminary results did reveal a substantial national electrical burden of 319.98MWp occurring between 8PM and 9PM. These findings support the urgent need to address the electrical burden. Management of the urban electrical burden will relieve the generation industry of a large electrical burden in addition to reducing substantial losses in the transmission network

Keywords: *Generation, Domestic, Electrical Burden/load, Urban, Transmission losses, surge power.*

1. INTRODUCTION

The Kenyan Electricity Supply Industry (KESI) power generation mix consists of: 716MW of hydro, 135MW of geothermal, 307MW of thermal diesel and 5.1MW of wind. This power is then committed into the power supply network to meet the national electrical peak power demand of 1176MWp.

The load demand in Kenya can be classified as Industrial at 60%, commercial at 20% and domestic at 20%. The industrial and commercial loads attain their peak during the day. On the other hand, the domestic burden attains its peak at 8-9PM in the night.

Most of the electrical domestic burden is located in the urban areas which are far from the electrical power generating stations. This distance contributes to large electrical power losses during transmission and distribution to the urban load centers. These losses cause stress on the network and affect the life span and general performance of the network. Further these losses increase the generation demand which is currently being bridged using fossil fuels electricity power generators. The cost of the generation fuel is later passed on to the consumer resulting in inflating of the electricity bill.

The new emerging electrical power generation methods like solar PV are readily available for use to establish their role in this situation. The investigations should reveal the amount of

domestic electricity burden that can be off loaded by these methods from the national grid.

A detailed literature review has shown that the urban areas of Kenya consume most of the electrical energy generated in the country with Nairobi leading at 60%. Out of this load, 20% consists of the domestic electrical burden. The review further revealed that rural domestic electricity burden is negligible and so it will not be considered in the analysis.

To evaluate the amount of the national urban domestic electrical burden, individual domestic loads were collected, compiled and analysed as accurately as possible. The collection methods, compilation methods and analysis methods will be discussed.

2. THEORY AND METHODOLOGY

The study observed that even in urban areas, there are some consumers who contribute negligibly to the total domestic electricity burden or load. These consumers live in the high density settlement estates of the urban areas and only use electricity for lighting. The study therefore restricted itself to consumers who live in houses which have two bedrooms and above. In the case study, only three bed-roomed apartments, bungalows and maisonettes were considered.

Embakasi Nyayo Estate in Nairobi was chosen as the case study. The estate was chosen because of its size (accommodating some 4770 3bed-roomed

master en-suit units), infrastructure, accessibility and location.

Picture 1: View of Embakasi Nyayo Estate



Source: Generated by the Study

Picture 1 show a section of the Embakasi Nyayo Estate phase 1. One block consists of eight 3 bedroom *master en suite* apartments.

2.2. Load Data Collection

Load data was collected from some 100 homes using questionnaires and direct interviews, and power consumption data using pre-paid metering system logging method. The methods of data collection are explained in the following sections.

2.2.1. The Questionnaires Method

The study developed questionnaires for collecting the domestic load data. The questionnaires were sent out to 100 randomly chosen residents who filled them and returned to the researcher.

2.2.2 The Direct Interview Method

The study conducted direct interviews with the respondents of the questionnaires to physically pose questions to the respondents. The purpose of the interviews was to confirm that the respondents understood and answered the questions accurately. Further, the study was able to gather technical information from the name plates of some domestic appliances in the homes.

2.2.3. Power Consumption data

The study collected power consumption data from the Kenya Power and Lighting pre-paid meters, using data collection assistants. The data collection assistants logged the hourly power consumption

data from some 20 homes for 7 days in the case study estate.

2.3. Data Consideration

During the interview the study realized that the appliances in homes were of different types and operated differently. Some appliances were purely resistive and stationary while some were inductive and had rotating parts. The inductive appliances required surge power to start and then settle to the rated power when running. This surge power had to be considered for peak power rating purposes.

Table 1 shows the power rating of some appliances used in a typical household in Embakasi Nyayo Estate and require surge power to start.

Table 1: Steady State and Surge Power

S/N	Type of Load	Power (W)	Surge Power (W)
1	Fridge	300	1500
2	D/Washer	700	1500
3	C/Washer	650	1150
4	D/Freezer	450	1800

Source: Generated by the Study.

This study uses the surge power to estimate the peak power of a typical house hold. The study considered the highest peak power in the case study as a typical peak in its analysis. Summation of the peak power ratings gave the total peak load of the entire estate.

Further the study compiled a list of appliances from the questionnaires to develop a typical appliance list for the case study. The duty cycle of each appliance was tabulated to arrive to the daily energy consumed in a typical home of the case study.

Table 2: Domestic Load Analysis

S/N	Appliance	No	Watt	Hour	Whr	Watts	Whr
	1	2	3	4	5	6	7
1	Cf lamps	10	11	2	220	0	0
2	Radio	1	22	8	176	9.8	235
3	TV 21	1	50	4	200	5.1	122
4	Iron	1	1000	1	1000	0	0
5	Cooker	1	1000	0.5	500	0	0
6	Microwave	1	1100	0.5	550	0	0
7	Toaster	1	1500	0.5	750	0	0
8	Hair dryer	1	1500	0.5	750	0	0
9	Coffee Mix	1	1200	0.5	600	0	0
10	DVD	1	50	2	100	5.9	142
11	Computer	1	110	4	440	2.2	53
12	Lap top	1	65	4	260	2	48
13	Fridge	1	300	2	600	0	0
14	D/ Freezer	0	500	2	0	0	0
	Total	22	11458	31.5	6646	25	600
	Daily energy consumed in Whrs				7246		

Source: Generated by the study

Table 2 shows the details of domestic appliances.

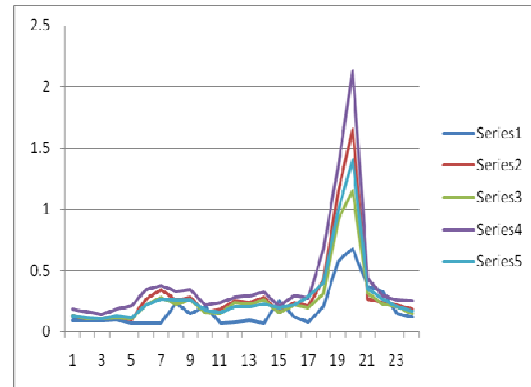
1. The appliance type on column 1.
2. The number of appliances in column 2.
3. The power rating of the appliance in column 3.
4. The duty cycle of the appliance in column 4 in hours.
5. The energy consumption of the appliance in column 5.
6. The stand-by power rating of the appliance in column 6.
7. The stand-by power consumption in column 7.

Table 2 shows the total installed electrical burden as 11458watts. From the same Table 2 the total daily energy consumed is 7246Whrs. This total energy consists of active appliance energy consumption of 6646Whrs and stand-by appliance energy consumption of 600Whrs.

3 RESULTS AND DISCUSSION

Figure 1 shows the daily power consumption for 4 sample houses in the case study estate. This data was collected using pre-paid meter data logging methods on 20 houses for 7days then an average was taken for each house. The figure only shows

the sample houses for comparison and clarity of the figure



Series 1- Court 87-House 9, 13, 15, 17,
 Series 2 Court1111-House 5, 9, 16, 25, 32
 Series 3 Court 116-House 2, 5, 7, 9.
 Series 4 – Court 5-House 1, 5, 7, 22
 Series 5 – Average of the Houses

Figure 1: Hourly Power Consumption (kW)

Source: Generated by the study

Table 3: Data Logging Burden Collection Average

Time	7-8	8-9	9-10	10-11	11-12	12-13
kWhrs	0.27	0.26	0.26	0.18	0.16	0.21
Time	13-14	14-15	15-16	16-17	17-18	18-19
kWhrs	0.21	0.23	0.2	0.22	0.29	0.4
Time	19-20	20-21	21-22	22-23	23-24	24-0
kWhrs	1	1.4	0.35	0.27	0.21	0.17
Time	0-1	1-2	2-3	3-4	4-5	5-6
kWhrs	0.13	0.12	0.11	0.13	0.12	0.22
Time	6-7	Total kWhrs consumed				
kWhrs	0.27	7.135				

Table 3 shows the daily total average energy requirement to be 7135Whrs using the data logging method while the daily total energy demand using the appliance ratings was 7246Whrs. This energy demands closely compares.

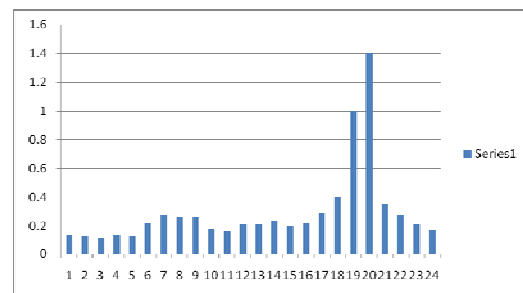


Figure 2: Daily Consumption in (kW)

Source: Generated by the study

Figure 2, shows the average daily peak power as 1.4kW which occurs between 8.00PM and 9.00PM or 20hours and 21hours. This information was used to obtain the total domestic burden of the study estate. The study would further extrapolate to get the Nairobi city total domestic burden and eventually the national domestic electricity burden.

3.1 Estimation of the Study Estate Domestic Electricity Burden

The study estate total domestic electricity burden is calculated as;

Domestic Electricity Burden = Total number of houses in the estate X typical peak power rating

Study Estate Burden,
 $\beta_e = 4774 \times 1400 = 6,683,600\text{Watts} = \mathbf{6.683MW}$

The Nairobi city domestic burden is calculated by estimating using the number of all similar units to the one considered in the study. The number of the units can only be estimated because the number is changing every day. Estimated number from Kenya Bureau of Statistics and the city council of Nairobi is 142,672 units. The city's domestic electrical burden is then;

City Burden,
 $\beta_c = 142672 \times 1400 = \mathbf{199.740MWp}$

The national domestic electricity burden is calculated by using the estimated number all similar units in the country. The estimated number of such similar units' country wide is 228557

Thus;
National Burden,
 $\beta_n = 228,557 \times 1400 = \mathbf{319.98MWp}$

3.2 Domestic Burden versus National Demand

The domestic burden is estimated at 319.98MWp and the national peak demand at 1176MWp. Expressing the domestic burden as a percentage of the national peak;

Percentage = $319.98 / 1176 = \mathbf{27.21\%}$

When we compare the national domestic electricity burden peak demand to the national peak demand, a substantial percentage is realized. This substantial burden on the electricity generation has far reaching negative effects on both the generation industry and the transmission network.

4 CONCLUSION AND RECOMMENDATION

The conclusions of this paper are summarized as follows.

1. The case study results have shown that the domestic electricity burden is large enough at 6.683MWp to deserve management.
2. The study has further shown by extrapolation that the city and national domestic electricity burden is 27.21%. This percentage is large enough to warrant Government intervention.
3. Localized domestic power generation systems are recommended as the most suitable intervention measure to take the burden off the generation industry and the grid.

5 ACKNOWLEDGEMENTS

The authors acknowledge the National Council for Science and Technology (NCST) for funding the study, the National Social Security Fund (NSSF) and Jomo Kenyatta University of Agriculture and Technology for facilitating the study.

6 REFERENCES

- [1] Kenya Bureau of Statistics (2006). Nairobi Kenya
- [2] KenGen, National energy report (2006)
- [3] Ministry of Energy, Electrical power status (2008)
- [4] KPLC Annual report (2008/2009). Renewable energy focus solar PV
- [5] Nairobi metropolitan development strategy report (2009)
- [6] Embakasi Nyayo Estate project report NSSF 1997
- [7] Arbi Gharakhani; Pragasen Pillay and Sheldon S. Williamson. 'A case study of PV installation for an Urban Building in Downtown Montreal' IEEE 2009, Grid connected solar PV, pp 1- 4
- [8] Woyte A., Van den Keybus, J. Belmas, Nijs J. Grid connected PV in the urban environment and experimental approach to system optimization 8th IEEE international conference on electronics and variable speed drives 2000, pp 548 -553
- [9] Bahaj A.S.; Braid, R.M.; James, P.A.B.; Post installation optimization of building integrated photovoltaic system at the Southampton University (Photovoltaic Specialists Conference, 2002.), pp: 1504 – 1507

ACTIVE POWER FILTER CONTROL USING A COOPERATIVE NEURO-FUZZY SYSTEM FOR HARMONIC MITIGATION

N. Bett
nkbett2002@yahoo.com

K.Hinga
pkhinga@yahoo.com

J.N. Nderu
jnnderu@yahoo.com.

Department of Electrical and Electronic Engineering, Jomo Kenyatta University of Agriculture and Technology,

Abstract—This paper presents a cooperative neuro-fuzzy based generation of gating signals for control of active power filter. The application of cost effective power converter circuits which enhance the overall performance, efficiency, and reliability of industrial process is common in all industries has led to serious concerns about the source of line pollution and resulting impacts on system equipment and power distribution systems. Active power filters have proven to be effective way of compensating harmonic component s in a nonlinear load. Various digital signal processing techniques are used to estimate the magnitude of harmonic distortion. Presently, neuro –fuzzy systems have proved to work better in nonlinear systems and it has attracted much attention from researchers due to its simplicity, learning and generalization ability of nonlinear quantities. This paper presents a neuro-fuzzy algorithm for estimating and generation of gating signals in real-time and high accuracy.

1. INTRODUCTION

The widespread and increasing use of solid state devices in power systems which enhance the overall performance, efficiency, and reliability of industrial processes has lead to escalating ambient harmonic levels in public electricity supply systems. These harmonic levels are subject to limitations in order to safeguard consumers' plant and installations against overheating and overvoltage. The effects of harmonics in power distribution systems are not new, but only recently the effects of these problems have gained more research attention. Advancement in semiconductor devices technology has also fuelled a revolution in application of power electronic devices over the last decade, and there are indications that this trend will continue [1]. Use of AC/DC and DC/AC power conversion commonly present in equipments such as converters, variable speed drives, arc equipment, uninterruptable power supply and many other household equipments are responsible for the rising problems related to power quality.

Power systems disturbance is often generated by non-linear loads. It is well known that a non linear load draws non sinusoidal periodic current even though sinusoidal voltage is applied [2].

There are many methods for harmonic extraction such as synchronous reference frame (dq) [3], discrete Fourier transform, fast Fourier transform [4] and instantaneous power (pq) theory [5].

The pq theory is associated with a limitation of determining harmonic components under load conditions only [6]. Fourier transform is the mostly used method for specific harmonic component compensation [7]. However it requires one more cycle of the voltage waveform data and corresponding time such that the delayed harmonic cancellation can occur.

The dq technique is substantially slow in responding to harmonic distortion and gives inaccurate result though it is within the acceptable range. Artificial neural network is a method with learning ability and high speed recognition in the field of electric power. It has been applied in several areas such as load forecasting [8]

In this study, feed forward neural network multilayer perceptron is used for harmonic detection processes as such obtain the input variables for the fuzzy controller to generate gating signal for the inverter. The distorted wave includes 5th, 7th, 11th, 13th, 17th, 19th, 23rd and 25th harmonics are used to be the input signal for the neural network at the training stage. The output layer of network is consisted of 8 units in according to each order of harmonic. By effect of learning representative data, each component of harmonic is detected to each according unit. That means neural network structures can decompose each order of harmonic and detect only harmonic without fundamental wave in the same time.

The outputs are summed-up together and compared to the distorted wave to obtain a reference signal

2. Structure of APF

The typical components of an active power filter system are the mains supply, nonlinear load, harmonic current detector, gating signal generator and voltage source inverter with interface reactor. The magnitude of harmonic current generated by a nonlinear load is supplied to the harmonic current detector together with information about other system variables. The reference signal from the current estimator, as well as other signals provides the control for gating signals controller. The output of the gating signals controller controls the voltage source inverter via a suitable interface reactor [9]. The main components of an active power filter system are shown in Figure 1.

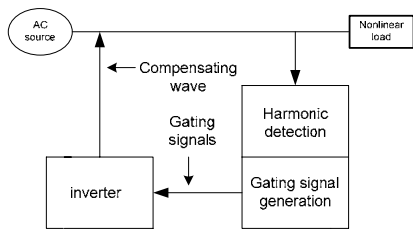


Figure 1: General Structure of APF

3. Cooperative Neuro-Fuzzy structure

Nuck [10] describes cooperative neural fuzzy model as a system where a neural network is used to determine several parameters (rules, rule weights and/or fuzzy sets) of the fuzzy system. Cooperative models can be further divided [11].

- (a) The neural net drives the parameters of membership functions from training data. The fuzzy sets are learned offline and are used with predefined fuzzy rules to implement a fuzzy controller.
- (b) The neural net drives linguistic control rules from training data. The learning is done offline and the fuzzy sets have to be defined in another way.
- (c) The neural net adapts the parameters of fuzzy sets online, i.e. while the fuzzy controller operates. It is necessary to know the fuzzy rules and initial fuzzy sets. In addition an error measure has to be defined that guides the learning process.
- (d) The neural net learns weights factors applied to the fuzzy rules in an online or offline mode. The weights are usually interpreted as the “importance” of the rule, and it modifies the output of the rule. Fuzzy rules and fuzzy sets have to be known in advance.

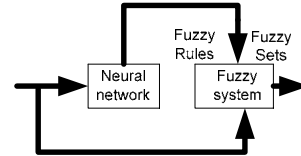


Figure 2: Cooperative Neuro-Fuzzy general structures

APF control using Cooperative Neuro-Fuzzy system.

Figure 3 shows the proposed application of a cooperative neuro-fuzzy network to detect and control APF. The distorted current is used in APF as the reference signal for controlling of the power stage. The acquired signal is sequentially introduce to cooperative neuro-fuzzy system and as a result, this network outputs the gating signal in real time.

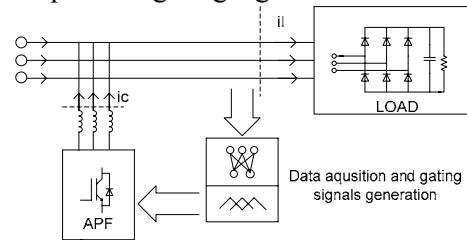


Figure 3: Neuro-Fuzzy controlled APF

- a) Harmonic detection and generation of gating signals.

Suppose the ideal supply voltage without any distortion,

$$v_s = V_p \sin \omega t \dots \dots \dots (1)$$

The periodic non-sinusoidal currents of nonlinear loads can be represented by Fourier progression as follows

$$i_l(t) = I_1 \sin(\omega t + \phi_1) + \sum_{n=2}^{\infty} I_n \sin(n\omega t + \phi_n) \dots (2)$$

Where ω is the angular frequency of signal, t is the time, I_1 is the fundamental component, ϕ_n is the respective angle and I_n is the harmonic component. In a three phase six switches system the active harmonics is as follows

$$n = 6k \pm 1, \text{ for } k = 1, 2, 3 \dots \dots (3)$$

where n is the active harmonic component and k is the sequence.

- b) System operation

The feed forward multilayered perceptron with the system will approximate the fundamental wave then compared with input distorted wave as such the reference signal is obtain. The train is done offline using the undistorted wave. It is then

compared with the out of the APF to generate an error. The error and change in error is then used as the inputs to the fuzzy logic system within the network to obtain the gating signal.

c) Simulation results
 Computer simulation results are presented to evaluate the performance of the cooperative neuro-fuzzy controller under industrial operating conditions. The MATLAB GUI representation of the proposed cooperative neuro-fuzzy controlled APF is shown in figure4.

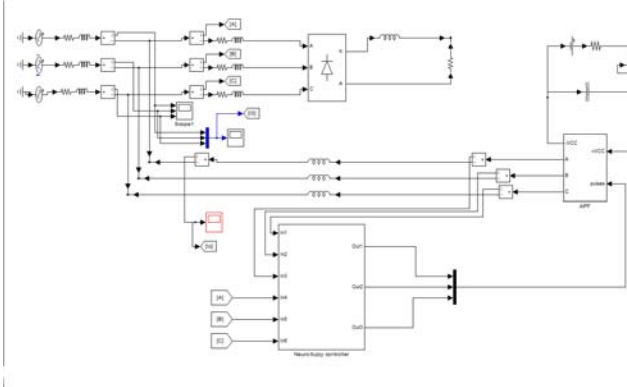
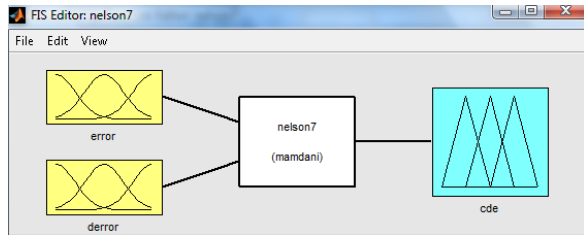


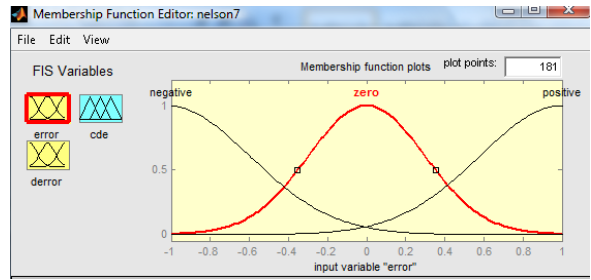
Figure 4: Simulated system

The output of APF is used to compensate for the harmonic distortions introduced by a nonlinear load in an electrical supply. After having identified the distortion harmonics, the resulting reference currents have to be injected phase-opposite in the electrical power systems. This is done by the APF's scheme with an inverter associated with an output passive filter.

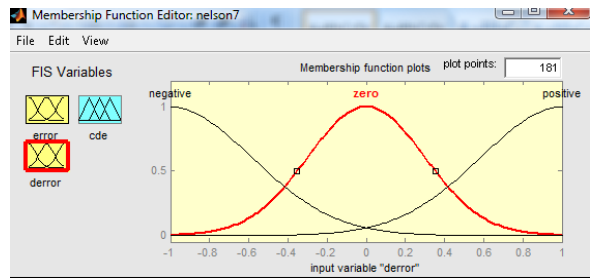
The fuzzy logic membership and its decision tale are shown in figure5 (a)-(d)



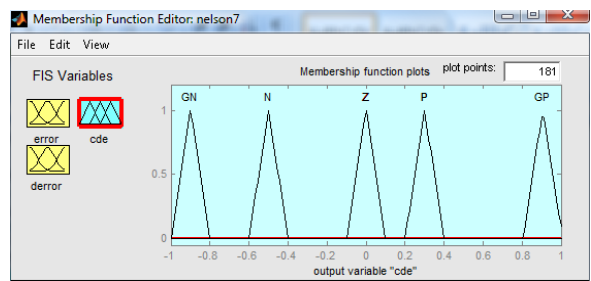
(a)



(b)



(c)



(d)

Figure5. (a). Fuzzy logic block diagram, (b) error membership function, (c) derror membership function and (d) output membership function

The fuzzy rules used for this case were as follows;

1. If error is zero then cde is Z
2. If error is positive (P), then cde id big positive(BP)
3. If error is negative, the cde is big negative (BN)
4. If the error is zero and derror is positive then cde is negative(N)
5. If the error is zero and derror is negative then cde is positive (P)

The power system is simulated with a sampling frequency of 50 Hz. The source characteristics are $RS = 0.001\Omega$, and $LS = 30\mu H$. The nonlinear load is composed of a Graetz's bridge of consisting of six valve functions with an angle $\beta = 0^\circ$ and with $RL = 0.5 \Omega$ and $LL = 300\mu H$. Figure6 (a)-(c)shows simulation results of the system.

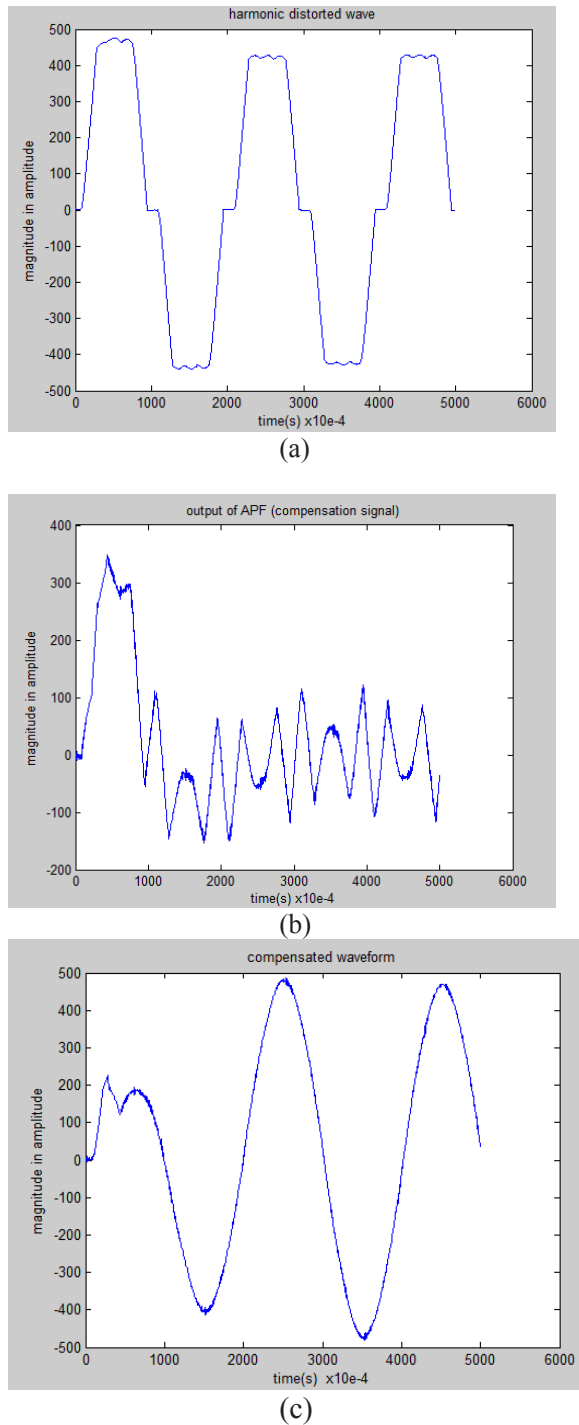


Figure 6. (a) harmonic distorted waveform, (b) compensation wave from APF and (c) compensated waveform

4. Conclusion

The effectiveness of the proposed cooperative neuro-fuzzy APF has been verified using MATLAB-simulink which allows real-time visualization, adjustment and control of all parameters. The proposed work shows promising

results to be investigated further in the hardware implementation.

6. References

- [1]. H. Akagi. "Trends in Active Power Line Conditioners", IEEE Transactions on power electronics, Vol.9, No.3, May 1994
- [2]. Balda, J. C. et al. Effects of Harmonics on Equipment. IEEE Trans. on Power Delivery. 1993. 8(2): 672-680.
- [3]. Gannett RA, Sozio JC, Boroyevich D (2002) Application of synchronous and stationary frame controllers for unbalanced and nonlinear load compensation in 4-leg inverters. Applied Power Electronics Conference and Exposition, 2002. APEC, Seventeenth Annual IEEE. Volume 2, 10-14 March 2002 Page(s):1038 - 1043 vol.2
- [4]. Asiminoaei L, Blaabjerg F, Hansen S (2005) Evaluation of harmonic detection methods for active power filter applications. Applied power electronics conference and exposition, 2005. APEC2005, Vol.1 March 2005 pgs 635-641
- [5]. Czarnecki Ls (2006) Instantaneous reactive power p-q theory and power properties of three-phase systems. Power Delivery, IEEE Transactions on Volume 21, Issue 1, Jan. 2006 Page(s):362 - 367
- [6]. Srinivasan D, Ng WS, Liew AC (2004) Neural-Network based signature recognition for harmonic source identification. Power Delivery, IEEE Transactions on Volume 21, Issue 1, Jan. 2006 Page(s):398 - 405
- [7]. Pecharanin N, Mitsui H, Sone M (1995) Harmonic detection by using neural network. Neural Networks, 1995. Proceedings, IEEE International Conference on Volume 2, 27 Nov.-1 Dec. 1995 Page(s):923 - 926
- [8]. Daneshdoost M, Lotfalian M, Bumroonggit G (1998) Neural network with Fuzzy based classification for short-term load forecasting. ". IEEE Transactions on Power systems, Vol. 13, NO. 4, November 1998.
- [9]. K.M. Tsang and W.L. Chan,(2006) "Design of single-phase active power filter using analogue cascade controller". IEE Proc.-Electr. Power Appl., Vol. 153, No. 5, September 2006.
- [10]. Detlef Nauck, (1995)"Beyond Neuro-Fuzzy: Perspectives and Directions", EUFIT '95, 1995, pp. 1159-1164.
- [11]. Jang R, Neuro-Fuzzy modeling: architecture, analyses and application, PHD Thesis, university of California Berkeley, July 1992.

DETERMINATION OF REACTIVE POWER COMPENSATION AND TRANSMISSION LINE POWER TRANSFER CAPABILITY IMPROVEMENT OF THE KENYAN POWER SYSTEM

Njoroge R.K.¹
rnjoroge@kplc.co.ke

Kaberere K.K.¹
kkanuthu@yahoo.com

Akumu A.O.²
AkumuAO@tut.ac.za

¹Jomo Kenyatta University of Agriculture and Technology, Kenya, ²Tshwane University of Technology, South Africa

Abstract—It is important to carry out regular power system analysis in the expanding power utilities in order to assess and plan for adequate reactive power. In this paper we look at why it is important to carry out reactive power compensation in a transmission network. A case of an emergency diesel plant that was first installed in a system during drought but could not be retired when the hydrology became favorable due to ensuing low bus voltages because of lack of adequate reactive power has been presented. The software package PSS/E has been used to simulate scenarios presented in this paper.

Keywords: *Power flow, bus voltage, system load demand, reactive power, compensation and emergency diesel plant*

I. INTRODUCTION

To supply power to consumers, utilities usually sign a supply agreement with a consumer that states details of power supply to be connected. This allows the consumers to specify the voltage rating of any electrical equipment procured for use in their premises. Once the supply is connected, the consumer expects the voltage and frequency to be maintained constant within the statutory tolerances and to experience minimum interruptions so that they can maximize the use of power.

For a utility to effectively meet the requirements of the consumers, the power system must be properly controlled. The main parameters to be controlled are voltage and frequency. To supply the system loads, a number of generating stations are interconnected through transmission lines and distribution network.

The frequency of the system is controlled by ensuring real power balance of supply and demand; it is controlled centrally. However, unlike frequency the transmission and distribution lines need voltage control at various points in the system to maintain the voltage at the consumer premises within permissible limits.

Voltage control is achieved by the control of reactive power flow in the system. The control of reactive load at the station bus is achieved by the adjustment of excitation of the station generators [1]. The voltage at different points of the power system may be controlled by introducing suitable reactive power compensating apparatus at various locations in transmission and /or distribution network.

One of the main causes of recent major outages in the power systems around the world was reported as insufficient reactive power of the system resulting in the voltage collapse [2]. Thus reactive power is essential for integrity of the power system. The amount of reactive power losses due to inductive nature of the transmission lines is significant as it can be about ten times greater than active power losses [2]. Under heavy load conditions, the total amount of reactive power losses may exceed the reactive power demand of the system loads. Accordingly, reactive power losses should be considered in the evaluation of the system's total reactive power requirements. In view of the high transmission losses (Figure 1), reactive power cannot be transmitted over long distances. Consequently, it must be produced close to where it is needed [2].

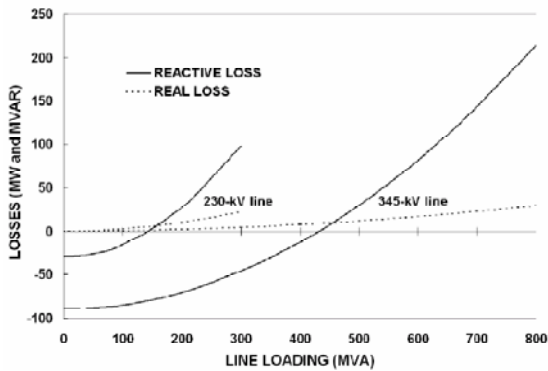


Figure 1: Transmission Line Real Power and Reactive Power Losses versus Line Loading (source [5])

II GENERATION AND TRANSMISSION NETWORK IN KENYA

Generation development in Kenya was initially concentrated in the hydro power resources along the Tana River. This led to the development of five hydro stations in a cascade, with installed capacity of about 550MW. The hydro power complex where the stations are located is known as the Seven Forks. To transfer this power to the load centres, five transmission lines were constructed to connect Seven Forks to Nairobi and Mombasa. Nairobi Area load demand is about 50% of the country's total demand. Mombasa Area has local thermal generation that meets the requirement of coast area and therefore most of the power generated in Seven Forks is transmitted to substations in Nairobi.

In 2006, there was a drought that affected the output of the Seven Forks hydro stations severely. In order to alleviate energy problems during the drought, an emergency diesel plant was installed at Embakasi (one of the main substations in Nairobi), with the generation tied to the 66kV bus. After the drought was over in mid 2007, the plant has been useful in maintaining voltage profiles in Nairobi area.

The transmission network comprises 220kV and 132kV transmission lines. In Nairobi area, there are sub-transmission lines with at voltage level of 66kV. All the lines at 33kV and below are considered to be distribution lines. Kenya Power and Lighting Company had a vertical structure until 1997 when it was unbundled to two entities; a generating company (KENGEN) and a transmission and

distribution company (KPLC). The new generating company formed became the Kenya Electricity Generating Company while the transmission and distribution company remained as Kenya Power and Lighting Company. With the separation, all the generating assets and facilities were transferred to KenGen, thus relieving KPLC not only the total control of generation of active and reactive power but also the planning of new energy resources.

III. VOLTAGE PROFILE PROBLEM

In Kenya bulk of the power supplied to consumers is generated by KenGen, contributing 80% and the other 20% is shared among the IPPs [4]. Though the IPPs are located close to the load centres, they operate their generators at a power factor close to unity and therefore do not generate much reactive power. KenGen's power stations are located far away from the load centres, and they generate most of the reactive power required in the power system. Thus, reactive power is transmitted over long distances, resulting in the low voltage profile at times experienced during evening peak. The low voltage (below 0.95pu) is due to high voltage drop along the transmission lines as the reactive current demand rises [6]. This phenomenon is experienced mostly when the water level in the reservoirs is high and the available hydro machines in the Seven Forks are loaded to the maximum available capacity for economic dispatch.

During and after heavy rains, the reservoirs store a lot of water. Instead of spilling, attempts have been made to maximize on hydro generation so as to save on fuel costs. However this has not always been successful because of the low voltage profile experienced in Nairobi. The low voltage profile is a symptom of reactive power imbalance between supply and demand at the receiving end substations in Nairobi [3]. This calls for an urgent reactive power planning in the transmission system in order to utilize all the available capacity of cheaper hydro power when the water is available in the reservoirs

and to improve voltage profiles (within $\pm 5\%$ of nominal) in order to maintain voltage levels at the consumer’s end within acceptable limit ($\pm 6\%$ of nominal) [3].

IV. RESEARCH FINDINGS

To address this voltage profile problem a research was carried out to determine the reactive power compensation requirements of the transmission network (132kV and 220kV) in Kenya in order to improve the voltage profile at the load centres and to enable the transfer of all the available hydro power from the Seven Forks hydro stations.

In this paper we shall demonstrate through power flow analysis carried out in the research that it was not possible to replace the emergency plant with power from Seven Forks hydro when the hydrology improved. The research findings are arranged as follows: Transmission network model; a base case - a peak load of 1024MW with emergency diesel plant in service; and a Case 1 where the emergency plant was replaced with generation from Seven Forks hydro.

A. Single line model of the transmission network

A single line model of Kenya transmission system was created using PSS/E. The transmission network model has included buses in sub-transmission and generation that were considered relevant for this research work.

B. Power flow scenarios

- *Base case data*

In order to model a running network, data records for the Kenya transmission network was used. The snapshot details on topology, system loading, generation, demand, and branches’ loading was based on the system control records of 21st November, 2007. Generation dispatch is seen in Table 1. Since it was not possible to freeze the system loading and generation demand from on line system, the evening peak, light load and branch loading as recorded in the transmission system

log-sheets as at 20.00hrs and 3.30hrs were used. The source of the data was National Control Centre (NCC).

- *System during evening peak demand-1024MW*

A peak demand of 1024 MW was recorded at 20.00Hrs by the National Control Centre on 21st November, 2007. The system load demand for that day is seen in the daily load curve of figure 2. This was the highest demand recorded in the system so far and that was the reason why it was chosen.

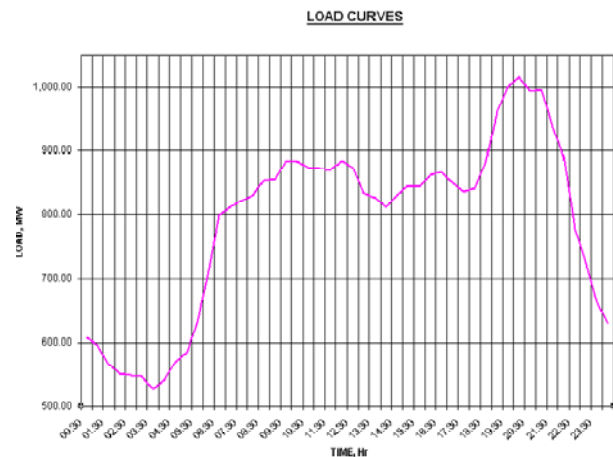


Figure 2: Daily Load Curve of 21st Nov. 2007

The generating plants and their loads during evening peak demand and during minimum demand at night are shown in Table 1.

- *Power flow for 1024MW load demand with emergency generator in service*

The following power flow results were obtained for this scenario.

1. Generation and loads summary

	MW	MVAR
From generation	1024.1	382.3
To constant power load	988.8	424.5
To constant current load	0.0	0.0
To constant admittance load	0.0	0.0
To bus shunt	0.0	0.0
To facts device shunt	0.0	0.0
To line shunt	0.0	0.0
From line charging	0.0	336.4

Table 1: Generation Log data for system demand.

STATIONS	EVENING	NIGHT
Gross Imp From Uetcl	6.368	1.344
Wanjii	4.57	4.55
Tana	9.60	9.80
Masinga	38.00	20.00
Kamburu	80.00	66.00
Gitaru	206.00	76.00
Kindaruma	40.00	24.00
Kiambere	110.00	100.00
Ndula	1.33	1.33
Mesco	0.37	0.37
Sagana	0.84	0.84
Sosiani	0.28	0.28
Gogo	0.15	0.15
Sondu Miriu	0.00	0.00
Turkwel	92.00	0.00
TOTAL		
HYDRO+UETC IMP	589.51	304.67
Iberafrica	50.60	11.00
N/S Fiat Gt	10.00	0.00
Olkaria 1	46.00	46.00
Orpower4 Steam	10.16	10.87
Kipevu Steam	0.00	0.00
Kipevu Gt1	0.00	0.00
Kipevu Gt2	30.00	0.00
Kipevu Diesel	50.00	20.00
Tsavo	74.40	53.20
Olkaria 2	66.00	66.00
Aggreko(Embakasi)	61.45	6.24
Aggreko(Eldoret)	36.02	10.11
Mumias Power	0.00	0.00
Total Thermal	434.63	223.42
System Gross	1,024.14	528.09

2. Losses and line charging summary

Voltage Level	Branches	x-losses-x		Charging
		MW	MVAR	MVAR
220.0	15	14.01	75.61	174.4
132.0	57	16.43	66.07	158.7
66.0	26 4	88	60.49	3.2
33.0	5	0.00	6.31	0.0
15.0	3	0.00	23.63	0.0
11.0	31	0.00	62.06	0.0
TOTAL	137	35.33	294.16	336.4

3. Bus voltage limit summary

a) Buses with voltage greater than 1.0500:

None

b) Buses with voltage less than 0.9500:

BUS	BASKV	V (PU)
19	132.00	0.9253
20	132.00	0.9025
48	132.00	0.9292
49	132.00	0.9309
52	132.00	0.9299
88	66.00	0.9488
90	66.00	0.9219

4. Branch loading above 100.0 % of rating:

None

5. Overloaded machine summary:

None

6. Generators at VAR Limits:

BUS	MW	MVAR	QMAX	MVABASE
82	30.0	20.0	20.0	36.0
88	17.0	6.0	6.0	30.0
102	5.9	4.0	4.0	120.0
104	61.3	30.0	30.0	95.0
TOTAL	114.1	60.0	60.0	281.0

Four machines reached VAR limit

The generating plants and their loads during evening peak demand and during minimum demand at night are shown in Table 1.

- Replacing emergency generator at Embakasi with generation from Seven Forks hydro-Case 1

In this case, the 61.4 MW generation from the emergency plant (Embakasi) was replaced by generation from Seven Forks hydro and the plant was shut down. The network model remained as before except for the plant at Embakasi that was switched off.

- Assessing reserves at Seven Forks hydro stations

There was need to assess whether the available machines at Seven Forks hydro had enough reserve capacity to take up the loads of the Emergency Plant.

The following table shows the machines that were running and their spinning reserves before the plant was shutdown. These data shown on running machines and their available reserve was derived from the machine summary of the base case.

Available generation and reserves in Seven Forks

BUS	PGEN (MW)	PMAX (MVAR)	BASE MVA (MW)	RESERVE (MW)
28	55.2	72	85.0	16.8
29	55.2	72	85.0	16.8
30	26.1	33	37.5	6.9
31	27.1	33	37.5	5.9
32	27.1	33	37.5	5.9
55	76.2	81	95.0	4.8
56	65.2	72	85.0	6.8
57	65.2	72	85.0	6.8
58	20.0	20	23.5	0.0
59	20.0	20	23.5	0.0
60	19.1	20	23.5	0.9
61	19.1	20	23.5	0.9
TOTAL	383.2	547	618	72.7

From the above table, the estimated reserve was 72.7MW. This was sufficient theoretically to replace the emergency generation of 61.4 MW. A power flow analysis was carried to confirm whether it was practically possible.

- Power flow results -Case 1

1. Generation and Load Summary

	MW	MVAR
From generation	1031.0	486.3
To constant power load	988.8	424.5
To constant current	0.0	0.0
To constant admittance	0.0	0.0
To bus shunt	0.0	0.0
To facts device shunt	0.0	0.0
To line shunt	0.0	0.0
From line charging	0.0	321.0

The generation went up to 1031MW because of increased losses.

2. System losses and line charging

Voltage Level	Branches	x-losses-x		charging
		MW	MVAR	MVAR
220.0	15	19.54	106.69	166.8
132.0	57	17.79	72.52	151.3
66.0	26	4.82	92.50	2.9
33.0	5	0.00	6.53	0.0
15.0	31	0.00	74.98	0.0
TOTAL	137	42.16	382.82	321.0

3. bus voltage limits summary

a). buses with voltage greater than 1.0500:

None

b) Buses with voltage less than 0.9500.

BUS	BASKV	V (PU)
1	220.00	0.9246
2	132.00	0.9446
3	132.00	0.9446
4	220.00	0.9162
5	66.000	0.8826
6	132.00	0.9423
7	66.000	0.9416
19	132.00	0.9083
20	132.00	0.8850
24	220.00	0.9344
34	220.00	0.9336
47	132.00	0.9294
48	132.00	0.9010
49	132.00	0.9027
52	132.00	0.9018
84	66.000	0.9484
88	66.000	0.9247
90	66.000	0.8972
92	132.00	0.9430
93	132.00	0.9309
94	132.00	0.9309
96	66.000	0.9223
97	66.000	0.8525
98	66.000	0.9416
99	6.000	0.8627
100	33.000	0.9447
101	132.00	0.9430
104	11.000	0.8695
9801	66.000	0.8704

From the above table, 29 buses had their voltage level below 0.95pu when generation was shifted from Embakasi to Seven Forks hydro. Seven of these buses (highlighted in yellow) had bus voltage below 0.90pu.

4. Branch loadings above 100.0 % of rating

Two branches were over loaded as seen in the table. These were the two transformers at Embakasi 220/66kV substation that were overloaded by 137.6% and 138.2 %

bus			current loading	rating	
From bus#	To bus #	CKT ID	loading (MVA)	rating A (MVA)	percent
4	5	1	123.8	90	137.6
4	5	2	124.4	90	138.2

5. Overloaded machine summary.

None

6. Generator at VAR limits

BUS#	MW	MVAR	QMAX	MVABASE
39	15.0	10.0	10.0	18.8
40	15.0	10.0	10.0	18.8
41	16.0	10.0	10.0	18.8
42	36.0	22.0	22.0	50.0
53	10.1	15.0	15.0	45.0
55	80.0	8.0	48.0	95.0
60	20.0	12.0	12.0	23.5
61	20.0	12.0	12.0	23.5
62	33.1	20.5	20.5	42.0
63	33.1	20.5	20.5	42.0
82	30.0	20.0	20.0	36.0
86	10.0	8.0	8.0	15.0
88	17.0	6.0	6.0	30.0
102	6.8	4.0	4.0	120.0
TTL	342.1	218.0	218.0	578.2

From the table, 14 Machines reached the VAR limit and therefore would not generate further reactive power to support the system voltage which was already below 0.95pu in 29 buses.

V. SUMMARY OF TABULATED RESULTS

From base case bus voltage limits, most buses had their voltage limits within the requirements except for seven buses. There were no buses with voltage above the limit, 1.05pu

Only four plants reached VAR limit. In case1 when generation was shifted to Seven Forks hydro, 29 bus voltages went below the limit,0.95pu

The loading on two transformers increased far above the limit of 100% to 137.6% and 138.2%.

Fourteen generating units reached their reactive power limit and they would therefore not support the system voltage.

The reactive power losses increased from 294.16MVAR to 382.82 MVAR, an increase of 88 MVAR.

The active power losses increase by 6.8MW

VI. CONCLUSION

Transferring generation from Embakasi to Seven Forks created a voltage profile problem in the network because 29 buses experienced low voltage and two transformers got overloaded to 137% and 138% at bus 4. There was a need according to these results to do address voltage support issues if the power were to be generated in Seven Forks hydro stations instead of using the emergency plant at Embakasi.

REFERENCES

[1] Arther R. Bergen and Vijay Vittal, "Power Systems Analysis", 2nd Edition, Publisher, Pearson, 2003
 [2] Ali H, Amjady N and Rabiee A, "Reactive Power Pricing Problems & Proposals for a Competitive Market", IEEE Power & Energy magazine, Vol.7 Number1, January/February, 2009
 [3] Mehta V.K and Rohit Mehta, "Principles of Power System", S.Chand Company Ltd, 2005
 [4] Gichuhi N. W, "Distributed Generation of Green Electricity for Sustainable Rural Electrification", Msc. Thesis, University
 [5] Federal Energy Regulatory Commission, "Principle for Efficient and Reliable Reactive Power Supply and Consumption", February 4th, 2005
 [6] Wadhwa C.L, "Electrical Power Systems", 4th Edition, New Age International, 2005

MODELLING AND CONTROL OF A FLEXIBLE MANIPULATOR USING FORMULA MANIPULATION

Minoru Sasaki¹, Hiroyuki Shimazaki¹, Toshimi Shimizu² and Satoshi Ito¹

*e-mail: sasaki@gifu-u.ac.jp 13028025@edu.gifu-u.ac.jp toshimi@mx.ibaraki.ac.jp
satoshi@gifu-u.ac.jp*

¹ Department of Human and Information Systems Engineering, Faculty of Engineering, Gifu University, Gifu, 501-1193, Japan

² Department of Mechanical Engineering, Faculty of Engineering, Ibaraki University, Hitachi, 316-8511, Japan

Abstract—This paper describes modeling and motion control of a flexible manipulator using a formula manipulation. Flexible arm is defined as low stiffness of a robot arm. We create a flexible manipulator model by using the formula manipulation language software MapleSim™ using the multi-body dynamics model of the flexible manipulator. We investigate the effect of elastic deformation and elastic vibration of the manipulator. The physical parameters are identified from the experimental data of the real manipulator experimental setup. Comparing between the simulations and experiments, the effectiveness of the modeling is evaluated and clarified. PD control of the joint angle and the feedback control of the link base strain are applied to motion control of the flexible manipulator. We confirm the effectiveness of the proposed control method and modeling of the manipulator.

1 INTRODUCTION

This paper presents modeling and motion control of a flexible manipulator using a formula manipulation. In the past several decades, there has been increasing interest in modeling and control of flexible manipulators [1-13]. There are a number of potential advantages stemming from the use of light-weight flexible-link manipulators, such as faster operation, lower energy consumption, and higher load-carrying capacity for the amount of energy expended. However, structural flexibility causes many difficulties in modeling the manipulator dynamics and guaranteeing stable and efficient motion of the manipulator end-effector. The control difficulties are mainly due to the non-collocated nature of the sensor and actuator positions, which results in non-minimum phase behavior. Further complications arise because of the highly nonlinear nature of the system. Satisfactory control of these systems is hampered by many difficulties related to sensing and identification. MapleSim™ is a collection of Maple™ routines that will automatically generate the symbolic equations of motion for an inter-connected system of rigid bodies and flexible beams, given only a description of the system as input. In other words, MapleSim™ is a symbolic package for

multibody dynamics and good tools for analyzing such as the flexible manipulators. This paper presents modeling and motion control of a flexible manipulator using a formula manipulation and comparing with experimental results and numerical simulation results. The effectiveness of the proposed control method and modeling method of the flexible manipulator is confirmed.

2 FLEXIBLE MANIPULATOR SYSTEM

The experimental system consists of highly flexible links as shown in Figure 1 whose parameters are shown in Table 1. A schematic of the experimental test-bed is shown in Figure 2. High performance drives were assembled consisting of PWM amplifiers that operate in speed feedback mode, DC servo motors with optical encoders and harmonic drive speed reducers. The digital controller consists of a dSPACE™ system based on the PowerPC. 16 channels of 16 bit A/D and D/A and 6 counters are also provided. In earlier experiments on this test-bed, the authors designed a PD controller. The identified model of the manipulator was derived and there was good agreement between experiment and model. Figures 4-6 show the time response of the identified models. The experimental results and the identified results match closely

except where hub friction or viscous damping dominates. The above analysis demonstrates that a linear model can approximate the actual system reasonably well and is suitable for defining the new output and designing the controllers.

Table 1: Parameters of the system.

Motor 1	Type	V511-012EL8	
	Rated power	105	W
	Rated spindle speed	3000	Rpm
	Rated torque	0.326	N·m
	Maximum torque	0.784	N·m
	Mass	1.1	Kg
Motor 2	Type	V404-012EL8	
	Rated power	39	W
	Rated spindle speed	3000	Rpm
	Rated torque	0.11	N·m
	Maximum torque	0.323	N·m
	Mass	0.55	kg
Encoder	Resolution	1000	P/R
	Type	Incremental	
Reduction Gear Joint 1	Reduction ratio	1/100	
	Mass	0.15	kg
	Type	CSF-40-100-2AR-SP	
Reduction Gear Joint 2	Reduction ratio	1/100	
	Mass	0.09	kg
	Type	CSF-17-1002 ^a -R-SP	
Link 1	Length	0.44	m
	Radius	0.005	m
	Material	Stainless	
Link 2	Length	0.44	m
	Radius	0.004	m
	Material	Aluminum	
Strain Gauge	Type	KGF-2-120-C1	
		-23L1M2R	

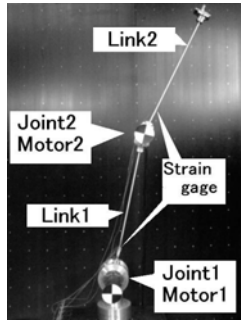


Figure 1: Flexible arm.

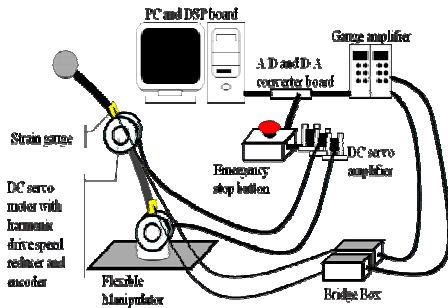


Figure 2: Experimental setup.

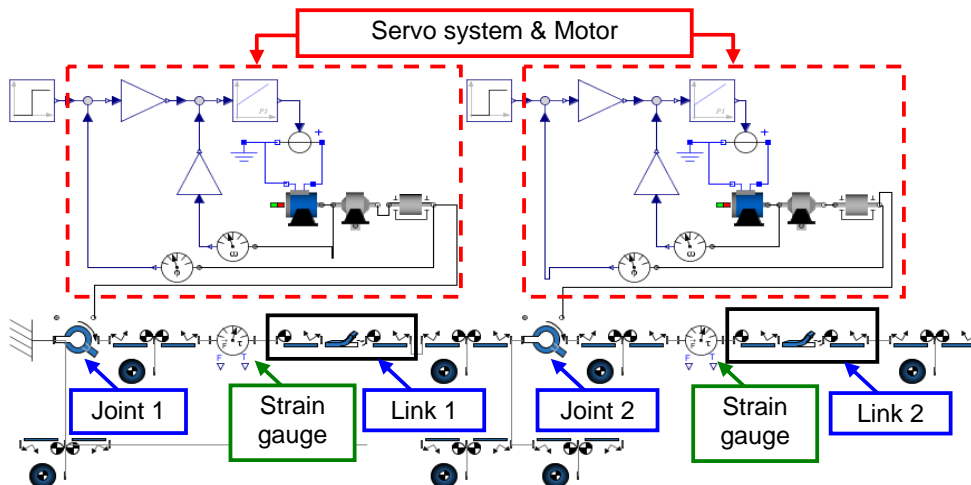


Figure 3: Model of the system

3 SYSTEM MODELLING

MapleSim™ supports a library of modelling components, including rigid bodies, flexible beams, forces, torques, springs, dampers, and a variety of joints (revolute, spherical, universal, etc) and includes fully validated Modelica components for modelling mechanical, electrical, hydraulic, thermal, and signal-flow systems. Model diagrams map directly to our physical systems, so they are easy to construct and validate. MapleSim™ lets us rapidly create custom components from first principles, by allowing you to specify the mathematical equations that define the dynamic behavior of our system.

With the physical modelling techniques in MapleSim™, we simply re-create the system diagram on a screen and the equations of the model are automatically generated. A model maps directly to each physical component, showing how those components are connected together, as shown in Figure 3 and the equations of motion are generated. This approach can save anywhere from hours to months on complex applications.

After our model is constructed, the MapleSim™ simulation engine automatically animates the model in 3-D, enabling us to visualize its behaviour.

State-of-the-art algorithms for multibody system handling automatically generate optimized model equations for our system. In MapleSim™, powerful code generation routines can then convert these equations into compact and numerically efficient code, which can be quickly and easily exported to other applications such as MATLAB™ in the tool chain.

4 CONTROL SYSTEM DESIGN.

A control law for a flexible manipulator can be developed using the Lyapunov control design method. Before designing the tracking control law, the procedure by developing a control law that drives the manipulator to a

given set of joint angles while suppressing the flexible motions will be illustrated. The Lyapunov function for the non-tracking controller is a weighted average of structural energy of each element of the manipulator, plus extra terms that force the Lyapunov function to be a minimum at the desired configuration of joint angles. The Lyapunov function is:

$$U = a_1 E_1 + a_2 E_2 + a_3 E_3 + a_4 E_4 + \frac{1}{2} b_1 (\theta_1 - \theta_{1ref})^2 + \frac{1}{2} b_2 [\theta_2 - \dot{r}'_1(l_1) - \theta_{2ref}]^2 \quad (1)$$

where E_1 is the kinetic energy of the hub of the first link, E_2 is the kinetic energy plus the strain energy of the first beam and its tip mass, E_3 is the kinetic energy of the hub of the second link, E_4 is the kinetic energy plus the strain energy of the second beam and its tip mass and payload, and θ_{1ref} and θ_{2ref} are the desired reference joint angles. The quantity $\dot{r}'_1(l_1)$ represents the angular deflection of the tip of the first link.

Since the elements of the arm are passive structural members, the rate of change of their energies is simply the applied external forces and moments times the velocities at the corresponding points of action. The rate of change of the Lyapunov function can be made negative by choosing the control torques to be

$$u_1 = -g_{11}(\theta_1 - \theta_{1ref}) - g_{12}\dot{\theta}_1 - g_{13}(M_1 - r_1 S_1) \quad (2)$$

$$u_2 = -g_{21}[\theta_2 - \dot{r}'_1(l_1) - \theta_{2ref}] - g_{22}[\dot{\theta}_2 - \dot{r}'_1(l_1)]$$

where $g_{11} = b_1/a_1$, $g_{12} = g_{13} = (a_1 - a_2)/a_1$, $g_{21} = b_2/a_2$ and g_{22} are the weighting constants. The quantity $M_1 - r_1 S_1$ can be measured using strain gauges at the base of link 1, whereas the angular positions and velocities can be measured using angle encoders and tachometers. Using these control laws, the rate of change of the Lyapunov function becomes

$$\dot{U} = -g_{12}\dot{\theta}_1^2 - g_{22}[\dot{\theta}_2 - \dot{r}'_1(l_1)]^2 \quad (3)$$

which is negative for all nonzero joint velocities. While this expression is only

negative semidefinite, the closed-loop system is in equilibrium only when $U=0$, so eventually the Lyapunov function must go to zero. The resulting system is asymptotically stable.

5 SIMULATION RESULTS AND DISCUSSION.

Figure 4 shows the time response of the joint angle of the flexible manipulator. Figure 5 demonstrates the time response of the root strain of the flexible manipulator.

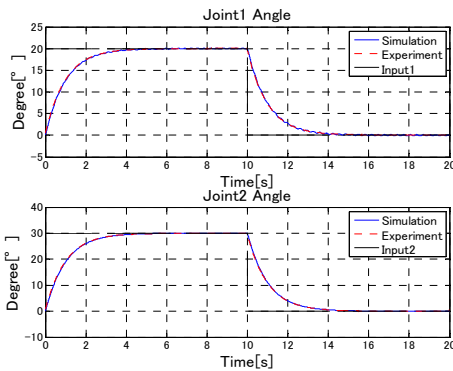


Figure 4: Joint angle response.

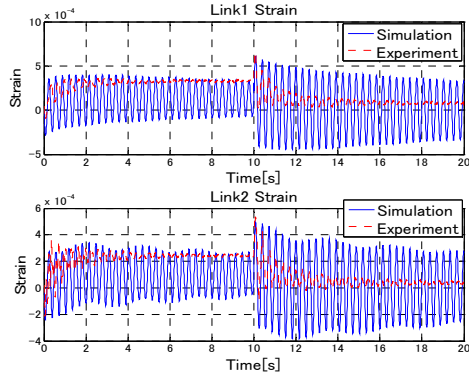


Figure 5: Root strain response.

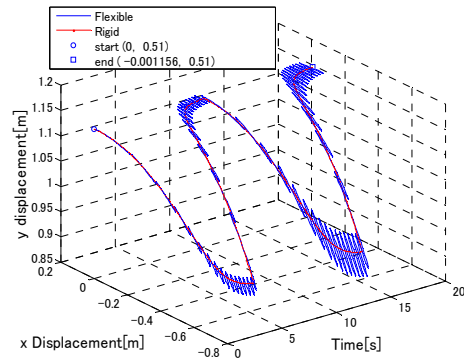


Figure 6: End point response.

Figure 6 shows the time response of the end point of the flexible manipulator.

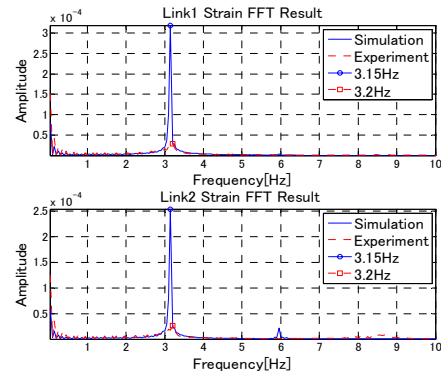


Figure 7: Power spectrum of the root strains.

Figure 7 shows the power spectrum of the root strains of the flexible manipulator. In these figures the red line shows the experimental result and the blue line shows the simulation result. The experimental results and the simulation results almost coincide with each other except damping phenomenon. In the FFT analysis results the experimental first natural frequency and the simulation first natural frequency are almost same.

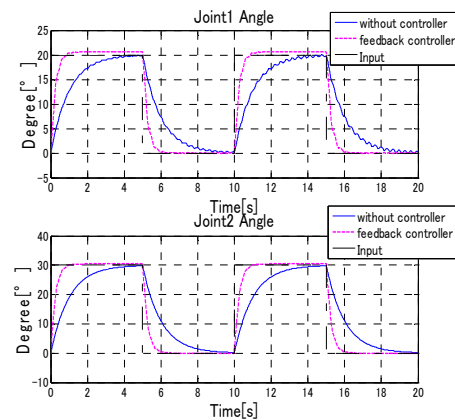


Figure 8: Joint angle response.

The end point vibration is occurred around the direction changed points. Figure 8 shows the time response of the root strain of the flexible manipulator with joint angles feedback and strain feedback. Figure 9 demonstrates the time response of the root strain of the flexible manipulator with the feedbacks.

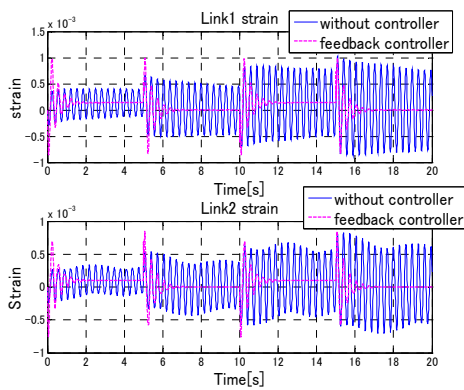


Figure 9: Root strain response.

Figure 10 shows the time response of the end point of the flexible manipulator with the feedback law. The feedback gains of the joint angles are 4 and the feedback gains of the root strains are 0.45 by the trial and error method. In these figures the residual vibrations are attenuated within 2 seconds and the end point of the manipulator and the joint angles can track the desired trajectory and the desired angles

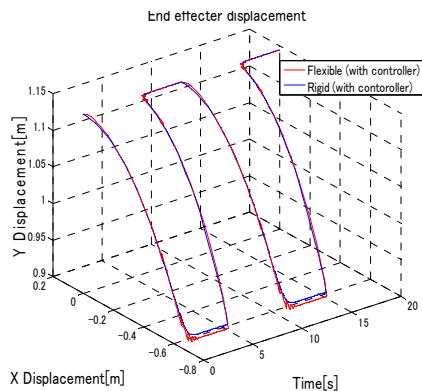


Figure 10: End point response.

6 CONCLUSION

This paper has presented modeling and motion control of a flexible manipulator using a formula manipulation. The flexible manipulator model has been created by using the formula manipulation language software MapleSim™ using the multi-body dynamics model of the flexible manipulator including the DC servo motor models and the electrical circuits. The effect of elastic deformation and elastic vibration of the manipulator has been investigated. The physical parameters have been identified from the experimental data of the real manipulator experimental setup. Comparing between the simulations and experiments, the effectiveness of the modeling is evaluated and clarified. The control law developed for the two-link manipulator allowed the flexible motions to be stabilized without any finite-dimensional estimation of the flexible modes, thus avoiding any

spillover problems. The effectiveness of the proposed control method and modeling of the manipulator has been confirmed.

7 REFERENCES

1. H.A. Talebi, R.V. Patel and K. Khorasani, Control of Flexible-link Manipulators Using Neural Networks, Springer, 2001.
2. F. M. Caswara, Neurofuzzy Network Based Control of a Multi-Link Flexible Manipulator, Shaker Verlag, 2001.
3. Eric H. K. Fung and Cedric K. M. Lee, Variable Structure Tracking Control of a Single-Link Flexible Arm Using Time-Varying Sliding Surface, Journal of Robotic Systems, Vol. 16-12, pp.715-726, 1999.
4. A. G. Cree and C. J. Damaren, Causal Approximate Inversion for Control of Structurally Flexible Manipulators Using Nonlinear Inner-Outer Factorization, Journal of Robotic Systems, Vol. 18-7, pp.391-399, 2001.
5. J. Cao and J. X. Xu, A Learning Variable Structure Controller of a Flexible One-Link Manipulator, ASME Journal of Dynamic Systems, Measurement, and Control, Vol. 122-4, pp. 624-631, 2000.
6. M. Moallem, R. V. Patel, and K. Khorasani, Nonlinear tip-position tracking control of a flexible-link manipulator: theory and experiments, Automatica, Vol. 37-11, pp. 1825-1834, 2001.
7. P. Bigras, M. Saad, and J. O'Shea, Robust Trajectory Control in the Workspace of a Class of Flexible Robots, Journal of Robotic Systems, Vol. 18-6, pp. 275-288. 2001.
8. C. I. Byrners, A. Isidori, J. C. Willems, Passivity, Feedback Equivalence, and the Global Stabilization of Minimum Phase Nonlinear Systems, IEEE Transactions on Automatic Control, Vol. 36-11, 1991.
9. Z. H. Luo and B. Guo, Further Theoretical Results on Direct Strain Feedback Control of Flexible Robot Arms, IEEE Transactions on Automatic Control, Vol. 40-4, pp. 747-751, 1995.
10. X. Zhang, W. Xu, S. S. Nair, and V. Chellaboina, PDEModeling and Control of a Flexible Two-Link Manipulator, IEEE Transaction on Control Systems Technology, Vol. 13-2, pp.301-312, 2005.
11. C. J. Damaren, Passivity and Noncollocation in the Control of Flexible Multibody Systems, ASME Journal of Dynamic Systems, Measurement, and Control, Vol. 122-1, pp. 11-17, 2000.
12. R. Ortega, A. Loria, R. Kelly, and L. Praly, On Passivity-Based Output Feedback Global Stabilization of Euler-Lagrange Systems, International Journal of Robust and Nonlinear Control, Vol. 5-4, pp. 313-323, 1995.
13. K. Okuda, M. Sasaki, F. Fujisawa, and T. Shimizu, Motion Control of Flexible Cartesian Robots, Proc. of 20th International Symposium on Space Technology and Science, pp.1-8, 1996.

LIST OF PARTICIPANTS

	NAME	ORGANIZATION	ADDRESS
1.	Andieri A.M.	MMUST	andieriam@yahoo.com
2.	Bett N.	JKUAT	nkbett2002@yahoo.com
3.	Chomba J.M.	MMUCK	jmchomba@gmail.com
4.	Dare A.A.	University of Ibadan	ademola_dare@yahoo.com
5.	Dharmadhikary V.	UON	dhamavasudha@gmail.com
6.	Gitonga T.	MMU	thogitgat@yahoo.com
7.	Hinga P.K.	JKUAT	pkhinga@yahoo.com
8.	Jallango Akello	MMUST	rjakello@yahoo.com
9.	Kanai M.M.	JKUAT	cheptora@yahoo.com
10.	Kidegho G.G.	JKUAT	kideghogee@gmail.com
11.	Kihato P.K.	JKUAT	kamitoza@yahoo.co.ke
12.	Kipyegon E.K	JKUAT	ekipyegon@yahoo.com
13.	Kiragu K.K	JKUAT	kckiragu@yahoo.com
14.	Kojima K.	Gifu University	03128010@queda.gifu-u.ac.jp
15.	Konditi D.B.O	MMUCK	onyango_d@yahoo.co.uk
16.	Kuriyama Y.	Gifu University	3812202@edu.gifu-u.ac.jp
17.	Maina C.	JKUAT	cmmurithi@eng.jkuat.ac.ke
18.	Mburu D.N.	MMUCK	da_mburu@yahoo.com
19.	Minoru S.	Gifu University	sasaki@gifu-u.ac.jp
20.	Muiga N.R.	JKUAT	muigarugera@gmail.com
21.	Muigai A	MU	muigai@mu.ac.ke
22.	Munda J.L.	TUT (RSA)	mundajil@tut.ac.za
23.	Mureu E.	JKUAT	ewmureu@yahoo.com
24.	Musyoki S.	JKUAT	smusyoki@yahoo.com
25.	Nderu J.N.	JKUAT	jnnderu@yahoo.com
26.	Njoroge R.K	JKUAT	rnjoroge@KPLC.co.ke
27.	Obadha J.A.	JKUAT	josephajok@yahoo.co.uk
28.	Ochieng T.	KPUC	ochiengtoni@yahoo.com
29.	Odhiambo D.	MMU	dodhiambo@mmu.ac.ke
30.	Odondo S.	MMUST	sodondo@yahoo.com
31.	Ojenge W.	KPUC	tojenge@yahoo.com
32.	Ombati D.O.	JKUAT	denis_2009@yahoo.com
33.	Otieno C.A.	JKUAT	otychriss@yahoo.com
34.	Ouma H.A.	UON	houma@ieee.org
35.	Saito A.	Japan	asaito1944920@ybb.ne.jp
36.	Senthil K.	St. Joseph College(DSM)	ksenthil_856@yahoo.com
37.	Sitati S.	MU	simiyusitati@yahoo.com
38.	Tanabe S.	Japan	tanas@tnb.bbia.jp
39.	Waguchu G.	JKUAT	gwaguchu@yahoo.com
40.	Yano K.	Mie University	yano-k@gifu-u.ac.jp

Key to Abbreviations:

JKUAT – Jomo Kenyatta University of Agriculture and Technology
 KPUC – Kenya Polytechnic University College
 MMUCK – Multimedia University College of Kenya

MMUST – Masinde Muliro University of Science and Technology
 MU – Moi University
 TUT (RSA) – Tshwane University of Technology, South Africa
 UON – University of Nairobi